Macromolecular network structuring effects on quasi-static and fatigue properties of natural rubber

Grégoire Delahaye

COLLEGE SCIENCES DE LA MATIERE
DOCTORAL DES MOLECULES
BRETAGNE ET MATERIAUX

Université de Rennes

THESE DE DOCTORAT DE

L'UNIVERSITE DE RENNES

ECOLE DOCTORALE N° 638
Sciences de la Matière, des Molécules et Matériaux
Spécialité : *Sciences des matériaux*

Par

Grégoire DELAHAYE

Effets de la structuration du réseau macromoléculaire sur les propriétés mécaniques quasi-statiques et en fatigue du caoutchouc naturel

Thèse présentée et soutenue le 07 novembre 2024 à Rennes
Unité de recherche : IPR UMR UR-CNRS 6251

Rapporteurs avant soutenance :

Stéphane MEO	Professeur des Universités – Université de Tours
Nicolas SAINTIER	Professeur des Universités – Université de Bordeaux

Composition du Jury :

Présidente :	Sandrine THUILLIER	Professeure des Universités – Université de Bretagne Sud
Examinateurs :	Stéphane MEO	Professeur des Universités – Université de Tours
	Nicolas SAINTIER	Professeur des Universités – Université de Bordeaux
	Grégory CHAGNON	Professeur des Universités – Université Grenoble Alpes
	Pierre-Antoine ALBOUY	Directeur de recherche CNRS – Laboratoire de Physique des Solides
Dir. de thèse :	Jean-Benoît LE CAM	Professeur des Universités – Université de Rennes

Invitées

Isabelle JEANNEAU	Contitech AVS France
Sophie GUILLAUME	Directrice de recherche CNRS – Institut des Sciences Chimiques de Rennes

Remerciements

Nous y voilà... il est temps d'écrire les dernières pages. Ces quelques derniers moments devant mon clavier me permettent non-seulement de clore ma thèse, mais surtout de remercier chaleureusement toutes les personnes ayant contribué à sa réussite. Le fruit de ce travail est collectif, et j'espère que ces mots sauront témoigner combien je vous en suis reconnaissant.

Je tiens tout d'abord à adresser de profonds remerciements aux membres du jury. Merci à Madame Sandrine Thuillier d'avoir accepté de présider ma soutenance de thèse. Messieurs Stéphane Méo et Nicolas Saintier, je vous remercie pour vos rapports avant soutenance et votre analyse très poussée du sujet. Vos questions et vos remarques m'ont fait prendre du recul et aborder les choses différemment. J'adresse également de profonds remerciements à Messieurs Pierre-Antoine Albouy et Grégory Chagnon, nos échanges ont été un moment particulièrement enrichissant.
Comme j'ai pu le souligner précédemment, une thèse est le fruit d'un travail collectif. Je souhaite en ce sens adresser mes plus profonds remerciements à mon directeur de thèse, Jean-Benoît Le Cam, pour ses conseils avisés, sa rigueur et les enseignements qu'il m'a transmis. Notre rencontre a définitivement marqué ma carrière professionnelle et mon avenir : merci pour tout ! Je tiens à remercier également mes encadrants industriels. Je remercie Benoît Ruellan pour sa patience, sa disponibilité sans faille et pour m'avoir fait découvrir (ou plutôt adorer) la course à pied ! Un grand merci à Isabelle Jeanneau de m'avoir accueilli au sein de son laboratoire, et pour nos échanges au sujet de la formulation de pièces. Je souhaite aussi remercier les membres de mon comité de suivi individuel, Florence Razan et Lionel Léotoing.

Je tiens à remercier chaleureusement Sophie Guillaume et Julien Rosselgong pour leur bienveillance et leur accueil au sein de l'ISCR. On peut dire que ça a plutôt bien "gonflé" là-bas ! Un grand merci à l'équipe IQ2M pour ces beaux moments passés ensemble lors de séminaires et au quotidien; Eric Robin, Mathieu Miroir, Romain Laniel et Mickaël Le Fur. Je remercie aussi Fabienne Blanchet pour les nombreuses découpes d'échantillons.

Je souhaite adresser de sincères remerciements à toutes les personnes de l'IPR pour leur accueil et leur gentillesse.
Je remercie Isabelle Delanoë, Pierrick Coirre et Maxime Gandeboeuf du labo. C'est toujours un plaisir de passer au laboratoire ! Merci aussi à Sylvain Larivière, ton travail précieux de préparation des mélanges fut indispensable. Je remercie très chaleureusement Charles Labouère, sans qui aucun essai de fatigue n'aurait été lancé. Merci également aux autres membres du laboratoire essais, Frédéric Mortier, Gildas Buisson, Anthony Le Guevel et Pascal Surget. Je remercie également Stéphane Gillet pour nos échanges lors des séminaires et parfois aux vestiaires après une sortie course à pied. Je souhaite remercier particulièrement l'équipe de l'innovation de Franck Kerguelen pour son accueil chaleureux et notamment Thomas Jacopin pour son aide dans la concrétisation de mon projet professionnel. Plus largement, je tiens à remercier l'ensemble du personnel de Contitech AVS France pour l'accueil qui m'a été réservé.

Je souhaite remercier la dream team du laboratoire, j'ai nommé Adel, Yasser et Adrien. Nous sommes passés par des phases de travail très intense, entrecoupées de moments de rire. Nous retiendrons surtout les chansons d'Adel, garantes de la bonne humeur. Je remercie bien évidemment la nouvelle dream team du laboratoire, Maria, Aminata, Doriane, David et Ismahen. Grâce à vous, l'avenir du laboratoire est assuré. Gauthier, je souhaite aussi te remercier pour ton fabuleux stage et nos moments de partage. Jules, mon compagnon de toujours, je te remercie pour ton soutien et je te félicite pour ta thèse. Mes amis du fabuleux groupe d'amis MPC, sachez à quel point je vous remercie d'avoir été à mes côtés jusqu'au bout de cette thèse.

Ma très chère famille, je vous remercie pour votre soutien. Oui, il n'est pas facile de comprendre exactement ce que Grégoire faisait avec le caoutchouc, mais vous vous y êtes toujours intéressés. Merci à mes parents, à qui je dois tout. Merci à ma sœur pour sa grande empathie, sa bienveillance et sa douceur. Merci à mes grands-parents pour leur soutien et leur grande gentillesse. Merci à ma marraine, à mon parrain, à mes oncles et tantes, à mes cousins et à ma cousine pour leur soutien, mais surtout pour m'aider à me changer les idées lors de nos rencontres en famille. Merci également à mes beaux-parents et à ma belle-famille, de France comme d'Italie, pour votre soutien et tous les moments conviviaux que nous avons partagés.

Clémentine, tu m'as accompagné pendant ces trois années. Tu as été là dans tous les moments, les bons comme les moins bons. Vivre au quotidien avec un doctorant peut sembler relever du défi, mais tu m'as toujours soutenu et aidé à avancer. Malgré la légèreté de ces quelques mots, je tiens à te remercier sincèrement pour tout ce que tu m'as apporté, et ce que tu m'apportes au quotidien.

Contents

Introduction générale

Les systèmes antivibratoires (AVS pour « Anti-Vibratory Systems ») sont utilisés dans l'industrie automobile afin de réduire le bruit, de filtrer les vibrations mais aussi d'améliorer la sécurité des véhicules. Ces pièces sont en grande partie composées d'élastomères, et sont dimensionnées de manière à respecter des spécifications mécaniques imposées par les constructeurs automobiles ; la raideur statique et la tenue au vieillissement par exemple. En fonctionnement, les sollicitations cycliques subies par les pièces provoquent un endommagement en fatigue qui conduit à la perte de leur fonctionnalité. Depuis plusieurs années, l'Université de Rennes, Continental et le CNRS ont œuvré à mieux comprendre et modéliser le comportement mécanique des pièces, réduisant considérablement le temps et les coûts nécessaires à leur développement ainsi que l'impact carbone des pièces. Cette collaboration a pris la forme d'un laboratoire commun créé en 2020. Il porte le nom d'ELAST-D^3 et a pour objectif de contribuer à la décarbonation de la mobilité. Dans ce cadre, les travaux de thèse respectifs de Benoît Ruellan et de Yasser Mouslih ont permis de mieux comprendre et caractériser l'effet de la température sur la résistance à la fatigue, pour des cas de chargements uni- et multi- axiaux. Aujourd'hui, l'électrification des véhicules automobiles conduit à une évolution substantielle des cahiers des charges des pièces antivibratoires. Cela nécessite d'adapter la boucle de conception des pièces, notamment en maîtrisant encore davantage le lien entre formulation, process de fabrication et propriétés mécaniques. Les travaux de la présente thèse s'inscrivent dans ce contexte.

Le caoutchouc naturel chargé de noir de carbone (CB-NR pour « Carbon Black filled Natural Rubber ») est l'élastomère le plus utilisé dans les systèmes antivibratoires. Il se distingue des autres élastomères par sa fascinante capacité à cristalliser sous déformation (SIC pour « Strain-Induced Crystallization ») et présente une résistance à la fatigue et des propriétés dynamiques remarquables. En effet dès 1940, les travaux de Cadwell *et al.* ont permis de mettre en évidence un renforcement de la durée de vie en fatigue du CB-NR sous chargement non-relaxants, c'est-à-dire pour un minimum de chargement strictement positif. Ce renforcement ne s'observant pas dans les élastomères non-cristallisables, il est

généralement imputé à la capacité du CB-NR à cristalliser sans pour autant que cela ait été démontré. Bien que beaucoup d'études traitent de la fatigue du CB-NR, peu d'entre elles questionnent le lien entre ces propriétés et la structure du réseau macromoléculaire, à savoir la densité de chaînes actives et la longueur des ponts soufrés. Ce réseau macromoléculaire acquiert sa structure au cours de la vulcanisation, on parle également de cuisson, laquelle dépend de la formulation chimique du matériau et des conditions de mise en œuvre (temps, température). Depuis sa découverte par Katz en 1925, on sait aujourd'hui que la SIC dépend fortement de la structuration du réseau macromoléculaire. Malgré un nombre conséquent d'études, le lien entre le réseau macromoléculaire et la SIC n'est pas encore bien établi. Pour autant, des résultats contradictoires ont été reportés sur un nombre limité de matériaux et comprenant de grandes différences en termes de de formulation et de conditions de vulcanisation, complexifiant leur interprétation. Ainsi, pour optimiser la formulation et les conditions de mise en forme des pièces en CB-NR, il convient de mieux comprendre le lien entre la structuration du réseau macromoléculaire et ses propriétés mécaniques, et plus particulièrement sa résistance à la fatigue et le renforcement de la durée de vie. Ces présents travaux de thèse ont vocation à revisiter et clarifier les effets de la structuration du réseau macromoléculaire sur le comportement mécanique du NR.

Dans cette étude, des essais quasi-statiques et en fatigue uni-axiaux sur une large gamme de matériaux ont été menés, et les objectifs sont les suivants :

- caractériser le lien entre formulation, conditions de vulcanisation et structuration du réseau macromoléculaire,
- caractériser l'effet de la structuration du réseau macromoléculaire sur le comportement mécanique quasi-statiques,
- établir un lien entre la structuration du réseau macromoléculaire et la résistance à la fatigue, et plus particulièrement le renforcement de la durée de vie,
- investiguer l'origine du renforcement de la durée de vie à l'échelle du réseau macromoléculaire.

Le Chapitre 1 dresse un état de l'art sur la structuration du réseau macromoléculaire et les propriétés mécaniques et cristallines du NR. Le chapitre détaille également le comportement du NR en fatigue. Le Chapitre 2 présente les matériaux de l'étude, destinés à l'exploration des propriétés mécaniques d'une large gamme de structures de réseau macromoléculaire. Les essais à réaliser pour caractériser le réseau macromoléculaire, les propriétés mécaniques quasi-statiques et en fatigue sont décrits. Ce chapitre se clôture par la présentation de résultats préliminaires sur la rhéométrie, le gonflement par solvant et

la traction monotone. La caractérisation de l'effet Mullins, réalisée au travers d'essais de traction cycliques, est présentée dans le Chapitre 3. L'effet de la structuration du réseau macromoléculaire sur l'effet Mullins pour des matériaux chargés est distingué de celui des non-chargés. Les mécanismes physiques à l'origine de l'effet Mullins sont discutés, notamment la contribution de la SIC, en lien avec la structure du réseau macromoléculaire. Le Chapitre 4 explore le comportement en fatigue, en différenciant les cas de chargements relaxants des non-relaxants. Pour chaque cas de chargement, une analyse des durées de vie est complétée par une analyse post-mortem des faciès rompus. L'effet de la structuration du réseau macromoléculaire sur la résistance à la fatigue et le renforcement de la durée de vie est discuté au travers de divers diagrammes. Le manuscrit se clôture avec la conclusion générale de l'étude et les perspectives pour poursuivre la discussion. Trois annexes complètent le document, elles portent respectivement sur la méthode de gonflement, les réponses mécaniques en traction monotone et sous chargement de traction cyclique.

Chapter 1

State of the art

Preamble

The fatigue properties of rubbers are influenced by a wide range of factors such as the formulation, vulcanization and testing conditions to name a few [1]. Clearly, these properties are intimately related to the macromolecular network, more precisely the cross-link length and active chain density [2, 3]. Surprisingly, crystallizable rubbers such as NR, exhibit a typical fatigue behavior characterized by a strong lifetime reinforcement observed in the case of non-relaxing loadings [4]. As the ability of NR to crystallize is driven by its macromolecular network, it appears essential to understand what are the parameters that affect the macromolecular network structure. To go further, understanding the multiple relations between macromolecular network, fatigue resistance, lifetime reinforcement and SIC is therefore essential. The present chapter addresses a state of the art on these relations.

This state of the art is divided into three sections. Section 1.1 gives generalities about NR. The rubber formulation and process conditions are presented, before its main mechanical properties are addressed. Section 1.2 presents the SIC and its links to the macromolecular network. A special attention is paid on the active chain density, as it seems to drive the mechanical and physical properties of NR. Finally, Section 1.3 reviews the fatigue properties, their generalities, and the factors affecting the fatigue life, with a particular emphasis on the effect of the macromolecular network. This section ends with a presentation of the damage mechanisms through post-mortem failure surface analyses.

1.1 Generalities on NR

In this section, the history of rubber field is firstly reported. Then, the macromolecular network of NR is introduced and the importance of the formulation and vulcanization conditions on its structuration are highlighted. Finally, the mechanical properties of NR are described, by attempting to relate them to the macromolecular network. Elasticity, viscoelasticity, hysteresis, Mullins effect, and calorimetric response are successively presented.

1.1.1 History

Originally, NR has been discovered by the Mayas, the Incas and the Olmecs. Years later, it has been used to produce objects such as balls and recipients [5]. It is now widely used with an annual consumption estimated at 13.8 million tons over the period 2012-2021[1]. NR originates from plants such as the *Hevea Brasiliensis*, *Guayule* and *Gutta-Percha* [6]. The main producers are Thailand and Indonesia. For the *Hevea Brasiliensis*, it is obtained by extracting the secreted latex. After extraction by a bleeding process, the latex is first filtered and coagulated with acid, and then washed and dried. The resulting product formed is called "gum".
Several important dates have punctuated the history of NR:

- **1736:** De La Condamine, a french explorer and scientist, imported the latex from South America to Europe. Furthermore, he also imported the name "caoutchouc" (in French) coming from the words "cao" and "tchu", literally meaning "crying wood" in quechua language.
- **1826:** Faraday discovered the NR formula $(C_5H_8)_n$.
- **1839:** Goodyear accidentally discovered the vulcanization process. By adding sulphur and a sufficient source of heat, rubber becomes elastic and acquires properties that lead to a wide range of applications. Later, Thomas Hancock will apply for a patent relative to vulcanization.
- **1888:** the rivalry between John Dunlop and the Michelin brothers starts with the expansion of the tyre industry. Rubber became indispensable in every types of vehicles.

Several other dates marked major contributions to the understanding and characterization of its mechanical and physical properties, non-exhaustively:

[1]From the "Ministère de la Transition écologique et de la cohésion des territoires": https://www.deforestationimportee.ecologie.gouv.fr/.

- **1805:** Gough reported the thermo-sensitivity of NR, which was then further investigated by Joule in the 1850s.
- **1903:** Bouasse and Carrière highlighted the stress softening effect in NR.
- **1925:** Katz provided the first X-ray diffraction (XRD) pattern of a stretched NR. This opened the way for numerous studies to characterize the crystalline phase structure, chain orientations, and crystallization kinetics of NR.
- **1940:** Cadwell *et al.* were the first to study the fatigue behavior of CB-filled NR. They highlighted the fascinating property of "lifetime reinforcement" under non-relaxing tensile loadings. Along with Fielding, they have been among the pioneers of crack initiation approaches for fatigue.
- **1953:** Rivlin and Thomas introduced the crack growth resistance approach for studying the fatigue of NR.
- **2000:** authors started exploring the damage mechanisms involved in the deformation of NR.

1.1.2 Macromolecular network of NR

NR has a complex chemical structure. As such, the NR gum does not present sufficient mechanical properties to be used in most of industrial applications. It therefore needs to be coupled with adjuvants and be subjected to several process steps. These differents aspects are detailed in this section.

1.1.2.1 Chemical composition

From a chemical point of view, NR can be classified as a natural polymer, whose polymerization is a product of C_5H_8 isoprene monomer, as established by Faraday. This diene monomer possesses two C = C double bonds that are separated by a single bond C − C as shown in Figure 1.1.

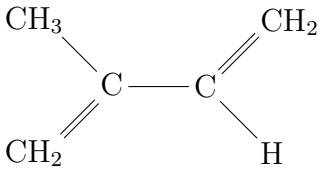

Figure 1.1: Isoprene unit semi-developed formula.

The polymerization leads to the formation of a macromolecule constituted by the addition of *cis*-1,4-polyisoprene units (see Figure 1.2), interacting with each other through covalent bonds.

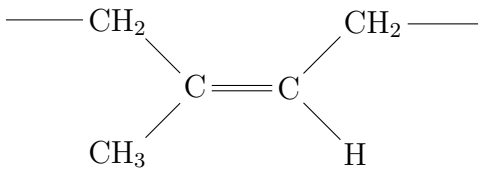

Figure 1.2: NR semi-developed formula.

It is noteworthy that NR contains C and H elements that form its backbone. It is a non-polar and hydrophobic polymer [7]. Additionally, NR includes "non-rubber components" [8] such as lipids of different nature for the most parts, and proteins, which are composed mainly of C, H and N elements. These variety of organic elements are present in a proportion ranging from 5% to 6%.
More importantly, NR from the *Hevea Brasiliensis* differenciates itself from synthetic rubber and NR from other sources by its high stereoregularity. For instance, the *Guttapercha* rubber is mainly constituted of the *trans* configuration structures, while the *Hevea Brasiliensis* rubber is composed of more than 99% of *cis* configuration structures [8]. Nevertheless, it was shown that chain-ends are mainly composed of the *trans* configuration structure [8], even for the *Hevea Brasiliensis* rubber. The high stereoregularity of NR is recognized as being responsible for its great mechanical properties, especially its ability to crystallize under a certain level of stretch. In this sense, rubbers with a more random structure would require more energy to crystallize [7]. Then, the *α-methylene* allylic hydrogen (CH_2) also appears as an important feature. In fact, it is very unstable and is likely to react with free elements [7, 9]. Consequently, since the ageing and the vulcanization mechanisms are driven by cleavage and cross-linking, the allylic hydrogen constitutes the preferred reaction site in the rubber chains.

1.1.2.2 Vulcanization

As already mentioned, the rubber gum is composed of long polymeric molecules of a thousand or more of the structural units that are linked together by entanglements, *i.e.*, physical links, in a completely random manner [10]. Despite its high deformability [11], the mechanical properties of the gum are poor, making it impossible to be used in most of industrial applications. However, the vulcanization process enables to structure the rubber gum network and therefore improve its properties. Vulcanization consists in using appropriate additives and applying particular temperature and pressure conditions during a determined amount of time. The principle lies in the formation of chemical bonds, *i.e.*, cross-links on random structural units, and thereby leading to the creation of

a structured three-dimensional network: it is called the macromolecular network, or the rubber network. These cross-links are on average of one for two hundred structural units [10]. They act as springs and give rubber its elastic properties [12], thanks to active chains, which physically corresponds to the portion of a macromolecule between two cross-links [10]. The active chains number is generally characterized by the active chain density. The chemical nature of the cross-link depends on the vulcanization agent used. The main vulcanization agents used in industrial applications are sulphur and peroxide [12]. Figure 1.3 gives an illustration of a macromolecular network.

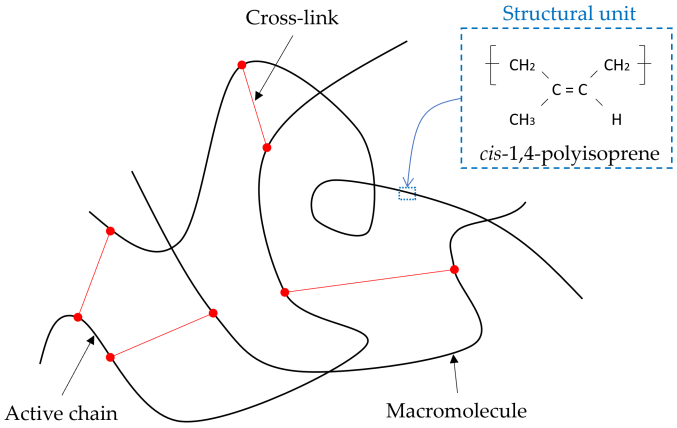

Figure 1.3: Illustration of a macromolecular network structure.

At least three conditions are necessary to achieve vulcanization: *(i)* a sufficient heat source *(ii)*, the existence of active sites, typically double and triple unsaturations on the carbon backbone and *(iii)* a reactive or vulcanization agent which drives the nature of the formed cross-links.

Prior to vulcanization, a preliminary manufacturing step is required. This step consists in mixing the NR gum with the adjuvants, and leads to the creation of an un-vulcanized NR compound. A mixer is used to mechanically masticate the components in order to reduce the molecular weight of the rubber gum. The mixing process is generally carried out in two successive stages. Once the mixed compound is obtained, the vulcanization kinetics is generally characterized by rheometry, which consists in shearing the rubber compound with an oscillating disk in a cavity at a given temperature [13]. At this stage, it is assumed that the increase in torque during vulcanization is proportional to the formation of cross-links. In practice, a moving die rheometer (MDR) is used. Figure 1.4 shows a typical torque evolution with time during the vulcanization process, at a given temperature. Three phases can be described: *(i)* the scorch during which no cross-link is created yet, *(ii)* the curing phase characterized by the torque increases with the formation of cross-links up to its stabilization and *(iii)* overcuring. At this point, different scenarios may occur depending on the formulation and temperature considered. It is to be noted

that this type of curve is called "MDR curve" and will be used in the following to show the effect of the formulation adjuvants, and the vulcanization conditions on the vulcanization kinetics.

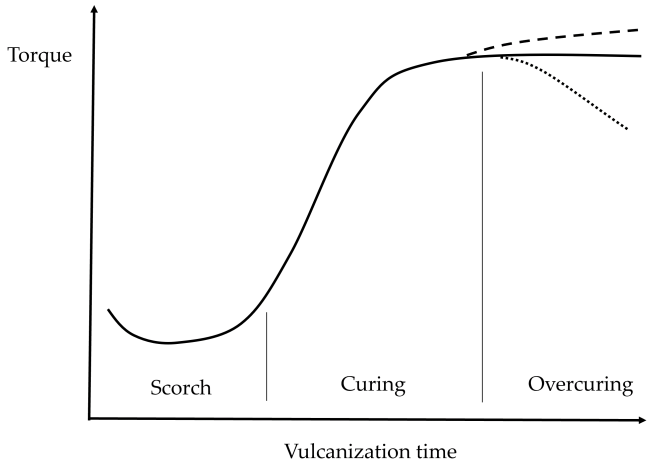

Figure 1.4: Typical vulcanization kinetics curve from [13].

1.1.2.3 Formulation

Even when vulcanized, the rubber gum is not adapted to the serial industrial process, nor does it have sufficient mechanical properties. This is the reason why adjuvants are commonly used in NR formulation. Consequently, selecting the appropriate adjuvants nature and content is of primary importance since it drives the processability of the compound, and also the final mechanical and physical properties of the vulcanizate. In this sub-section, the most commonly used adjuvants are presented. It is to be noted that adjuvant content is given in part per hundred of rubber (phr), in weight.

Type of accelerators	**Abbreviations**	**Relative curing speed**
Guanidines	DPG	Slow
Thiazoles	MBT, MBTS, ZMBT	Moderate
Thiophosphates	DIPDIS	Semi-fast
Thioureas	ETU	Fast
Sulfenamides	CBS, MBS	Fast
Dithiocarbamates	ZDBC	Very fast
Thiurams	TMTD, TMTM, DPTTS	Very fast

Table 1.1: Vulcanization speed as a function of the accelerator type [12].

Vulcanization system

Vulcanization agents are used to create cross-links between the macromolecular chains. Historically, sulphur was used as the vulcanization agent. This so-called "free sulphur vulcanization" consists in the creation of sulphur cross-links by homolytic or heterolytic cleavage of pure sulphur S_8. It is noteworthy that the formed cross-links are for the most part attached to unsaturations, through the allylic hydrogen. Nowadays, this technique is no longer used because of its relative inefficiency, *i.e.*, it takes a too long time to achieve complete vulcanization. This justifies why sulphur is at least combined with an accelerator, forming the "vulcanization system". Three types of system are used for sulphur vulcanization:

- **Type 1. Sulphur - accelerator system:** it is the most commonly used system and presents the main advantage of drastically decreasing the vulcanization time due to the presence of an organic accelerator. The TMTD from dithiocarbamates, the CBS and TBBS from the benzothiazolesulfenamides and the MBT from benzothiazoles are the most widely used [14]. Their action is initiated by the N=C-S structural functionality. Table 1.1 presents a classification of the accelerator type as a function of the curing speed [12]. Both the type and content of accelerators influence the vulcanization kinetics. Figure 1.5 (a) shows the effect of the accelerator type on the vulcanization kinetics, given by a MDR curve. Furthermore it can be seen that accelerators such as TMTD and ZDMC are likely leading to overcuring. In addition, for a given accelerator type, increasing the accelerator content increases the number of active chains, but not necessarily its speed. This is illustrated in Fig. 1.5 (b).

- **Type 2. Sulphur - primary and secondary accelerators system:** for which a secondary accelerator is combined to the primary one, as described above. The role of this secondary accelerator is to further reduce the vulcanization time. It can be referred to as a booster [15]. Combining two accelerators leads to synergetic effects that could also improve the properties of the vulcanizates [14]. For instance, Aprem *et al.* used 1-phenyl 2-4 dithiobiuret (DTB) with TBBS, and DTB with dicyclohexyl benzothiazole sulfenamide (DCBS) for NR [16, 17]. Additional information on the use of accelerator pairs can be found in [18] for styrene butadiene rubber (SBR) and in [19] for NR/SBR blends.

- **Type 3. Sulphur-donor system:** the last type of vulcanization system does not require any sulphur properly speaking, as the accelerator used contains activated sulphur in its chemical structure, which is released during a reaction mechanism [12].

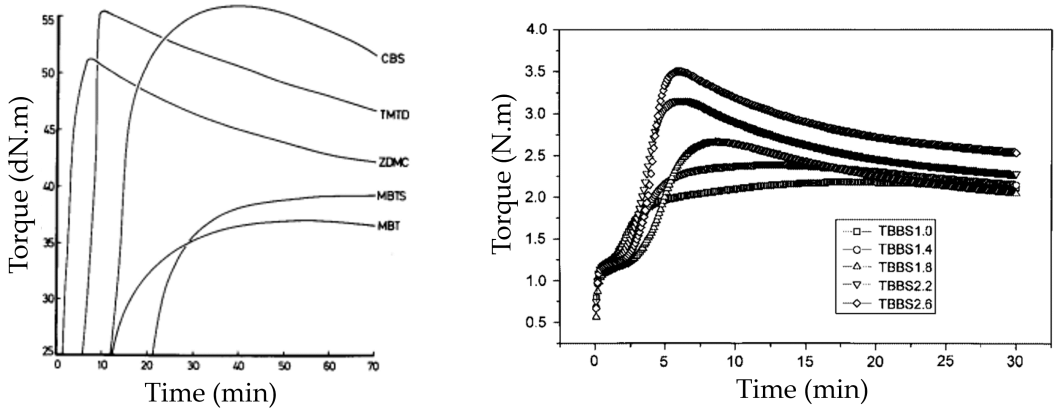

Figure 1.5: Effect of (a) the accelerator type on the vulcanization kinetics at 140°C [20], and (b) the TBBS accelerator content (in phr) on the vulcanization kinetics for a given formulation and vulcanization temperature [21].

In addition to the fact that the vulcanization system encourages the vulcanization to occur, it also drives the macromolecular network structure. In the following, a focus will be made on a sulphur - accelerator system as it is the one used in this study.
The sulphur [S] and accelerator [A] contents determine the length and the number of cross-links formed, which is related to the number of active chains. According to the classical theory of rubber elasticity, active chains confers the rubber its elastic properties [22]. In practice, the higher [S] and [A], the higher the active chain density. In addition to that, the accelerator-to-sulphur ratio [A]/[S] drives the cross-link length [12], and can consequently either leads to the formation of polysulphide, disulphide or monosulphide cross-links [15]. In practice, the higher the [A]/[S], the lower the cross-link length. The vulcanization systems are generally classified according to the [A], [S] and [A]/[S] ratio, regardless of the accelerator chosen. A conventionally vulcanized (CV) rubber is mainly composed of polysulphide cross-links $C-S_x-C$, with $x > 3$. A semi-efficient vulcanization (SEV) leads to a similar proportion of poly-, di- and- monosulphide cross-links $C-S_x-C$, $C-S_2-C$ and $C-S-C$, respectively. Finally, an efficient vulcanization (EV) mostly provides monosulphide $C-S-C$ cross-links. Quirk introduced a denomination for the system out of this, it is summarized in Table 1.2 [23].

Type of vulcanization system	**Sulphur [S] (phr)**	**Accelerator [A] (phr)**	**[A]/[S] ratio (-)**
Conventional (CV)	2.0-3.5	1.2-0.4	0.1-0.6
Semi-efficient (SEV)	1.0-1.7	2.5-1.2	0.7-2.5
Efficient (EV)	0.4-0.8	5.0-2.0	2.5-12

Table 1.2: Vulcanization system distinction according to Quirk [23].

Fillers

Since the 20^{th} century, the rubber industry commonly employed CB in rubber formulations to enhance its mechanical properties [24], namely the stiffness, the hardness, the tear strength, the resistance to abrasion and rupture [25]. From a chemical point of view, CB is a material close to pure carbon form, and is obtained from the combustion of products derived from hydrocarbon or biomass [26]. Typically, CB is predominantly composed of carbon, about 92%, and is characterized by its specific surface area, structure and surface chemistry [27]. There are different grades of CB, such as High Abrasion Furnace (HAF) CB, Channel CB and Thermal CB, which are distinguished by their production process [24]. It is noteworthy that it also implies different chemical composition, for example the HAF differs in the surface oxidized groups, nature and quantity [24, 28, 29].

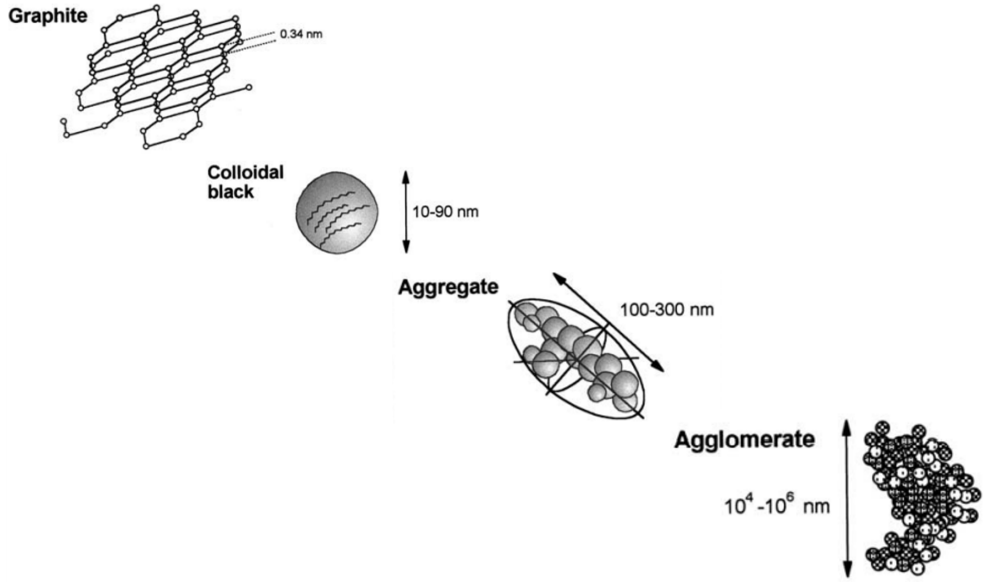

Figure 1.6: From primary elements to CB agglomerate [25].

From a process point of view, CB is introduced in agglomerates and required to be masticated and mixed with rubber to be dispersed and degrades into aggregates. If not sufficiently dispersed, crack initiation is likely to be promoted in the final product [5]. Among other types of fillers, silica is also widely used. However, its polar surface makes it more challenging to interact and disperse with the gum [30], which implies a lower reinforcement in comparison to CB. Nowadays, the development of fillers presenting a lower environmental impact has become one of the priorities [31]. In practice, in CB-filled NR, the macromolecular network coexists with large and rigid particles that also form their own "fillers network". Both macromolecular and fillers networks form a composite involving strong and complex interactions. Figure 1.7 gives the functional groups present at the CB surface.

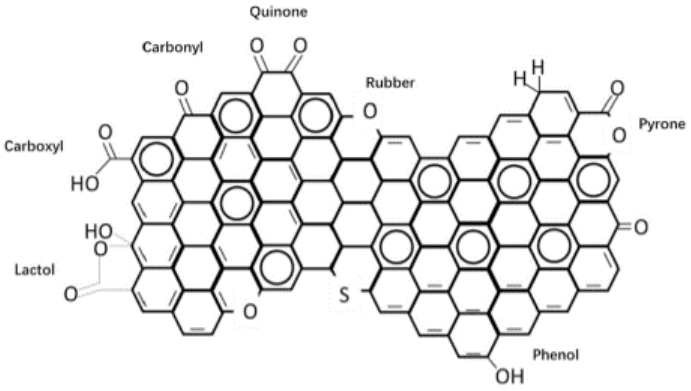

Figure 1.7: Main functional groups at the CB surface [31].

Weak Van Der Waals bonds link elements such as O and N, with the CB structure [24]. The work of Stearn and Johnson [28] showed that more complex organic functional groups could also be present at their surface. It also appears that possible bonds such as an unsaturation similar to ethylene would allow the fillers to be linked to the macromolecular network. A few decades later, Boehm [32] described the main functional groups that populate the surface of CB. These are mainly coupled with H atoms, but it is possible to find other groups from the oxide family. Furthermore, these functional groups are likely to interact with one another. In other words, two groups can react to form much more complex structures. This demonstrates that the CB structures and the CB-rubber matrix interactions are very complex. However, it is known that in the vicinity of CB particles, strong interactions that alter the NR chains organization occur, while far into the bulk, the rubber matrix is similar to that of unfilled NR. More details are given in the work of Leblanc [25].

Plasticizers

Plasticizers were originally used to make the vulcanized rubber more stretchable, flexible and consequently easier to be manufactured. The plasticizer is chosen to optimize its compability with the rubber [33], but mineral oils are mainly used. As NR is non-polar, a non-polar plasticizer is required. For instance, NR is compatible with aromatic and naphthenic plasticizers but this is not the case with paraffinic and ester ones. From a manufacturing point of view, the plasticizer reduces the mixing time and facilitates lamination. Plasticizers are generally presented as the only ingredients that can modify the glass transition temperature (T_g). When plasticizers are added to the macromolecular network, they insert themselves between the chains, reducing viscosity, pulling the chains apart and thus increasing the mobility of additives such as CB [25]. For instance, Surya *et al.* showed that plasticizers ease the integration of CB into the macromolecular network and maximize the reinforcement of the mechanical properties [30].

Activators

In the early 1900s, zinc oxide (ZnO) was first used as a reinforcing filler in order to enhance the mechanical properties of rubber parts. However, the latter was rapidly replaced by CB. A few years later, a novel application for ZnO was discovered. When combined with a fatty acid, the vulcanization time for accelerated and un-accelerated compound is reduced. Thus, this discovery enriched the knowledge and drastically improved the vulcanization process efficiency [15]. The ZnO and fatty acid are hereafter denoted as "activators". It is worth emphasizing that they are still widely used to date, although questions have been raised about environmental concerns.
Generally, the fatty acid used is a stearic acid or a lauric one. They react with ZnO to form a zinc stearate salt [34], which constitutes complex intermediate species. These complex species are known to be more effective to activate sulphur cross-linking [35]. More precisely, the stearic acid weakens the $Z_n - S$ bonds from the complex species [36] and facilitates the inclusion of sulphur molecules. One can note that stearic acid is not always necessary, in the sense that their action can be replaced by free amides.

Protection agents

Once vulcanized, NR parts are exposed to hostile environments that are likely to cause the degradation or their macromolecular network. Protection agents are therefore used to prevent from thermal and thermo-oxidative ageing. It is noteworthy that UV and ozone ageing occur, but their effects seem of minor importance in comparison to oxidative ones. Protection agents are generally amines, phenols and paraphenylene diamines to ensure protection against thermo-oxidative ageing. Typically, a formulation is made up of 1 or 2 different types of these chemicals to take advantage of multiple protective properties. In practice, they act by delaying ageing reactions so that the properties of the part are remain unchanged.
From a molecular point of view, thermo-oxidative ageing can lead to either chain scission or post cross-linking. For instance, ageing at 100°C leads to an increase and then a decrease in active chain density for unfilled NR [37]. This indicates that a cross-linking reaction occurs first, followed by a predominant chain scission mechanism. Cross-linking mechanism generally involves extra-cross-linking from oxidative groups [38]. Depending on the sulphur cross-link length, ageing is generally more severe for CV systems due to its thermally unstable polysulphide cross-links [39]. Short cross-link length of EV systems are preferred since they are more resistant to heat, and consequently to ageing.

1.1.2.4 Vulcanization conditions

Appropriate vulcanization conditions to be chosen in order to optimize the macromolecular network. A focus is here paid on the vulcanization time and temperature, as they appear to be the most impactful.

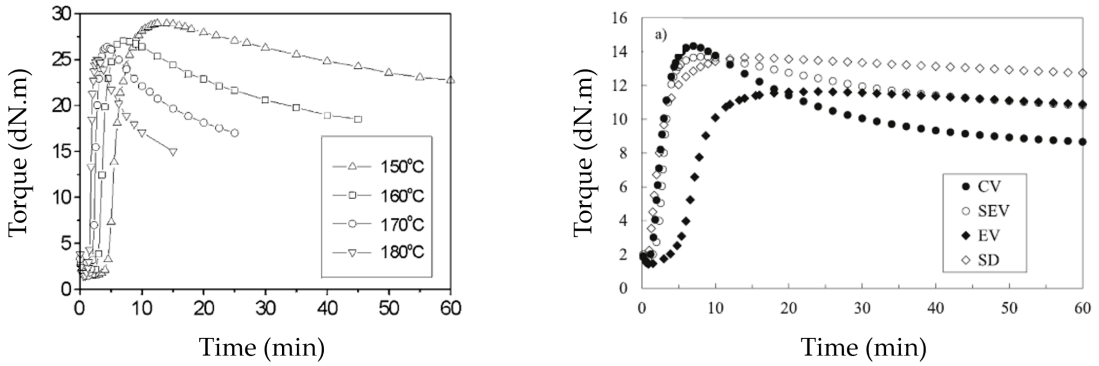

(a) (b)

Figure 1.8: Effect of (a) the vulcanization temperature [40] and (b) the vulcanization system type on vulcanization kinetics [41], for unfilled NR.

Vulcanization temperature

The vulcanization temperature is generally set between 140 and 170°C. For NR, the optimal temperature would be around 160-165°C. Figure 1.8 (a) illustrates the effect of the vulcanization temperature for unfilled NR [40]. The higher the vulcanization temperature, the faster the vulcanization and the lower the maximum torque achieved [40]. Moreover, a high vulcanization temperature has more pronounced effect on CV systems which show many changes in the reversion region while SEV and EV systems do not seem as impacted by prolongated curing [40]. For instance, CV systems show a high decrease in maximum torque above a certain vulcanization time. These changes in vulcanization kinetics reflect changes in macromolecular network. Indeed, this is due to the fact that polysulphide cross-links are highly thermosensitive, whereas shorter cross-links are much more stable and can easily withstand high vulcanization temperatures. In this sense, the overall number of cross-links are likely to decrease for CV systems, which results in a drop of torque during vulcanization. Consequently, EV systems are preffered for high vulcanization temperatures.

For a given vulcanization system, the vulcanization temperature has a significant effect on the active chain density and the cross-link length. Polysulphide cross-links are likely to decrease, *i.e.*, to break and reform in shorter cross-links when the vulcanization temperature is increased [42–44]. This could also be accompanied by macromolecular chain

modifications [44]. Among them, rubber chains can change their confirmity from *cis* to *trans* configuration, which affects their stereoregularity.

Vulcanization time

The vulcanization time drives the cross-linking [13, 45] and its effect is inseparable from the effect of the vulcanization temperature. In the rubber field, the vulcanization time is given by t_X, corresponding to the time required to reach $X\%$ of the maximum torque measured. The optimal vulcanization time corresponds to the time needed to achieve the optimal properties of the final parts [35]. However, there is no consensus on the optimal torque, *i.e.*, the X value, for maximizing the mechanical properties. The vulcanization time vary from t_{80} to t_{100}. Above this value, the rubber compound is likely to degrade due to over-vulcanization depending on the vulcanization system. As above-mentioned, this is related to the thermal sensitivity of the cross-links. Consequently, this reversion permanently changes the macromolecular network and the elastic properties. It is noteworthy that the rubber type, the rubber grade and the vulcanization temperature can also modify the kinetics in the overcuring region [35]. For instance, EV systems are likely to show a broad maximal vulcanization plateau whereas CV systems are more prone to reversion [40]. This indicates that CV systems are more subjected to active chain density loss with reversion [41]: the higher the reversion level, the higher the loss of active chain density [46]. Figure 1.8 (b) shows the effect of the vulcanization system type on the vulcanization kinetics.
From a molecular point of view, the number of elastically inactive structures such as "cyclic sulphides" (it is termed a "closed loop" by Treloar [47]) or "pendant side groups" [12, 35], increases as a consequence of the decrease in active chain density. Inactive structures contribute to permanently change the physical, chemical and mechanical properties of the rubber, in most cases by reducing the contribution to stress. Thus, these inactive structures can be considered as network defects and are difficult to quantitatively quantified [47]. It is worth noting that EV systems are more prone to form pendant side groups, whereas CV ones tend to form cyclic sulphides. To go further, prolonged vulcanization will encourage the NR to lose the stereoregularity of the structural units by passing from a *cis* to a *trans* configuration [45].

1.1.2.5 Summary on the macromolecular network of NR

In light of the literature on both the formulation and the vulcanization conditions, it is proposed to provide a complete description of the NR macromolecular network. Figure 1.9 gives an overview of the main structures constituting the NR macromolecular network. It is is mainly composed of NR chains (*cis*-1,4-polyisoprene) and cross-links of different length achieved during the vulcanization process. Possible elastically inactive structures

such as pendant residual accelerators, or cyclic sulphides can also be formed. Some residual accerelators, un-reacted sulphur and protection agents exist without being attached to the rubber chains. When filled, fillers form their own network and are physically bound to the macromolecular network, the nature of the interactions depending on the filler type. In the present study, the NR macromolecular network is defined as the combination of *(i)* the active structures corresponding to the rubber and the filler networks and the resulting interactions between them, and *(ii)* the inactive structures such as cyclic sulphides, pendant groups and rubber chain modifications. The vulcanization system (sulphur and accelerator contents), fillers content and type as well as the vulcanization conditions (time and temperature) are the main parameters driving the macromolecular network structure.

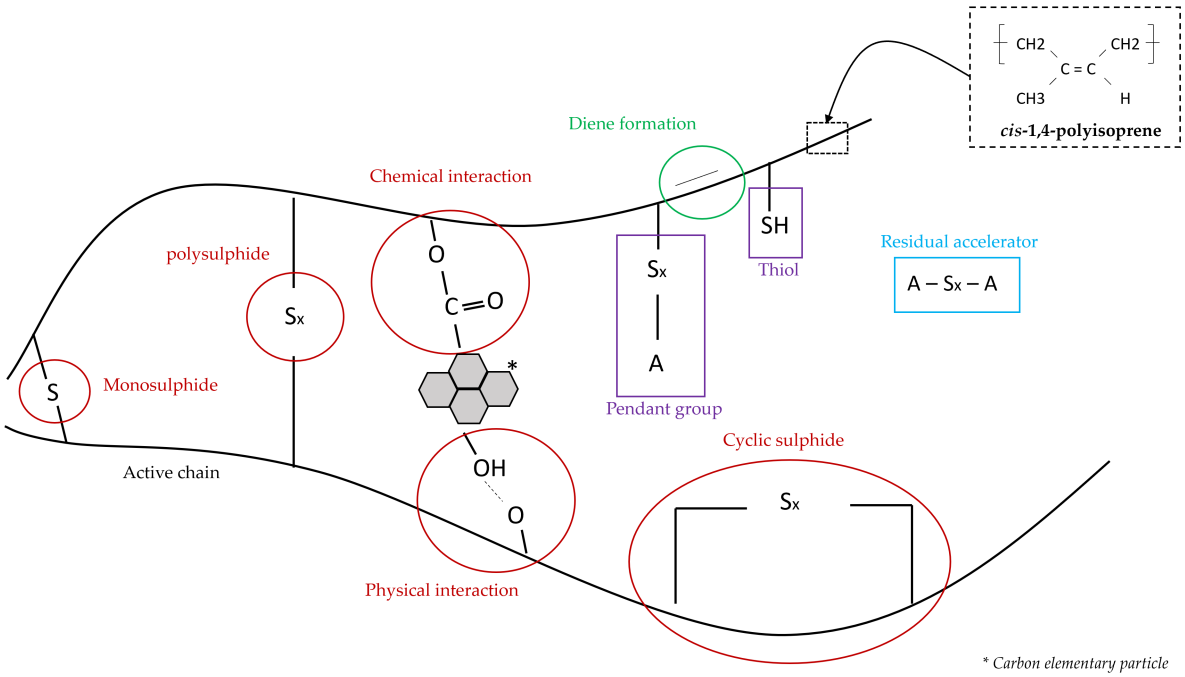

Figure 1.9: Schematic representation of the macromolecular network of NR.

The macromolecular network of NR drives its mechanical properties. This will be discussed in the next section.

1.1.3 Mechanical properties of NR

Vulcanized rubber is highly deformable, and exhibits an elastic behavior. However, the stress-strain response is generally accompanied by viscoelasticity, hysteresis, the Mullins effect and temperature variation. These are hereafter described.

1.1.3.1 Elasticity

For uniaxial monotonic loadings, rubbers can be stretched from one hundred to one thousand percent of their initial length in a reversible manner to a certain extent. In the early 20^{th} century, the development of rubber thermodynamics elasticity provided an understanding of the deformation process. As postulated by the kinetic theory, the reaction force of the macromolecular network during extension is proportional to the absolute temperature [47], assuming a purely entropic behavior, *i.e.*, no changes in internal energy. As experimentally shown by Meyer and Ferri [48], this is true for high deformation levels. But below 10% of strain, deviations were observed indicating a non-negligible non-entropic contribution to the reaction force, calling into question the origin of rubber elasticity. It therefore seems that the source of rubber elasticity lies in two contributions: an entropic and an enthalpic one. The entropic contribution is related to the changes of the macromolecular network configuration [47]. For the enthalpic contribution, it is related to volume changes, possibly explained by changes in intramolecular internal energy [49].
An example of a stress-strain response is shown in Figure 1.10 (a) for an unfilled vulcanized NR. The stress response is highly non-linear with different stages:

- from 0 to 25% of strain, the elastic response is linear. The weak physical bonds are likely to break and NR chains unfold,
- up to 400%, NR chains continue to unfold, disentangle and orient in the stretching direction,
- around 400%, the stress response upturn. The maximum extensibility is reached for shorter active chains and a strong stiffening occurs. This is generally attributed to SIC effect.

For NR, both stiffness and deformability are triggered by the macromolecular network and fillers, *i.e.*, by the formulation and process conditions. Concerning the effect of the macromolecular network on the elasticity, the stiffness is driven by the active chain density [47, 52] and the cross-link length [53]. In practice, the higher the number of polysulphide cross-links, the higher the elongation at break for CBS-accelerated unfilled NR. The opposite trend will be achieved for monosulphide cross-links. For a given level of strain, monosulphide cross-links induce more stiffness because of their shorter length and reduced mobility. Moreover, fillers induce a strong stiffening which is due to local strain amplification [54]. The effect of the fillers depends on their content and type. For instance, the effect of the N550 CB content on the stress-strain response is presented in Figure 1.10 (b) for NR [51]. Increasing the CB content increases the stiffness, while the elongation at break increases at 20 phr and then decreases with 43 and 55 phr. It is to be

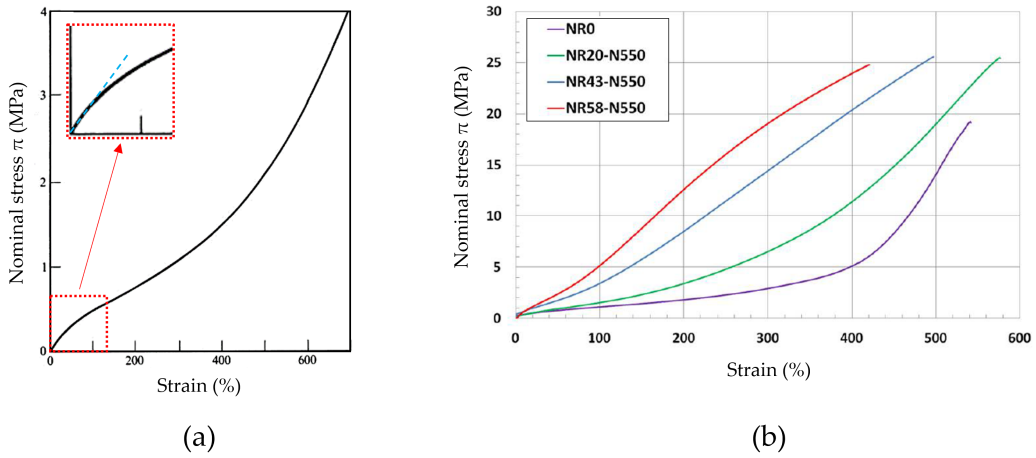

Figure 1.10: Stress-strain curve of (a) unfilled NR from [50] and (b) unfilled NR and CB-filled NR at different content from [51].

noted that, for unfilled NR, a very high active chain density makes the material "brittle" and drastically reduces the tensile strength and elongation at break. However, when CB is added to a macromolecular network with a high active chain density, a significant increase in tensile properties is obtained [55]. In summary, the main parameters driving the stress-strain response are the active chain density, the cross-link length and the filler content and type.

1.1.3.2 Viscoelasticity

Viscoelasticity characterizes the time dependency of the mechanical response. It depends on several parameters such as the maximal applied stretch, strain rate and temperature [56]. This viscoelasticity can be seen in the stress-strain response of the quasi-static monotonic tensile response, which changes as a function of strain rate. In the case of cyclic loading conditions, a mechanical hysteresis loop can be formed due to viscosity. Finally, long-term tests reveal significant changes in stress as a function of the applied strain, indicating a non-linear viscoelastic response. From an experimental point of view, viscoelasticity is generally evaluated through cyclic, relaxation, creep or dynamic mechanical analyses (DMA) tests, that correspond to dynamic loadings carried out at small amplitudes. For DMA, viscoelasticity is quantified by the phase between the prescribed signal and the material mechanical response. Figure 1.11 (b) presents the evolution of the stress for different extensions reported in [57].
The origin of the viscosity in a CB-filled NR comes from fillers, which induce and amplify viscosity by creating macromolecular friction. In addition, both the cross-link length and the active chain density also affect the dynamic mechanical response, typically when they evolve due to ageing [58]. Indeed, polysulphide cross-links induce high changes in the dynamical response, *i.e.*, the elastic part of the response, when vulcanized at high tem-

perature, and for too much time whereas EV systems were much more resistant [40]. This was explained by the low thermal resistance of polysulphide cross-links. When aged under aerobic and anaerobic ageing, CV systems also lead to the worst mechanical properties [59]. Finally, the vulcanization agent type is known to affect the dynamical response, more details can be found in the study of Baruel *et al.* who compared sulphur and peroxide vulcanization for NR [60].

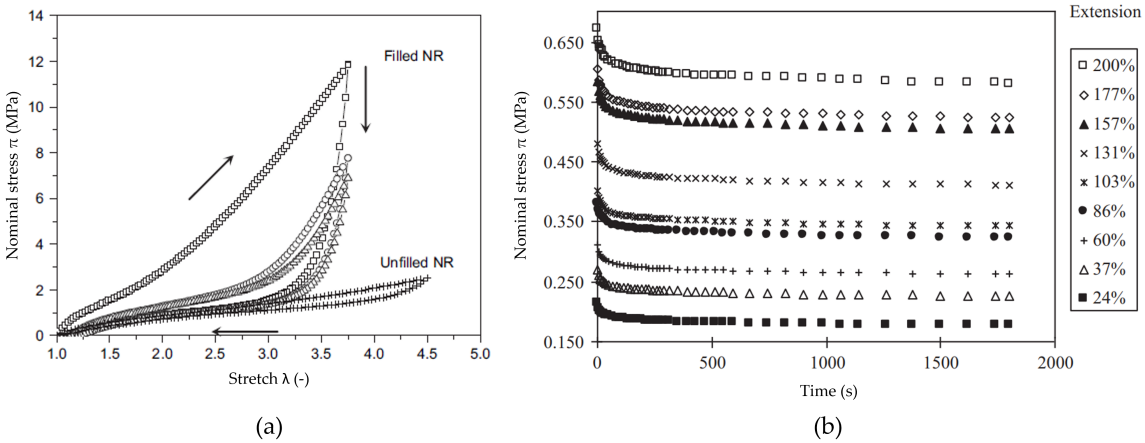

Figure 1.11: (a) Hysteresis of both unfilled and filled NR [61], and (b) evolution of the nominal stress with respect to the time, for different maximum extensions [57].

1.1.3.3 Hysteresis

Whether filled or not, the stress of NR is lower during the unloading than during the loading. This is materialized by a lower strain energy density and by the presence of an hysteresis in a stress-strain plot. Fig. 1.11 (a) shows the hysteresis of a CB-filled and an unfilled NR. This apparent loss in strain energy density is generally considered to be due to viscosity. This paragraph reviews the main differences between hysteresis for unfilled and filled rubber. On the one hand, the hysteresis loop of unfilled NR have no intrinsic dissipation. Indeed, no dissipation of mechanical energy into heat under adiabatic conditions was found by Samaca-Martinez *et al.* [62–64]. This means that there are no viscoelastic effects associated with the hysteresis, the latter being solely driven by structural changes which is predominantly the SIC. More precisely, this hysteresis loop is due to the difference in kinetics between crystallization and melting of crystallites [62, 63, 65]. It is noteworthy that as SIC starts after a certain stretch threshold, around $\lambda_c = 4$ for unfilled NR, no hysteresis loop is observed for stretches below this threshold. On the other hand, contrarily to unfilled NR, the contributions of the hysteresis for filled NR are due to a competition between *(i)* viscosity induced by fillers and *(ii)* structural changes due to the reorganization of the filler network [66] and SIC [67]. Note that their relative contribution can be quantified by using surface calorimetry [68].

1.1.3.4 Mullins effect

Under cyclic loadings, rubber exhibits a singular mechanical behavior: when a rubber specimen is stretched to a given elongation and then retracted, a lesser stress is required to reach this elongation at the next cycle. First observed by Bouasse and Carrière in 1903 [69], the softening effect was then extensively studied by Mullins [70], which is why the phenomenon is now referred to as the "Mullins Effect". Figure 1.12 illustrates the mechanical response of a CB-filled NR at different stretch levels at (a) 23°C and (b) 90°C [71].

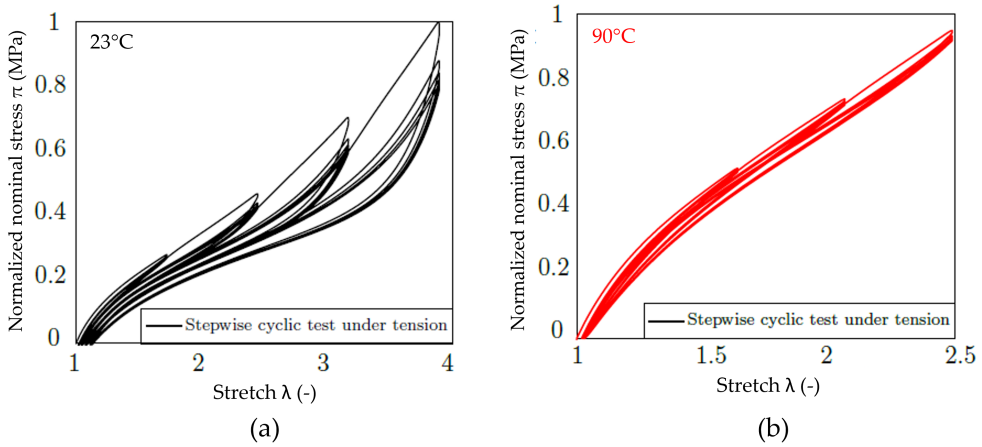

Figure 1.12: Example of the Mullins effect at different stretch levels for CB-filled NR from [71].

The Mullins effect includes different changes in the mechanical response, that are summarized as follows:

- after a first cycle, a softening effect appears for stretches lower than or equal to the maximum stretch previously applied,
- the higher the stretch reached at the first cycle, the higher the softening effect,
- during the next cycle, the material stiffens as the current stretch is closed to the maximum stretch previously applied,
- when applying a higher stretch than the maximum stretch previously reached, the mechanical response follows the same path as the one of a virgin material,
- the softening effect is maximal during the first cycle. The mechanical response stabilizes during the first few cycles at the same stretch.

The Mullins effect has been observed in many filled rubbers such as NR [72, 73], SBR [74], ethylene propylene diene monomer (EPDM) [75], nitrile butadiene rubber (NBR)

[76], silicone [77, 78] non-exhaustively. More surprisingly, the Mullins effect has also been evidenced in unfilled rubbers such as NR by Harwood *et al.* [79] and NBR by Kakavas [80]. Three different physical interpretations of the Mullins effect are found: *(i)* the rubber matrix damaging such as disentanglement, changes in the active chain density, rubber chain scission, appearance of cavities, *(ii)* the filler network alteration such as loss of percolation, filler aggregate and agglomerate fracture and *(iii)* the modification of the rubber-filler interface such as bonds breakage at the filler surface, slipping of molecules, desorption/adsorption [74, 81].

The relationship between the macromolecular network and Mullins effect is not yet fully understood. Several studies reported in the literature investigated the dependency of the Mullins softening to the active chain density and cross-link length. For CB-filled SBR with 50 phr, Kraus *et al.* conducted swelling tests in n-heptane before and after various cyclic tests in order to compare relative changes in the volume fraction of rubber at equilibrium with respect to the softening [82]. The softened specimens were obtained by a cycle at 250% of strain, at various strain rates and temperatures. The softening was estimated by a ratio between the area under stress-strain curves of virgin and softened specimens. Their results showed only small changes in the volume fraction of rubber at equilibrium in comparison to the level of softening. Thus, breakage in the SBR macromolecular network is not sufficient to explain the softening. Dannenberg and Brennan also conducted swelling tests with unfilled SBR, NR and *cis*-polybutadiene, on softened specimens after 3 cycles. They evaluated the softening from the ratio of the area under the loading curves of the virgin and softened specimens [83]. Their results showed no significant changes in active chain density between the virgin and softened specimens, and concluded that the Mullins softening is unrelated to cross-links breakage. Later, Roland studied one NR and five SBR, both vulcanized with peroxide, whose respective active chain density were different. He concluded that the macromolecular network had no effect on the softening since comparable results were obtained for each materials [84]. However, the six materials in this study do not allow conclusions to be generalized to the case of unfilled NR. More recently, Wan *et al.* showed a dependence of the softening on active chain density for unfilled NR from coarse-grained molecular dynamics simulation [85]. Even more recently, Lin *et al.* also found that active chain density has an effect of on the softening for unfilled NR with [A]/[S]=1 [46]. The authors observed an increase in the softening level with an increase in active chain density. This raises the following question: "What is precisely the effect of the macromolecular network on the Mullins effect?".

1.1.3.5 Calorimetric response

As mentioned by Le Cam [86], the purely mechanical response of rubbers has been studied since the beginning of the 20^{th} century, whereas the first work on its thermo-

mechanical behavior was carried out in the 1970s. Rubber elasticity is driven by both entropic and non-entropic contributions. However, it is not possible to deconvolute these effects from purely mechanical tests. Thermal and calorimetric measurements were more recently used to provide additional information [62, 63]. Consequently, evaluating the calorimetric response is of first importance to compare rubbers from a different and complementary point of view, to the purely mechanical one. In practice, heat sources are calculated from thermal measurements during mechanical testing [87]. It is noteworthy that the measured temperature cannot be used as it is affected by conducto-convective effects with the surroundings, *i.e.*, heat exchanges with the air and the grips. For the sake of clarity, the theroritical background of heat source calculation is not detailed, but the interested reader can refer to the work due to Le Cam *et al.* [87, 88].

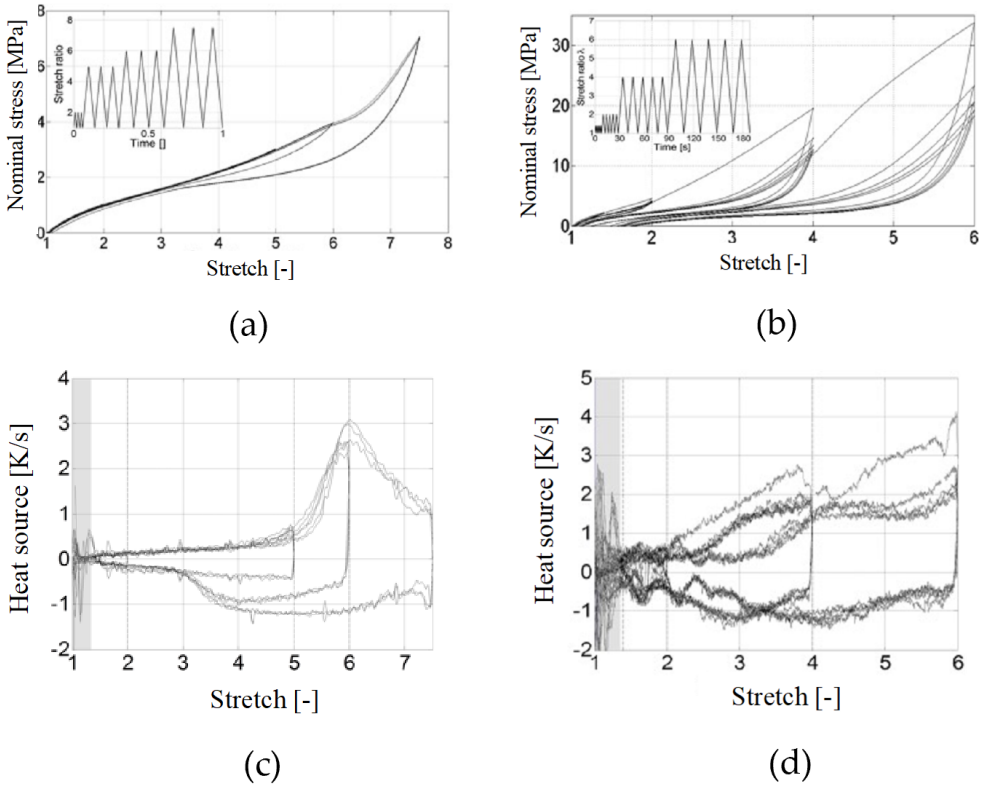

Figure 1.13: Mechanical response of (a) unfilled and (b) filled NR. Calorimetric response of (d) unfilled and (d) CB-filled NR from [86].

For NR, the calorimetric response depends on whether it is filled or not. Figure 1.13 shows the classical response for both unfilled and CB-filled NR.

- In the case of unfilled NR, the heat sources during the loading are the same as those during the unloading. As soon as SIC takes place, *i.e.*, for stretch higher than 4, the calorimetric response changes: a strong exothermal peak due to SIC occurs. Furthermore, even though the heat sources are equal in absolute value during the

loading and the unloading phase, they show different kinetics. This phenomenon is explained by the difference of kinetics between crystallization and crystallite melting.

- In the case of CB-filled NR, the heat sources are different from those of unfilled NR. The heat sources drastically increase above $\lambda = 2$, and there is no strong exothermal peak. As the fillers network reogarnization contributes to energy storage and release, this affects the heat sources during the loading and unloading. Further elements on SIC are given in Section 1.2.

1.2 SIC of NR

This second section of the state of the art addresses the relationship between the macromolecular network and SIC. Firstly, a short description of the SIC phenomenon is proposed. The physical origin of SIC and its consequences on the mechanical properties are then examined. Secondly, the main parameters affecting SIC are discussed, with a focus on the effect of the tests conditions, and the macromolecular network. More specifically, the effects of both active chain density and cross-link length for filled and unfilled NR on SIC features, namely the stretch ratio to crystallization onset, maximum of crystallinity and crystallinity rate are described.
This non-exhaustive review focuses on the most important aspects of SIC. However, for more information on SIC, the reader can refer to the following Refs [89–91].

1.2.1 Generalities on SIC

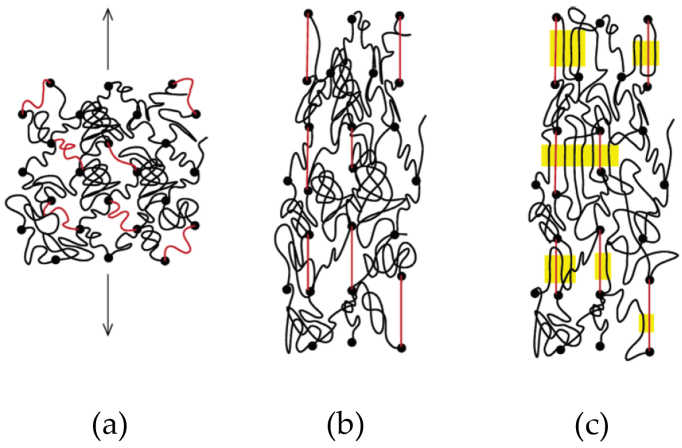

Figure 1.14: SIC nucleation mechanism proposed by Tosaka *et al.* [92]: (a) before deformation (b) after deformation, short active chains are fully extend and (c) act as nucleus of crystallites.

1.2.1.1 SIC phenomenon description

First evidenced by Katz in the early 20^{th} century, the fascinating SIC phenomenon is related to the ability of the rubber to crystallize when stretched [93]. Thiw was observed in NR, synthetic polyisoprene rubber (IR), polybutadiene rubber (BR), butyl rubber (IIR) and also polychloroprene rubber (CR). Generally, SIC is driven by the alignments of the rubber chains, and occurs in two steps: *(i)* crystallites nucleation, which is follows by *(ii)* crystallites growth. From a phenomenological point of view, when a specimen is uniaxially stretched, the rubber chains unfold and orient themselves parallel to the direction of loading. Then, at a sufficiently high strain level, a fraction of the rubber chains organizes into crystallites. This is generally associated with the shorter active

chains reaching their maximum extensibility limit [94]. At this point, the macromolecular network is composed of a crystallized phase, ranging from a few to 30% for a given volume depending on several factors. It is to be noted that, for unfilled NR, rubber chain orientation is mainly driven by stretch, while temperature and active chain density have no significant effects, as shown by Trabelsi *et al.* [95]. Figure 1.14 presents a schematic representation of a nucleation mechanism based on the extensibility limit of shorter active chains, introduced by Tosaka *et al.* in the early 2000s [92].

From an experimental point of view, SIC can be evaluated by numerous methods, XRD being the most widely used [90]. A more recent technique based on surface calorimetry has been developed by Le Cam [88]. Since SIC is strongly exothermal, the heat sources calculated during a tensile test have a specific signature. Thus, crystallinity can be calculated from these heat sources. This technique has the advantage of being accessible in a laboratory, allowing a rapid evaluation. However, no information on chain orientation are provided. Consequently, surface calorimetry and XRD are complementary. It is noteworthy that surface calorimetry has been validated by cross-testing and has shown satisfactory results on both unfilled [96] and CB-filled [67, 97] NR. Figure 1.15 shows a comparison between the techniques for (a) unfilled and (b) filled NR.

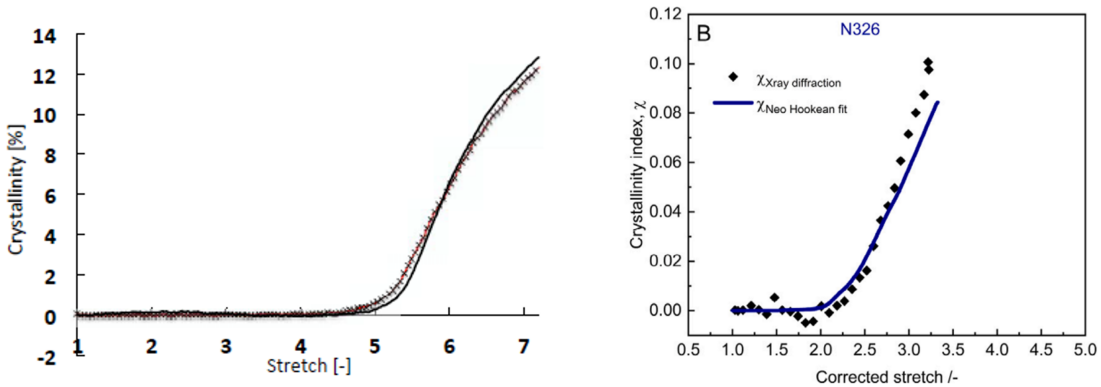

Figure 1.15: SIC measurement from XRD and surface calorimetry for uniaxial tension loading for (a) unfilled NR [96] and (b) CB-filled NR [97].

1.2.1.2 Physical origin of SIC

The intriguing property of NR to crystallize when stretched has been the focus of numerous studies and continues to be intensively investigated. This sub-section is devoted to understanding and discussing the origin of SIC.

Effect of the rubber macromolecules on SIC

According to Flory [98], the reason why the rubber crystallizes is fairly obvious: when stretched, the active chains are elongated, which reduces the configurational entropy of the macromolecular network. Less entropy is necessary in passing to crystalline state, where the configurational entropy is equal to zero. In this sense, the overall entropy of the macromolecular network is drastically decreased by SIC. Following this idea, we might expect any rubber to crystallize under the effect of strain, since it is highly beneficial to minimize energy. Nonetheless, as SIC was only observed for some rubbers, this suggests that the rubber type is important. So why is NR able to crystallize? On the scale of a single chain, NR has a high degree of stereoregularity, *i.e.*, the chains are already well-organized thanks to the high proportion of *cis* configurations. Consequently, this could at least explain why IR has lower crystalline properties than NR [99], since it contains less *cis* configurations [100]. It is noteworthy that the onset of stretch for crystallinity is higher, and the crystallinity is lower for IR in comparison to NR [94]. However, the symmetry of a chain is not the essential point for crystallization to occur.

Effect of the non-rubber components on SIC

Considering that the macromolecular network is not the only parameter inducing SIC, further questions about its origin arise. A different interpretation based on the non-rubber components is generally found in the literature. Indeed, SIC could be related to the proportion of non-rubber components, *i.e.*, naturally occuring and remaining components such as proteins and phospholipids [8]. These "naturally occuring impurities", not present in IR, are of great benefit to SIC. They could explain why NR exhibits such a behavior. In the work of Amnuaypornsri *et al.*, it was shown that these impurities form a kind of "network structure". This structure is believed to improve the SIC ability of the un-vulcanized and vulcanized NR [101]. From the work of Toki *et al.*, it was shown that un-vulcanized NR presents a very interesting mechanical response under uniaxial tension loading: it can be stretch up to $\lambda = 7$ [102]. Its stress-strain response is highly non-linear, and presents both hysteresis and permanent set. This is analogous to the stress-strain response of a vulcanized NR, *i.e.*, a macromolecular network structure. Furthermore, the un-vulcanized NR is also able to crystallize under strain. Thus, the authors concluded that this final network structure - which is the combination of chemical and naturally occuring network - is able to promote and drive SIC. This raises more questions about the physical origin of SIC.

1.2.1.3 Effect of SIC on the mechanical properties

The effect of SIC on the stress-strain response for uniaxial mononotic, cyclic and fatigue tension loadings is presented hereafter.

Uniaxial monotonic tension

For uniaxial monotonic tension, the SIC effect is generally associated with a significant stiffening, observed in a stress-strain plot. Figure 1.16 shows (a) the mechanical response for unfilled NR and (b) the corresponding crystallinity obtained from XRD measurements. The stress upturn is observed around $\lambda = 4.5$. Furthermore, a hysteresis loop is observed in both crystallinity and mechanical behavior. Clark *et al.* [103] were the first to suggest that a correlation exists between SIC and the mechanical hysteresis loop.

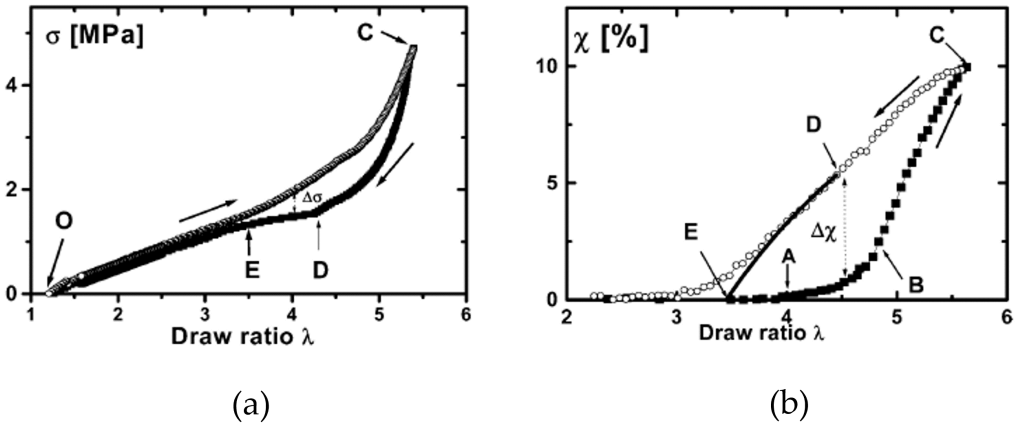

Figure 1.16: Example of SIC for unfilled NR: (a) stress-strain response and (b) crystallinity as a function of applied stretch [65].

Generally, the stress upturn is associated to the onset of SIC [61]. For unfilled NR, the stress upturn is affected by the active chain density. By increasing the active chain density, the stress upturn is observed at a lower strech [61, 65]. This suggests that the network restrictions induced by more active chains promote SIC. For filled NR, Chenal *et al.* observed a similar stress upturn for different CB grades, and for similar active chain densities. Furthermore, for the same CB grade and content but different active chain densities, no effect of the active chain density was found on the stretch at which the stress upturn occurs. This suggests that the effect of active chain density is completely overcome by fillers, resulting in no effect on stiffness from a macroscopic point of view.

Uniaxial cyclic tension

The effect of SIC on the stress-strain behavior of NR, for cyclic loadings, is not yet fully understood. As above-mentioned, NR exhibits a stress softening, namely the Mullins

effect, when cycled to a given stretch level.

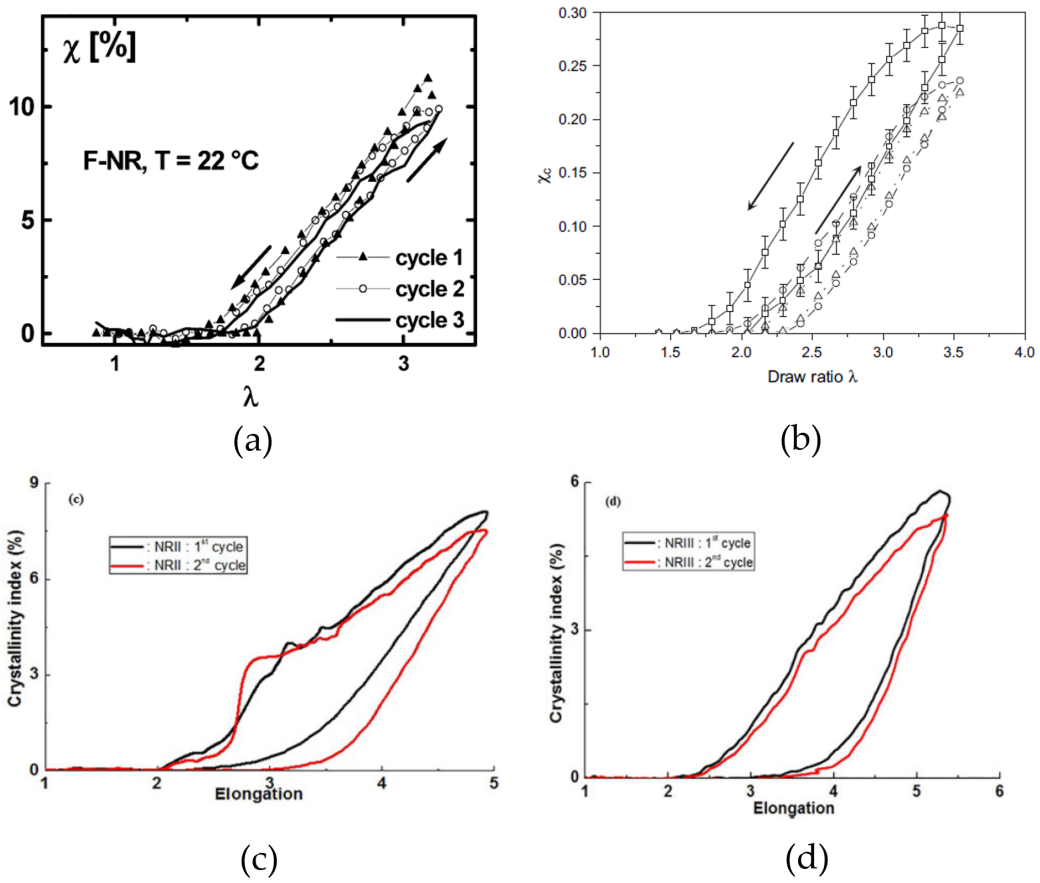

Figure 1.17: Evolution of the crystallinity as a function of the stretch, for successive loadings, on CB-filled NR from (a) Trabelsi *et al.* [95] (b) Chenal *et al.* [61] and on unfilled NR from (c,d) Zaghdoudi *et al.* [104].

The fact that the Mullins effect can be observed in unfilled NR questions the contribution of the SIC. Several authors performed SIC measurements by XRD during cyclic tests. Trabelsi *et al.* observed a strong softening between the first and second cycles, for a CB-filled NR [95]. However, the authors did not measure a significant decrease in SIC and concluded that "the Mullins effect does not play any role during stress-induced crystallization (stretching) and during melting (recovery)." (Fig. 1.17 (a)). Based on this finding, Diani *et al.* noted that "the Mullins' softening does not affect the strain-induced crystallization". However, Chenal *et al.* showed a non-negligible decrease in SIC, also on a CB-filled NR [61] (Fig. 1.17 (b)). The authors attributed this discrepancy to the difference in strain rate and concluded that in the case of Trabelsi *et al.* "the stress in the matrix network is sufficiently low to avoid any important modification of the rubber filler network and consequently of SIC.". More recently, Zaghdoudi *et al.* observed a decrease in SIC for two unfilled NR (Fig. 1.17 (c) and (d)), and attributed this decrease in SIC to the breakage of the shorter active chains which "will no longer take part of the stretching

process for the subsequent cycles." [104].

Uniaxial fatigue loading

Beurrot-Borgarino *et al.* carried out fatigue tests while measuring SIC with XRD [105]. They showed that the cristallinity index was increasing, at a constant λ_{max} and an increasing λ_{min}. For a minimum strain higher than the strain at which crystallites melt (λ_m), the crystallinity index was found to increase with the accumulation of loading cycles. Conversely, for a lower minimum strain, the crystallinity index decreases. The authors questioned the effect of the SIC on the amorphous phase to explain their results. These results may also explain the loading ratio dependence of crack growth resistance in NR. Additionally, the dependence of SIC at the crack tip on the loading ratio was highlighted by Bruening [106]. The authors observed an increase in SIC at the crack tip when increasing the loading ratio. At the crack tip of CB-filled NR and for relatively low prescribed stretch, Trabelsi *et al.* showed that the local stretch field is very heterogeneous [107]. These stretch heterogeneities result in a heterogeneous crystallinity index. This was later confirmed by other authors [108, 109]. Since these results were obtained for a few formulation and vulcanization conditions, it seems logical to hypothesize that changes in the macromolecular network would induce changes in the SIC at a crack tip.

1.2.2 Parameters affecting SIC

Crystallinity is generally plotted as a function of the stretch. In this type of representation, important features can be observed such as the maximum of crystallinity reached, the crystallinity rate, *i.e.*, the slope, and the macroscopic stretch at the onset of crystallization λ_m. These features depend on several parameters, related to: *(i)* the mechanical test conditions, and *(ii)* the macromolecular network. These are independently addressed in the following.

1.2.2.1 Mechanical loading and testing conditions

Crystallinity is affected by the loading type, testing temperature and strain rate. It is to be noted that multiaxial loading has also an effect [67, 110], but this is not addressed since only uniaxial loadings were performed in this work.

Stretch at the onset of crystallization

For uniaxial tensile loading, Candau *et al.* showed that both the testing temperature and strain rate influence the stretch at onset of crystallization, for unfilled NR [111]. Indeed, for a given strain rate, the stretch at onset of crystallization was almost constant

from -50 to 0°C, but tended to increase from 0 to 80°C. Furthermore, the values were strongly influenced by the strain rate, especially at low temperatures below -20°C: an increase in strain rate from 10^{-3} s^{-1} to 10^{-1} s^{-1} leads to an increase in crystallization onset. It is noteworthy that above -20°C, the effect of the strain rate was almost negligible. Furthermore, the authors showed that the strain rate effect competes with the active chain density: at low active chain density and strain rate, the crystallization onset occurred at a greatly reduced stretch [112]. To continue with the effect of the temperature on the SIC onset, Trabelsi found that increasing the testing temperature increases the stretch at onset of crystallization [65]. This was then confirmed by Bruening *et al.* on unfilled NR [113], for temperatures ranges from -25 to 50°C. In the case of filled NR, Candau *et al.* showed that the temperature has no effect on the local stretch at the onset of crystallization [114]. The authors concluded that the chains involved in the first crystallites formed have a similar local active chain density. In filled NR, Rault *et al.* showed that the macroscopic stretch at onset of crystallization was found independent on the maximum applied stretch [115].

Crystallization rate and maximum of crystallinity

Generally, in the case of uniaxial tensile loadings, the stretch level drives the crystallinity: the higher the applied stretch, below the elongation at break, the higher the maximum of crystallinity reached [61, 116, 117]. In the case of cyclic loading, the maximum of crystallinity is governed by both the maximum and the minimum applied stretches [105, 118]. Indeed, Beurrot *et al.* showed that the minimum prescribed stretch and its relative value compared to the stretch at crystallites melting, drives the crystallite volume and the maximum of crystallinity reached. Concerning the testing temperature, Trabelsi *et al.* showed that an increase in temperature in the range [0;90]°C leads to a decrease in crystallinity [65], for every maximum stretch prescribed. This result was confirmed by Albouy *et al.* [117] and Bruening *et al.* [113].

1.2.2.2 Macromolecular network

Since the present study focuses on the effect of the macromolecular network structure on the mechanical properties, it is necessary to clarify the links between crystallization, active chain density, cross-link length and fillers. Given the large number of studies, this literature review is not exhaustive but it will hopefully provide an overview of the main findings.

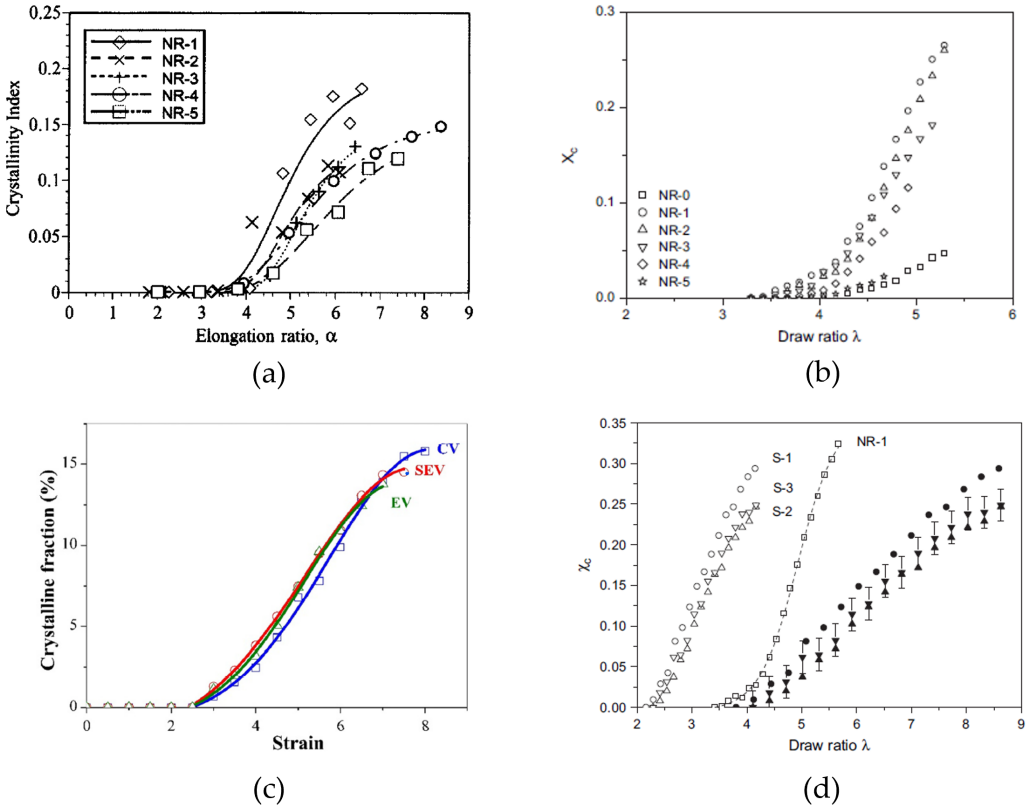

Figure 1.18: Effect of active chain density for (a) Tosaka *et al.* [94] and (b) Chenal *et al.* [116], and effect of (c) the cross-link length from Tosaka *et al.* [119] and (d) fillers from Chenal *et al.* [61] on SIC, for NR.

Stretch at the onset of crystallization

For an unfilled NR, the active chain density is generally considered to have no effect on the stretch at onset of crystallization, for sulphur vulcanization. This is illustrated in Figures 1.18 (a) and (b). The value is approximately equal to $\lambda_c = 4$, and was found several times in literature. For instance, Grasland [120] and Sainumsai *et al.* found $\lambda_c = 4$ for CV systems [121], while Trabelsi *et al.* [65], Ikeda *et al.* [122], Chenal *et al.* [116], Tosaka *et al.* [94], Sainumsai *et al.* [121] and Candau [123] for SEV ones. However, this is no more the case at high and low strain rate since the active chain density was found to have an effect on SIC onset [112]. Recently, for a fixed active chain density, Sainumsai *et al.* showed a slightly lower onset of SIC for an EV and SEV systems [119] in comparison to a CV one, as shown in Fig. 1.18 (c). The authors suggest that shorter cross-links have less mobility; however, their alignment is facilitated. It is noteworthy that for peroxide-vulcanized unfilled NR, the stretch at onset of crystallization depends on the active chain density [124]. In the case of filler NR, it was observed that the SIC onset was lower than for unfilled NR, when macroscopic stretch is considered. The higher the CB content, the lower the onset [61]. This is due to the fact that CB fillers act as topological constraints in the network, inducing SIC earlier. At low strain rate and for a

large temperature range of [0;80]°C, the local stretch at SIC onset was equal for unfilled and CB-filled NR, regardless of the CB content [114]. This confirmed the results obtained by Chenal *et al.* [61], which are shown in Fig. 1.18 (d).

Crystallization rate and maximum of crystallinity

In the late 1940s, Goppel and Arlman investigated the effect of the vulcanization time on SIC [125]. They found that increasing the vulcanization time conducted to a drop up to 50% of the crystallinity. According to the authors, crystallinity was reduced due to reversion by *(i)* a too high active chain density or *(ii)* rubber chains scission, but they did not address the possibility that reversion could lead to structural changes such as an increase in *trans* configurations. However, this point was addressed by Lin *et al.* who observed a strong decrease of SIC with over-vulcanization [46]. CV systems were much more impacted than EV ones, which is correlated with their poor resistance to long-time vulcanization. The cross-link length was found to have only a slight effect on the maximum of crystallinity, due to the work of Sainumsai *et al.* [119]. Indeed, it was shown that for a given active chain density, CV system demonstrated a little higher maximum of crystallinity compared to EV one. To go further, as mentioned by Treloar [47], the maximum of crystallinity is mainly affected by the active chain density. To date, the relation between the active chain density and crystallinity is still under debate since contradictory results exist. Nevertheless, the main results on the links between the active chain density and SIC, for unfilled NR, are hereafter reviewed. The active chain density is given in $\times 10^4$ mol/cm^3, under the assumption of an affine deformation network.

- **For CV systems:** Tosaka *et al.* observed that an increase in the active chain density led to a decrease in the maximum of crystallinity reached in the range of [1.01;2.12], for CV systems vulcanized at 140°C [94]. However, they reconsidered their values a few years later, and showed that the maximum of crystallinity could be maximized for 1.31, while the crystallinity rate for 1.46 [126]. To continue, Sainumsai *et al.* found an optimum value of 1.73 in the range [1.12;2.26] for a vulcanization temperature of 150°C and for a time corresponding to t_{90}. Finally, Grasland showed a decrease in the maximum of crystallinity in the range [1.5;2.5], for CV systems vulcanized at 150°C for a time corresponding to t_{98} [120].

- **For SEV systems:** Trabelsi *et al.* showed that, for an active chain density comprises in the range [0.8;1.94], increasing the active chain density decreases the maximum of crystallinity [65]. This result was then questioned by Chenal *et al.* since they observed an increase in the maximum of crystallinity reached in the range [0.23;1.63] and then a decrease in the range [1.63;1.95] [116], for different [A]/[S] ra-

tio[2] and a vulcanization temperature of 150°C. Ikeda *et al.* showed that maximum of crystallinity is the highest for highly cross-linked material [122]. From their work, it can be concluded that in the range [1.02, 1.83], increases the active chain density increases the maximum of crystallinity reached. These results were obtained for a vulcanization temperature of 140°C.

- **For EV systems:** Wang *et al.* found a similar maximum of crystallinity in the range [1.08;1.84], while above 2.18, a sharp decrease in crystallinity was obtained [127].

To sum-up, several studies reported a strong effect of the active chain density on SIC. However, since contradictory results were obtained on different formulations, and vulcanized with different conditions, it is difficult to draw conclusions. But we wonder if there is an optimal active chain density that maximizes SIC?

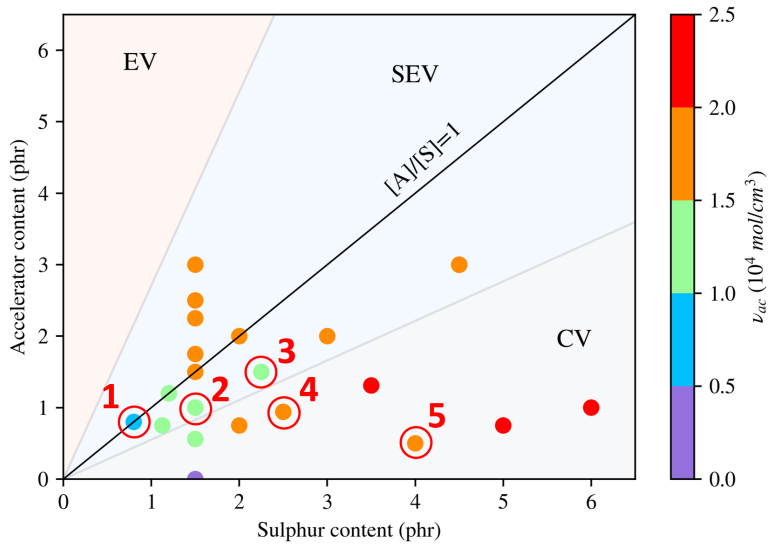

Figure 1.19: Vulcanization system maximizing SIC, deduced from: (1) Trabelsi *et al.* [65] (2) Ikeda *et al.* [122] (3) Sainumsai *et al.* [121] (4) Tosaka *et al.* [126] and (5) Grasland *et al.* [120].

Chenal *et al.* proposed to compare materials in terms of the crystallinity rate. With this approach the authors unified their results with the ones of Trabelsi *et al.* and concluded on the existence of an optimal active chain density around 1.20 $\times 10^4$ mol/cm^3. However, Tosaka *et al.*, after reconsidering their initial results, came to an optimal active chain density of 1.46 $\times 10^4$ mol/cm^3 [126, 128]. More recently, Hassoune *et al.* found an active chain density of 1.50 $\times 10^4$ mol/cm^3 optimizing the energetic behavior, *i.e.*, SIC and entropic elasticity. This further reduce the range of active chain density that could optimize the SIC, *i.e.*, between 1.20 and 1.50 $\times 10^4$ mol/cm^3. In order to give a different

[2]the sulphur content [S] was fixed, the authors varied both the cross-link length and the active chain density by changing the accelerator content [A]. This is unusual in light of the literature formulations investigated classically.

point of view on these results from the literature, they were plotted in a 3D graphic. The X and Y axes correspond to the sulphur and accelerator contents, while the active density is given by the colorbar. The vulcanization systems that promote the best the SIC are circled in red (Fig. 1.19). This could help to identify the sulphur and accelerator contents that structure a macromolecular network with high crystallinity.

Concerning the effect of fillers, altough fillers act as topological constraints and promote SIC, they reduce the rubber chain orientation [61]. Furthermore, for a given active chain density and CB content, the maximum of crystallinity was enhanced by N234 in comparison to N347 and N330 grades. However, for a given CB content and grade, there is an optimum active chain density maximizing both the maximum of crystallinity and the crystallinity rate, similarly to unfilled NR. Considering the macroscopic stretch, Demassieux showed that increasing the CB content from 0 to 70 phr induced a strong increase in the crystallinity index for a given stretch [129]. However, as the elongation at break decreases with increasing CB content, the maximum of crystallinity reached was the highest for unfilled NR.

1.3 Fatigue properties of NR

This last section explores the fatigue properties of NR. First, generalities on the fatigue properties of NR are given and the fatigue tests are described. The types of diagram used to analyze the results are presented. Then, the main factors affecting the fatigue response are discussed. Special attention is paid on the relationship between the fatigue behavior and the macromolecular network. To continue, damage mechanisms are investigated. Finally, the relation between SIC and fatigue properties is discussed and closes this section.

1.3.1 Generalities on uniaxial fatigue tests

The fatigue properties of NR have been intensively studied since the pioneering work of Cadwell *et al.* [4]. Historical results are recalled, before the experimental conditions generally found in the literature are detailed, for both the crack initiation and propagation approaches.

1.3.1.1 History and context

Fatigue is the ability of a material to withstand cyclic loadings without failure. Although it has been intensively studied for metallic materials since the 19^{th} century, it was not until the middle of the 20^{th} century that fatigue was first studied for rubber materials. Cadwell *et al.* [4] were the first to study the fatigue properties of a CB-filled NR. They opened up the field of research into understanding the fatigue properties of NR by highlighting a surprising and unique behavior under non-relaxing loading. As written by Beatty, "the really important fact is that cyclic stressing below the failure limit of a material will *never* cause failure even for an infinite number of cycles unless *some physical properties change as a result of this stressing.*" [130]. The fatigue analysis is in fact an evaluation of the fatigue life, by trying to understand what caused the specimen failure. In the rubber field, two main approaches are generally used. The first one is the crack propagation approach in which a pre-cutted planar specimen is tested. The aim is to characterize the evolution of the crack size during the cyclic test. The second approach is the crack initiation, where volumetric specimens are used. These specimens are not pre-cut and are considered to be free of cracks. The aim is to cyclically stretch the specimen up to the micro-crack initiation and propagation, and ultimately a macroscopic crack initiation. The resulting lifetime is then analyzed in relation to a mechanical quantity that is assumed to drive the damage.

Even though the present study focuses on the crack initiation approach, it has been chosen to provide some results related to the crack propagation approach. They will ease the comprehension of damage mechanisms since they traduce the propagation of the

crack. For more information on the crack growth approach, the reader can refer to the article of Robertson *et al.* [131].
Rivlin and Thomas were the first to define a criterion for the tearing of a rubber specimen, which is related to the tearing energy (T). In their methodology, the tearing energy is independent of the specimen geometry, and it could be used to describe crack growth [132]. This criterion showed good prediction for the crack growth of NR specimens, carried out on different geometries by Thomas [133, 134]. A few years after the work of Thomas and co-workers, Lake and Thomas studied other aspects of crack propagation [135]. They considered the relation between the crack propagation rate and tearing energy to be an intrinsic property of the rubber. They theorized that a crack can only propagate and grow above an energy threshold (T_0). From a molecular point of view, they interpreted and showed that rubber chains contribute to the network resistance. As a result, a crack needs to break each rubber chain that crosses its path in order to grow. The amount of energy required for the crack to grow thus depends on the number of rubber chains. A typical crack growth response is shown in Figure 1.20. Below T_0, the material can be considered undamaged, *i.e.*, the pre-cut crack does not propagate. Above T_0, the crack propagates with different regimes until a complete failure corresponding to the ultimate tear strength (T_C). We can naturally wonder how this approach can be used to link the macromolecular network structure on the ability of the material to resist to crack growth. This will be further discussed in Chapter 4.

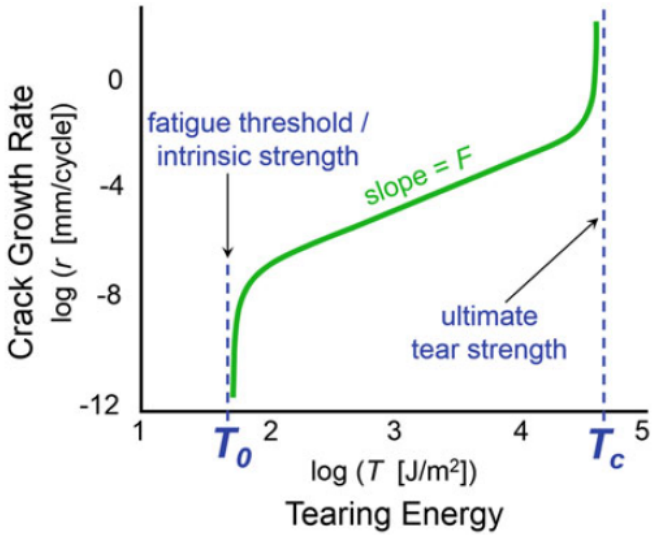

Figure 1.20: Relation of the crack growth rate and tearing energy, from [131].

1.3.1.2 Experimental fatigue tests

This non-exhaustive state of the art focuses exclusively on the crack initiation approach. In the following, several mechanical quantities are used. For the sake of clarity, the mechanical quantities and their respective abbreviations are given: displacement U (mm),

force F (N), stress σ (MPa), nominal stress π (MPa), strain ε (%) and stretch λ (-).

Specimens geometry

Volumetric specimens are generally used since they are more representative of the parts used for AVS applications. Several geometries have been employed. Initially, geometries with a constant cross-section were used. They are known as the "Dumbell" and were first introduced by Beatty [130]. Later, André introduced a radius of curvature to locate the failure at the half of the Dumbell specimen, and was named "Diabolo" [136]. Today, most studies use axisymmetric specimen, namely "AEX", derived from the Diabolo developed by André. It refers to "axy-symmétrique entaillé" with a radius of curvature of X mm. The radius of curvature enables to modify the triaxality level and varied depending on the authors. For instance, the AE5 specimen was generally used for multiaxial loading conditions [71, 137]. The Diabolo specimen has the advantage of not buckling under compression. Stress and strain are concentrated at half of its height, and damage generally occurs at the surface. As reviewed by Ruellan, there is unfortunately no standard geometry for using Diabolo. In the case of uniaxial loading condition, authors used Diabolo with radius of curvature of 2 mm [51, 137–139], 15 mm [140], 40 mm [5] and 42 mm [138, 141]. More information on the specimen geometries used in the crack initiation approach are provided in the review of Tee *et al.* [142]. Figure 1.21 presents the dimensions of (a) AE40 and (b) AE2 Diabolo specimens, from PhD thesis by Mouslih [71].

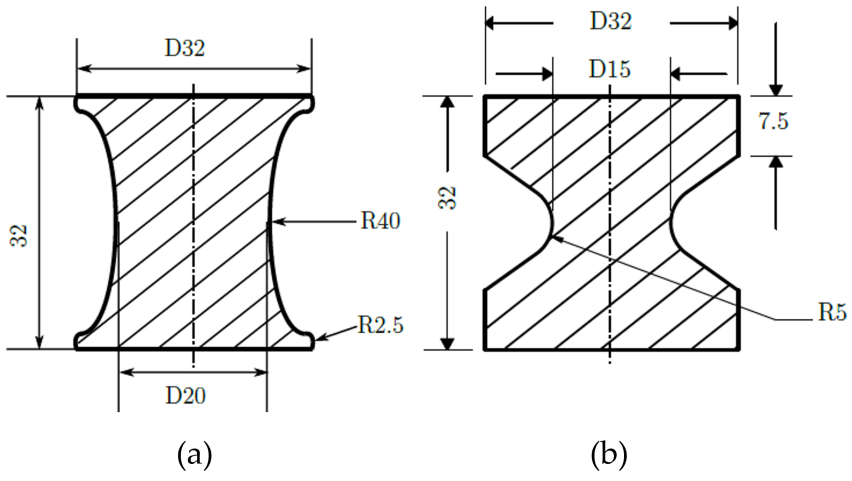

Figure 1.21: Dimensions of (a) AE40 and (b) AE2 Diabolo specimens [71].

Testing conditions

A fatigue test is carried out by applying a cyclic load to the specimen. An illustration of a fatigue test is given in Figure 1.22, in which M refers to the mechanical quantity used

to prescribe the test. Tests are generally prescribed under displacement U [5, 51, 137, 143, 144]. However, in some studies, tests are prescribed under force F [140, 145]. The loading ratio R_M is defined as the minimal over maximal value of M with $R_M = \frac{M_{min}}{M_{max}}$.

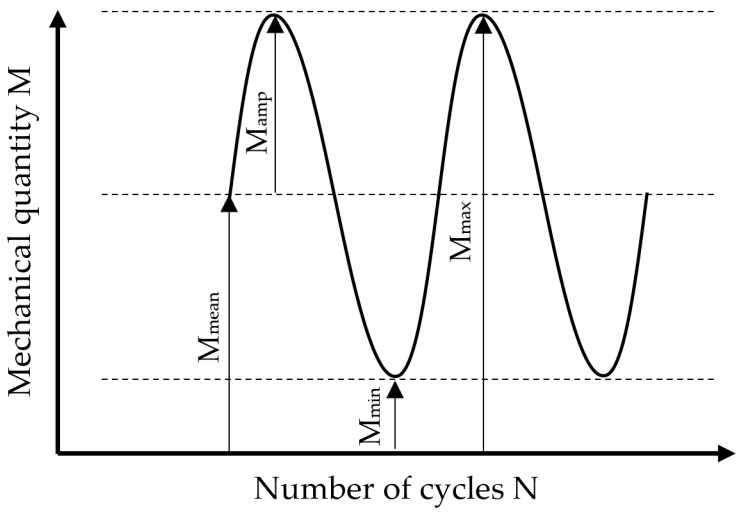

Figure 1.22: Illustration of the loading profile.

Depending on R_M, both the mean M_{mean} and amplitude M_{amp} of the loading changed. They are given by: $M_{mean} = 0.5 * (M_{max} + M_{min})$ and $M_{amp} = 0.5 * (M_{max} - M_{min})$, respectively. The calculation of M_{mean} and M_{amp} is particularly useful in the construction of Haigh diagram that will be presented in the following. The loading ratio types are given in Table 1.3. In practice, for $R_M < 0$, the loading cycle exhibits a compression phase while it remains under tension for $R_M > 0$.

In the case of uniaxial fatigue tests, the pioneering work of Cadwell *et al.* was dedicated to study the effect of the loading amplitude at a fixed minimum, and *vice-versa* [4]. They performed compression-compression, compression-tension, repeated tension and tension-tension tests. Beatty worked on the effect of the minimum loading on the lifetime for both NR and SBR [130]. André and Saintier conducted a fatigue campaign for both relaxing and non-relaxing loadings [136, 137]. Raoult worked on the lifetime prediction and carried out fatigue tests for compression-tension, repeated tension and tension-tension [144]. Bennani conducted a large fatigue campaign for both relaxing and non-relaxing loadings [146]. Masquelier conducted repeated tension loadings ($R_U = 0$) on NR filled with different contents and grades of CB [51]. Ruellan investigated the effect of the temperature on the lifetime reinforcement of a CB-filled NR, and performed compression-tension, repeated tension and tension-tension loadings ($R_\varepsilon \in [-0.25; 0.8]$). Champi *et al.* performed a wide range of non-relaxing loadings on a CB-filled NR/IR blend [147]. Even though uniaxial fatigue tests are mandatory, they are not discriminating for lifetime prediction

R_M	**Loading case**
<-1	Compression-tension
-1	Symmetrical tension-compression
]-1;0[	Tension-compression
0	Repeated tension
>0	Tension-tension

Table 1.3: Loading case given by the loading ratio R_M.

because industrial parts are subjected to multiaxial loadings. For more information on multiaxial fatigue tests, please refer to the state of the art of PhD thesis by Mouslih [71].

End-of-life criterion

The end-of-life criterion links a mechanical quantity to a number of cycles corresponding to the end-of-life. Defining an appropriate criterion is therefore of primary importance in the analysis. Ruellan distinguished four criteria in the literature: *(i)* the complete specimen failure [4] *(ii)* the apparition of a crack of a critical length at the specimen surface [148] *(iii)* a critical value of a macroscopic parameter such as a percentage of loss [140] and *(iv)* the brutal drop of force [143]. The most important point is to establish a satisfactory criterion for analyzing the fatigue data in a consistent and uniform way. Since the criterion *(iv)* is used in this study, it will be further detailed in the following. For more information on the other criteria, the reader can refers to PhD thesis by Ruellan [5].

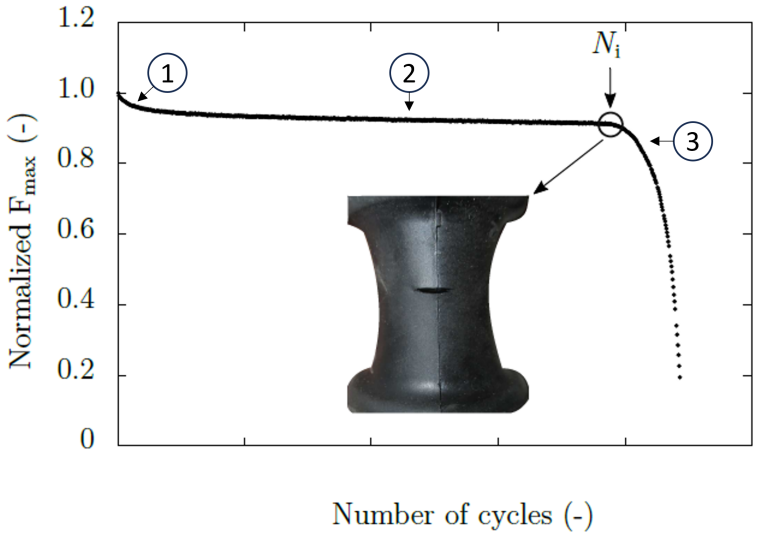

Figure 1.23: Example of the end-of-life criterion from Ruellan [5].

Originally developed by Lu, the end-of-life correlates with the loss of stiffness, and is materialized by the decrease of the macroscopic force [149]. In the early 2000s, Ostoja-Kuczynski *et al.* formalized this criterion, and proposed to associate the number of cycles N_i to the brutal drop of force observed during fatigue test [143]. Figure 1.23 illustrates a typical evolution of the maximum force with the number of cycles [5]. Three distinct stages occur. First, there is a stress softening leading to a reduction in force (stage 1). Then, a broad plateau is reached (stage 2) until a brutal drop in force (stage 3) indicating the specimen failure. The number of cycles is taken at the end of the plateau, in stage 2, and is denoted N_i. This criterion has been used for instance in Refs [5, 51, 71, 150, 151].

Fatigue life representation

The fatigue results are generally represented according to two different diagrams. They both aim at giving the evolution of the fatigue life with respect to a mechanical quantity derived from the continuum mechanics. Firstly, a two-dimensional graph which gives the evolution of the fatigue life with respect to a fatigue predictor [51, 140, 152], for a given R_M value. It is referred to as "endurance curve", "Wöhler curve" or "S-N" curve in the literature. Secondly, a three-dimensional Haigh diagram, which maps the fatigue tests according to the mean and amplitude of the loading applied. The fatigue life is given as a third axis and iso-lifetime curves are used to represent the fatigue life under non-relaxing loadings [5, 137, 153–156]. In the case of uniaxial fatigue loading, different quantities issued from continuum mechanics were used such as the maximum stress σ_{max}, the maximum strain ϵ_{max} and the strain energy W_{strain} [5, 157]. It is to be noted that these mechanical quantities unified the fatigue results in the case of proportional loading [157], but not in the case of more complex loadings [71].

1.3.2 Parameters affecting the fatigue resistance

Beatty [130], Mars and Fatemi [1], Tee *et al.* [142], Robertson *et al.* [131] and Gehling *et al.* [3] have reviewed the main parameters affecting the fatigue properties. These parameters can be grouped into four categories: *(i)* the mechanical loading *(ii)* the vulcanization conditions *(iii)* the chemical composition and *(iv)* the ageing. Figure 1.24 summarizes these categories and lists the corresponding effects. In this sub-section, results from both the crack propagation and crack initiation approaches are considered. Indeed, it can be stated that the crack initiation at the macroscopic scale actually corresponds to the propagation of a microscopic crack. Results can in some extent be transposed from one approach to another.

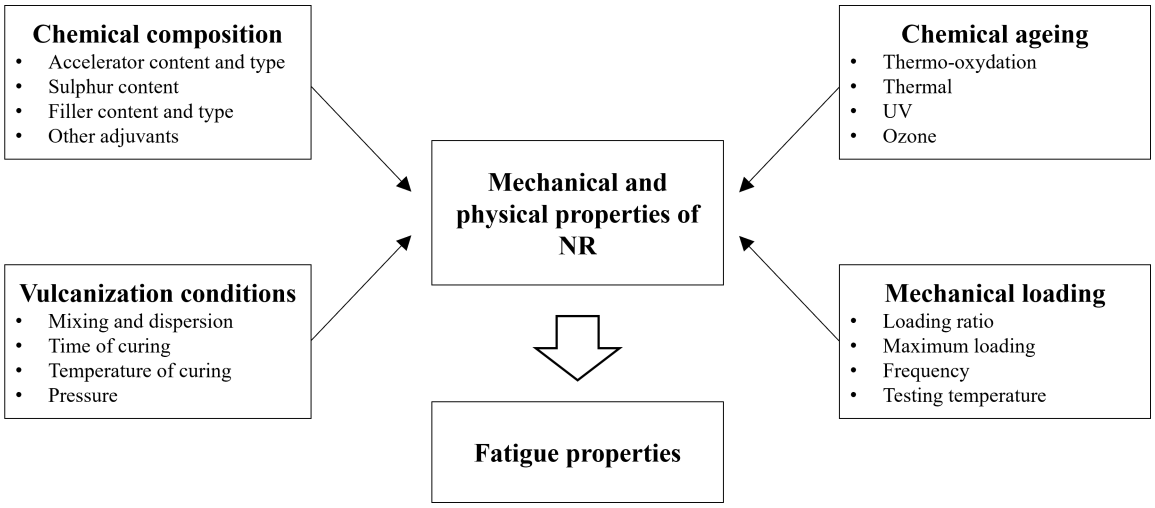

Figure 1.24: Main factors affecting the fatigue resistance.

1.3.2.1 Mechanical loading

Type of loading

The fatigue response of CB-filled NR is driven by the loading conditions, typically M_{min}, M_{max} and the corresponding R_M. Cadwell *et al.* [4] were the first to highlight the now well-known fatigue life reinforcement under positive R_M. It was further discussed by Fielding [158] and Beatty [130], who compared the fatigue behavior of non-crystallizable and CB-filled NR. Since the end of the 20^{th} century, more studies have been devoted to understanding the loading case effect on the fatigue behavior of CB-filled NR, such as the work of André [136], Saintier [137], Ostoja Kuczynski *et al.* [143], Bennani [146], Ruellan [5], Warneboldt *et al.* [139] and Mouslih [71], non-exhaustively.
For a fixed R_M, fatigue tests are conducted at different M_{min} and M_{max}. For relaxing loading conditions, the higher the M_{max}, the lower the fatigue life. Figure 1.25 (a) shows an example of an endurance curve plotted as a function of F_{max} and for $R_U = 0$, from Ruellan [5]. In this case, the maximum of the loading M_{max} is assumed to drive predominantly the fatigue damage. However, for non-relaxing loading conditions, *i.e.*, for $M_{min} > 0$, the maximum of the loading no longer solely drives the fatigue properties. The minimum of the loading M_{min} becomes more important. When R_M is varied, a second parameter is needed to represent the effect of the loading. The Haigh diagram is generally used for that purpose, as first introduced for CB-filled NR by André [136]. In such a diagram, the fatigue life reinforcement is characterized by the change of slope of the isolifetime curves in the positive R_M loading zone. It is to be noted that there is no change in the slope of the isolifetime curves for for non-crystallizable rubbers [130, 158]. An example of a Haigh-diagram is given in Fig. 1.25 (b). It is noteworthy that the lifetime reinforcement is equal between uniaxial tension and torsion loadings [156].

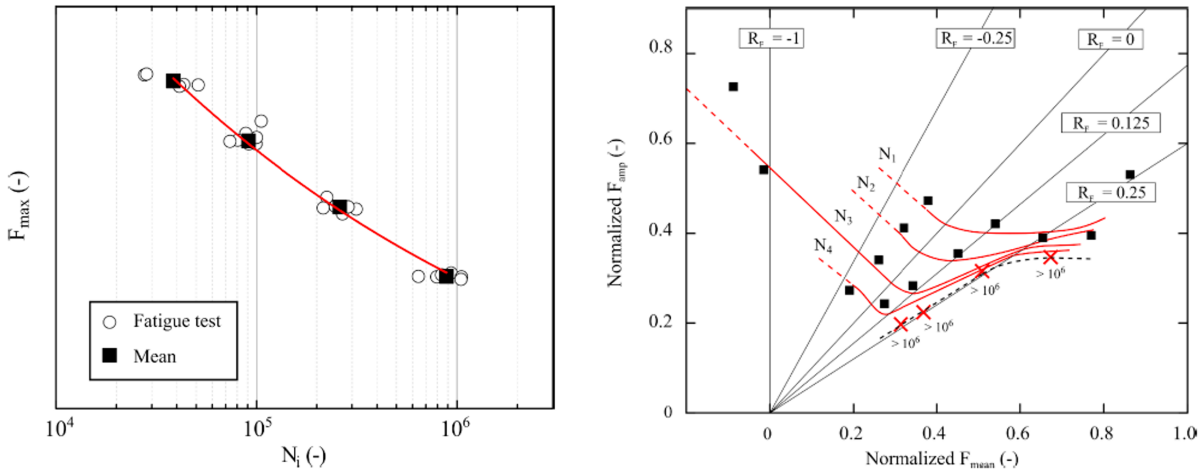

Figure 1.25: Representation of the fatigue results in an (a) endurance curve for $R_U = 0$ and in a (b) Haigh diagram, at 23°C from Ruellan [5].

Test frequency and heat build-up

As already described above, rubbers and more particularly filled rubbers exhibit a viscoelastic and hysteretic behavior, which leads to heat production and thereby heat build-up. This heat build-up is unable to be fully dissipated as the thermal conductivity of rubbers is low. In general, the frequency test ranges from 1 to 10 Hz. As increases the loading frequency increases the heat build-up, several authors wondered what was its effect on the fatigue life. It is to be noted that, apart from frequency, other parameters affects the heat build-up, such as: *(i)* the rubber type [1, 159] *(ii)* the filler type and content [151, 160] *(iii)* the specimen geometry, volumetric specimens leading to higher heat generation than planar ones [1] *(iv)* the maximal strain applied [140] and *(v)* the cross-link length [161].
The effect of the heat build-up on the fatigue life can be reviewed with respect to the specimen type:

- **Planar specimens:** Firstly, Young showed that the fatigue properties of unfilled NR are not affected by the heat build-up, for a frequency range from 1 to 20 Hz [159]. For a 50 phr CB-filled SBR the heat built-up had no effect on the crack growth resistance for frequency between 1 to 5 Hz [162]. Contrarily, it has been shown that the crack growth rate of a 20/80% NR/SBR blend filled with 80 phr of CB, was lower at 1Hz. The lower crack growth rate of the NR/SBR blend was also observed at 3 and 5 Hz, in comparison to the SBR compound. The authors questioned these results, which appear inconsistent with the literature. Indeed, frequency is generally considered to have no effects on the fatigue resistance for crystallizable rubbers [163]. In addition, the very unusual CB content makes any

conclusions difficult to be drawn. On the contrary, the crack growth resistance of NBR filled with 42 phr of CB was found to depend on the frequency [164]. The authors observed that the higher the frequency, the higher the heat build-up, and the higher the crack growth resistance, from 0.25 to 10 Hz.

- **Volumetric specimens:** For a NR/SBR/BR blend filled with 79 phr of different CB grades (N330 and N550), Seichter *et al.* found that the fatigue resistance was constant between 1 to 5 Hz [165]. They observed a strong increase in temperature at higher frequencies, but this was not correlated with any reduction in fatigue life. This results was confirmed by Neuhaus *et al.* on a NR/BR (90/10%) blend filled with CB between 1 and 4 Hz [140]. The authors demonstrated despite a temperature raise increasing from 8 to 34°C at the sample surface, no shift in endurance curve was observed. To go further, it should be noted that Ruellan measured a heat build-up of up to 20°C at the higher prescribed maximum displacement [5], and Mouslih measured a temperature of up to 10°C [71] on CB-filled NR under tension and torsion, respectively. Masquelier limited the frequency in order to limit the self heating to 5°C [51]. In the case of a 34 phr CB-filled SBR, no effect of the frequency on fatigue life was observed from 3 to 5 Hz [138].

A few comments are added regarding the origin of the heat build-up. From a molecular point of view, the heat build-up is generally attributed to internal molecular friction and depends on the rubber type [1, 159]. As reported by Medalia, the effect of the rubber matrix on heat generation comes from the sliding of the chain segments, with the dangling chain producing a viscous effect [160]. The author also reported that increasing the number of cross-links has the effect of *(i)* constraining the entanglements which ultimately becomes trapped, and *(ii)* reducing the number of dangling chains, which consequently decreased the frictional effects. In addition, fillers induce a high viscous effect, which could be explained by the interaction between filler and matrix. For CB-filled NR, heat generation is related to surface characteristics [166], which triggered the interaction with the rubber matrix. Surface functionality is also an important parameter, especially for silica fillers [160]. As fillers content increases, heat build-up also increases as a consequence of higher viscosity induced [167]. To date, the relationship between the frequency, the heat build-up and the macromolecular network is not yet fully understood.

Testing temperature

During service life, AVS parts are subjected to a combination of high temperature variations and dynamic mechanical loadings. Generally, when tested at high temperature (90-110°C), CB-filled NR exhibits a significant lifetime reduction in comparison to ambient temperature [4, 130, 149]. For instance, Neuhaus *et al.* observed a strong shift

of endurance curves under relaxing loadings on CB-filled NR/BR blend (90/10%). For the authors, the fatigue life reduction is due to the combined effects between *(i)* the temperature causing a thermo-oxidative ageing of the NR macromolecular network and *(ii)* the aged macromolecular network causing a supplementary sensitivity to temperature [140]. However, the effect of the testing temperature on the fatigue reinforcement, *i.e.*, for non-relaxing loadings, was first investigated by Ruellan [168] for CB-filled NR. The authors showed that the fatigue life reinforcement still occurred at 90°C but in a lesser magnitude than at 23°C. At 110°C, the lifetime reinforcement disappeared, suggesting that the phenomena responsible for this reinforcement depends on temperature. To go even further, on the same CB-filled NR, Mouslih *et al.* demonstrated that the lifetime reinforcement was similar between torsion and tension loading, at 23°C and 90°C [155, 156]. This shows that the phenomenon responsible for the lifetime reinforcement is independent to the loading multiaxiality. Furthermore, this also suggests that this phenomenon is temperature-driven. The effect of the macromolecular network as well as the fillers content and type on the fatigue resistance at high temperatures remains unexplored.

1.3.2.2 Macromolecular network

NR exhibits a remarkable fatigue resistance under relaxing loadings, espacially in comparison to other rubber types such as SBR, EPDM, IR and CR [130]. However, many other parameters impact the fatigue response. This sub-section is dedicated to understanding the relation between the macromolecular network and the fatigue resistance. The macromolecular network structure can be modified by the formulation, and more precisely by the vulcanization system as well as by adding fillers. The vulcanization conditions also impact the macromolecular network structure. It is noteworthy that both thermal and thermo-oxidative ageing affect the fatigue properties of NR, but they will not be addressed in the present state of the art. For information on these effects, the interested reader can refer to Refs [120, 140, 152, 169–171].

Cross-link length

In the early 1950s, Dogadkin and Tarasova studied unfilled NR and SBR for different vulcanization system types [172]. They performed anaerobic fatigue tests at 100°C, and showed that the fatigue resistance generally depends on the thermal resistance of the cross-links. They also showed that polysulphide cross-links are better than shorter cross-links are room temperature. Years later, several studies demonstrated that the fatigue resistance was influenced by the cross-link length: for instance, this has clearly been shown for NR in the study of Yanyo [173], who demonstrated that polysulphide cross-links lead to a higher crack growth resistance than monosulphides and carbon-carbon ones (Fig. 1.26). The author interpreted them by the greater ability of longer cross-

links to provide mobility to the active chains. This would enable them to be stretched and relaxed cyclically without undergoing any damage. It became generally accepted that longer cross-links were beneficial for fatigue life. Other authors explained the superiority of longer cross-links by their ability to break and rearrange [130, 174]. According to Beatty, contrarily to polysulphide cross-links, short monosulphide cross-links cannot rearrange at the ultimate local strain, and therefore break [130]. This explanation is close to the one proposed by Bhowmick, who stated that both the rearrangement of the cross-links and their scission, before the active chains failure, has the effect of dissipating the strain energy [174]. For Lake and Lindley, the explanation lies in the flexible nature of such long cross-links. This would be responsible for stresses relieving that has the consequence of increasing the energy required to break the active chains of the macromolecular network [175]. Following this idea of local stresses reduction, chain slipping was also proposed as a phenomenon that would increase the resistance to failure [176]. For Chan, polysulphide cross-links lead to a better fatigue resistance by at least a factor two or three, than for shorter cross-links, for relaxing loading conditions [177]. Nevertheless, the author mentioned that the temperature and the strain level have an effect on this behavior.

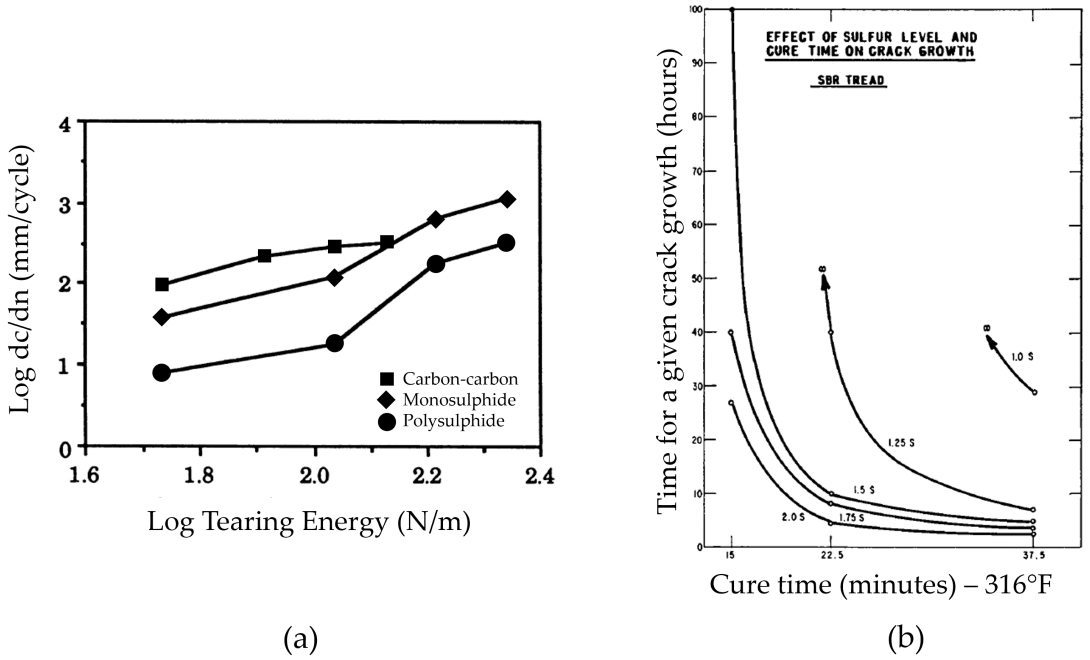

Figure 1.26: Effect of (a) the cross-link length from Yanyo [173] and (b) the sulphur content and time of vulcanization from Beatty [130] on the crack growth resistance.

Active chain density

As mentioned by Mars and Fatemi [1], an optimal active chain density exists, for which the fatigue life is maximized. This optimum is the consequence of the competition between strengthening effects that are maximized at higher active chain densities and ability to

dissipate energy that are encouraged for lower ones. It is worth remembering that an increase in active chain density leads to stiffening and a decrease in hysteresis [13]. In the 1980s, the effect of the active chain density on the threshold tear strength T_0 was investigated by Gent [178]. Several rubbers were compared in their work, including NR. By varying the proportion of peroxide in the formulations, the molecular weight varies as a consequence of the number of carbon-carbon bonds created. The T_0 value appears to depend on the active chain density, as described by Lake and Thomas [135]. This indicates that decreasing the active chain density tends to increase T_0 and consequently delay the crack propagation phenomenon [178]. As shown by Beatty, the sulphur quantity governs the crack growth resistance for SBR compounds [130]. The author reported the existence of combined effect of vulcanization time and sulphur content, as shown in Figure 1.26 (b). However, without active chain density calculation, it is difficult to further discussed on the results of Beatty. Chan also mentioned that excessive cross-linking increases the fatigue failure sensitivity of NR. These results imply that an optimal active chain density exists for fatigue applications [177]. More recently, Grasland showed that for a fixed cross-link length, the crack growth rate depends on the active chain density [120]. It is noteworthy that the active chain density and SIC are intimately related. In this sense, the active chain density drives the stiffness, which impacts the fatigue life. To go further, it could also act on the fatigue behavior by influencing SIC. Therefore, as the stiffness and SIC are related to the active chain density by antagonist phenomenon, its real contribution to the fatigue life appears complex. Carrying out an exhaustive fatigue campaign on a large active chain density, covering different crystallinity rates and maximums, could provide further elements.

Fillers

Kim and Lee compared CV, SEV and EV systems for a CB-filled with 40 phr, and also an unfilled NR. For each formulation, it was shown that the propagation had two regimes: a slow one followed by a brutal acceleration. The unfilled CV, SEV and EV presented similar propagation rates, indicating no effect of the cross-link length for unfilled NR. But, the addition of CB drastically reduced the crack propagation rate, but did not have any impact on the vulcanization system, *i.e.*, cross-link length has no effect. However, the brutal propagation regime was amplified for the EV system. This indicates that CV systems are to be preferred for CB-filled NR. The authors reported that CV are better due to the influence of the chain extensibility limit and a lower stretch at crystallization initiation [179]. Finally, it was shown that the crack growth resistance is higher for N330 CB grade than for a N770, on CB-filled NR [180]. It is worth noting that both the CB grade and content have an effect on the threshold tear strength T_0. A higher content leads to a higher stiffness and also higher T_0 value. For CB grade, N220 and N330 greatly

increases T_0 [181]. Also, Masquelier show that the CB grade seems to predominantly drive the endurance curve, more than the CB content [51]. These results show that CB drives the fatigue resistance. However, to the best of the authors knowledge, the effect of the active chain density and cross-link length on the fatigue resistance for filled NR remains unclear.

Vulcanization conditions

The vulcanization conditions, namely the vulcanization time and temperature, affect the fatigue resistance. For SBR, it was for example shown that increasing the vulcanization time beyond a certain value has the effect of drastically reducing the crack growth resistance [130]. Furthermore, it seems there is an optimal vulcanization time for the fatigue life, that would correspond to a sufficiently high stiffness and hysteresis [1]. However, for CB-filled NBR, Gehling *et al.* measured that increasing the vulcanization time above an optimal value leads to a decrease in crack growth resistance [182]. The authors also showed that the higher the vulcanization temperature, the higher the crack growth resistance. Concerning vulcanization temperature, Mukhopadhyay showed that a high vulcanization temperature is likely to reduce the cross-link length. The consequence is a lesser crack growth resistance for CV, which is significantly better for low vulcanization temperature [44]. It is clear that literature on the effect of vulcanization conditions on the fatigue properties of NR is limited.

Summary

This state of the art highlighted that polysulphide cross-links are of beneficial for fatigue life. It could be hypothesized that the longer the cross-link length, the higher the fatigue life. In addition, authors have reported an optimal range of active chain density that maximizes the fatigue life without clearly establishing it. This is particularly true for NR, for which there is a lack of data. To go further, there is no information on possible combined or competing effects of the cross-link length and the active chain density on the fatigue resistance. Fillers and vulcanization conditions are also of primary importance. In summary, the literature has provided initial answers, but has not been able to establish clear links between the effect of macromolecular network and fatigue resistance for both filled and unfilled NR. This is all the more complex as each parameter is of primary importance and there may be combined effects.

1.3.3 Damage mechanisms

Since the beginning of the 2000s, a focus has been made on the analysis of the failed specimens: it is called a "post-mortem" analysis. It appears that the damage analysis

is indisociable from considering the fatigue lives, as it provides further information on the elementary mechanisms that lead to failure. For example, it was able to provide information on the activation of SIC which was put into perspective with the fatigue reinforcement under non-relaxing loadings.
The analysis of damage mechanism is generally performed at two scales: *(i)* the macroscopic scale that locates the crack at the specimen scale and *(ii)* the microscopic scale that considers the failure surface and enables to determine the elementary crack initiation and propagation patterns. For more details on damage mechanisms in non-crystallizable rubber and for CB-filled NR for multiaxial loading conditions, the reader can refer to Refs [5] and [183], respectively.

1.3.3.1 Macroscopic scale

At the macroscopic scale, the damage mechanisms are related to the loading conditions. Authors introduced a pseudo Haigh diagram to map the effect of the loading conditions on the damage mechanisms observed on Diabolo specimens. More importantly, the "damage modes" were introduced by Le Cam *et al.* in order to classify the type of damage mechanisms [183, 184]. In their former work, 7 damage modes were identified. Lately, on the basis of the work of Le Cam *et al.*, Ruellan used 3 damage modes depending on the loading case for uniaxial fatigue loading. This type of diagram was also used for instance by Mouslih [71].

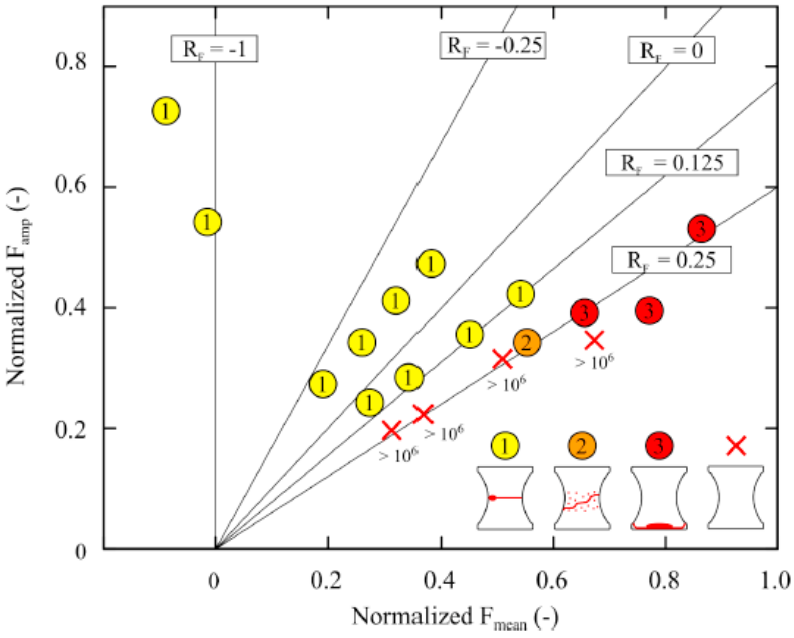

Figure 1.27: Relation between loading case and damage modes from Ruellan *et al.* [168]. Damage modes are categorized into Damage mode 1, 2 and 3.

The work of Le Cam *et al.* [184] highlighted a dependence of the damage mechanisms on the loading conditions. The main results are illustrated in the pseudo Haigh diagram in Figure 1.27, and can be commented as follows:

- **Relaxing tension:** the crack initiates and propagates at the surface of the median section of the Diabolo. The crack is visible in the median section until the specimen fails (see Damage mode 1). It is to be noted that this damage mechanism is the only one reported for relaxing loadings.
- **Non-relaxing tension loading:** the crack developed in the median region, but some crack bifurcations can be observed (see Damage mode 2). According to the authors, they reflect the crack propagation resistance induced by SIC. This phenomenon is even more pronounced in the case of Damage mode 3, where the reinforcement in the median zone is too high for any crack to develop. In this case, the damaged zone is shifted under the inserts. This is obtained in the case of highly non-relaxing loadings.

1.3.3.2 Microscopic scale

At the microscopic scale, the crack first initiates and then propagates by forming characteristic patterns. Figure 1.28 shows the crack propagation zones in (a) a specimen and (b, c) from a schematic point of view.

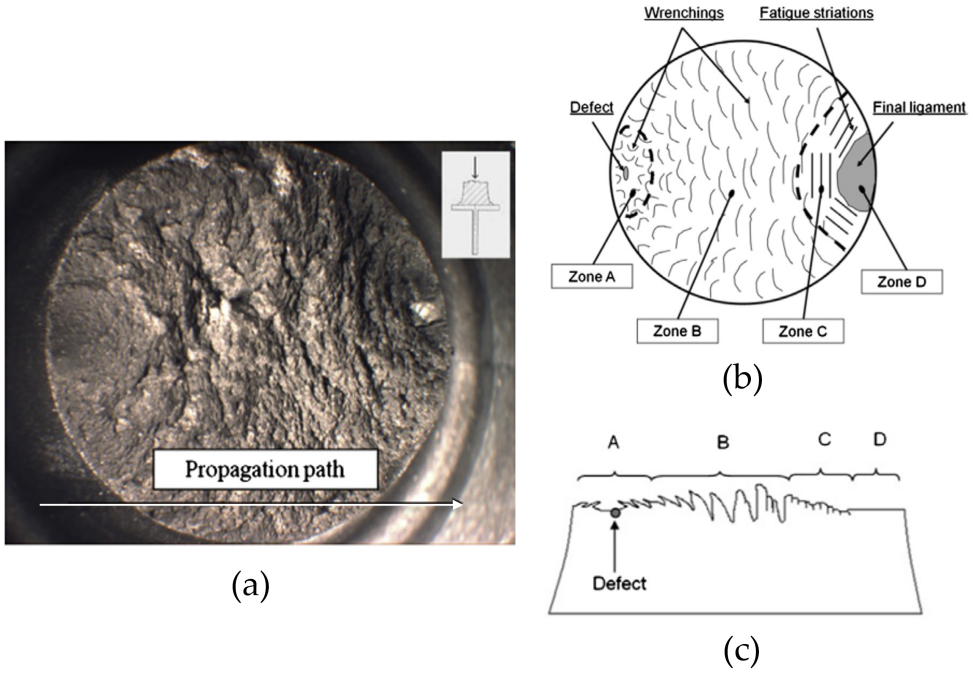

Figure 1.28: Crack propagation zones from Le Cam *et al.* [183].

Crack initiation

Diabolo specimens are not free of defects, which are generally randomly localized. The crack generally initiates around a defect or a singularity that concentrates stress. As the Diabolo undergoes a cyclic loading, stress and strain are concentrated in the middle of the Diabolo, near the surface which constitutes a preferred zone for crack initiation. However, some heterogeneities in terms of vulcanization state might exist due to the molding process. In most cases, the crack initiates around defects near the specimen surface due to high stress concentration [51, 137, 157]. The crack precursors can be: *(i)* ZnO particles [137, 183] *(ii)* pollution [137] or *(iii)* geometrical aspiration [51]. Ruellan observed predominantly defects being CB agglomerate, which is explained by a cavitation phenomenon [5]. It has to be noted that multi-initiations may occur, before one of them predominates and develops [143]. In the study due to Ruellan *et al.* [168] for non-relaxing loadings (see damage mode 2), multi-initiations occur predominantly around the surface. The authors interpretation was the activation of SIC, which prevented any crack from propagating, thereby allowing the initiation of several cracks in parallel.

Crack propagation

For damage mode 1 corresponding to relaxing loadings, after the crack is initiated, the crack propagates elliptically (Zone A). Once it reaches the surface, it propagates toward the opposite side of the failure surface by forming wrenchings (Zone B). The size of the wrenchings increases as the crack propagates and the stress level increases. These wrenchings are formed by highly stretched ligaments at the crack tip [185]. As the local stress continues to increase with the reduction of the surface, fatigue striation might form, depending on the loading and temperature (zone C). Finally, the crack leads to complete failure and a very smooth final ligament is visible (Zone D). This suggests that these zones may vary depending on the macromolecular network, and the resulting mechanical and SIC properties.

Under non-relaxing loadings (Damage mode 2), the fatigue life reinforcement is generally accompanied with SIC markers at the failure surface. As explained by Le Cam and Toussaint, high stress at the crack tip locally increases the crystallinity, preventing the crack from propagating in a direction perpendicular to the applied load and therefore causing the crack to bifurcate. Consequently, the fracture surfaces experience simultaneous tearing, sliding, and relaxation along the highly crystallized tip, leading to the formation of fatigue striations [186]. This was observed for both repeated tension and non-relaxing tension loadings [154]. However, for non-relaxing loadings, it appears that the fatigue striations are more numerous and their structure is more pronounced. It is

to be noted that Ruellan introduced the term "regime of striation" to differentiate these well-formed striations. A new pattern referred to as "cones" also forms in the case of multiple initiations. These cones are an indication that multi-crack initiations are deviated by the SIC reinforcement, and propagate perpendicular to the loading direction. This is indicative of a high reinforcement and was first observed by Ruellan [168]. Figure 1.29 shows the fatigue striations (a, c) and cones (b, c).

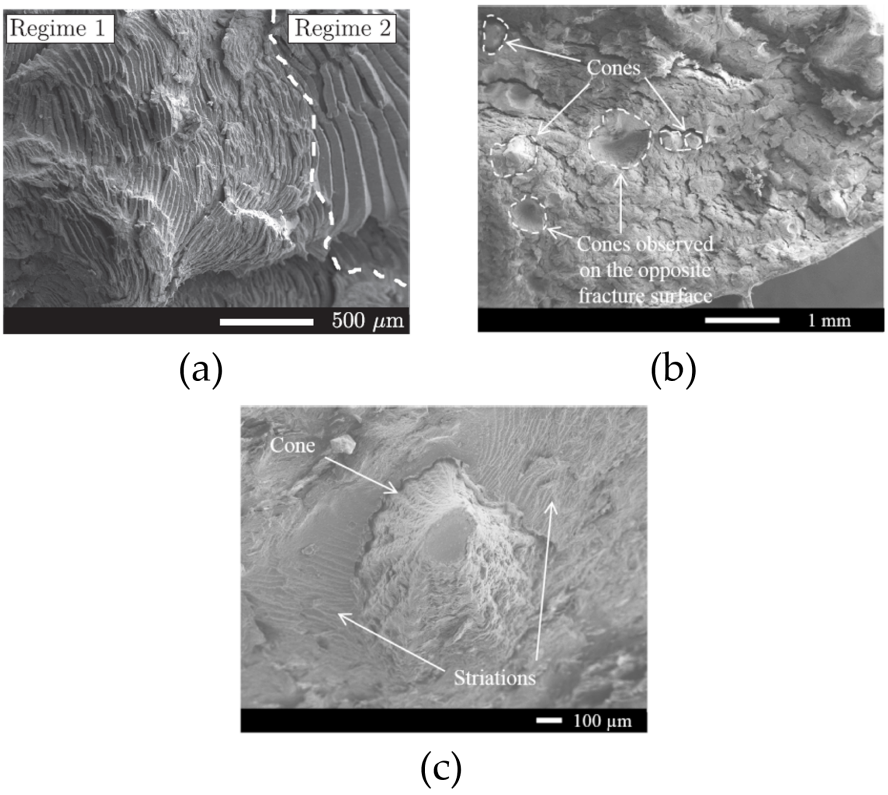

Figure 1.29: SIC markers: (a) fatigue striations of regime 1 and 2 (b) cones and fatigue striations and (c) focus on a cone [154].

1.4 Conclusion of the chapter

The first section of the state of the art was devoted to the generalities concerning NR. In this section, fundamental notions on the macromolecular network of NR were presented, and the vulcanization process was described. The recipes imply several adjuvants, but the macromolecular network structure is governed mainly by the filler content and type, as well as the vulcanization system. Additionally, it was also shown that vulcanization conditions are of primary importance and their effects depend on the vulcanization system. Concerning the mechanical properties of NR, the effect of the macromolecular network on elasticity, viscoelasticity, hysteresis, Mullins effect and calorimetric response were addressed. It was shown that both the active chain density and cross-link length, for filled and un-filled NR are important parameters governing the physical and mechanical properties. Nevertheless, how these parameters affect the Mullins effect, which is one of the main features of the mechanical response, is not fully characterized and understood.

The second section was dedicated to the understanding of the SIC of NR. Fundamental notions about SIC were recalled as well as a discussion on the physical origin of this phenomenon. Then, its effects of the mechanical properties were addressed, especially on the stress-strain behavior in the case of monotonic tensile and cyclic loading, and also fatigue. Finally, the factors affecting SIC were examined, focusing first on mechanical loading aspects and then on macromolecular network ones. It was shown that the active chain density and SIC have a very peculiar relationship, which is not yet fully understood. For instance, SIC could be maximized by an optimal active chain density.

The third section focused on the fatigue behavior of NR. A description of the fatigue property was firstly carried out, by describing both crack initiation and crack propagation approaches. The specific behavior of NR under fatigue loading was then discussed, and the relationship between fatigue and SIC was questioned, as the effect of the macromolecular network on the fatigue properties is not clearly established. This is due to the fact that the formulations and vulcanization conditions used in the litterature strongly differ from one study to another. Namely, the vulcanization time and temperature, the vulcanization system type, the filler quantity and the rubber matrix type. Since the aforementioned parameters affect the macromolecular network structure, understanding its relationship with the fatigue properties therefore requires a dedicated study including an exhaustive and comprehensive material formulations. More importantly, the relationship between the macromolecular network structure and the fatigue is even more complex since lifetime reinforcement is generally attributed to SIC. To conclude, the understanding of how the macromolecular network structure impacts the mechanical properties requires further investigations.

Chapter 2

Materials, specimens and experimental techniques

Preamble

The previous state of the art showed that the macromolecular network structure drives the mechanical properties of NR. In addition, it drives the crystallinity, and the active chain density might have an "optimal" value that would maximizes it. If the lifetime reinforcement is driven by SIC, investigating different macromolecular network structures would result in different reinforcement. On this basis, the purpose of the experimental framework is to provide both the appropriate NR materials and tests to be performed, in order to carry out a complete characterization of the macromolecular network, and its mechanical and fatigue properties.

This chapter is composed as follows. First, Section 2.1 presents the materials definition considered here. Vulcanization systems and conditions were varied to ensure significant variations in the macromolecular network structure. Then, the three different specimen geometries used, namely the swelling specimen, simple tension specimen and AE40 Diabolo specimen, are presented in Section 2.2. Note that the AE40 Diabolo is the same as the one introduced by Ruellan [5], and later used by Mouslih [71]. These specimens are used to characterize the macromolecular network, and to characterize the mechanical and fatigue properties, respectively. To continue, Section 2.3 describes the swelling test protocole as well as the data-processing procedure. This section also provides a description of the quasi-static tensile tests performed, and fatigue tests facilities and conditions. This is followed by a description of the equipments used to perform the damage mechanisms analysis in Section 2.4. The chapter ends with Section 2.5, which is dedicated to the presentation of the first results on the rheometric characterization, swelling tests and uniaxial monotonic tension tests.

2.1 Materials

In the following, a "material" stands for a formulation and a curing condition.

2.1.1 Formulations

The material considered here is a NR (*cis*-1,4-polyisoprene) of Standard Malaysian Rubber (SMR) grade. As mentioned in Chapter 1, it is made of more than 99% of *cis*-configuration monomers. Consequently, NR macromolecules are highly stereoregular which is of benefit for mechanical and physical properties. Components used in NR formulations are given in phr. In practice, X phr corresponds to X g per 100 g of NR. Some components in the materials formulation studied are common to all of them. Indeed, 10 phr of ZnO is used, as this high content is beneficial for AVS applications [5]. It is accompanied by 2 phr of stearic acid. For the antioxidants and plasticizer, 3 and 2 phr are used, respectively. Note that plasticizers are solely used in filled formulations. For the other components, namely sulphur, accelerator and fillers, they are variable. Table 2.1 presents the formulation used for a given NR, with the content of the common components given in phr. The variable components are marked with "V".

Component	Content (phr)
NR	100
CB	V
Plasticizer	V
ZnO	10
Stearic acid	2
Antioxydants	3
Accelerator	V
Sulphur	V

Table 2.1: Components used in the materials formulation, in phr. The variable components are denoted "V".

In the present study, only sulphur (S) vulcanization is studied, accelerated with CBS (A). In order to vary the macromolecular network structure, *i.e.*, both the cross-link length and active chain density, several vulcanization systems were defined. They were chosen in agreement with the standard distinction proposed by Quirk [23], in which three principal types of material are distinguished: CV, SEV and EV systems. This distinction is given in Table 1.2 in Chapter 1. The difference between them lies in the length of the cross-links formed, which is driven by the ratio between the accelerator [A] and sulphur

[S] contents, denoted [A]/[S]. The smaller the ratio, the longer the cross-link length. On a first hand, to vary the cross-link length, a total of five content ratios are defined; 0.2 and 0.6 for CV, 1.5 and 2.5 for SEV, and 4 for EV. On a second hand, in order to vary the active chain density, both accelerator [A] and sulphur [S] contents are changed while keeping a fixed content ratio. Additionally, in order to evaluate the contribution of fillers relatively to the cross-link length and active chain density, NR has been filled with 20 phr of N330 HAF grade CB. This grade of CB is considered as a reinforcing filler [25]. [A], [S], [A]/[S], and CB content are given in Table 2.2. The "0 and 20" in the CB content indicates that both unfilled and 20 phr CB-filled formulations exist.

Designation	[A]	[S]	[A]/[S]	CB
$NR^{2}_{0.2}$	0.4	2	0.2	0 and 20
$NR^{3}_{0.2}$	0.6	3	0.2	0
$NR^{4}_{0.2}$	0.8	4	0.2	0 and 20
$NR^{6}_{0.2}$	1.2	6	0.2	20
$NR^{2}_{0.6}$	1.2	2	0.6	20
$NR^{4}_{0.6}$	2.4	4	0.6	20
$NR^{6}_{0.6}$	3.6	6	0.6	20
$NR^{0.8}_{1.5}$	1.2	0.8	1.5	20
$NR^{1.2}_{1.5}$	1.8	1.2	1.5	0 and 20
$NR^{1.6}_{1.5}$	2.4	1.6	1.5	20
$NR^{0.8}_{2.5}$	2	0.8	2.5	20
$NR^{1.2}_{2.5}$	3	1.2	2.5	0 and 20
$NR^{1.6}_{2.5}$	4	1.6	2.5	20
$NR^{0.5}_{4}$	0.5	2	4	0
$NR^{0.8}_{4}$	0.8	3.2	4	0 and 20
$NR^{1.2}_{4}$	1.1	4.4	4	0

Table 2.2: Materials formulations of the study. They are denoted NR^{J}_{I}, with I the sulphur content [S] and J the accelerator-to-sulphur [A]/[S] ratio. For the sake of clarity, designation are classified in accordance with the vulcanization system type: CV, SEV and EV in black, blue, and red, respectively.

2.1.2 Vulcanization conditions

The specimens were obtained by a molding process. All the components were incorporated into the internal mixer except those for the vulcanization system, which were added during external mixing, in an open-roll mill, to ensure a temperature of the mix

lower than 100°C in order to prevent the compound from early cross-linking reactions. The specimens were molded at a temperature of 160 °C, and at a time corresponding to t_{98} (condition N°0 in Table 2.3), determined with a rheometer (Rubber Process Analyzer 1000, Alpha Technologies). The specimens are presented in next Sub-section 2.2.

Since the vulcanization conditions strongly affect the macromolecular network structure, filled $NR^{4}_{0.2}$, $NR^{1.2}_{1.5}$ and $NR^{0.8}_{4}$ were also molded with four other conditions, detailed in Table 2.3. These three NR were chosen since they cover the range of CV, SEV and EV systems of the present study. First, the vulcanization time is changed: condition N°1 corresponds to an under-vulcanized material, while the condition N°2 corresponds to an over-cured one. For the over-vulcanized materials, since the torque kinetics strongly depend on the vulcanization system, it would have been trivial to set a time corresponding to a torque value. For instance, CV system tends to rapidly reverse, while the EV one forms a torque plateau and decreases only slightly. Consequently, it is preferred to use an additional period of time, defined as 40% of the total time corresponding to t_{98}. Then, the temperature of vulcanization is changed. A vulcanization at low and high temperature of 150 °C and 170 °C were defined as the conditions N°3 and 4, respectively.

Condition N°	Time (-)	Temperature (°C)
0	t_{98}	160
1	t_{80}	160
2	t_{98} +40% of time	160
3	t_{98}	150
4	t_{98}	170

Table 2.3: Changes in the vulcanization time and temperature for filled $NR^{4}_{0.2}$ (CV), $NR^{1.2}_{1.5}$ (SEV) and $NR^{0.8}_{4}$ (EV).

2.2 Specimen geometries

The specimens used to perform the swelling, quasi-static and fatigue tensile tests are described hereafter.

2.2.1 Pure shear specimen

Pure shear specimen was used since it allows to cut both simple tension and swelling specimens. First, the simple tension specimen is cut by water jet cutting, which is performed at the University of Rennes. This cutting method is preferred to manual cutting

because it ensures a clean and repeatable cut. This type of specimen is used for quasi-static tension tests. Its extremeties allow the specimen to be easily mounted, without slipping into the grips. The dimensions are given in Figure 2.1, the cross-section is equal to 8×2 mm^2, with a length between the cylindrical extremities of 23 mm. Secondly, the swelling specimen is cut by a circular punch. The main advantage is that both uniaxial tension and swelling specimens are obtained from the same pure shear specimen. Thus, they should have a very similar macromolecular network, which allows for representativeness and comparison of the different types of test. Figure 2.1 gives a representation of the pure shear specimen. The cutted specimens are also illustrated in red.

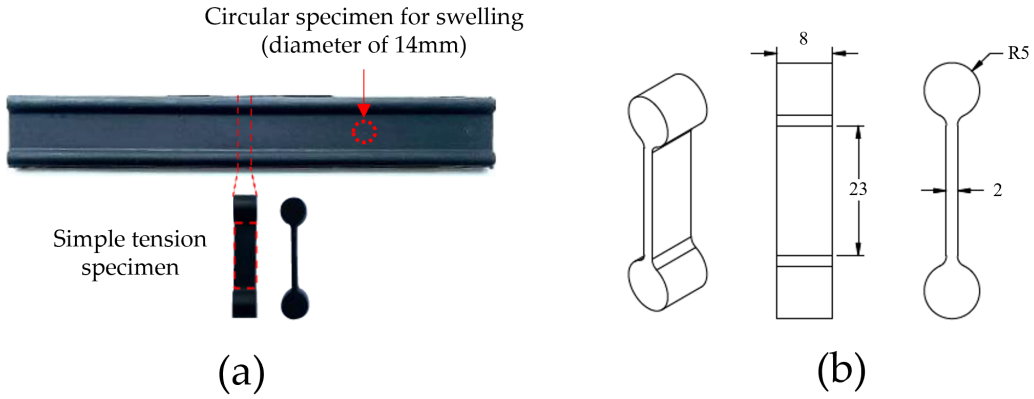

Figure 2.1: Illustration of (a) a pure shear specimen with the cutted swelling and simple tension specimens adapted from [5] and (b) the geometry of a uniaxial tension specimen from [71].

2.2.2 Diabolo specimen

The Diabolo specimen introduced by Ruellan is used in this study [5]. It is denoted "AE40" and refers to as "axy-symmétrique entaillé" in French, with a radius of curvature of 40 mm. The stress and strain are concentrated at the half of its height [5], but complex multiaxial deformation occurs in the vicinity of metallic inserts [184]. The triaxiality level of this type of specimen is slightly higher than 0.33 (uniaxial state) [71]. The geometry of the specimen is presented in Figure 2.2. The metallic inserts are used to mount the Diabolo specimen on the fatigue machine. Rubber is adhered to the metallic insert with a special coating, called "enduction". In addition, before any fatigue test is performed, the molded Diabolo specimens rest for at least 24 hours to stabilize. It is noteworthy that this volumetric geometry is preferred to planar specimens since it is more representative of the industrial rubber parts.

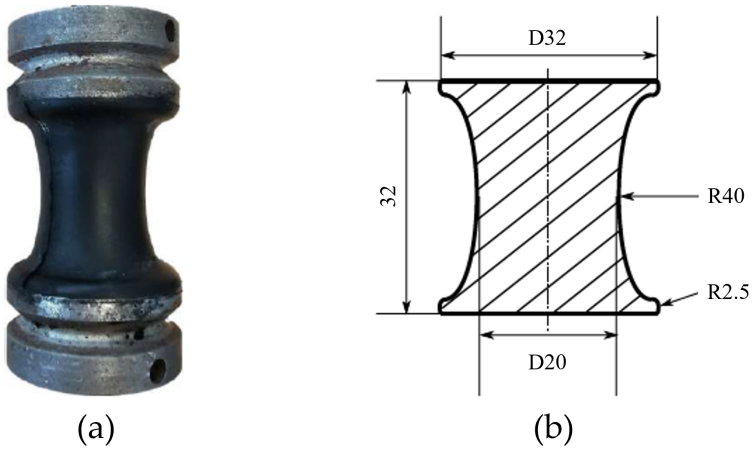

Figure 2.2: Illustration of a AE40 Diabolo specimen in (a) isometric view and (b) its dimensions from [71].

2.3 Mechanical tests and chemical analyses

This section summarizes the experiments conducted to investigate the relationship between the macromolecular network structure and mechanical properties. First, the swelling test used to evaluate the macromolecular network is described. Then, the uniaxial tension tests are presented, highlighting the experimental set-up. Details on calculating stress and strain from the continuum mechanics relation are then given. This section ends with a presentation of the fatigue tests, from the facilities to the data-processing.

2.3.1 Swelling tests

In Section 2.1, a wide range of formulations and vulcanization conditions have been defined. This ensures studying materials with large differences in macromolecular network structure, *i.e.*, active chain density and cross-link length. This section explains how the active chain density, or the cross-link density, is determined. The active chain density corresponds to the number of active chains in moles per unit volume, and is closely related to the cross-link density. There are several techniques that can be used for evaluating the active chain density such as *(i)* stress-strain analysis *(ii)* swelling test *(iii)* nuclear magnetic resonance (NMR) and *(iv)* DMA. Each technique has its own advantages and drawbacks, the interested reader can refer to Ref [53] for more information on their comparison. Considering the large number of materials studied, the swelling test was chosen as it is a good compromise between simplicity, cost and repeatability.

A swelling test consists in immersing a specimen in a "good" solvent. The solvent molecules incorporate in the rubber while filling the free spacing in the macromolecular network. The solvent penetrates the available empty spaces until an equilibrium state is reached. At this point, the network is fully constrained by topological constraints such

as cross-link junction points and entanglements, and no more solvent can be absorbed. Then, the samples are dried, and the solvent trapped in the rubber evaporates. By following the sample's weight during these two successive stages, it is possible to calculate different quantities which are used in the Flory-Rehner relationship to determine the active chain density.

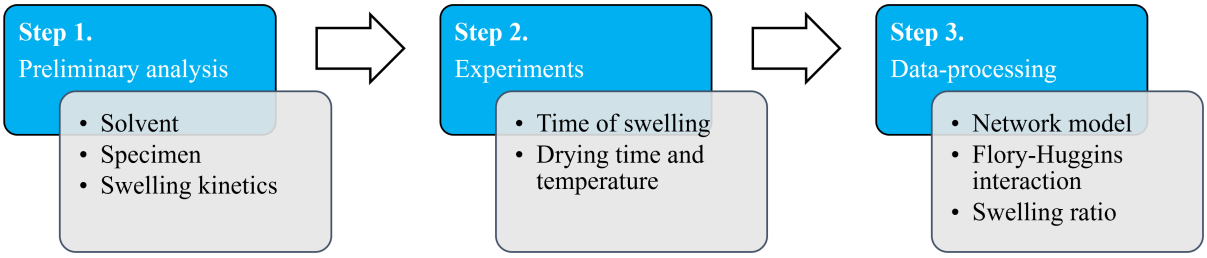

Figure 2.3: Definition of the three steps necessary to perform swelling test.

In practice, a swelling test is generally made with respect to the three steps described in Figure 2.3. First, a preliminary analysis is required to define the appropriate specimen geometry and solvent (Step 1). A swelling kinetics is performed to obtain information in order to define the protocole for the experiments (Step 2). Then, the experiments are made on this basis. Finally, the parameters and assumptions need to be properly defined in order to process the data (Step 3). These steps are addressed hereafter.

2.3.1.1 Preliminary analysis

The choice of the solvent depends on its compatibility with the rubber. For NR, toluene is generally used. A swelling kinetics is necessary to characterize the swelling process during the immersion time. The objective is to reach a plateau, corresponding to the equilibrium. If the time is not sufficient, the calculation of the active chain density may be overestimated. For this reason, one of the unfilled NR, here the $NR^2_{0.2}$, was characterized by measuring the evolution of the weight of the samples during several days, while immersed in a toluene vial in order to determine the equilibrium swelling time. This swellings kinetics is given in Figure A.1, from Appendix A. The crude weight ratio w_t is given as a function of the time of immersion t, calculated with the relation proposed by Ellis and Welding [187]. The swelling kinetics indicates that an equilibrium state is reached around 20 h of immersion. On this basis, an immersion time of 72 h has been chosen. Furthermore, different geometries and initial weight were defined, and showed no differences on the weight measurements. These results are presented in the Appendix A.

2.3.1.2 Experimental procedure

The swelling experiments were performed at the Institute of Chemical Sciences of Rennes (ISCR) of the University of Rennes. They are made by using the circular specimens presented in Section 2.2. The reported values are the average of the weight of three samples.

The specimens of weight w_i are immersed for 72 h in a closed vial of toluene, high performance liquid chromatography (HPLC) grade. Then, specimens are released, and a paper cloth is used to dry the solvent excess from their surface. The weight at swollen state (w_s) is then measured. In order to evaporate toluene trapped in the specimens, they are dried in a vacuum-oven until a constant weight is obtained, typically for 24 h at 60 °C. The specimens are finally weighed at the considered dry state (w_d). The weight is measured with a model XT-220A (Precisa scale) balance. These tests were performed at ambient temperature, without isolating the vial from the light. UV light is known to cause a chemical degradation of unfilled NR and could affects the swelling measurements [188]. However, by looking at the swelling kinetics of Candau on similar materials, the degradation happened only at a relatively long time, around 300 h [123]. Since it is considerably longer than the chosen immersion time, UV exposure is assumed to have no effect.

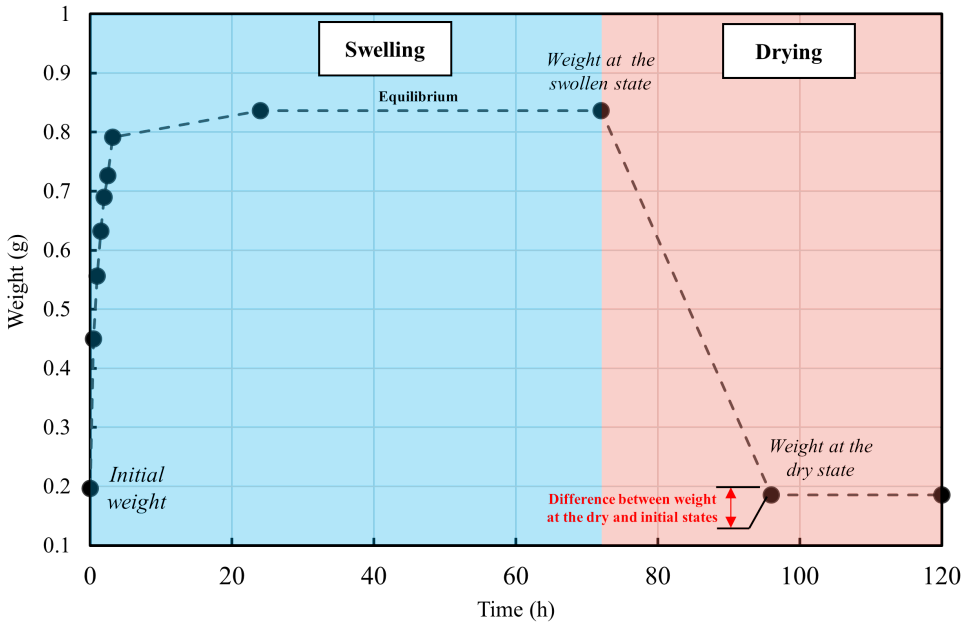

Figure 2.4: Complete swelling kinetics of the unfilled $NR^4_{0.2}$ during several days. The first step (blue area) corresponds to the swelling during 72 h. Then, the second step (red area) consists in two successive drying of the specimens.

An illustration of the complete swelling test of the unfilled $NR^4_{0.2}$ is shown in Figure 2.4. The evolution of the weight during the successive swelling and drying is presented. First, when put into solvent, a very rapid increase in weight occurs during the first few hours and stabilizes. A plateau is then reached. At 72 h, the weight remains the same

as 20 h, indicating that the time of immersion is correct. Then, the specimen is put into the oven. The weight remains the same between 24 h and 48 h of drying. Importantly, a difference is observed between the initial weight and weight at the dry state. This is due to the extraction of soluble components in toluene, *i.e.*, low molecular weight components such as un-reacted rubber chains and accelerator residues.

2.3.1.3 Data-processing

Description of the parameters

Once the tests are performed, the active chain density can be calculated by using the Flory-Rehner relationship [22, 52, 189]. This relation is written as follows (Eq. 2.1) for an affine network [47] assumption :

$$M_c = -\frac{\rho \upsilon_s (\upsilon_r^{\frac{1}{3}} - \frac{2\upsilon_r}{\phi})}{\log(1-\upsilon_r) + \upsilon_r + \chi \upsilon_r^2} \tag{2.1}$$

with M_c the molecular weight between cross-links, ρ the rubber density, ϕ the cross-link functionality, υ_r and υ_s the rubber and solvent volume fraction at equilibrium. For a phantom network [190] assumption, the relationship (Eq. 2.2) is written:

$$M_c = -\frac{\rho \upsilon_s \upsilon_r^{\frac{1}{3}} (1 - \frac{2}{\phi})}{\log(1-\upsilon_r) + \upsilon_r + \chi \upsilon_r^2} \tag{2.2}$$

The calculation strongly depends on the assumptions made. Consequently, it is very difficult to compare results from literature when assumptions are not given. The parameters that require special attention are summarized below:

- **The swelling ratio Q:** it represents the volume expansion of the swollen specimen V_{swo} over the virgin one V_{ini}: $Q = V_{swo}/V_{ini}$. Even if it is generally calculated by using the weight measurement at the initial state, the weight at the dry state is sometimes used instead of the weight at the initial state [188]. This is due to the "soluble components" in solvent affecting the weight measurements. To go further, "non-soluble components" remain in the specimen during swelling, which significantly decrease the weight measurements. Consequently, a correction is generally considered in Q calculation [191].

- **The polymer volume fraction υ_r:** it is equal to the inverse of the swelling ratio: $\upsilon_r = 1/Q$.

- **The Flory-Huggins interaction χ:** it is generally taken as 0.39 [116, 123, 188] for NR-toluene pair. However, it was found to depends on υ_r due to the work of

Horkay *et al.* [192]. Thus, it can be calculated as follows: $\chi = \chi_0 + \chi_1 \upsilon_r + \chi_2 {\upsilon_r}^2$. Further elements are given in the Appendix A.

- **The network functionality φ:** the network functionality gives the number of chains attached to a given cross-link junction point. In most studies, this value is taken as 4, corresponding to tetra-functional cross-links.
- **The network model:** these models dictate how the macromolecular network deforms, and are very important as they strongly affect the calculations. Generally, the affine network model is used.

Assumptions used in this study

The data-processing of the results presented in the following chapters is presented hereafter. The term υ_r is equal to the inverse of the swelling ratio Q. The swelling ratio Q is equivalent to $Q = V_{swo}/V_{dry}$, the volume at the dry state is considered as it takes into account the soluble components in toluene. Finally, the active chain density ν_{ac} is calculated from M_c by using the following relation: $\nu_{ac} = \rho/M_c$.
For Chapter 3, the active chain density is calculated under the assumption of a phantom network model, and with a Flory-Huggins interaction considered dependent on the polymer volume fraction [193]. This is believed to be more representative of the macromolecular network. However, for Chapter 4, since the studies from the literature devoted to SIC used specific assumptions, it was decided to use the same ones in order to facilitate the comparison. Thus, the analysis is carried out by using the Flory-Rehner relationship with the affine network model and a Flory-Huggins interaction equal to 0.39.

Importantly, as ZnO and CB are insoluble in toluene, they lead to a swelling restriction and thereby an overestimation in the calculation of ν_{ac}, when not corrected. As a result, a correction of the insoluble components in toluene is employed. This correction consists in two successive steps. First, the volume fraction of ZnO is corrected in the swelling ratio Q, by using the correction proposed by Valentín *et al.* [188]. Then, the effect of CB is corrected by using the active chain densities values of an unfilled NR, determined with an empirical relationship. More details are given in Appendix A.

2.3.2 Uniaxial tension tests

As different macromolecular network structures imply different mechanical properties, uniaxial tension tests are used to characterize each mechanical response. These responses will be used for modeling purposes, in the following. First, the experimental set-up for both tension and cyclic loading is presented. Then, some elements of the stress-strain relationship are recalled.

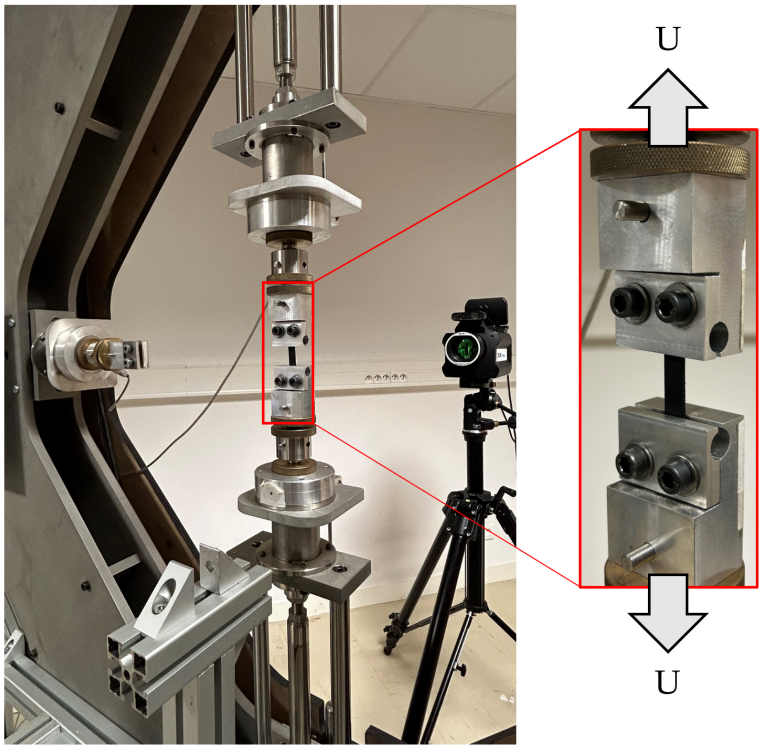

Figure 2.5: Home-made biaxial testing machine used for the the tests.

2.3.2.1 Experimental set-up

Uniaxial mechanical tests were carried out with a home-made biaxial testing machine, presented in Figure 2.5. The tests are prescribed under displacement, specimens being mounted in the vertical direction, and stretched symmetrically. The loading rate is set to $\pm$ 250 *mm/min*. Two types of tests were used to compare the stress-strain response of each material.

- A monotonic tension test: this type of test is performed up to $\lambda = 11$ or until the specimen slides or fails. This type of test provides information on the stiffness and elongation at break.

- A set of five mechanical cycles: it is applied at different levels from λ=1.5 to λ=7.5, with an increment of 1. This cyclic test brings information on the Mullins effect and the mechanical hysteresis loop. Furthermore, such a procedure induces a non-negligeable permanent stretch of the specimens. Indeed, the length of the unbuckled state is then increased. This induce a difference between the prescribed stretch and the actual stretch undergone by the specimen, as shown for instance in similar materials in the recent study of le Cam *et al.* [97]. As a result, a correction of the initial length of the specimens is performed. It should also be noted that for some materials the cyclic stress-strain response deviates from the monotonic stress

response, as initially pointed out by Harwood and Payne [73]. Consequently, in Chapter 3, the cycles performed at a prescribed stretch of 7.5 were not considered for the analysis of the results.

2.3.2.2 Stress-strain relation from continuum mechanics

The output of the quasi-static tension tests is the displacement U and measured reaction force F. From these two mechanical quantities, the nominal stress π, Cauchy stress σ, strain ε and stretch λ can be calculated on the basis of continuum mechanics described by Treloar [47]. In the following, the classical theory of rubber elasticity as well as the Mooney-Rivlin model are described. Since the present study deals with uniaxial tension loading, no information is provided for other loading cases.

Theory of network elasticity

The theory of the network elasticity is based on a gaussian network theory. Two major assumptions are made: *(i)* an affine network deformation and *(ii)* a deformation without volume changes, *i.e.*, $\lambda_1\lambda_2\lambda_3 = 1$. In an orthonormal (x, y, z) reference frame where the principal axes of strain are parallel to the x, y and z axes, the components of chain length change with deformation are $(\lambda_1 x, \lambda_2 y, \lambda_3 z)$. By considering the number of chains per unit volume N, the entropy of deformation ΔS of the macromolecular network is given by:

$$\Delta S = \frac{1}{2} Nk(\lambda_1^2 + {\lambda_2}^2 + \lambda_3^2 - 3) \tag{2.3}$$

By considering that all deformation states have the same internal energy ($\Delta U = 0$) and an isothermal reversible process ($\Delta A = W$), the work of deformation per unit volume W is deduced from Helmholtz relation ($\Delta A = \Delta U - TS$). It is written:

$$W = \frac{1}{2} NkT(\lambda_1^2 + \lambda_2^2 + \lambda_3^2 - 3) \tag{2.4}$$

In the case of uniaxial simple tension, where $\lambda_1 = \lambda$ and $\lambda_2 = \lambda_3 = \lambda^{-1/2}$, the Equation 2.4 becomes:

$$W = \frac{1}{2} NkT(\lambda^2 + \frac{2}{\lambda} - 3) \tag{2.5}$$

The stress for the unstrained configuration, *i.e.*, nominal stress π (F/S_0), is given by Equation 2.6. It is noteworthy that NkT is equal to the shear modulus.

$$\pi = NkT(\lambda - \frac{1}{\lambda^2}) \tag{2.6}$$

Phenomenological model

The previous developments were physically-based. More generally, constitutive model are classified into three types of models, as discussed by Marckmann and Verron [194]. As some deviations were found from the physical model proposed by Treloar, other authors worked on phenomenological model, such as Mooney [195], and Rivlin [196]. The principal strain invariants are equal to: $I_1 = \lambda_1^2 + \lambda_2^2 + \lambda_3^2$, $I_2 = \lambda_1^2\lambda_2^2 + \lambda_2^2\lambda_3^2 + \lambda_3^2\lambda_1^2$ and $I_3 = \lambda_1^2\lambda_2^2\lambda_3^2$. From this, for an incompressible material assumption, Mooney [195] obtained the following relation:

$$W = C_1(I_1 - 3) + C_2(I_2 - 3) \tag{2.7}$$

The relations between the principal stresses and the principal stretches, in a pure homogeneous strain, are obtained by the partial derivatives of W with respect to the principal strain invariants. For the uniaxial simple tension loading case, the stress-strain relationship is given Equation 2.8. The stress for the strained configuration is denoted σ (F/S). For this type of loading, it is related to π with: $\sigma = \pi\lambda$.

$$\sigma = 2(\lambda^2 - \frac{1}{\lambda})(C_1 + \frac{C_2}{\lambda}) \tag{2.8}$$

For more details about the existing constitutive models, the different model types and their relative comparison, the reader could refer to the review written by Marckmann and Verron [194].

2.3.3 Uniaxial fatigue tests

The fatigue tests are defined in order to provide information on both the fatigue resistance and lifetime reinforcement. Consequently, this experiment is very important and had to be well-defined to highlight the lifetime reinforcement. This is described in detail below. It should be noted that main parts of these fatigue tests were defined on the basis of the PhD thesis by Ruellan [5] and Mouslih [71].

2.3.3.1 Fatigue tests facilities

The fatigue tests were carried out using an uniaxial MTS Landmark machine, equipped with a home-made apparatus. It is presented in Figure 2.6. As above-mentioned, AE40 axisymmetric specimen were used for the fatigue tests. Thanks to the home-made apparatus, a total of height specimens can be tested simultaneously. This is of great benefit since it *(i)* drastically reduces the fatigue campaign duration and *(ii)* compensates the inherent fatigue life dispersion and *(iii)* it also contributes to characterize better the fatigue life

dispersion. The reaction force was retrieved individually, which enabled to determine the fatigue life of each sample independently.

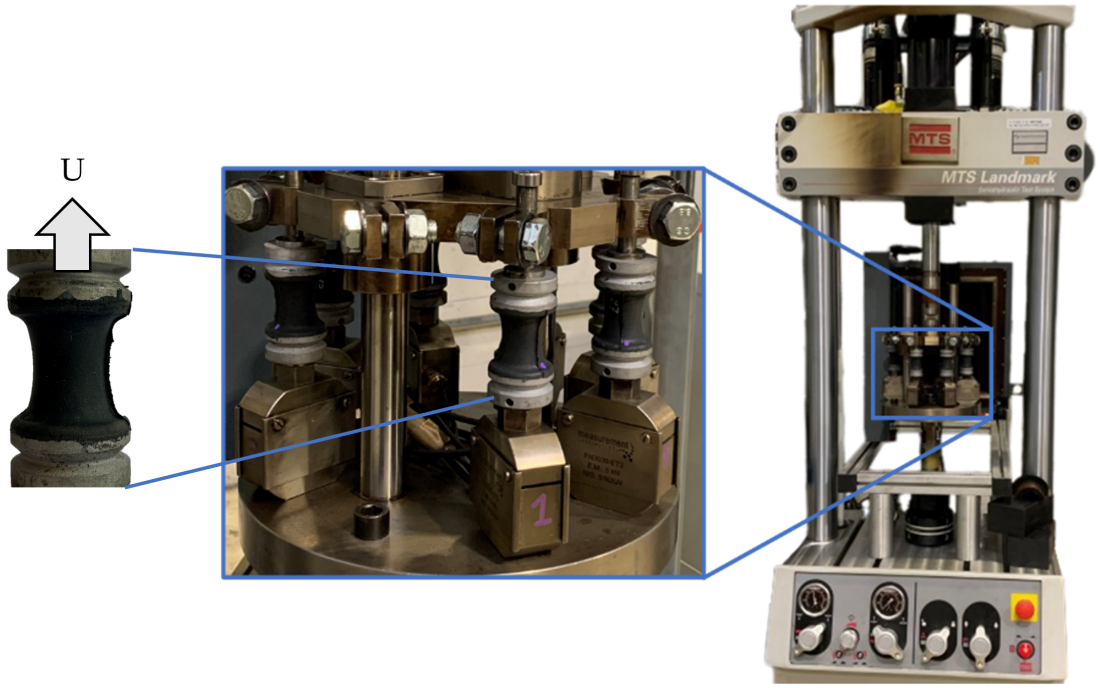

Figure 2.6: Presentation of the fatigue machine used, with the home-made apparatus equipped and a single Diabolo specimen.

2.3.3.2 Experimental procedure

The fatigue tests were conducted under uniaxial tension loading conditions at room temperature. They were prescribed under displacement. In regards to the large number of tests in the present study, two formulations were tested simultaneously, with 4 Diabolos each. Two different loading ratios were applied in order to investigate the lifetime reinforcement. The loading ratios investigated are $R_U = 0$ and $R_U = 0.25$, corresponding to repeated tension and non-relaxing tension loading, respectively. For the sake of clarity, repeated tension loading is denoted "relaxing tension loading" in the following. For each loading ratio, three maximum displacements U_{max} were imposed. The tests were carried out with a frequency ranges from 2 to 4 Hz in order to limit the self-heating at the specimen's surface and to prevent the material from further damage due to additional thermal degradation. For comparable materials, these conditions were found to limit self-heating to 15 °C at the sample's surface [5].

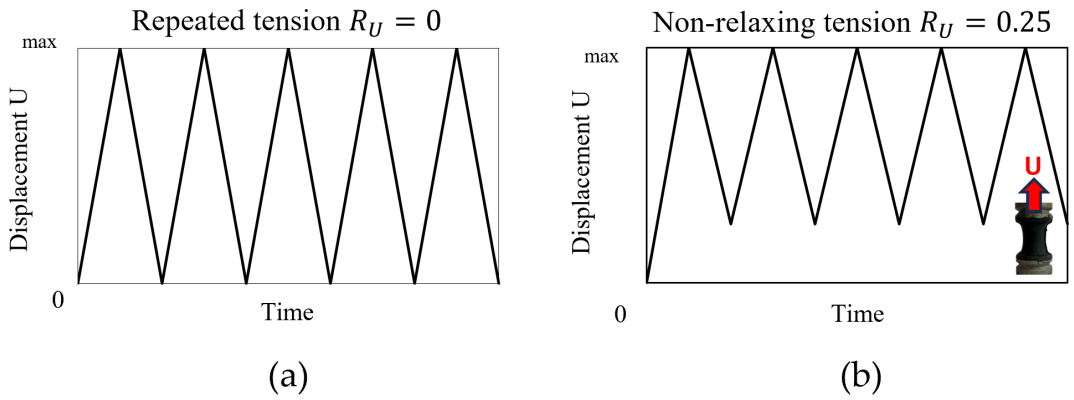

Figure 2.7: Experiments performed: (a) repeated tension loading and (b) non-relaxing loading.

The summary of the testing conditions is given in Table 2.4. It has to be mentioned that other maximum displacements were applied for materials presenting a higher fatigue life at $R_U = 0.25$. In this case, higher displacements were used to reach fatigue lives lower than 10^6 cycles. In practice, the tests were conducted until failure, or stopped at 1.7×10^6 cycles.

Condition	R_U (-)	U_{max} (mm)	U_{min} (mm)	ε_{max} (-)	ε_{min} (-)	**Frequency (Hz)**
1	0	11.31	0	60	0	4
2	0	16.89	0	90	0	4
3	0	23.26	0	120	0	4
4	0.25	16.89	4.58	90	22.5	4
5	0.25	36.79	8.30	172	43	2
6	0.25	45.15	9.57	200	50	2

Table 2.4: Summary of the fatigue tests performed.

2.3.3.3 Representation of the results

The two main approaches generally used to represent the fatigue life of rubber are adopted in this study. An endurance curve is used to account for the effect of the macro-molecular network for $R_U = 0$. Since the physical and mechanical properties of each material are very different, the use of an appropriate predictor is of great importance for the analysis of the fatigue results. The question of the damage predictor is addressed in Chapter 4. Then, a Haigh diagram is chosen to investigate the fatigue properties at both $R_U = 0$ and $R_U = 0.25$ loading conditions, *i.e.*, to represent the fatigue life reinforcement. Before going any further, it is necessary to ensure that the mechanical state of the Diabolo is correctly predicted. This will be discussed in the next Sub-section 2.3.3.4.

2.3.3.4 Prediction of the mechanical state

Predictive models are used to link the stress and strain. The choice of an appropriate model is of major importance to interpret the fatigue results. Finite element analysis (FEA) is used to calculate the mechanical state at any point of the Diabolo. The constitutive model proposed by Mouslih *et al.* is used here [156], since it accounts for the Mullins effect, and showed good predictions of the mechanical state. The nominal stress, or the first Piola-Kirchhoff stress, is defined as the ratio of the force over the initial cross-section area. It is denoted π in the following. Figure 2.8 shows the experimental and predicted stress-strain curves for $NR^2_{0.2}$, $NR^4_{0.2}$ and $NR^6_{0.2}$, which are representative of the active chain density range measured on the formulations used in this study. Note that these tests were performed in the same simple tension specimen as the one used by Ruellan [5] and Mouslih [156] and presented in Section 2.2. As shown in Figs 2.8 (a) and (b), this model accounts well for the Mullins effect, which is of great interest since the Diabolo specimens soften.

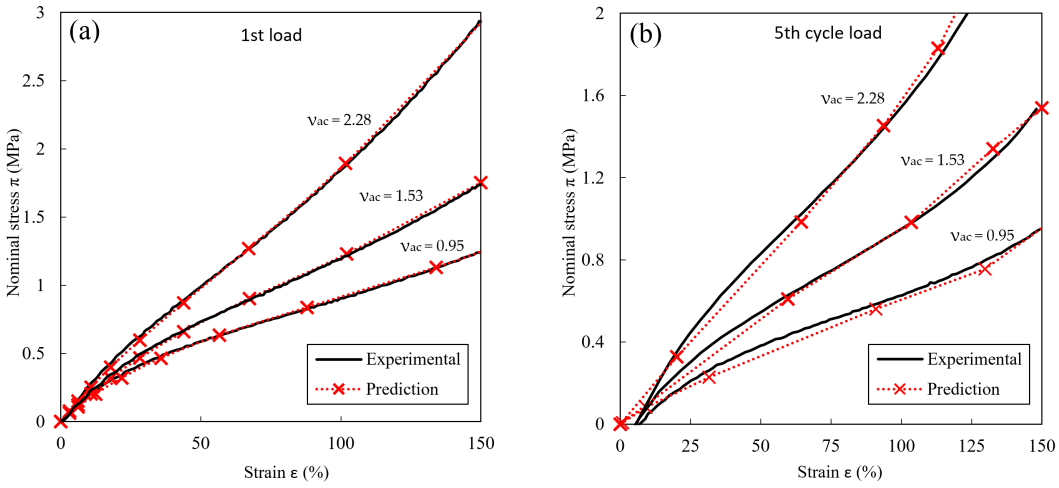

Figure 2.8: The prediction of (a) the 1^{st} and (b) the 5^{th} loads for uniaxial tension.

This model was used to calculate the stress-strain field in the Diabolo specimens. The predicted force was compared to the experimental one to validate the model. Figure 2.9 gives the correlation between the experimental and the predicted reaction forces for each formulation. In these graphs, the predicted and experimental reaction forces are given in X and Y axes, respectively. A perfect prediction is given by the straight dotted line representing x=y. Since all data is within a 10% scatter band, the constitutive model is considered representative of the formulations behavior, and therefore validated for the range of active chain density studied. Thus, the stress and strain can be used to represent the lifetime.

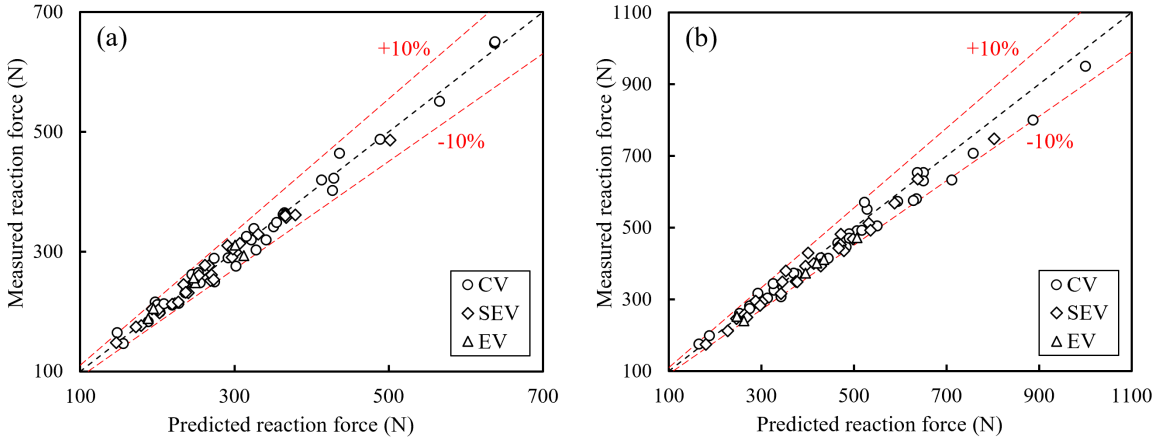

Figure 2.9: Correlation between the measured and predicted reaction force (a) $R_U = 0$ and (b) $R_U = 0.25$. The black dashed line stands for perfect prediction. The red dashed lines represents +/- 10% error.

2.4 Microscopy

A post-mortem analysis was conducted in order to correlate the fatigue life analysis with the damage mechanisms. This study is believed to add a complementary point of view to the fatigue resistance analysis. In this study, two types of microscopes were used for different purposes. The first one is a scanning electron microscope (SEM), which is located in the University of Rennes. The second one is an optical microscope microscope, which is located in Contitech AVS France. They are hereafter described.

2.4.1 Scanning electron microscope

A JEOL IT 300 LA SEM was used to analyze the failure surface with a high magnification. It is coupled with an Oxford Instrument X Max Energy Dispersive Spectrometer (EDSX) probe in order to quantify the atoms present on the specimen surface. This has been used by Ruellan, for instance, to study the chemical nature of defects in the microscopic crack initiation area [5]. Secondary and back-scattered electrons were used for imaging and composition analysis, respectively. In this study, only secondary electron scanning is used to provide information on surface variations.

The specimen preparation was performed with respect to the protocol described by Mouslih [71]. The Diabolo specimens were first cut in order to separate the metallic insert. Then, the failure surface is cleaned by high pressure air-cleaning. Specific subsequent cutting was used to make some slices from 2 to 5 mm. Since secondary electron scanning requires the specimen to conduct electrons, a metallic conductive layer is deposited on the surface. This is made by coating the specimen surface with a thin *Au-Pd* layer of about 2 nm.

In this study, SEM was used as a preliminary analysis in order to verify whether or not a change in macromolecular network could induce a change in damage mechanisms. For this purpose, filled $NR^{2}_{0.2}$, $NR^{6}_{0.2}$ and $NR^{0.8}_{4}$ were selected since they are representative of a wide range of both cross-link length and active chain density. Failure surface analysis did not provide any new information that was not already reported in literature. No new characteristics were discovered on the fracture surfaces. However, it was found that the macromolecular network structure has a strong influence on the different areas such as the final ligament surface, the relative number of SIC markers, and the stable crack propagation area. This justifies the use of the optical microscope, as it is less time consuming and allows a complete characterization of the very high number of specimens to be tested. The optical microscope is described in the following.

2.4.2 Optical microscope

A wide field ZEISS Axio Zoom V16 microscope was used to analyze and observe the characteristic features present on the fracture surfaces. This microscope is equipped with two lenses that provide magnifications ranging from $\times 7$ to $\times 112$ and $\times 16$ to $\times 256$. It is able to deal with non-planar areas due to its ability to perform scans for different depths, and then to reconstruct 2D images. No further preparation was required as the specimens were cleaned with air. Each Diabolo specimen was analyzed and various indicators were studied at both the macro- and- microscopic scales. It should be noted that the stable propagation area, the presence of fatigue striations and their regime, the presence and location of cones, the final ligament surface area and the presence of cavitations will be investigated to analyze our Diabolo specimens.

2.5 First results

The macromolecular structure, *i.e.*, the active chain density and cross-link length, depends principally on the vulcanization system and conditions, but also on the fillers due to their strong interactions with the rubber matrix. The first results concern the effects of the macromolecular network structure on the rheometric behavior, active chain density and stress-strain response under monotonic tension loading conditions.

2.5.1 Rheometric behavior

The rheometric behavior of NR varied as a function of the vulcanization system and conditions, and fillers. Figure 2.10 presents the effect of these parameters on the vulcanization kinetics in a MDR curve, representing the evolution of the torque measured as a function of the vulcanization time. The specimens used are un-vulcanized rubbers, taken at least 24 h after mixing.

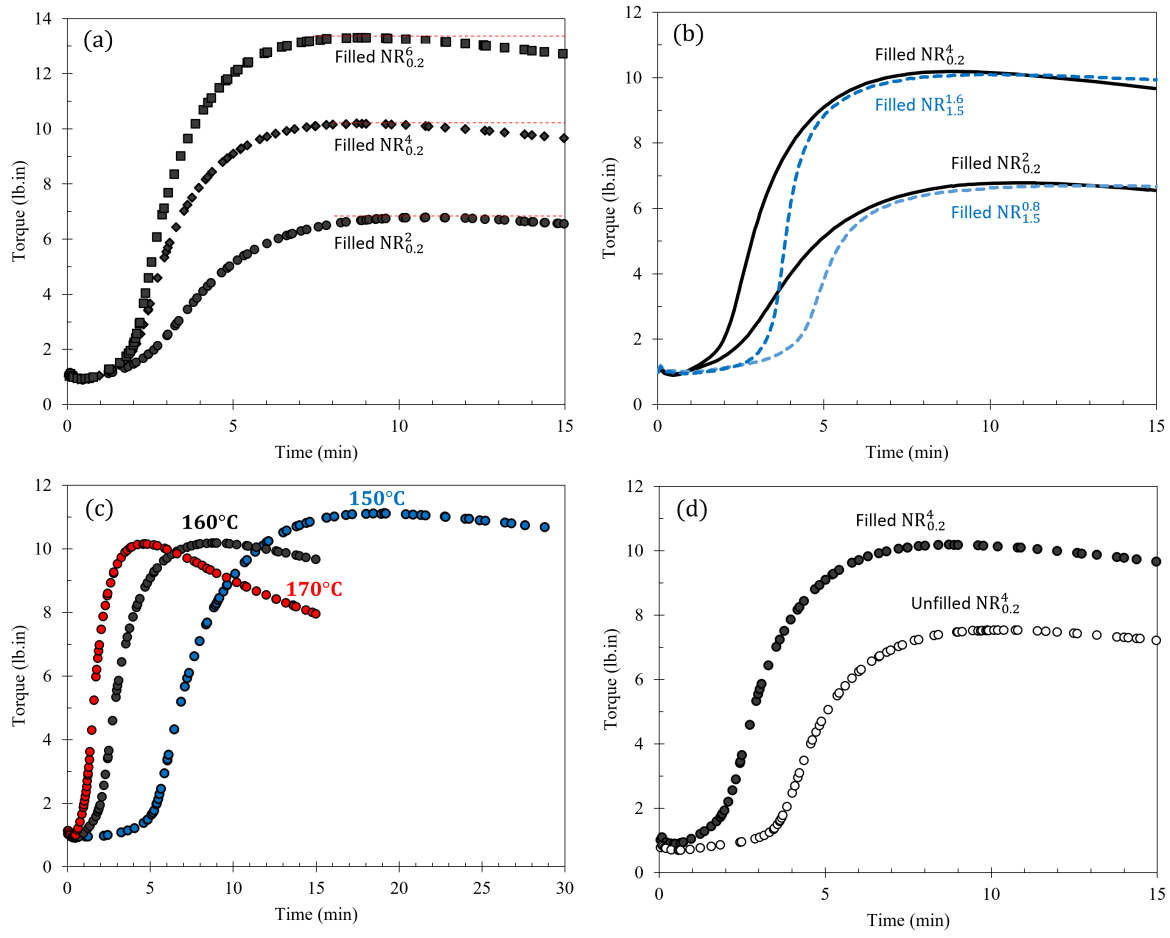

Figure 2.10: Effect of the (a) sulphur and accelerator contents for CV systems, *i.e.*, filled $NR^2_{0.2}$, $NR^4_{0.2}$ and $NR^6_{0.2}$ (b) vulcanization system type for filled $NR^2_{0.2}$ and $NR^4_{0.2}$ (CV) and $NR^{0.8}_{1.5}$ and $NR^{1.6}_{1.5}$ (SEV) (c) vulcanization temperature and (d) fillers for $NR^4_{0.2}$, on the vulcanization kinetics.

Figure 2.10 (a) shows that, for a given [A]/[S], increasing the sulphur and accelerator contents increases the maximum torque achieved. This is expected as more cross-links are created causing a strong stiffening. In addition, it appears that the maximum torque is reached earlier for $NR^6_{0.2}$ than for $NR^2_{0.2}$ with could be due to the higher content of accelerator used. Nevertheless, the latter is more prone to reversion with a decrease in the torque above the maximum torque reached. This indicates that a CV system is very sensitive to the vulcanization time. A comparison of the vulcanization kinetics of CV and SEV systems, having similar maximum torque reached, is presented in Fig. 2.10 (b). A wide plateau is found for SEV systems while CV systems show a decrease in torque. To continue, the higher the temperature, the lower the time needed to reach the maximal torque, for $NR^4_{0.2}$ (Fig. 2.10 (c)). However, at a low temperature of 150°C, the maximum torque is much higher, resulting in a higher number of cross-links formed in the macromolecular network. To conclude, the vulcanization temperature is likely to break the cross-links and reduce the stiffness of the specimen, but it drastically reduces

the vulcanization time. This is consistent with the results of the literature, presented in Chapter 1. Finally, adding CB induces a strong increase in the maximum torque measured, which is due to the increase in stiffness induced by these rigid particles (Fig. 2.10 (d)). In addition, vulcanization operates faster, which correlates with the ability of the fillers to transfer heat.

2.5.2 Active chain density

As above-mentioned, the active chain density is an intrinsic parameter that is evaluated from the swelling measurements. By changing the vulcanization conditions or/and system, this parameter varies as a consequence of a variation of the macromolecular network structure. The effect of the formulation and the vulcanization conditions on the active chain density is addressed here. For the sake of clarity, the active chain density is referred to as ν_{ac}.

2.5.2.1 Vulcanization system effect

The effect of the sulphur [S] content, accelerator [A] content and the [A]/[S] ratio on ν_{ac} is summarized in the diagram presented in Figure 2.11. This diagram enables us to gather all the information about the different vulcanization systems and their effect on ν_{ac}. It is to be noted that ν_{ac} is given in $10^4\,\mathrm{mol/cm^3}$, and for the assumption of an affine network and for χ=0.39. The X and Y axes represent the sulphur and accelerator contents, respectively. The dotted lines represent the different [A]/[S] ratios, which is a qualitative information on the length of the sulphur cross-links. As indicated by the red arrow in the middle of the diagram, the length of the cross-link decreases as the slope of the lines increases. Thus, the five cross-link length investigated in the present study are shown. Then, for a given [A]/[S], the cross-link length is fixed and only ν_{ac} can be varied by sulphur and accelerator contents. This is illustrated by the red arrow below the [A]/[S]=1. For instance, for [A]/[S]=0.2 which corresponds to $NR^2_{0.2}$, $NR^3_{0.2}$, $NR^4_{0.2}$ and $NR^6_{0.2}$, increasing the sulphur and accelerator contents increase in consequence ν_{ac}. This is the case for every other ratios, *i.e.*, 0.6, 1.5, 2.5 and 4. For the materials of the present study, ν_{ac} covers a range from 0.95 to 3.20 $\times 10^4\,\mathrm{mol/cm^3}$. It is noteworthy that a value superior to 2 $\times 10^4\,\mathrm{mol/cm^3}$ corresponds to very highly cross-linked NR, which is consequently very stiff. Further discussion of the effect of ν_{ac} on the stiffness is given in the following Sub-section 2.5.3.

For the sake of clarity, values are compiled in Table 2.5, for the different assumptions used in this study.

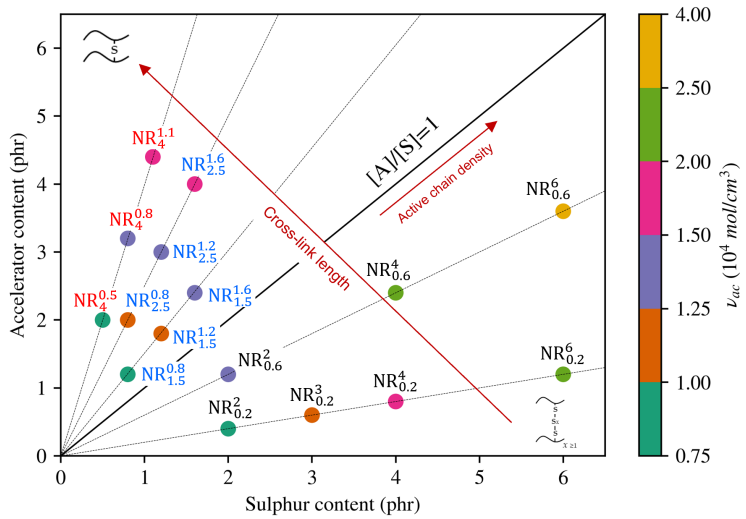

Figure 2.11: Effect of the vulcanization system on ν_{ac} for filled and unfilled NR, vulcanized for condition N°0 in Table 2.3. ν_{ac} is calculated by using the Flory-Rehner relationship with the assumption of an affine network, and for χ=0.39.

A few details concerning the $NR_{1.5}^{0.8}$ and $NR_{0.2}^{2}$ is also given, as they provide some important information of the effect of the vulcanization. As shown in Figure 2.5, these two materials have the same ν_{ac}, even though they have a very different vulcanization system, *i.e.*, cross-link length. Since they have the same maximum torque (Fig. 2.10 (b)), this is very consistent. In fact, this result highlights that for filled $NR_{0.2}^{2}$, within a low content of accelerator, a much higher content of sulphur is necessary to obtain such quantity of active chains. But, for filled $NR_{1.5}^{0.8}$, its significant content of accelerator is known to rapidly decomposed the polysulphide cross-links into shorter cross-links such as mono- and- disulphide cross-links [177]. Consequently, this decomposition increases the overall number of cross-links.

Material	$NR_{0.2}^{2}$	$NR_{0.2}^{3}$	$NR_{0.2}^{4}$	$NR_{0.2}^{6}$	$NR_{0.6}^{2}$	$NR_{0.6}^{4}$	$NR_{0.6}^{6}$
affine network, χ=0.39	0.95	1.26	1.53	2.28	1.41	2.27	3.20
phantom network, χ=f(υ_r)	1.15	1.63	1.97	2.93	1.79	2.96	4

$NR_{1.5}^{0.8}$	$NR_{1.5}^{1.2}$	$NR_{1.5}^{1.6}$	$NR_{2.5}^{0.8}$	$NR_{2.5}^{1.2}$	$NR_{2.5}^{1.6}$	$NR_{4}^{0.5}$	$NR_{4}^{0.8}$	$NR_{4}^{1.1}$
0.95	1.24	1.49	1.11	1.38	1.71	0.95	1.29	1.83
1.15	1.52	1.89	1.38	1.75	2.19	1.20	1.68	2.30

Table 2.5: Summary of ν_{ac}, for vulcanization condition N°0 in Table 2.3. Values are given in 10^4 mol/cm^3, for an affine network model and χ=0.39 in black, and a phantom network model and $\chi = f(\upsilon_r)$ in magenta, respectively.

2.5.2.2 Vulcanization conditions effect

Table 2.6 presents the effect of vulcanization time and temperature on ν_{ac}. For the effect of vulcanization time, filled $NR^{4}_{0.2}$ shows the largest variations of ν_{ac}. Indeed, the lower the time of vulcanization the higher ν_{ac}. At first sight, this result is surprising, but it correlates with the thermal sensitivity of CV system. This is discussed in more detail in Chapter 3. For filled $NR^{1.2}_{1.5}$ and $NR^{0.5}_{4}$, vulcanization time showed only a slight effect. This could be due to the fact that SEV and in particular EV have a very wide plateau before reversing, as illustrated in Sub-section 2.5.1 (Fig. 2.10 (c)). For the vulcanization temperature, filled $NR^{1.2}_{1.5}$ and $NR^{0.5}_{4}$ exhibited the same trend: temperature tends to reduce ν_{ac}. However, for filled $NR^{4}_{0.2}$, it is unlikely that a temperature of 160°C gives a lower ν_{ac} than a temperature of 170°C. This could be due to process issue, and further demonstrates the high thermal sensitivity of long cross-link [40, 43, 59], which could justify why CV are more complicated to manufacture. As above-mentioned, the maximum torque reached for the filled $NR^{4}_{0.2}$ was very similar for 160°C and 170°C.

Condition N°	Time (-)	Temperature (°C)	$NR^{4}_{0.2}$	$NR^{1.2}_{1.5}$	$NR^{0.8}_{4}$
1	t_{80}	160	1.61	1.23	1.34
			2.02	1.55	1.69
2	t_{98} +40% of time	160	1.43	1.22	1.31
			1.82	1.53	1.65
3	t_{98}	150	1.70	1.34	1.38
			2.18	1.60	1.74
4	t_{98}	170	1.63	1.20	1.30
			2.10	1.51	1.65

Table 2.6: Effect of the vulcanization conditions on ν_{ac} for $NR^{4}_{0.2}$, $NR^{1.2}_{1.5}$ and $NR^{0.8}_{4}$. Values are given in 10^4 mol/cm^3, for an affine network model and χ=0.39 in black, and a phantom network model and $\chi = f(\upsilon_r)$ in magenta.

2.5.3 Stress-strain response

As shown in Chapter 1, the stress-strain response of NR can be fully triggered by the vulcanization system and conditions, and the fillers content. The purpose of this sub-section is to investigate the effect of the macromolecular network, *i.e.*, ν_{ac} and cross-link length, on the stress-strain response, for both filled and unfilled NR. For the sake of clarity, each stress-strain responses not provided are given in Appendix B. It is to be noted that ν_{ac} values are given for the assumption of an affine network, and χ=0.39.

2.5.3.1 Filler effect

It is well known that the stiffness of NR can be easily increased by adding fillers [24]. Different vulcanization systems have been formulated with and without fillers, and by varying the cross-link length and ν_{ac}: $NR^2_{0.2}$, $NR^4_{0.2}$ and $NR^4_{0.6}$ for CV, $NR^{1.2}_{1.5}$ and $NR^{1.2}_{2.5}$ for SEV and $NR^{0.8}_{4}$ for EV. Figure 2.12 shows their stress-strain response. From the stress-strain response of each material, it can be seen that the inclusion of fillers has the effect of drastically increase the stiffness. However, this increase in stiffness seems to be much more pronounced for the smallest ν_{ac}. On the macromolecular scale, these rigid inclusions form the filler network, and coexist with the macromolecular network. Their particular and strong interactions are also known to be of great benefit for the mechanical properties [25]. Furthermore, it appears that the elongation at break is not reduced by the addition of fillers, for the smallest ν_{ac}. By increasing ν_{ac}, the unfilled NR with the highest ν_{ac} shows a better elongation at break when filled. This indicates that fillers are of benefit for highly cross-linked NR, as already shown by Hamed *et al.* [55].
These curves also present the strengthening effect that correlates with the SIC phenomenon. This stiffening is easily observable in unfilled NR and happened above $\lambda = 4$. However, for filled NR, this stiffening occurred at lower macroscopic stretch since fillers act as topological constraints and promote SIC [61].

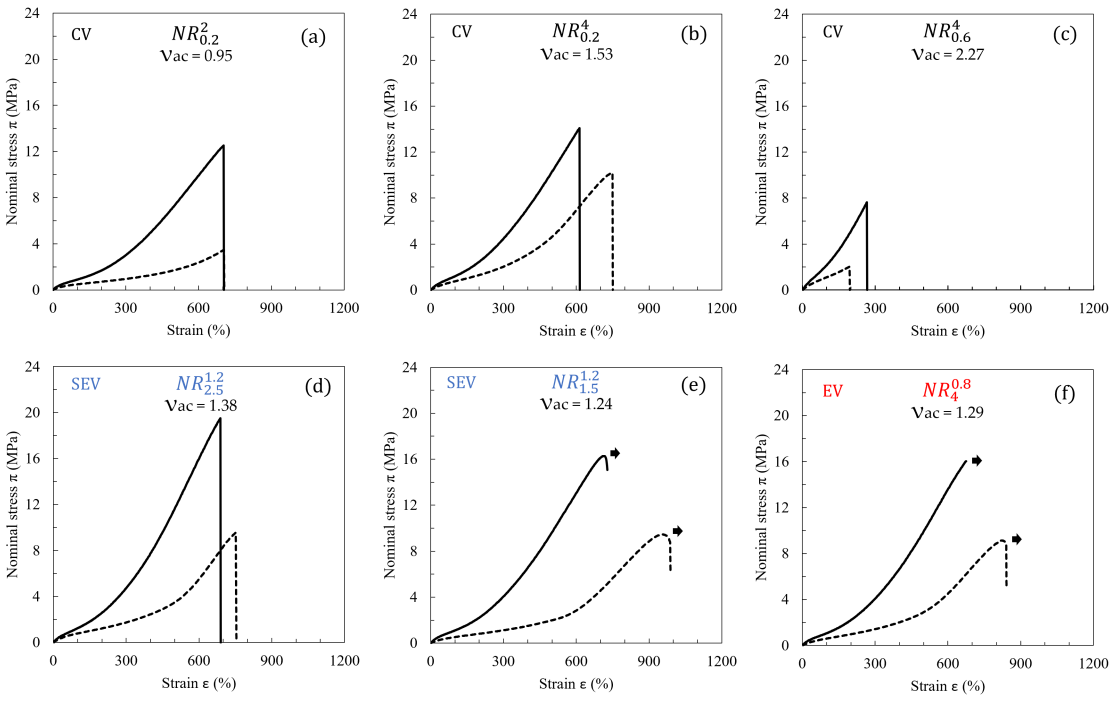

Figure 2.12: Stress-strain response for filled (–) and unfilled (- -) (a) $NR^2_{0.2}$ (b) $NR^4_{0.2}$ (c) $NR^4_{0.6}$ (d) $NR^{1.2}_{1.5}$ (e) $NR^{1.2}_{2.5}$ and (f) $NR^{0.8}_{4}$.

2.5.3.2 Active chain density effect

The effect of the active chain density on the stress-strain response is discussed here for both filled and unfilled NR, for a fixed cross-link length (fixed [A]/[S]). Figure 2.13 presents the stress strain response of (a) the three filled NR with [A]/[S]=2.5 and (b) the three unfilled NR with [A]/[S]=4. For the three filled NR, ν_{ac} triggers the stiffness, leading to a non-negligible increase in stress for a given strain, above 100% of strain. Furthermore, for this range of ν_{ac}, the elongation at break is reduced as ν_{ac} is increased. This demonstrates that, even for filled NR, ν_{ac} can be another parameter to further modify the stress-strain response. In the case of unfilled NR, the effect of ν_{ac} is much more pronounced. In the early percent of strain, the stiffness is already higher for the higher ν_{ac}. Even though the stiffness is higher, the elongation at break is not necessarily better. A perfect example of too high and too low ν_{ac} is drawn here. The unfilled $NR_4^{0.5}$ and $NR_4^{1.1}$ present a lower elongation at break than $NR_4^{0.8}$. On the contrary, the unfilled $NR_4^{0.8}$ can undergo large deformation and its tensile properties are drastically better than the others. This further demonstrates the primary importance of formulation, and ν_{ac} achieved.

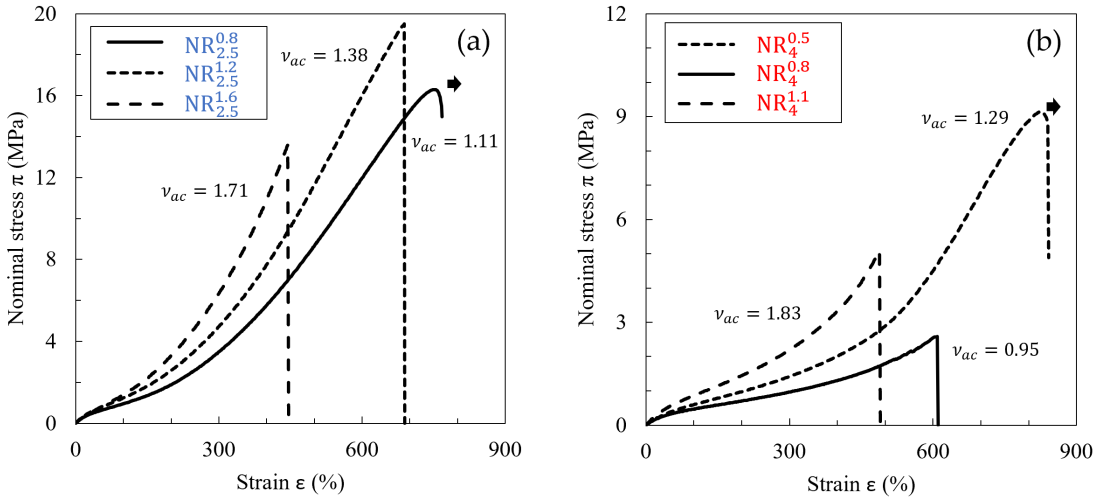

Figure 2.13: Effect of the active chain density on stress-strain response for (a) filled with [A]/[S]=2.5 and (b) unfilled NR with [A]/[S]=4.

2.5.3.3 Cross-link length effect

The effect of the cross-link length on the stress-response is discussed here for both filled and unfilled NR, for different fixed ν_{ac}. Figure 2.14 shows the stress strain response for filled (a) $NR_{2.5}^{1.2}$, $NR_{1.5}^{0.8}$, $NR_{0.2}^{2}$ and $NR_{0.6}^{2}$, and unfilled (b) $NR_4^{0.5}$, $NR_{0.2}^{2}$, $NR_4^{0.8}$ and $NR_{1.5}^{1.2}$.

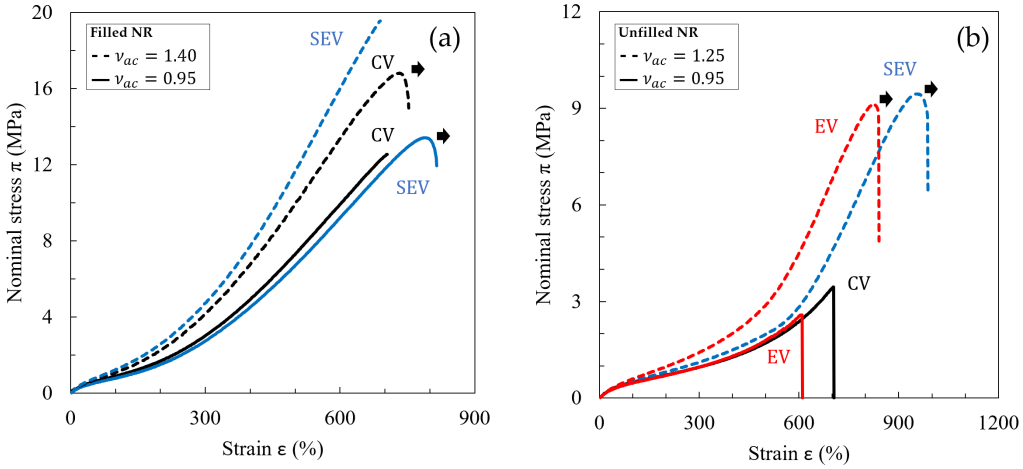

Figure 2.14: Effect of the cross-link length on stress-strain response for (a) filled and (b) unfilled NR, for different ν_{ac}.

For both filled and unfilled NR with a ν_{ac} of 0.95 $\times 10^4$ mol/cm^3, the effect of the cross-link length is negligible. The stress-strain response seems to be mainly driven by ν_{ac}. However, a strong difference in stiffness is obtained for ν_{ac} of about 1.25 $\times 10^4$ mol/cm^3 for unfilled NR. This shows that EV leads to a strong increase in stiffness. This is correlated with the lower chain extensibility limit of short cross-link length [135]. For a filled NR with a ν_{ac} 1.40 $\times 10^4$ mol/cm^3, there is a non-negligible cross-link length effect. Indeed, the SEV is stiffer than the CV. However, this effect seems to be less pronounced than for unfilled NR. In summary, the cross-link length effect depends on ν_{ac} and the fillers. For a ν_{ac} greater than 0.95 $\times 10^4$ mol/cm^3, it is possible to trigger the stress-strain response and to add a little more stiffness, by reducing the cross-link length.

2.6 Conclusion of the chapter

This second chapter of the manuscript presents the materials and the experiments carried out to explore the effect of the macromolecular network structure on the quasi-static and fatigue properties of NR. Formulation and vulcanization conditions were defined and varied to create a large range of macromolecular network structure, *i.e.*, active chain density and cross-link length, for filled and unfilled NR.

Different experiments were performed. The swelling tests were used in order to characterize the macromolecular network, and particular attention has been paid to the correct definition of the assumptions used in the calculations. Uniaxial tension tests were used in order to characterize the stress-strain response for quasi-static loading conditions. Furthermore, these tests are also used for modeling purposes, by following the methodology described by Mouslih [71]. Finally, a fatigue campaign was defined in order to characterize the effect of the macromolecular network on the fatigue resistance. Relaxing and

non-relaxing tension loadings were applied to evaluate the lifetime reinforcement. This fatigue campaign is accompanied by a post-mortem analysis of the Diabolo specimens with the purpose of correlating the damage mechanisms, and more specifically the SIC markers, with the macromolecular network structure.

Chapter 3

How do active chain density and cross-link length influence the Mullins softening in filled and unfilled natural rubber?

Preamble

As discussed in Chapter 2, the mechanical properties of NR depend mainly on the active chain density, the cross-link length and the fillers. This is true for the stress-strain response under monotonic tension loading. However, it is well known that filled NR, and less known that unfilled NR, show a specific stress softening under cyclic loading. This stress softening is called the Mullins effect, or the Mullins softening. This chapter is devoted to the characterization of the mechanical behavior of NR under cyclic loading conditions. Results are analyzed with respect to macromolecular network structure, *i.e.*, ν_{ac} and cross-link length, for filled and unfilled NR. Furthermore, important features and origins such as SIC of the Mullins effect accompanying the stress-strain response are discussed.
This chapter corresponds to an article accepted for publication in ACS Applied Polymer Science.

This chapter is organized as follows. Introduction and Experimental section corresponds to Section 3.1 and 3.2. Section 3.3 presents the results. First, ν_{ac} of each NR formulation is discussed in view of the formulation and vulcanization conditions. Then, cyclic mechanical responses are described and linked to the rubber network structure. The effect of the fillers, ν_{ac} and cross-link length on the stress-strain relation is discussed. Finally, the Mullins effect in both filled and unfilled NR is evaluated. Section 3.4 provides a discussion on the Mullins effect. Concluding remarks are given in Section 3.5.

Abstract

The present study investigates the effect of the active chain density and cross-link length on the Mullins softening in natural rubber by using a wide range of vulcanization systems (conventional, semi-efficient and efficient). For that purpose, sulphur [S] and accelerator [A] contents, as well as their ratio [A]/[S], have been varied. Different vulcanization conditions, corresponding to various time and temperature, have also been tested. In order to investigate how the fillers affect the relationship between the rubber network and the softening, the tests were conducted with the same natural rubber, unfilled and filled with carbon black. The active chain density was determined from equilibrium swelling test by applying the Flory-Rehner relationship and by removing the effect of the insoluble components. The Mullins softening was evaluated from sets of uniaxial tension cycles at increasing maximum stretches. The mechanical response showed that the Mullins softening in unfilled NR is significantly impacted by the active chain density. The higher the active chain density, the higher the softening. Furthermore, our results confirm that the strain-induced crystallization is necessary to induce the Mullins softening. The effect of the cross-link length was found negligible. In the filled NR, the addition of fillers drastically increases the Mullins softening and is the first effect compared to that of the active chain density. Moreover, the vulcanization conditions tested were found to have no significant effect on the softening. This study gathers a large amount of data on the effects of the rubber network and fillers on the Mullins softening and provides therefore information of importance to better model the softening with physically motivated approaches, especially those inspired from the molecular network description.

Keywords: Mullins softening, active chain density, natural rubber, carbon black filler, vulcanization conditions.

3.1 Introduction

Vulcanized rubber is used in many industrial applications for its specific mechanical properties. For instance, carbon black (CB) filled natural rubber (NR) is widely used in the design of antivibratory systems for its good damping and fatigue properties. Under cyclic loadings, rubber exhibits a singular mechanical behavior. When it is stretched to a given stretch and then retracted, less stress is required to re-stretch it to the same stretch. First observed by Bouasse and Carrière in 1903, the softening was then extensively studied by Mullins, which is why the phenomenon has been then referred to as the "Mullins Effect" [69, 70]. The Mullins effect, or the Mullins softening, includes different changes in the mechanical response, that are summarized as follows:

- after a first cycle, a softening appears for stretches lower than or equal to the

maximum stretch previously applied,

- the higher the stretch reached at the first cycle, the higher the softening,
- during the next cycle, the material stiffens as the current stretch is close to the maximum one applied previously,
- when applying a higher stretch than the maximum stretch previously reached, the mechanical response follows the same path as for the virgin material,
- the softening effect is maximal during the first cycle. The mechanical response stabilizes during the first ten cycles at the same stretch, the main softening being observed between the first and second cycles.

The Mullins softening has been observed in many filled rubbers such as NR [72], styrene butadiene rubber (SBR) [74], ethylene propylene diene monomer (EPDM) [75], nitrile butadiene rubber (NBR) [76] and silicone [77, 78], non-exhaustively. Three different physical interpretations of this phenomenon are found in the literature: *(i)* the rubber matrix damaging such as disentanglement, changes in the active chain density[1], rubber chain scission, appearance of cavities, *(ii)* the filler network alteration such as loss of percolation, filler aggregate and agglomerate fracture and *(iii)* the modification of the rubber-filler interface such as bonds breakage at the filler surface, slipping of molecules, desorption/adsorption [74, 81]. For further information on the different explanations summarized above, see for instance Refs [85, 197, 198] for bonds breakage, and Refs [83, 199–201] for the molecules slipping. Furthermore, and more surprisingly, the Mullins softening has also been evidenced in unfilled rubbers such as NR by Harwood *et al.* [79] and NBR by Kakavas [80]. Therefore, among the three interpretations previously mentioned, only the first applies for the Mullins softening in unfilled rubbers. More generally, the fact that the Mullins softening can be observed in filled and unfilled rubbers questions the contribution of the macromolecular network, especially the active chain density and the cross-link length. Several studies reported in the literature investigated the dependency of the Mullins softening to ν_{ac} and cross-link length. For CB-filled SBR with 50 phr, Kraus *et al.* conducted swelling tests in n-heptane before and after various cyclic tests in order to compare relative changes in the volume fraction of rubber at equilibrium with respect to the softening [82]. The softened specimens were obtained by a cycle at 250% of strain, at various strain rates and temperatures. The softening was estimated by a ratio between the area under stress-strain curves of virgin and softened specimens. Their results showed only small changes in the volume fraction of rubber at equilibrium in comparison to the level of softening. Thus, breakage in the SBR macromolecular network is not sufficient to explain the

[1]The active chain density is defined as the number of chain segments of a molecule between successive points of cross-linkage and is denoted ν_{ac} in the following [47].

softening. Dannenberg and Brennan also conducted swelling testswith unfilled SBR, NR and *cis*-polybutadiene, on softened specimens after 3 cycles. They evaluated the softening from the ratio of the area under the loading curves of the virgin and softened specimens [83]. Their results showed no significant changes in ν_{ac} between the virgin and softened specimens, and concluded that the Mullins softening is unrelated to cross-links breakage. Later, Roland studied one NR and five SBR, both vulcanized with peroxide, whose respective ν_{ac} were different. He concluded that the rubber network had no effect on the softening since comparable results were obtained for each materials [84]. However, the six materials in this study do not allow conclusions to be generalized to the case of unfilled NR. More recently, Wan *et al.* showed a dependence of the softening on ν_{ac} for unfilled NR from coarse-grained molecular dynamics simulation [85]. Even more recently, Lin *et al.* also found that ν_{ac} has an effect of on the softening for unfilled NR with [A]/[S]=1 [46]. The authors observed an increase in the softening level with an increase in ν_{ac}.
In view of the results presented in this literature, it appears that only few unfilled NR have been studied, and that the authors have more often varied the rubber network for filled SBR than for NR. Finally, the authors were more concerned about the effect of the softening on the rubber network than for the reverse situation, and the conclusion is that the Mullins effect has only minor effects on the network since it does not change significantly ν_{ac}. However, the results of Lin *et al.* suggest that a possible relationship between ν_{ac} and the softening exists.
This review highlights that the understanding of the macromolecular network - Mullins softening relationship has to be further explored, especially in the case of unfilled NR. To substantially advance the state of the art, a comprehensive characterization of the Mullins softening in different formulations of the same NR, to cover a large range of ν_{ac} and cross-link length, both filled and unfilled NR, must be carried out. This is the aim of the present study.

This paper is composed as follows. Section 3.2 presents the experimental setup and the data-processing. Materials are described as well as the swelling procedure and quasi-static cyclic tests performed. The specimens used for both experiments are presented. The methodology used to evaluate the Mullins effect is precisely explained. In Section 3.3, the swelling measurements are given and the mechanical response of the different NR tested are reported. and discussed according to the active chain density and cross-link length. The Section 3.4 focuses on the relative contribution of ν_{ac}, the cross-link length, fillers and strain-induced crystallization (SIC) to the Mullins softening. Concluding remarks and perspectives close the paper.

3.2 Experimental set-up

3.2.1 Materials

The material considered here is a NR of Standard Malaysian Rubber (SMR) grade. This type of rubber, *i.e.*, *cis*-1,4-polyisoprene is made of more than 98% of *cis*-configuration monomers. As a result, the macromolecules are highly stereoregular. The components of the formulation are given in parts per hundred of rubber (phr), in weight. Some components of the materials studied are common to all of them: 10, 2 and 3 phr of zinc oxide (ZnO), plasticizer, and antioxidants, respectively. In the present study, only vulcanization with N-cyclohexylbenzothiazol-2-sulphenamide (CBS) accelerator and sulphur is studied. In order to change both the cross-link length and ν_{ac}, several vulcanization systems were defined. They were chosen in agreement with the standard distinction proposed by Quirk [23], in which a distinction is drawn between CV, SEV and EV systems. The difference between them lies in the length of the cross-links formed, which is driven by the ratio between the accelerator and the sulphur contents, denoted [A]/[S]. The smaller the ratio, the longer the length of the cross-links formed. For instance, CV are mainly composed of polysuphide cross-links while shorter cross-links such as mono- and- disulphide cross-links are obtained for EV ones. It is noteworthy that cross-link length has an effect on the NR dynamics, shorter cross-links being more restrictive than longer ones [202].
On a first hand, to vary the cross-link length, a total of five content ratios are defined; 0.2, 0.6, 1.5, 2.5 and 4. These ratios were chosen to ensure significant differences in terms of cross-link length. By keeping the ratio constant, it is possible to ensure a fairly identical mean length of the sulphur cross-links [203]. On a second hand, in order to vary ν_{ac}, both accelerator and sulphur contents have been changed while keeping a fixed content ratio. Additionally, in order to evaluate the contribution of fillers relatively to ν_{ac} and the cross-link length, NR has been filled with 20 phr of N330 High Abrasion Furnace (HAF) grade CB. This grade of CB is considered as a reinforcing filler [25]. When filled, 2 phr of plasticizer has been added in order to facilitate the fillers dispersion.
Formulations are given in Table 3.1. The contents of accelerator [A], sulphur [S], the content ratio [A]/[S], and the content of CB are given. The "0 and 20" in the CB content indicates that both unfilled and 20 phr CB-filled formulations exist. It should be noted that CB structure has an effect on the mechanical behavior of NR, and the Mullins softening, see for instance Ref [204]. This is not addressed in the present study.

Vulcanization conditions

The specimens were obtained by a molding process. All the components were incorporated into the internal mixer except those for the vulcanization system, *i.e.*, sulphur and accelerator. They were added during external mixing, in an open-roll mill, to ensure a

Designation	[A]	[S]	[A]/[S]	CB	Vulcanization condition N°	ν_{ac}
$NR^{2}_{0.2}$	0.4	2	0.2	0 and 20	0	1.15
$NR^{3}_{0.2}$	0.6	3	0.2	0	0	1.63
$NR^{4}_{0.2}$	0.8	4	0.2	0 and 20	0	1.97
				20	1	2.02
					2	1.82
					3	2.18
					4	2.10
$NR^{6}_{0.2}$	1.2	6	0.2	20	0	2.93
$NR^{2}_{0.6}$	1.2	2	0.6	20	0	1.79
$NR^{4}_{0.6}$	2.4	4	0.6	20	0	2.96
$NR^{6}_{0.6}$	3.6	6	0.6	20	0	4
$NR^{0.8}_{1.5}$	1.2	0.8	1.5	20	0	1.15
$NR^{1.2}_{1.5}$	1.8	1.2	1.5	0 and 20	0	1.52
				20	1	1.55
					2	1.53
					3	1.60
					4	1.51
$NR^{1.6}_{1.5}$	2.4	1.6	1.5	20	0	1.89
$NR^{0.8}_{2.5}$	2	0.8	2.5	20	0	1.38
$NR^{1.2}_{2.5}$	3	1.2	2.5	0 and 20	0	1.75
$NR^{1.6}_{2.5}$	4	1.6	2.5	20	0	2.19
$NR^{0.5}_{4}$	2	0.5	4	0	0	1.2
$NR^{0.8}_{4}$	3.2	0.8	4	0 and 20	0	1.68
				20	1	1.69
					2	1.65
					3	1.74
					4	1.65
$NR^{1.1}_{4}$	4.4	1.1	4	0	0	2.3

Table 3.1: Materials of the study. They are denoted NR^{J}_{I}, with I the content of sulphur [S] and J the [A]/[S] ratio. For the sake of clarity, designations are classified in accordance with the vulcanization system type: CV, SEV and EV in black, blue, and red, respectively. The formulation is given in phr. Vulcanization conditions are given: N°0 t_{98} at 160°C, N°1 to t_{80} at 160°C, N°2 to $t_{98+40\% \text{ of time}}$ at 160°C, N°3 to t_{98} at 150°C and N°4 to t_{98} at 170°C.

temperature of the mix lower than 100°C in order to prevent the compound from early cross-linking reactions. The specimens were molded at a temperature of 160 °C, and at a time corresponding to t_{98} (condition N°0 in Table 3.1), determined with a rheometer (Rubber Process Analyzer 1000, Alpha Technologies). In the rubber field, rheometry is used to monitor the vulcanization kinetics. In practice, t_{98} corresponds to the time required to reach 98% of the maximal torque measured. This is related to the cross-linking process, its direct consequence is the stiffening of the compound. Time and temperature of vulcanization affect the rubber network formed. A too long vulcanization time is known to cause reversion. This reversion generally has an effect on the stereo-regularity of the macromolecules with *cis* to *trans* structures changes, and can also induce chain scission [13, 177]. For vulcanization temperature, it can be stated that increasing the temperature, for a corresponding optimal time, decreases ν_{ac} and cross-link length [42–44]. This is why, in the present study, filled $NR^{4}_{0.2}$, $NR^{1.2}_{1.5}$ and $NR^{0.8}_{4}$ were also molded with four other conditions in order to vary the vulcanization time as well as the vulcanization temperature; condition N°1 corresponds to an under-vulcanized material, while condition N°2 corresponds to an over-cured one, and condition N°3 corresponds to low temperature (150°C) while condition N°4 to high one (170°C).[2]

3.2.2 Evaluation of the active chain density

In this section, the swelling test procedure is first detailed. Then, the data-processing as well as the assumptions used for the calculation are presented.

3.2.2.1 Swelling tests procedure

The swelling experiments were made by using circular specimens cut with a punch in 2 mm thick sheet of initial weight equal to 0.4 g. The result, *i.e.*, the weight lost, was averaged over three specimens.

The specimens were immersed for 72 h in a closed vial of toluene, high performance liquid chromatography (HPLC) grade. Then, specimens were released, and a paper cloth was used to dry the solvent excess from their surface. The weight at swollen state was then measured. In order to evaporate toluene trapped in the specimens, they were dried in a vacuum-oven until a constant weight is obtained, typically for 24 h at 60 °C. The specimens were finally weighed at the considered dry state. The weight was measured with a model XT-220A (Precisa scale) balance. These tests were performed at ambient

[2]For the over-vulcanized materials, since the torque kinetics strongly depend on the vulcanization system, it would have been trivial to set a time corresponding to a torque value. For instance, CV system tends to rapidly reverse while for EV system, a torque plateau is formed, and it only decreases slightly. Consequently, it is preferred to use an additional period of time, defined as 40% of the total time corresponding to t_{98}. For more details on the effect of the vulcanization system on the vulcanization kinetics, the reader can refer to Refs [12, 45].

temperature, without isolating the vial from the light. UV light is known to cause a chemical degradation of unfilled NR and could affects the swelling measurements [188]. However, by looking at the swelling kinetics of Candau on similar materials, the degradation happened only at a relatively long time, around 300 h [123]. Since it is considerably longer than the chosen immersion time, UV exposure was assumed to have no effect.

3.2.2.2 Data-processing and assumptions

From swelling experiments, ν_{ac} can be calculated by using the following relation: $\nu_{ac} = \frac{\rho}{M_c}$, typically expressed in moles per unit volume [47]. The term ρ denotes the rubber density, and M_c the molecular weight between cross-links. They are obtained by using the Flory-Rehner relationship with the assumption of a *phantom* network model (Eq. 3.1), *i.e.*, cross-links junction points are considered to have a certain mobility [52, 190, 205]. This model is known to be more realistic than the affine network one [193, 203].

$$M_c = -\frac{\rho \upsilon_s \upsilon_r^{\frac{1}{3}} (1 - \frac{2}{\Phi})}{\log(1 - \upsilon_r) + \upsilon_r + \chi \upsilon_r^2} \tag{3.1}$$

with χ the Flory-Huggins interaction [189, 206], Φ the functionality of the rubber network, υ_r and υ_s the rubber volume fraction and the solvent volume fraction at equilibrium, respectively.

For the calculation of ν_{ac}, several assumptions are made. The functionality of the network Φ is taken as 4, which physically corresponds to a cross-link junction point joining on the average 4 rubber chains [10]. For the Flory-Huggins interaction χ, it is not defined as a constant, as it is the case in most studies. Indeed, since the parameter is dependant on υ_r, it is calculated through the relation: $\chi = 0.427 + 0.112\upsilon_r^2$ [203]. υ_r is equal to the inverse of the equilibrium swelling ratio (or degree of swelling) Q. The general assumption for the calculation of Q is to consider the volume at swollen state as the sum of the solvent and the rubber volumes. In this case, taking the initial weight has no signification since it changes during the swelling due to the extraction of the soluble components in solvent. As a result, weight at the dry state is obviously lower than the one of the initial state, and is therefore chosen for the calculations. Soluble components can be un-reacted rubber chains or adjuvants such as antioxidants [203]. It is to note that fillers and activators have an effect on the swelling: they limit the fraction of solvent volume absorbed by the rubber [207–209]. Since all of our materials are composed of 10 phr of ZnO, and 20 phr of CB for filled ones, their are subjected to this restriction phenomenon. The swelling restriction, which leads to an overestimation in the calculation of ν_{ac}, must therefore be taken into account and corrected. As a result, a correction of the insoluble components in toluene is employed. Details and procedure are given in our recent study, see Ref [191].

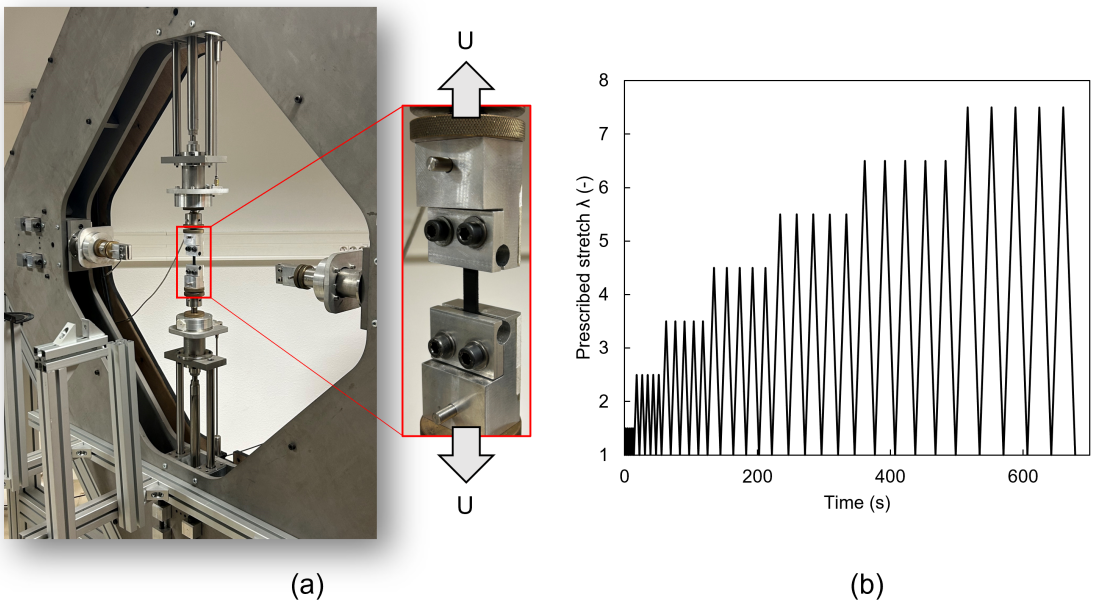

Figure 3.1: (a) Overview of the experimental set-up used (b) stretch-time curve performed at ± 250 *mm/min*.

3.2.3 Procedure for uniaxial tests and specimen geometry

Uniaxial mechanical tests were carried out with a home-made biaxial testing machine (see Fig. 3.1 (a)). 8 mm wide and 2 mm thick specimens were cut with a water-jet cutting device from pure shear specimens. The extremities of the specimens are composed of rolls of diameter equal to 10 mm. The distance between the rolls, *i.e.*, the initial length, is equal to 23 mm. Tests are prescribed under displacement, specimens being mounted in the vertical direction, and stretched symmetrically. Sets of five mechanical cycles are applied at different levels from λ=1.5 to λ=7.5, with an increment of 1 (see Fig. 3.1 (b)). The loading rate is set to ± 250 *mm/min*, which corresponds to strain rate equal to 0.18 s^{-1}.

3.2.4 Evaluation of the Mullins softening

Several methods for evaluating the Mullins softening from the strain-stress response are reported in the literature. Some of them are based on the ratio of stresses [79, 104], some others are carried out in terms of energy [82, 83, 210, 211]. Energy approaches are themselves numerous, especially when successive cycles are performed at increasing strain levels. In 2019 for instance, Lin *et al.* evaluated the Mullins softening from the area that is not common to hysteresis loops of two cycles performed at increasing strain levels [210]. In 2012, Machado and coworkers proposed to quantify the Mullins softening from a ratio between the strain energies brought during the second (W_{2L}) and the first (W_{1L}) loading

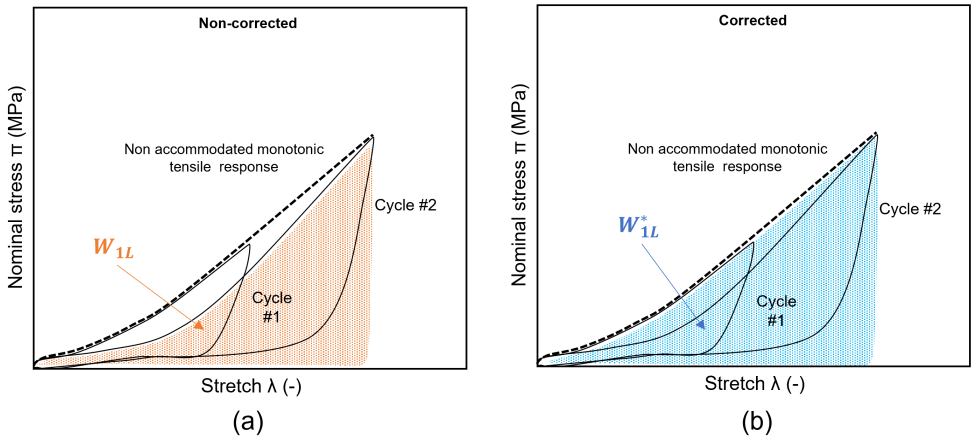

Figure 3.2: Schematic representation of two successive loadings (cycles #1 and #2) at a given stretch, for a material already softened at a lower stretch. The corresponding non-accommodated monotonic first load is given in dashed line. The determination of (a) W_{1L} and (b) W^*_{1L} of the cycle #2 are given with colored areas.

at the same maximum stretch [78]. The area under the loading curves was calculated as follows:

$$W_{iL} = \int_1^{\lambda max} \pi d\lambda, i = 1, 2 \tag{3.2}$$

When sets of cycles are performed at increasing strains, the first load W_{1L} is influenced by the previous load (at a lower strain). To address this issue, the method proposed by Machado *et al.* was subsequently extended to successive cycles at increasing strains by Lachhab *et al.* [212] The method enables us to determine the energy that would be brought during the first loading if no cycle were carried out previously at lower strains. In the present case, only the first load performed at $\lambda = 1.5$ could be estimated by using W_{1L}. Thus, the strain energy of the first load for the higher strain levels is calculated by fitting the monotonic tensile response, which corresponds to the non-accommodated state, as illustrated in Figure 3.2.[3] The corrected value of W_{1L} is denoted W^*_{1L} in the following. This method prevents us from carrying out all the tests independently at each stretch level, with different specimens. Finally, the Mullins softening is evaluated as follows:

$$C_W = \frac{W_{2L}}{W^*_{1L}} \tag{3.3}$$

This ratio quantifies the softening level. For instance, a ratio C_W=1 stands for no Mullins softening. As the ratio decreases, the Mullins softening becomes more pronounced, meaning that a lower quantity of strain energy is needed to reach the same prescribed stretch.

[3]The C_W calculation was limited to $\lambda = 6.5$ since a deviation of the cyclic response from the monotonic tensile response was observed at prescribed stretch of 7.5.

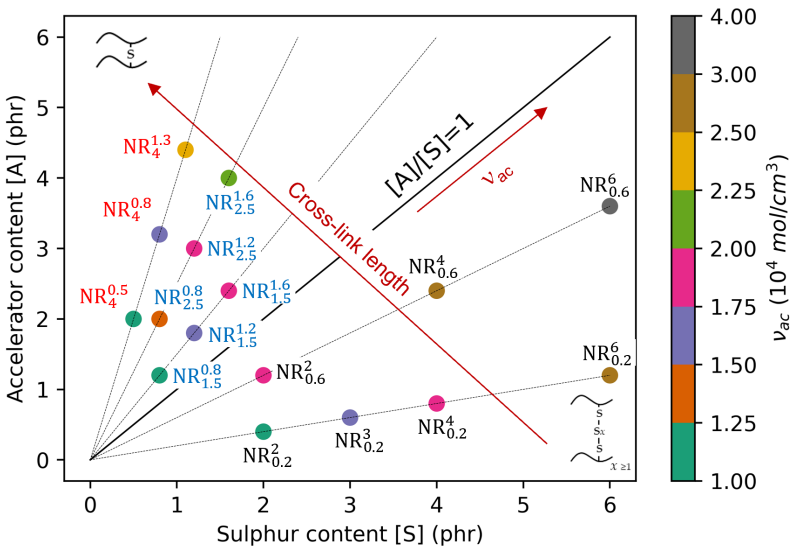

Figure 3.3: Effect of the vulcanization system on ν_{ac} for filled and unfilled NR, vulcanized for condition N°0 in Table 3.1.

3.3 Results

3.3.1 Effect of formulation and vulcanization conditions on active chain density

As above-mentioned, ν_{ac} was calculated from swelling measurements. Changing the vulcanization conditions or/and system, *i.e.*, the sulphur content [S], the accelerator content [A] and the [A]/[S] ratio has an effect on ν_{ac}. These different vulcanization systems are summarized in the diagram first introduced in Ref [191]. This diagram is presented in Figure 3.3, and enables us to gather all the information about the different vulcanization systems and their effect on ν_{ac}. The X and Y axes represent the sulphur and accelerator contents, respectively. The dotted lines represent the different [A]/[S] ratios, which is a qualitative information on the cross-link length. As indicated by the red arrow in the middle of the diagram, the cross-link length decreases as the slope of the lines increases. Thus, the five cross-link length investigated in the present study are shown. Then, for a given [A]/[S], the cross-link length is fixed and only ν_{ac} is changed by sulphur and accelerator contents. This is illustrated by the red arrow below the [A]/[S]=1. For instance, for [A]/[S]=0.2 which corresponds to $NR_{0.2}^2$, $NR_{0.2}^3$, $NR_{0.2}^4$ and $NR_{0.2}^6$, increasing the sulphur and accelerator contents increases ν_{ac}. This is the case for every other ratios, *i.e.*, 0.6, 1.5, 2.5 and 4. The ν_{ac} values of the NR materials of the present study cover a range from 1.00 to 4.00 $\times 10^4$ mol/cm^3. It is noteworthy that a value superior to 3.00 $\times 10^4$ mol/cm^3 corresponds to highly cross-linked NR, which are consequently very stiff.

Details concerning the $NR^{0.8}_{1.5}$ and $NR^{2}_{0.2}$ are also given, as they provide some important information of the effect of the vulcanization. As shown in Table 3.1, these two materials have the same ν_{ac}, even though they have a very different vulcanization system, *i.e.*, cross-link length. In fact, this result highlights that for filled $NR^{2}_{0.2}$, within a low content of accelerator, a much higher content of sulphur is necessary to obtain such quantity of active chains. But, for filled $NR^{0.8}_{1.5}$, its significant content of accelerator is known to rapidly decomposed the polysulphide cross-links into shorter cross-links such as mono- and- disulphide cross-links [177]. Consequently, this decomposition increased the overall number of cross-links. In this case, it is logical that they can have the same ν_{ac} even though they have very different cross-link lengths.
For the effect of vulcanization time, filled $NR^{4}_{0.2}$ shows the largest variations of ν_{ac}. Moreover, the lower the time of vulcanization, the higher the ν_{ac}. At first sight, this result is surprising. The fact that under-vulcanized filled $NR^{4}_{0.2}$ presents a higher ν_{ac} could be explained by the vulcanization process. Indeed, even though the specimens are removed early from the injection molding machine, they are still very hot: vulcanization can continue until the specimens have cooled sufficiently. Nevertheless, it is possible to avoid this effect by cooling the part after vulcanization [182]. Following this idea, the optimally vulcanized filled $NR^{4}_{0.2}$ could already be in the beginning of the reversion area. At this point, the polysulphide cross-links are likely to break. Two competitive phenomena occurred: *(i)* the cross-links decomposition which tends to increase the overall number of active chains and *(ii)* the formation of elastically inactive cross-links such as cyclic polysulphide cross-links [12]. Since ν_{ac} decreased, one can assume that the second phenomenon is predominant. For filled $NR^{1.2}_{1.5}$ and $NR^{0.5}_{4}$, vulcanization time showed only a slight effect. This could be due to the fact that SEV and EV have a very large plateau before reversing.
For the vulcanization temperature, filled $NR^{1.2}_{1.5}$ and $NR^{0.5}_{4}$ exhibited the same trend: an increase in temperature tends to decrease ν_{ac}. However, for filled $NR^{4}_{0.2}$, it is unlikely that a temperature of 160°C gives a lower ν_{ac} than a temperature of 170°C. This could be due to process issue, and further demonstrates the high thermal sensitivity of long cross-link [40, 43, 59], which could justify why CV are more complicated to manufacture.

3.3.2 Effect of active chain density, cross-link length and fillers on mechanical response

A large number of materials has been studied in this work. Consequently, only some of them have been chosen to illustrate the changes induced by the vulcanization conditions, vulcanization system (cross-link length and ν_{ac}), and fillers on the mechanical response. The results not presented here are given in Appendix B. Figure 3.4 present the mechanical responses of the chosen materials. The results are presented in terms of the nominal stress

expressed as a function of the prescribed stretch λ. The nominal stress, or the first Piola-Kirchhoff stress, is defined as the ratio of the force over the initial cross-section area. It is denoted π in the following. For the sake of clarity, ν_{ac} as well as the vulcanization system type (CV, SEV and EV) are also given on the figures. The effect of ν_{ac} and cross-link length on stiffness is shown in Figs. 3.4 (a-f) for unfilled NR and (g-l) for filled NR.

Figs. 3.4 (a), (b) and (c) present the mechanical response of unfilled CV $NR^2_{0.2}$, $NR^3_{0.2}$ and $NR^4_{0.2}$. As these three unfilled NR have similar cross-link length, only ν_{ac} is varying from 1.15 to 1.97 $\times 10^4$ mol/cm^3. As expected, increasing ν_{ac} has the effect of increasing the stiffness. For instance, for a prescribed stretch of $\lambda = 6.5$, the nominal stress is increased by a factor of 3 between unfilled $NR^2_{0.2}$ and $NR^4_{0.2}$, while at lower stretch, the nominal stress is increased by a factor 2. The evolution of the nominal stress as a function of ν_{ac} is shown in Appendix B. For prescribed stretch of 1.5 and 2.5, the nominal stress is linearly related to ν_{ac}, while for 3.5 and 4.5, this relation changed. However, ν_{ac} and consequently stiffness cannot be increased "infinitely", since failure occurs due to the high stiffening. This is why the unfilled $NR^4_{0.2}$ broke for a prescribed stretch of $\lambda = 7.5$. To go further on ν_{ac} effect, the mechanical responses of unfilled EV systems $NR^{0.5}_4$, $NR^{0.8}_4$ and $NR^{1.1}_4$, respectively given in Figs. 3.4 (d), (e) and (f), are examined. These materials have a similar cross-link length, but different ν_{ac} ranging from 1.20 to 2.30 $\times 10^4$ mol/cm^3. The increase in stiffness is once again correlated with the increase in ν_{ac}. The unfilled $NR^{1.1}_4$ broke for a prescribed stretch $\lambda = 6.5$, giving another illustration of the reduction of the elongation at break induced by an increase in ν_{ac}.
For every unfilled NR presented in Figure 3.4, a hysteresis loop forms once the SIC onset is exceeded [62, 63, 65]. Moreover, it is observed that below the SIC onset, non-significant softening occurs. This questions the relationship between SIC and softening in unfilled NR. In their review paper, Diani *et al.* stated that the SIC is necessary for the softening to occur [81]. Thus, our results confirm this statement. Nevertheless, no threshold effect was observed effect in the case of the unfilled NBR studied in [80]. As NBR does not crystallizes under strain, this topic calls for further investigations.

By comparing the mechanical responses in Figs. 3.4 (a) and (j) for $NR^2_{0.2}$, it can be concluded that adding 20 phr of CB fillers - which is relatively low as CB filler can generally be added up to 50 or 60 phr - causes a strong stiffening. Indeed, the stiffness is multiplied by a factor of 3 for the highest stretch. The effect of CB filler on the mechanical response for $NR^{1.2}_{1.5}$ and $NR^{1.2}_{2.5}$ also demonstrated a strong stiffening effect (see Appendix B). Adding CB changed the NR the macromolecular network: at the macromolecular scale, a rubber matrix coexists with a filler network. Strong interactions between macromolecules and CB particles exist [25]. Consequently, CB filler network is recognized to reinforce the NR properties [24]. For example, CB changes the elongation at break and improves the tensile

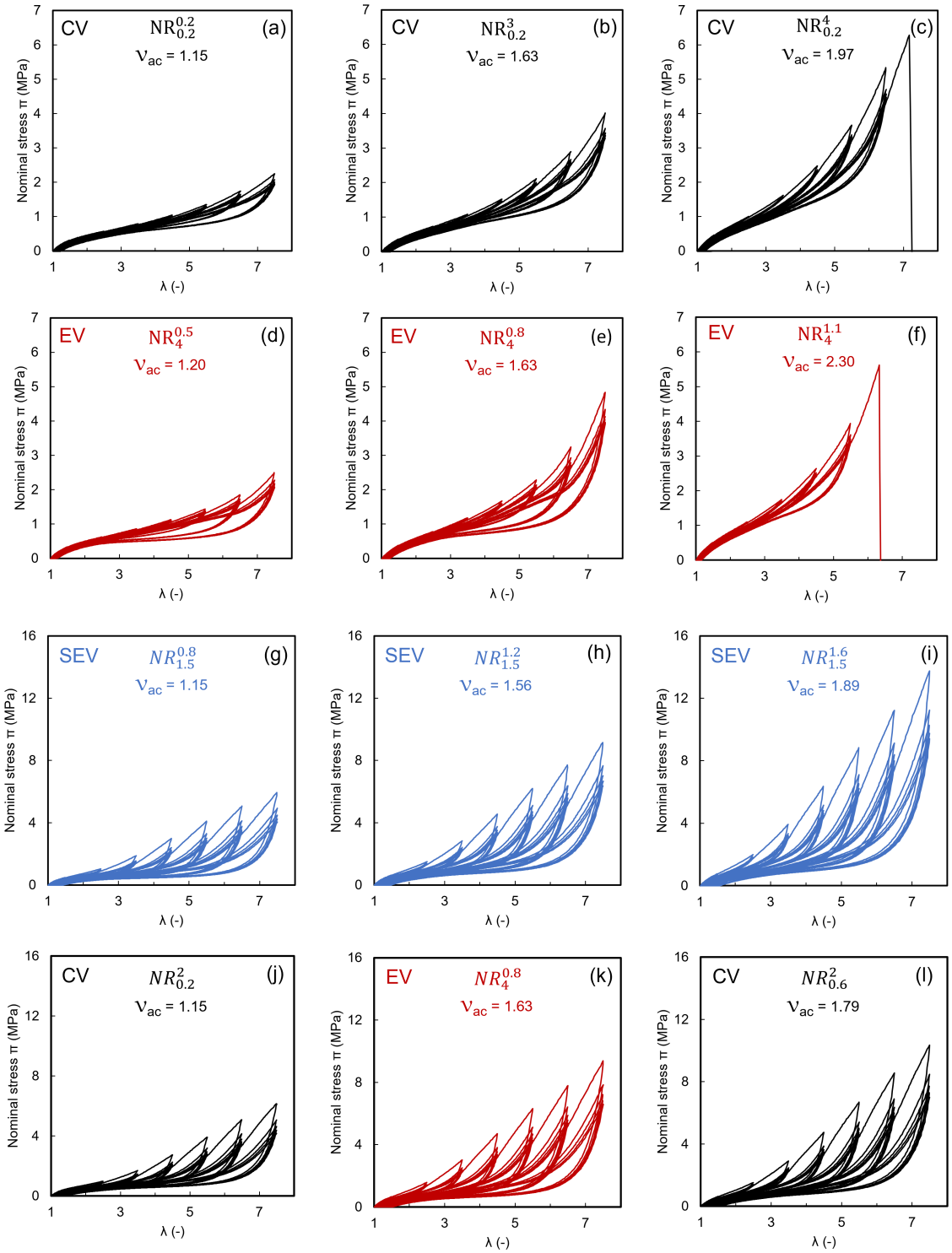

Figure 3.4: Effect of ν_{ac} and cross-link length on the mechanical response for (a-f) unfilled and (g-l) filled NR, plotted in terms of the nominal stress as a function of the prescribed stretch. Designation, vulcanization system type and ν_{ac} are given in the Figures. Two specimens broke (unfilled $NR^{4}_{0.2}$ and $NR^{1.1}_{4}$). The vertical line highlight the stretch at break.

strength, depending on both ν_{ac} and CB content [31]. It should be noted that the tensile properties of highly cross-linked unfilled NR are considerably enhanced by the addition of CB fillers [55].
Furthermore, CB-filled NR also presents a hysteresis in the mechanical response, which begins at around $\lambda = 3.5$. Contrarily to unfilled NR, the physical phenomenon associated with the hysteresis loop is not only due to SIC. In fact, this hysteresis is due to the coupled contribution of viscosity and structural changes such as reorganization of the filler network and SIC [66, 67]. Note that their relative contribution can be quantified by a surface calorimetry analysis during tensile test. For more details, see Ref [68]. It is also to be mentioned that SIC occurs in CB-filled NR, at a certain stretch threshold. For instance, Candau found a $\lambda_c = 3$ and 2.5 for NR filled with 20 and 50 phr of CB, respectively [123]. This is due to the the fact that fillers induce a strain amplification, the higher the filler content the lower λ_c value [61]. Indeed, in the bulk, the local stress is similar to those unfilled while in the vicinity of filler particles, stress is much higher [95].

Figs. 3.4 present the mechanical responses for filled $NR^{0.8}_{1.5}$ (g), for $NR^{1.2}_{1.5}$ (h) and for $NR^{1.6}_{1.5}$ (i), where only ν_{ac} is varied. As previously shown for unfilled NR, ν_{ac} also drives the stiffness for filled NR, with an increase in ν_{ac} leading to an increase in stiffness. Figs. 3.4 (j), (k) and (l) were added to investigate the effect of the cross-link length on the mechanical response. Results indicate that for a low ν_{ac}, stiffness is very similar between CV and SEV ((g) and (j)), which suggests that cross-link length has no effect. For an ν_{ac} of around 1.60 $\times 10^4$ mol/cm^3, SEV and EV also present similar stiffness ((h) and (k)). But for high ν_{ac} ((i) and (l)), SEV is much stiffer than CV, indicating that short cross-link length increased the stiffness. Thus, the cross-link length effect on the stress-strain response depends on ν_{ac}. CB-filled NR having an ν_{ac} of 3.00 $\times 10^4$ mol/cm^3 showed catastrophic failures at low stretch. To conclude, these results quantify how stiffness and deformability of NR can be completely tuned by CB fillers, ν_{ac} and cross-link length.

3.3.3 Mullins softening of unfilled NR

This section is dedicated to the evaluation of the Mullins softening for every unfilled NR. First of all, the softening effect is quantified by using C_W (see Equation 3.3). Then, the C_W values are related to ν_{ac} in Figure 3.5. This Figure maps the effect of ν_{ac} in the case of materials having the longest cross-links (Fig. 3.5 (a)) and the shortest cross-links (Fig. 3.5 (b)), for different prescribed stretches. First, it is observed that the Mullins softening depends on the maximum prescribed stretch, whatever the material considered. For stretch of $\lambda = 3.5$, the C_W values are closed to 1, *i.e.*, a negligible softening. From $\lambda = 4.5$, the ratio started to decrease: the higher the stretch, the lower the ratio. In view of the literature, this result confirms the fact that the maximum stretch applied drives

the Mullins softening for unfilled NR [72]. Furthermore, for each stretch presented here, increasing ν_{ac} leads to a decrease of C_W. This effect suggests that the Mullins softening depends on ν_{ac}, which is in good agreement with the results of Lin *et al.* obtained on unfilled NR with an [A]/[S] ratio of 1 [46]. Comparable results are obtained for the longest (Fig. 3.5 (a)) and shortest cross-link lengths (Fig. 3.5 (b)); ν_{ac} increases the Mullins softening, regardless of the cross-link length. It is noteworthy that there is much more effect for ν_{ac} higher than 1.60 $\times 10^4$ mol/cm^3. It is worth recalling the fact that no Mullins softening occurs before a certain threshold in terms of stretch.
In order to generalize the effect of ν_{ac} on the Mullins softening for every cross-link length, all the results obtained for the 8 materials are gathered in Fig. 3.5 (c), which gives the coefficient C_W as a function of ν_{ac} and the stretch level. As expected, the Mullins softening is confirmed to depend on the maximum applied stretch. The higher the stretch, the higher the softening. Furthermore, the ratio can vary up to 8% between the lowest and highest ν_{ac}, for the highest stretch. This highlights that the Mullins softening depends predominantly on ν_{ac} than on the cross-link length. Hence, the Mullins softening depends on ν_{ac} and stretch for unfilled NR, suggesting that ν_{ac} influences the physical phenomena responsible for the softening. Consequently, it is proposed to model C_W as a function of both the stretch and ν_{ac}. The Y-axis interception decreases as λ increases, and both λ and ν_{ac} drive the slope of the interpolated curves.The following empirical relationship is therefore proposed to link softening: $C_W = a\lambda(\nu_{ac}+1) + b\nu_{ac} + c$, with a=-0.017, b=0.04 and c=1.062. This means that an increase in ν_{ac} tends to reduce C_W, the magnitude of this reduction is directly depending on λ value.

3.3.4 Mullins softening in CB-filled NR

Since ν_{ac} was found to affect the Mullins softening for unfilled NR, it is of first importance to determine whether or not it still has an effect on the softening once the material is filled. This section also examines the effect of vulcanization system and conditions on the softening for filled NR.

3.3.4.1 Vulcanization system

Figure 3.6 (a) presents C_W as a function of ν_{ac}, for filled NR, and for different stretch levels ranging from 2.5 to 6.5. First, it is shown that the Mullins softening depends on the maximum applied stretch, which is in good agreement with the results from the literature [72]. It is perhaps worth emphasizing that *(i)* Mullins softening is sharply higher in CB-filled NR than in unfilled one, for a given stretch and *(ii)* C_W evolves linearly with ν_{ac}, showing that the effect of ν_{ac} depends on whether the NR is filled or not. Thus, these first results contrast sharply with those obtained in the case of unfilled NR. However, the trend in the interpolated scatter-plots reveals a slight decrease of C_W as ν_{ac} increases. In

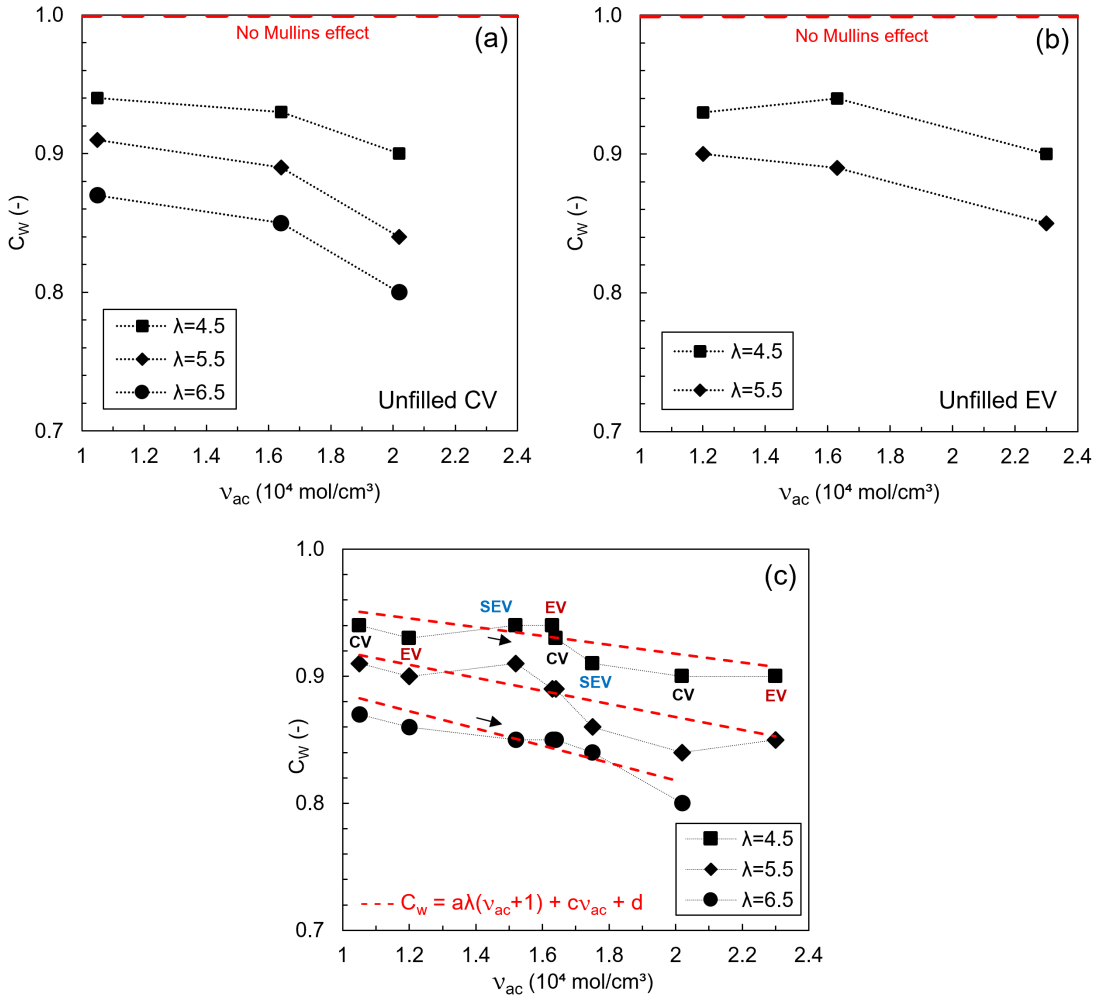

Figure 3.5: Effect of ν_{ac} on the Mullins softening for NR with (a) long cross-links types (CV) and (b) short cross-links types (EV). Dotted red lines correspond to zero Mullins softening, *i.e.*, C_W=1. The effect of ν_{ac} on the Mullins softening for every vulcanization system, *i.e.*, all the unfilled NR tested (CV, SEV and EV) is presented in (c).

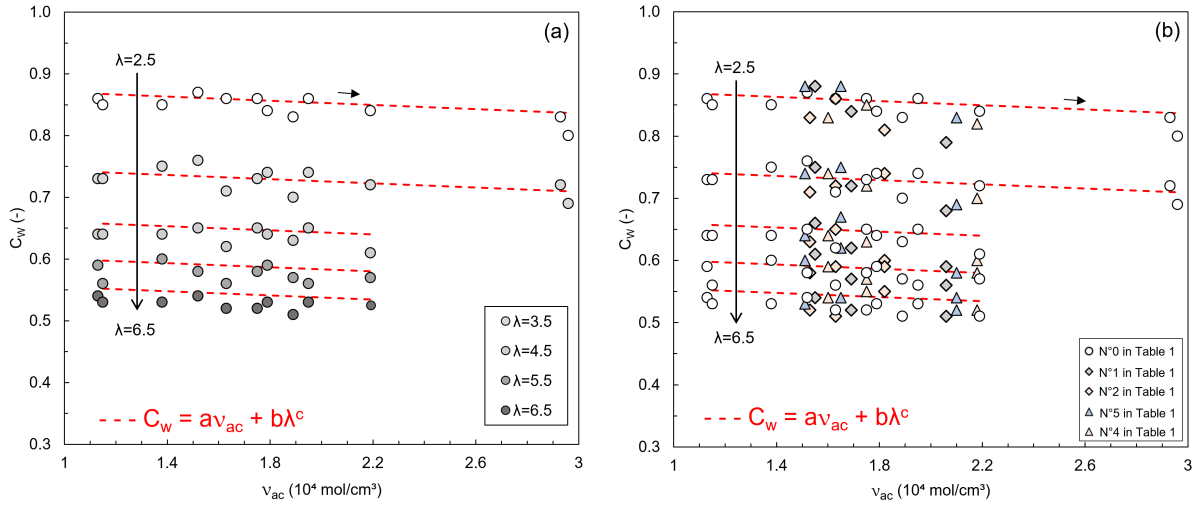

Figure 3.6: Effect of ν_{ac} on the Mullins softening for filled NR vulcanized with (a) condition N°0 in Table 3.1 and (b) condition N°0, 1, 2, 3, 4 and 5 in Table 3.1.

view of the linearity of the results, it is also important to notice that the Mullins softening seems to be independent of cross-link length, which is consistent with the previous results on unfilled NR (Fig. 3.5) (c). Thus, in the case of filled NR, the Mullins softening is mainly driven by the filler effect as well as the maximal stretch applied. Hence, it is proposed to model C_W as a function of these two parameters. The Y-axis interception of the linear trend curves varies as a function of the prescribed stretch. It should be noted that although ν_{ac} demonstrated only a small effect, it was therefore chosen to model it. The following empirical relationship: $C_W = a\nu_{ac} + b\lambda^c$, with a=-0.0158, b=1.3515 and c=-0.46. This relationship shows that an increase in λ value tends to reduce C_W, the magnitude of this reduction is slightly depending on ν_{ac} value.

3.3.4.2 Vulcanization conditions

The results presented previously were obtained with vulcanization conditions corresponding to condition N°0 in Table 3.1,*i.e.*, vulcanization at 160°C during a time corresponding to t_{98}. However, to give a complete understanding of the changes in mechanical properties induced by vulcanization conditions, these parameters are varied accordingly to Table 3.1. Since NR for industrial use are filled, the effect of the vulcanization conditions is only addressed for filled NR. Therefore, this sub-section aims at investigating in which extend the Mullins softening is affected by the vulcanization conditions, *i.e.*, by structural changes induced by variation in the time and temperature of vulcanization. Before presenting any data, few elements concerning time and temperature of vulcanization are recalled.

First, increasing the vulcanization temperature is known to reduce both ν_{ac} and cross-link length [42, 43]. Then, the vulcanization time strongly changes ν_{ac} as vulcanization process lies in cross-linking: increasing the time increases ν_{ac} up to a maximum [45]. But,

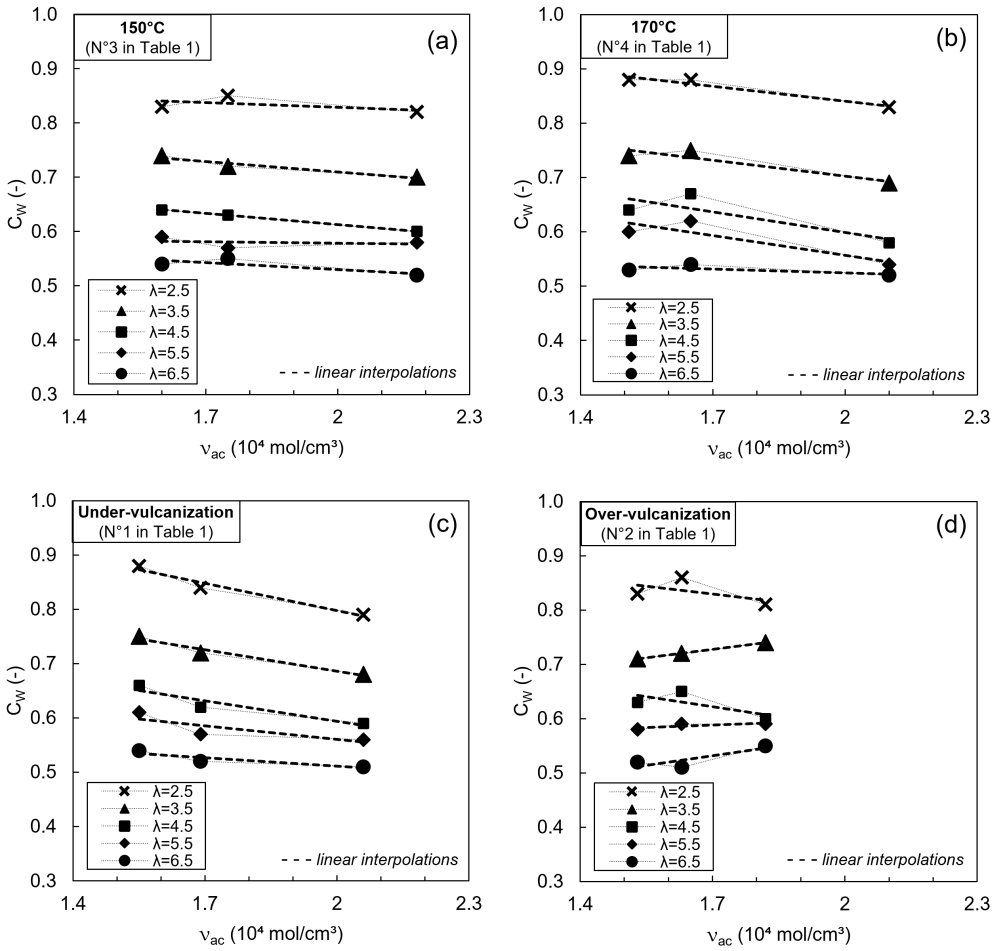

Figure 3.7: Effect of ν_{ac} on the Mullins softening for filled $NR^{4}_{0.2}$, $NR^{1.2}_{1.5}$ and $NR^{0.8}_{4}$ vulcanized with different conditions which are (a) 150°C (N°3 in Table 3.1), (b) 170°C (N°4 in Table 3.1), (c) under-vulcanized at 160°C (N°1 in Table 3.1), and (d) over-vulcanized at 160°C (N°2 in Table 3.1).

once the optimum time has been reached, it is known that other major reactions take place, leading to important structural changes such as the formation of: *(i)* dangling (or pendant) cross-links *(ii)* cyclic cross-links (cross-linking of a same macromolecule) *(iii)* decomposition of polysulphide cross-links into shorter cross-links and *(iv)* cross-links scission [12, 16, 35, 40]. These modifications are generally entered into competition. For instance, a CV system will be more affected by cyclic cross-links and decomposition of polysulphide cross-links into shorter cross-links, while an EV one mainly promotes dangling cross-links. Furthermore, EV systems are also prone to rubber chains modifications such as macromolecular scission. To go further, *cis* isomeric structure can also change into *trans* structure, which directly affects the stereoregularity of the rubber network. For more details, see Refs [12, 35].

Figure 3.7 presents the effect of the vulcanization conditions on the Mullins softening, in the same diagram as those introduced previously. C_W is given as a function of ν_{ac}

and λ, for vulcanization temperature of 150 °C (Fig. 3.7 (a)) and 170 °C (Fig. 3.7 (b)), and also for under-vulcanization (Fig. 3.7 (c)) and reversion (Fig. 3.7 (d)). First of all, vulcanization temperature led to similar results than the ones obtained at 160 °C. Indeed, for both temperatures of 150 °C and 170 °C, the Mullins softening depends slightly on ν_{ac}, and significantly on the maximal stretch applied. However, a vulcanization temperature of 170°C seems to be slightly more affected by ν_{ac}, the trend indicating that an increase in ν_{ac} decreases C_W. Since changing the temperature of vulcanization mainly resulted in changes in ν_{ac} and cross-link length, the results (Figs. 3.7 (a) and (b)) appear to be consistent with these possible structural changes. However, it is difficult to draw more conclusions on these results.

For a vulcanization time higher than the optimal time, the Mullins softening is no longer a function of ν_{ac}. Indeed, C_W varies slightly when increasing ν_{ac} for over-vulcanized materials. This is not the case for the under-vulcanized NR. In this sense, the different phenomena induced by reversion seem to affect the Mullins softening. So, among phenomena induced by reversion, changes in cross-link length is believed not to be the cause. Macromolecule scissions and/or changes in chain conformation, from *cis* to *trans* structures, could more probably be the reason. However, since reversion strongly depends on the vulcanization system type, it is complicated to discuss further about the results. It is recalled that only filled $NR^4_{0.2}$, which is mainly composed of long polysulphide cross-links, shows a strong decrease in ν_{ac} with over-vulcanization.

Thus, an attempt to compare relatively the values of C_W for the different vulcanization times and temperatures was carried out. Figure 3.6 (b) presents the results about the under- and over-vulcanized plotted with those optimally vulcanized, and also results obtained for vulcanization at 150 and 170°C. For each vulcanization conditions, a comparable Mullins softening is obtained.

3.4 Discussion

In order to link the Mullins softening with the rubber network parameters, a 3D plot is proposed to gather them. The X and Y axis referred to as the vulcanization system, *i.e.*, the sulphur and accelerator contents, respectively. The colorbar represents the values of C_W obtained for filled NR ((a), (b) and (c)) and for the unfilled one ((d), (e) and (f)) in Figure 3.8. Each subplot presents the values for a given level of stretch, the latter being indicated in the top right. It is decided to represent the C_W values for λ of 2.5, 4.5 and 6.5. The main analogy between filled and unfilled NR is the fact that they both depend on the maximal stretch applied, even though a much greater softening was obtained for the filled one. However, for unfilled NR, increasing ν_{ac} has the effect of amplifying the Mullins softening. On the contrary, when the same quantity and type of fillers are added, a comparable Mullins softening is finally obtained for each ν_{ac}. This indicates that in the

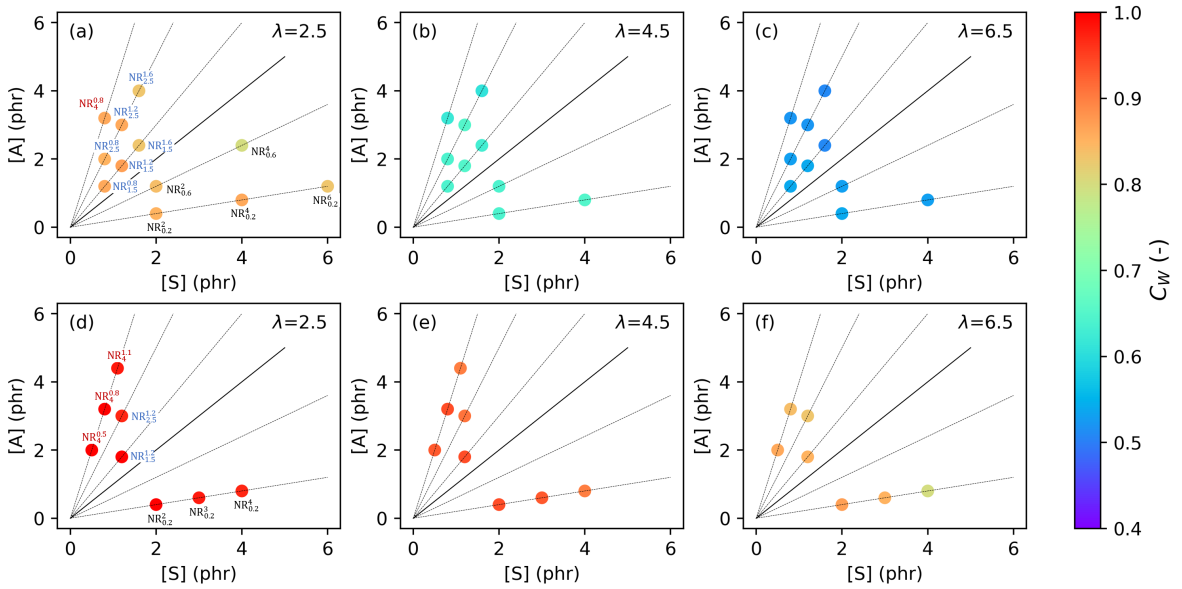

Figure 3.8: Effect of the vulcanization system on the Mullins softening for filled (a, b and c) and unfilled (d, e and f) NR. The colorbar is common to all 4 subplots, and the stretch level is given in the figures. [A] and [S] stand for the accelerator and sulphur contents, respectively.

case of filled NR, ν_{ac} effect is overcome by the filler effect.

Surprisingly, the softening for unfilled NR was not observed below $\lambda = 4.5$. We recall that Diani *et al.* stated that "presence of crystallites is necessary for the occurrence of Mullins' softening in unfilled rubbers" [81], which echoes our results. Considering that SIC starts around $\lambda = 4$ in unfilled NR [65, 92, 116], this suggests that SIC is necessary for the Mullins softening to occur. Furthermore, for an unfilled NR, Zaghdoudi *et al.* observed a significant reduction in softening for a test at 80°C, compared to 25°C, where the crystallinity is considered to be significantly decreased [104]. Thus, SIC seems to be the main condition for the softening to occur. We consider now the reverse situation, *i.e.*, whether or not the softening has an effect on SIC. Several authors performed SIC measurements by X-ray diffraction during cyclic tests. Trabelsi *et al.* observed a strong softening between the first and second cycles, for a CB-filled NR [95]. However, the authors did not measure a significant decrease in SIC and concluded that "the Mullins effect does not play any role during stress-induced crystallization (stretching) and during melting (recovery).". Based on this finding, Diani *et al.* noted that "the Mullins' softening does not affect the strain-induced crystallization". However, Chenal *et al.* showed a non-negligible decrease in SIC, also on a CB-filled NR [61]. The authors attributed this discrepancy to the difference in strain rate and concluded that in the case of Trabelsi *et al.* "the stress in the matrix network is sufficiently low to avoid any important modification of the rubber filler network and consequently of SIC.". More recently, Zaghdoudi *et al.* observed a decrease in SIC for two unfilled NR, and attributed this decrease in SIC to

the breakage of the shorter active chains which "will no longer take part of the stretching process for the subsequent cycles." [104]. In summary, the softening could reduce the SIC, but no consensus has yet been reached. Finally, since our results showed that increasing ν_{ac} increases the softening, we finally ask if a high crystallinity induces a high softening. It is to be noted that ν_{ac} drives the SIC properties [90, 94], which further questions the relationship between SIC and Mullins softening. Zaghdoudi *et al.* showed that the unfilled NR with the higher ν_{ac} has the higher maximum of crystallinity reached, and the higher level of softening [104]. Junkong *et al.* observed a negligible stress softening for synthetic rubber (IR), even though it crystallizes under strain [213, 214]. *A contrario*, the NR showed higher softening and crystallinity level. Thus, the relationship between SIC, ν_{ac} and softening remains an opened question.

In perspective, our results raise additional questions: does the Mullins softening depends on ν_{ac} for higher filler contents? What would be the effect of the filler type? Our results show that the Mullins softening is predominantly induced by fillers. Based on the principle that the Mullins softening is controlled by the deformation level and that adding fillers increases the deformation level, increasing the amount of filler leads to an increase in the Mullins softening. This has already been evidenced in the literature in various articles [72, 73]. Regarding the effect of the filler type and more especially its structure, it has been shown that the amount of different CB types does not lead to the same local amplification and therefore to the same softening (see Ref [204] for further information). Recently, a study by Liang and Nakajima investigated the Mullins softening at the local scale with the Atomic Force Microscopy (AFM) technique [215]. The results showed that for the filler type considered, the interaction mechanisms between the rubber matrix and the fillers depend on the deformation level. The interfacial region between the fillers and the rubber matrix exhibits different softening behaviors at different strains. The fact that the softening increases with the deformation level has therefore to be put into perspective with the fact that the mechanism of softening the interfacial region also changes with the deformation level.

3.5 Conclusions and perspectives

This study explores the effect of the macromolecular network structure, *i.e.*, active chain density and cross-link length as well as vulcanization conditions, on the Mullins softening of NR. Unfilled and filled NR have been considered. The Mullins softening was evaluated from the cyclic mechanical tests by using the ratio of the strain energy of the second cycle over the first one. As expected, the cyclic stress-stretch responses are driven by the active chain density, the cross-link length and CB. The Mullins softening was found to depend on the active chain density for unfilled NR: an increase in the active chain density led to

an increase in the softening level. The sulphur cross-link length has no significant effect on the softening. However, the active chain density had only minor effect on Mullins softening for filled NR. For filled NR, the temperature and time of vulcanization has no significant effect on the softening. This study provides results of importance and a large quantitative database to better model the softening with physically motivated approaches, especially those inspired from the molecular network description.

Chapter 4

Effect of the active chain density and cross-link length on the fatigue properties and damage modes of natural rubber under uniaxial loading conditions

Preamble

This chapter examines the effect of the macromolecular network structure, *i.e.*, ν_{ac} and cross-link length, on the fatigue resistance, for filled NR. As the materials showed very different stress-strain response in the case of quasi-static loadings, they are expected to present significant differences in fatigue life. The post-mortem analysis of the damage mechanisms is also expected to provide information of importance on SIC markers. This chapter is written as a paper to be submitted to International Journal of Fatigue. In the present manuscript, the information already given in Chapter 2 has been removed in order to avoid any redundancy.

This chapter is composed as follows. Introduction and Experimental section are presented in Section 4.1 and 4.2, respectively. Results and discussion are given in Section 4.3, and is divided into three sub-sections. First, the effect of the macromolecular network on the fatigue resistance and damage mechanisms is addressed for relaxing loading conditions. Then, non-relaxing loading conditions and lifetime reinforcement are analyzed. Finally, a discussion on the relationship between ν_{ac}, SIC markers and lifetime reinforcement is provided. Concluding remarks are given in Section 4.4.

4.1 Introduction

NR is a highly deformable material with a remarkable fatigue resistance and good damping properties. For these reasons, it is classically employed for anti-vibratory applications, where the numerous mechanical cycles applied induce fatigue damage. The fatigue properties[1] of NR has been intensively studied since the pioneering work due to Cadwell *et al.* [4], who highlighted the significant lifetime reinforcement when non-relaxing cyclic loading conditions are applied [153, 156, 168]. Since the 2000s, fatigue of rubbers has been reviewed several times [1, 130, 142], and the main factors that govern the fatigue properties have been identified. Among them, ageing [152] and mechanical loading conditions [153] were found the most impacting. The elastomer type, the vulcanization system and fillers were also identified as parameters of primary importance. During the vulcanization process, rubber macromolecules are chemically bonded by cross-links to form a network: it is generally denoted the macromolecular network, or rubber network. In the case of NR (*cis*-1,4-polyisoprene), sulphur is generally used as the cross-linking agent. The parts of macromolecules between cross-links are denoted "active chains" and are characterized by the active chain density. Usually, sulphur is associated with an accelerator, which controls the vulcanization reaction initiation.

Vulcanization system	**[A]**	**[S]**	**[A]/[S]**
Conventional (CV)	0.4 - 3.5	2 - 3.5	0.1 - 0.6
Semi-efficient (SEV)	1.2 - 2.4	1 - 1.7	0.7 - 2.5
Efficient (EV)	2 - 5	0.4 - 0.8	2.5 - 12

Table 4.1: Classification of the vulcanization system proposed by Quirk [23]. Accelerator [A] and sulphur [S] contents are given in parts per hundred of rubber rubber (phr), in weight. For the sake of clarity, CV, SEV and EV are given in black, blue and red, respectively.

The sulphur content [S], the accelerator content [A] and [A]/[S] ratio determine the macromolecular network structure, *i.e.*, the cross-link length and active chain density. It should be noted that the accelerator type also affects the macromolecular network formed [15]. In practice, a low [A]/[S] ratio leads mainly to polysulphide (long) while a high value leads to mono- and-disulphide (short) cross-links. A distinction is generally made between conventional (CV), semi-efficient (SEV) and efficient (EV) vulcanization systems, leading mainly to long, both short and long, and mainly short cross-links, respectively [23]. Table 4.1 recalls the vulcanization system classification according to the range of [A] and [S] contents as well as the range of [A]/[S] ratio. For a given vulcanization system, *i.e.*, given sulphur [S] and accelerator [A] contents, the vulcanization conditions, namely the time

[1]In the present paper, the fatigue properties characterize the ability of the material to preserve the initial mechanical properties under cyclic mechanical loadings.

and the temperature of vulcanization, also influence the macromolecular network structure. On the one hand, a high vulcanization temperature reduces the active chain density as well as the cross-links length by a desulphurization process [40, 42–44]. On the other hand, the vulcanization time directly controls the cross-linking, and thereby triggers the active chain density and cross-link length [12, 13, 35, 41, 216]. The active chain density and cross-link length significantly affect the physical, chemical and mechanical properties of rubbers. For instance, the ageing resistance is enhanced by short cross-links [37, 217, 218] and the static stiffness of the NR increases by increasing the active chain density [13, 219]. To go even further, the SIC ability, which is usually considered as responsible for the fatigue resistance especially under non-relaxing loading conditions, is closely related to the macromolecular network [61, 65, 92, 95, 116, 119, 121]. Moreover, in the early 1950s, Dogadkin and Tarasova were among the first to address the effect of the cross-links length on the fatigue resistance, for unfilled NR and SBR vulcanized with various vulcanization systems [172]. The authors showed that the longer the cross-links, the higher fatigue resistance at room temperature, while the reverse situation is at elevated temperatures. Years later, Yanyo demonstrated that polysulphide cross-links led to a higher crack growth resistance than monosulphide and carbon-carbon ones [173], which confirms the results due to Dogadkin and Tarasova. For the author, longer cross-link increases the active chain mobility. This would allow them to be cyclically stretched and relaxed without breaking. Other authors explained these results by the ability of the cross-links to break and rearrange [130, 174]. According to Beatty, contrarily to polysulphide cross-links, monosulphide ones cannot rearrange themselves at the ultimate local strain, and therefore break [130]. This explanation is close to the one proposed by Bhowmick, who states that both the rearrangement of the cross-links and their scission, before the active chains break, dissipate the strain energy [174]. For Lake and Lindley, the explanation lies in the flexible nature of those long cross-links. This would be responsible for stresses relieving, which increases the energy required to break the active chains of the macromolecular network [175]. Chain slipping phenomenon has also been proposed to explain this increased resistance to failure [176]. For Chan, polysulphide cross-links increase the fatigue resistance by at least a factor two or three compared to shorter cross-links, for relaxing loading conditions [177]. Nevertheless, the author mentioned that the temperature and the strain level have a significant effect on this behavior. As shown by Beatty, the sulphur content, *i.e.*, the active chain density, governs the crack growth resistance for SBR [130]. Chan mentioned that an excessive active chain density increases the sensitivity of NR to fatigue. Hence, this implies the existence of an optimal active chain density for fatigue application [177], as also suggested by Mars and Fatemi [1]. More recently, Grasland showed that for CV systems, the crack growth rate depends on the active chain density [120]. Finally, the vulcanization conditions, *i.e.*, the time and temperature, also affect the fatigue resistance. For SBR, it was shown that increasing the vulcanization time beyond

a certain value has the effect of drastically reducing the crack growth resistance [130]. Furthermore, it seems there is an optimum vulcanization time for the fatigue life, that would correspond to a sufficiently high stiffness and hysteresis [1]. However, for CB-filled NBR, Gehling *et al.* measured that increasing the vulcanization time above an optimal state leads to a decrease in crack growth resistance [182]. The authors also showed that the higher the vulcanization temperature, the higher the crack growth resistance. Finally, CB content and grade affect the fatigue resistance of NR [51, 180, 181].
To summarize, numerous results are available in the literature. Many parameters were found to affect the relationship between the macromolecular network and the fatigue properties, namely the curing time and temperature, the vulcanization system type, the fillers content and grade and the rubber matrix type. Nevertheless, these results were obtained with very different compounds and vulcanization conditions. No study investigates the effect of these parameters, especially a wide range of active chain densities and cross-link lengths on the fatigue resistance of the same elastomer filled with the same filler type and content.
In the present study, a wide range of vulcanization systems (accelerator, sulphurand accelerator-to-sulphur ratio) and conditions (time, temperature) have been considered for the same CB-filled NR. The fatigue properties have been characterized under relaxing and non-relaxing tensile loading conditions. Systematic post-mortem analyses have been carried out to understand the relationship between the fatigue damage mechanisms, fatigue resistance and the macromolecular structure.

The present paper is composed as follows. Section 4.2 presents the experimental set-up: the materials of the study and the specimens geometry, the swelling tests, the fatigue tests facilities and the fatigue loading conditions applied. The section closes with the end-of-life criterion, the prediction of the mechanical state and the choice of the damage predictor. Results are reported and discussed in Section 4.3. Concluding remarks and perspectives close the paper.

4.2 Experimental section

This section presents the material formulations, the active chain density evaluation from swelling tests, the fatigue tests and the fractographic analyses.

4.2.1 Materials

The material considered here is a NR (*cis*-1,4-polyisoprene) of a SMR grade. Components are given in phr. All formulations contain 10 phr of ZnO, 2 phr of plasticizer, 2 phr of stearic acid and 3 phr of antioxidants, respectively. Each material was filled

with 20 phr of N330 HAF CB grade. The vulcanization system is composed of sulfur and CBS as accelerator. Their contents were varied to vary the macromolecular network formed. First, five [A]/[S] ratios were defined to cover a large range of cross-link lengths. It corresponds to 0.2 and 0.6 for CV, 1.5 and 2.5 for SEV and 4 for EV. Then, for a fixed [A]/[S] ratio, [A] and [S] were varied in order to reach various active chain densities for a same cross-link length. For the sake of clarity, CV, SEV and EV will be respectively denoted in black, blue and red in the following. These recipes are in agreement with the standard distinction introduced by Quirk and presented in Table 4.1 [23].
Table 4.2 details the different formulations. They are denoted NR^I_J, with I the sulphur content [S] and J the [A]/[S] ratio, respectively.

Designation	**Vulcanization system**	**[A] (phr)**	**[S] (phr)**	**[A]/[S] (-)**	**CB (phr)**
$NR^2_{0.2}$	CV	0.4	2	0.2	20
$NR^4_{0.2}$	CV	0.8	4	0.2	20
$NR^6_{0.2}$	CV	1.2	6	0.2	20
$NR^2_{0.6}$	CV	1.2	2	0.6	20
$NR^4_{0.6}$	CV	2.4	4	0.6	20
$NR^6_{0.6}$	CV	3.6	6	0.6	20
$NR^{0.8}_{1.5}$	SEV	1.2	0.8	1.5	20
$NR^{1.2}_{1.5}$	SEV	1.8	1.2	1.5	20
$NR^{1.6}_{1.5}$	SEV	2.4	1.6	1.5	20
$NR^{0.8}_{2.5}$	SEV	2	0.8	2.5	20
$NR^{1.2}_{2.5}$	SEV	3	1.2	2.5	20
$NR^{1.6}_{2.5}$	SEV	4	1.6	2.5	20
$NR^{0.8}_{4}$	EV	0.8	3.2	4	20

Table 4.2: Material formulations of the study.

The specimens were obtained by a two-step mixing process. The NR gum and adjuvants were first incorporated into an internal mixer. The sulphur and accelerator were then added in an external mixing, in an open-roll mill, at a lower temperature below 100°C in order to prevent early cross-linking reaction from occurring. The vulcanization conditions, *i.e.*, time and temperature are hereafter denoted t_{vulc} and T_{vulc}, respectively. The specimens were molded at a temperature of 160 °C, at a time corresponding to t_{98}[2], determined with a Rubber Process Analyzer 1000 from Alpha Technologies. For $NR^2_{0.2}$, $NR^{0.8}_{1.5}$ and $NR^{0.8}_{4}$, additional curing temperatures of 150°C and 170°C were used. The

[2] t_X corresponds to the time required to reach X% of the maximum torque measured by a rheometer, during vulcanization.

rheometric behavior being dependent on temperature, the vulcanization times were adjusted to reach t_{98}. Under- and over-vulcanization were also investigated for these three materials[3]. The vulcanization times correspond to t_{80} and $t_{98}+40\%$. These conditions are numbered 1 to 4 and are recalled in Table 4.3. In the following, when the vulcanization condition number is not mentioned, results refer to materials cured for condition N°0 in Table 4.3, *i.e.*, t_{98} and 160°C.

Condition N°	$\boldsymbol{t_{vulc}}$ **(-)**	$\boldsymbol{T_{vulc}}$ **(°C)**
0	t_{98}	160
1	t_{80}	160
2	t_{98} +40% of time	160
3	t_{98}	150
4	t_{98}	170

Table 4.3: Description of the vulcanization condtions investigated for $NR^{2}_{0.2}$, $NR^{0.8}_{1.5}$ and $NR^{0.8}_{4}$.

4.2.2 Active chain density evaluation

The objective of evaluating the active chain density, denoted ν_{ac} in the following, is to provide a quantitative information on the macromolecular network. ν_{ac} was evaluated from swelling test and weight measurements. In practice, for a given initial weight, the higher the weight at swollen state, the lower the ν_{ac} value. The Flory-Rehner relationship, for a affine network assumption and $\chi = 0.39$, as well as a correction for the volume of insoluble components were used to calculate ν_{ac}. This is fully explained in Appendix A.

[3]For the over-vulcanized materials, since the torque kinetics strongly depends on the vulcanization system, it would have been trivial to set a time corresponding to a torque value. For instance, CV system tends to rapidly reverse while for EV system, a torque plateau is formed, and it only decreases slightly. Consequently, it is preferred to use an additional period of time, defined as 40% of the total time corresponding to t_{98}. For more details on the effect of the vulcanization system on the vulcanization kinetics, the reader can refer to Refs [12, 15, 45].

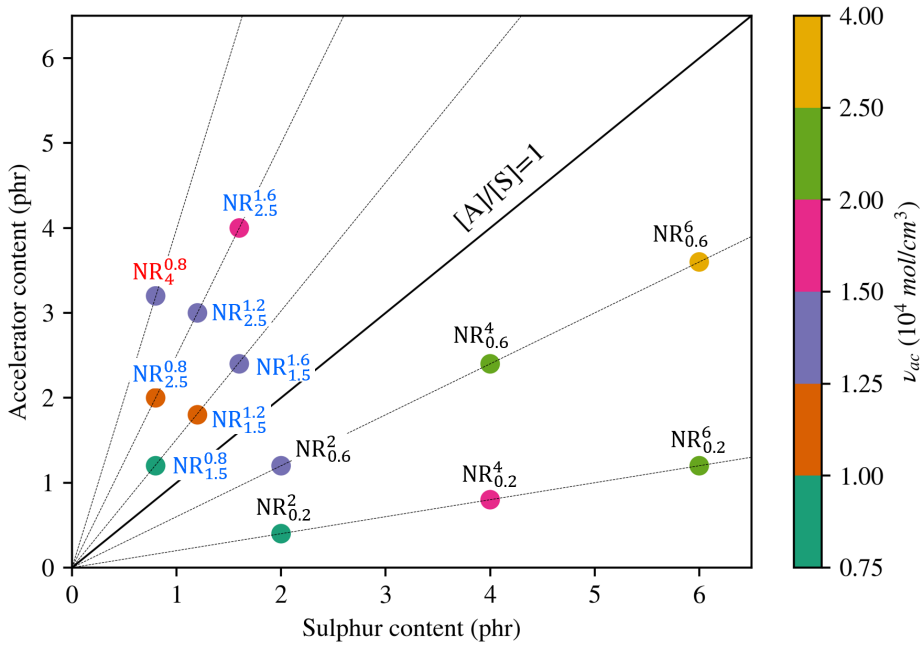

Figure 4.1: Vulcanization system mapping with respect to accelerator [A] and sulphur [S] contents. The qualitative colorscale gives the value of ν_{ac}.

ν_{ac} has been determined for each NR used in the present study. In order to present the results obtained for this large number of materials, ν_{ac} values are reported with respect to the sulphur [S] and accelerator [A] contents and their ratios [A]/[S], as first introduced in Ref [191]. It is given in Figure 4.1, for materials cured at t_{98} corresponding to condition N°0 in Table 4.3. In this figure, the X and Y axes represent the sulphur [S] and accelerator [A] contents, respectively. [A]/[S] ratios are constant along the half lines starting from the origin (0,0). Each material is therefore mapped according to its vulcanization system. ν_{ac} is characterized by the corresponding color level. The associated values are summarized in Table 4.4.

Formulation	$NR_{0.2}^{2}$	$NR_{0.2}^{4}$	$NR_{0.2}^{6}$	$NR_{0.6}^{2}$	$NR_{0.6}^{4}$	$NR_{0.6}^{6}$
$\boldsymbol{\nu_{ac}}$	0.95	1.53	2.28	1.41	2.27	3.20
$NR_{1.5}^{0.8}$	$NR_{1.5}^{1.2}$	$NR_{1.5}^{1.6}$	$NR_{2.5}^{0.8}$	$NR_{2.5}^{1.2}$	$NR_{2.5}^{1.6}$	$NR_{4}^{0.8}$
0.95	1.24	1.49	1.11	1.38	1.71	1.29

Table 4.4: Summary of ν_{ac}. Values are given in $\times 10^4$ mol/cm^3.

The effect of the vulcanization conditions on ν_{ac} are summarized in Table 4.5. It should be noted that the vulcanization time and temperature were found to have a pronounced effect on ν_{ac} for $NR_{0.2}^{4}$. These effects on the fatigue properties are discussed in Section 4.3.

Condition N°	t_{vulc} **(-)**	T_{vulc} **(°C)**	$NR^{4}_{0.2}$	$NR^{1.2}_{1.5}$	$NR^{0.8}_{4}$
1	t_{80}	160	1.61	1.23	1.34
2	t_{98} +40% of time	160	1.43	1.22	1.31
3	t_{98}	150	1.70	1.34	1.38
4	t_{98}	170	1.63	1.20	1.30

Table 4.5: Effect of the vulcanization conditions on ν_{ac} for $NR^{4}_{0.2}$, $NR^{1.2}_{1.5}$ and $NR^{0.8}_{4}$.

4.2.3 Fatigue tests

As mentioned in the preamble, the fatigue test facilities,the Diabolo specimens, the experimental procedure, the diagrams used to represent the results and the prediction of the mechanical state were presented in Chapter 2. For the sake of clarity, they are not recalled here. However, the definition of the end-of-life criterion as well as the choice of the damage predictor are detailed in the following.

4.2.3.1 End-of-life criterion

The end-of-life criterion can be defined as the loss of the specimen mechanical properties, which generally coincides with the appearance of the crack at its surface. It is similar to the one used in Ruellan *et al.* [5]. In practice, it corresponds to the development of a crack whose length is lower than 5mm [5, 156]. Figure 4.2 shows the evolution of the maximal reaction force during a fatigue test with a $NR^{4}_{0.2}$ specimen, and for the loading condition n°1, *i.e.*, relaxing tension at a maximal strain equal to 60%. Three steps are observed in the evolution of the reaction force during the test: *(i)* a slight decrease in the force at the beginning of the test corresponding to the stress softening, *(ii)* the stabilized maximal force state, which corresponds to the major part of the lifetime of the Diabolo specimen and *(iii)* the drop of stiffness. The end-of-life N_i is defined as the last cycle of step 2, *i.e.*, before the drop of stiffness.

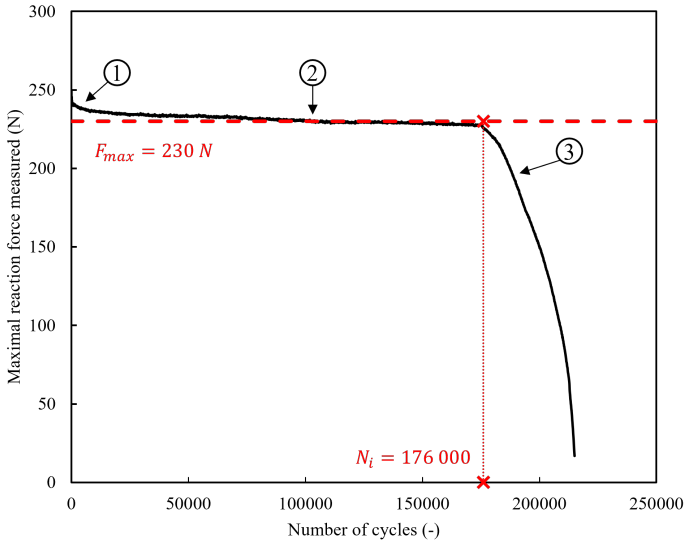

Figure 4.2: Evolution of the maximal reaction force over the number of cycles, for relaxing tension loading at $\epsilon_{max} = 60\%$, and for $NR^4_{0.2}$.

4.2.3.2 Choice of the damage predictor

In the case of uniaxial fatigue loading, different continuum quantities were used in the literature such as the maximum stress σ_{max}, the maximum strain ϵ_{max} and the strain energy density W_{strain} [157]. It is to be noted that these mechanical quantities unify the fatigue results in the case of proportional loading [157]. σ_{max}, ϵ_{max} and W_{strain} were calculated by FEA, and then compared in order to choose the damage predictor that will be used in this study. The comparison is again made on $NR^2_{0.2}$, $NR^4_{0.2}$ and $NR^6_{0.2}$ as they cover a large ν_{ac} range, and consequently very different stiffnesses. Figure 4.3 presents the fatigue life of the three materials with respect to (a) the maximal Cauchy stress σ_{max}, (b) the maximal strain ϵ_{max} and (c) the strain energy density W_{strain}, for relaxing tension loading conditions. The maximum stress and strain energy density show similar results and led to similar trends. However, the endurance curve plotted with respect to the maximal strain shows strong differences. Indeed, $NR^2_{0.2}$ is found to be greatly superior to $NR^4_{0.2}$ and $NR^6_{0.2}$. As the tests are prescribed under displacement and the constitutive behaviors are different, the responses in terms of stresses differ. The maximum Cauchy stress accounts for this effect, thus it is used to compare the different materials used in the present study[4].

[4]It should be noted that ν_{ac} drives the stiffness [47, 50], further demonstrating the close relationship between the macromolecular network and mechanical behavior.

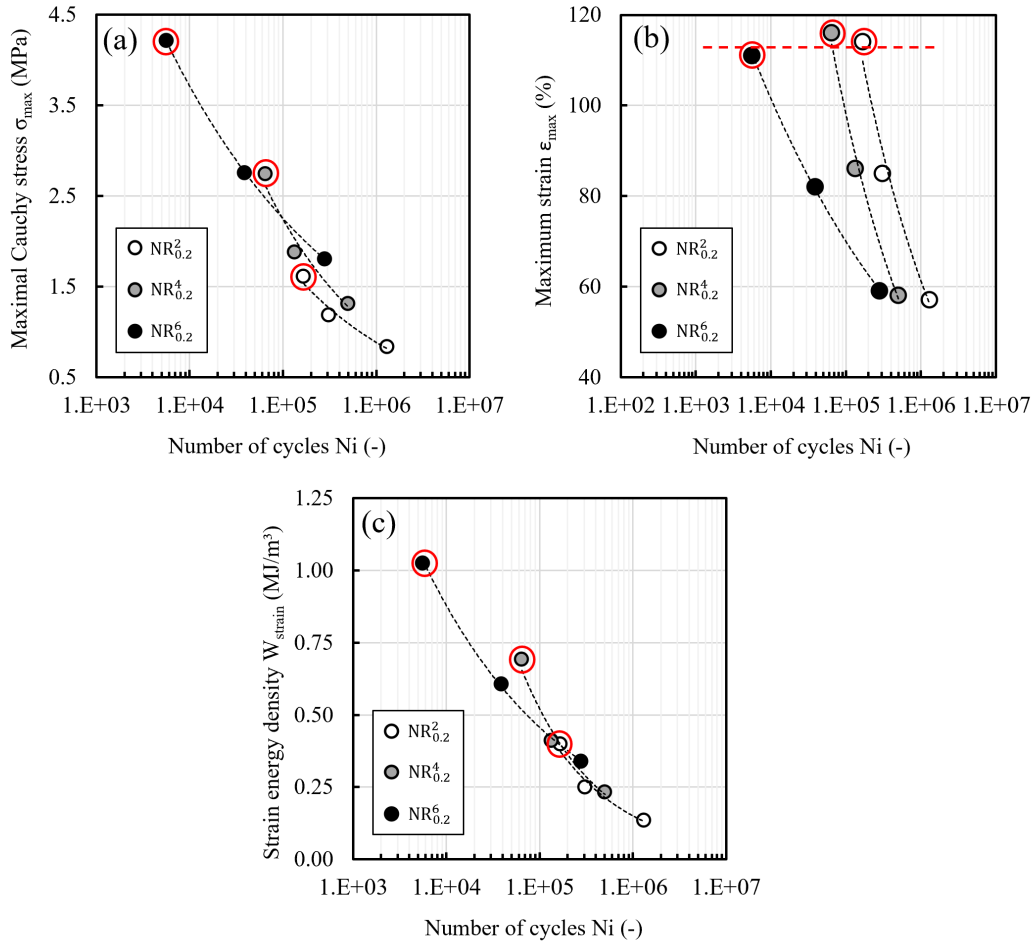

Figure 4.3: Endurance curves for the $NR^2_{0.2}$, $NR^4_{0.2}$ and $NR^6_{0.2}$ by using (a) the maximal stress σ_{max}, (b) the maximal strain ϵ_{max} and (c) the strain energy density W_{strain} as a damage predictor.

4.2.4 Microscopy

Microscopy was used to analyze the failure surface of the fatigue-tested Diabolos to provide additional information on the damage mechanisms and the effect of the materials. The fatigue damage mechanisms of NR under both relaxing and non-relaxing tension were already well-established, and highlight the strong influence of SIC. The present post-mortem analysis study does not aim to revisit the damage mechanisms of NR, but rather to investigate the extent to which the SIC markers form in relation to the macromolecular network structure, *i.e.*, ν_{ac} and cross-link length. The experimental procedure is first described before standard damage mechanisms are described.

4.2.4.1 Experimental procedure

A wide field ZEISS Axio Zoom V16 optical microscope was used to analyze and observe the fracture surface features. Each Diabolo specimen was analyzed and various features were studied at both the macro- and- microscopic scales. Table 4.6 summarizes the

different elements to be observed. The damage mechanisms considered for the analysis of these elements are presented hereafter in Section 4.2.4.2. It should be noted that the stable propagation area, presence of fatigue striations, presence and location of cones, final ligament surface area and presence of cavitations were used to compare the fracture surfaces. The other elements in the table were observed to compare with the literature [5, 183, 184], but do not provide any new information.

Macroscopic scale	**Microscopic scale**
Damage modes	Number of initiations
	Position of the defect relative to the injection point
	Defect-surface distance
	Defect length
	Stable propagation area
	Presence of fatigue striations and their regime
	Presence of cones and their location
	Final ligament surface area
	Presence of cavitations

Table 4.6: Summary of the analyzed elements on the fracture surfaces of the Diabolo specimens.

A JEOL IT 300 LA SEM was used to analyze some failure surface with a higher magnification. It is coupled with a EDSX probe in order to quantify the atoms present at the specimen surface. Secondary and back scattered electrons were used for imaging and composition analysis, respectively.

4.2.4.2 Damage mechanisms to be observed

The damage modes of NR under fatigue loading conditions are classified according to the classification introduced by Le Cam *et al.* [184], and then used and further enriched by Ruellan *et al.* [154]. This classification covers damages observed at both macro- and-microscopic scales.

At the macroscopic scale

Three main macroscopic damage modes are encountered. They are given in Figure 4.4. They can be described as follows:

- **Damage mode 1**: the failure occurs perpendicularly to the stretching direction, in the middle of the specimen (Fig. 4.4 (a)). It was generally observed for relaxing loading conditions [184],

- **Damage mode 2**: it involves multiple surface cracks at mid-height of the Diabolo specimen, propagating through the volume with successive bifurcations. It is exclusively observed when the applied load is non-relaxing, suggesting that the reinforcement due to SIC is activated (Fig. 4.4 (b)),
- **Damage mode 3**: it corresponds to a cohesive failure under the inserts, where the hydrostatic pressure is high. This damage mode is exclusively observed under highly non-relaxing conditions (Fig. 4.4 (c)).

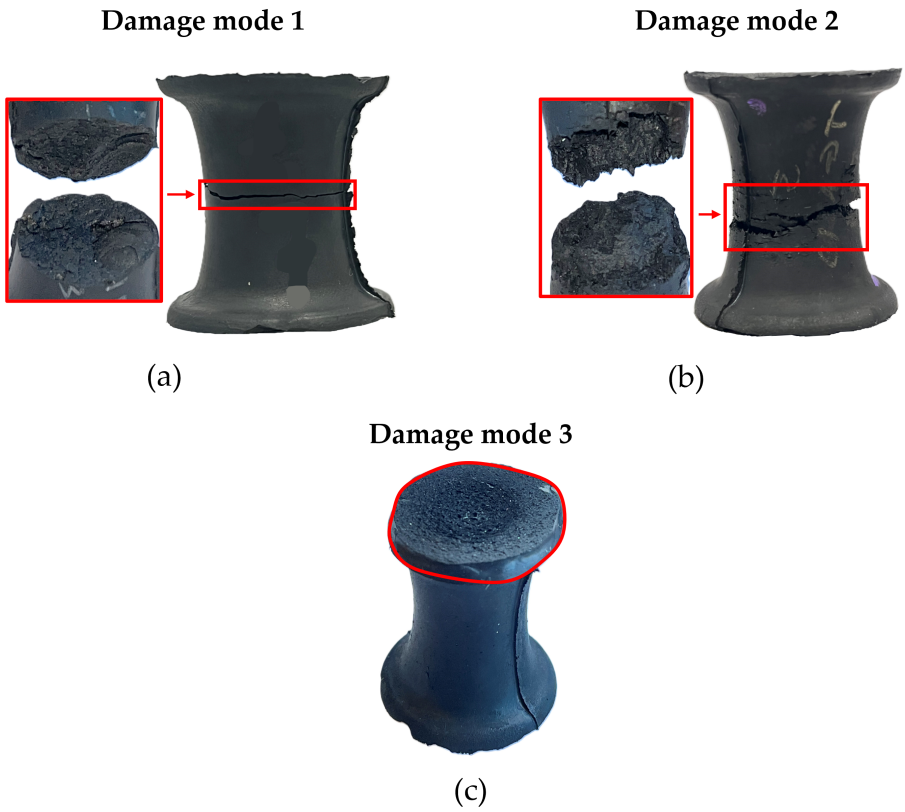

Figure 4.4: The tree main damage modes encountered at the macroscopic scale.

At the microscopic scale

At this scale scale, the crack initiates and propagates, revealing different patterns that differ according to the damage mode.

- **Damage mode 1**: for relaxing loading conditions, the crack initiates near the surface, either due to the presence of a particle part of the formulation (*i.e.*, CB or ZnO) that concentrates stresses [146, 153, 183, 220], or due to a geometric singularity such as a joint plane. The crack then propagates elliptically until it reaches the surfaces, thereby causing alteration of the mechanical properties. The stable propagation phase characterized by a rather smooth surface is followed by the unstable

one, during which wrenchings[5] and small regime 1 fatigue striations[6] are formed, depending on the strain level. When the stress exceeds the stress at break, the Diabolo fails monotonously, by forming a very smooth final ligament. This is summarized in Figure 4.5.

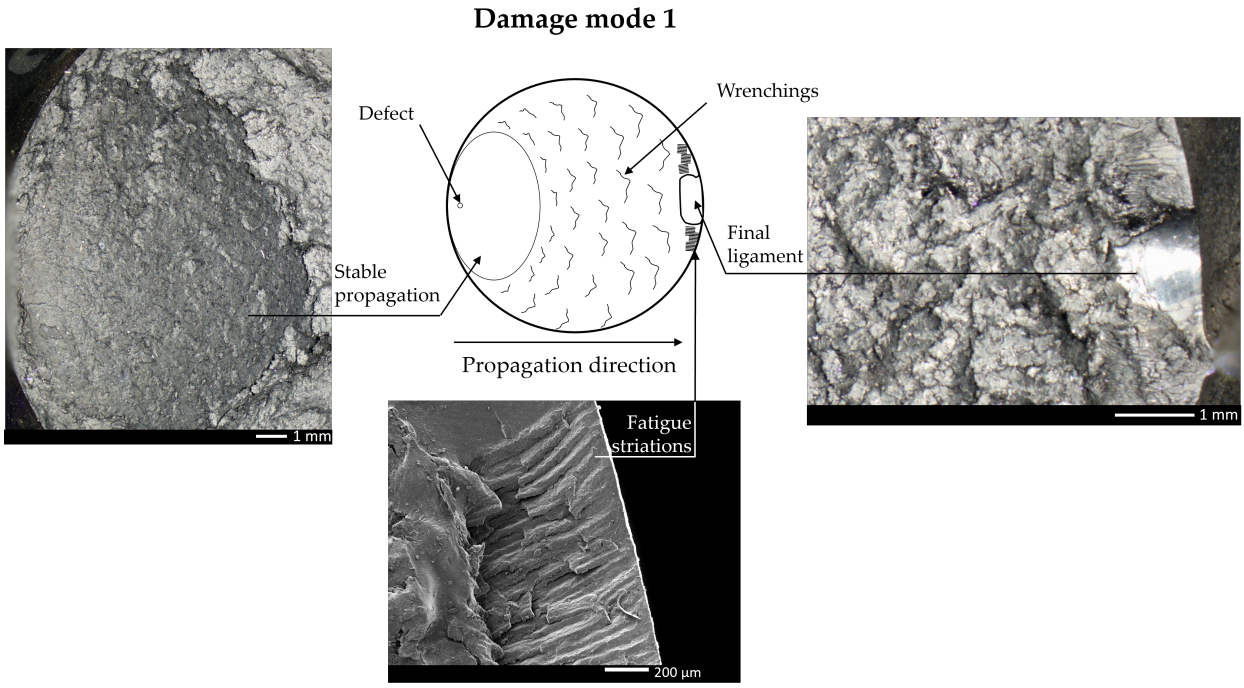

Figure 4.5: Schematic representation of a fracture surface of a filled NR Diabolo specimen tested under relaxing fatigue loading conditions at $R_U = 0$.

- **Damage mode 2**: under non-relaxing loading conditions, multiple initiations occur near the surface but do not propagate perpendicular to the direction of strain, contrarily to Damage mode 1, because of the high reinforcement due to SIC[7]. Instead, the crack propagates along the path of least energy, almost parallel to the strain direction. This mode of propagation leads to the formation of cones, further reflecting the strong activation of SIC. The crack then propagates from the main cone, similar to Damage mode 1 by successively forming wrenchings, well-formed fatigue striations according to Regime 2 [5] with lamellar and triangular shapes [186], and the final ligament. This is illustrated in Figure 4.6.

[5]Wrenchings has been defined as "highly stretched ligaments which break and shrink" by Le Cam *et al.* [185].

[6]Fatigue striations were first introduced by Le Cam *et al.* [185] and then their regimes were introduced by Ruellan *et al.* [154].

[7]It is noteworthy that neither fatigue striations nor cones were observed on SBR, which is non-crystallizable [221]. These features can therefore be considered as markers of crystallization.

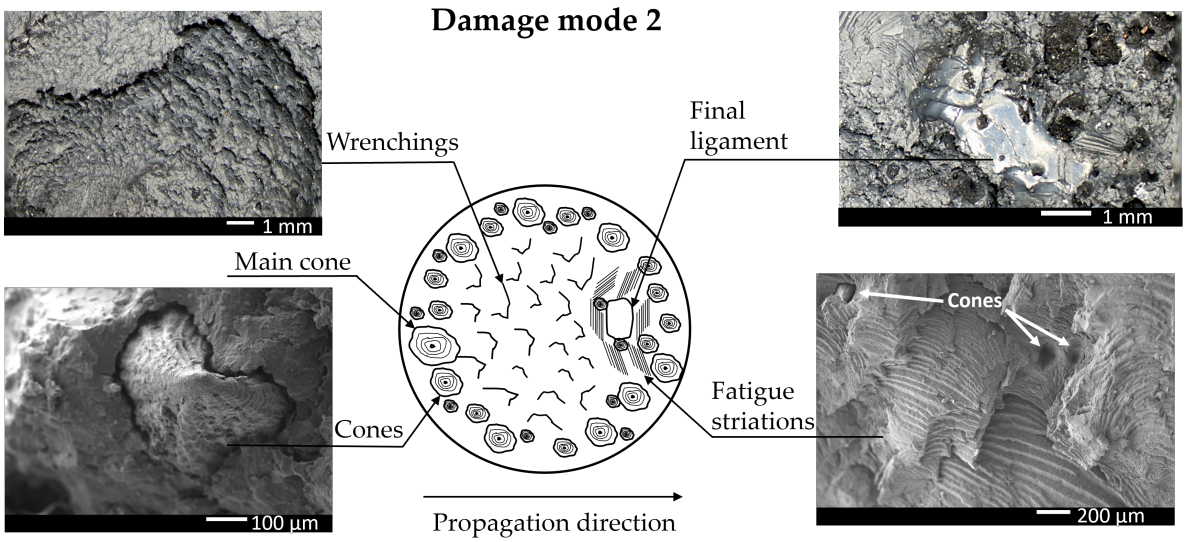

Figure 4.6: Schematic representation of a fracture surface of a filled NR Diabolo specimen tested under non-relaxing fatigue loading conditions at $R_U = 0.25$.

- **Damage mode 3**: in the case of highly non-relaxing loading conditions, the specimen middle section remains undamaged due to the high reinforcement, which prevents any crack from developing. The damage zone is shifted under the inserts where high hydrostatic pressures occur [184, 222]. This leads to the formation of cavitations that are close together and have jagged edges, creating a similar appearance to blooming flowers. These cavitations appear to form from the center outwards, indicating a radial crack propagation. This suggests that the location of the maximum stress zone is at the center, and as the pressure increases, the material yields by expanding outward. This is illustrated in Figure 4.7. Notice that competition between crack branching and crack below metallic inserts was observed by Le Cam *et al.* [184].

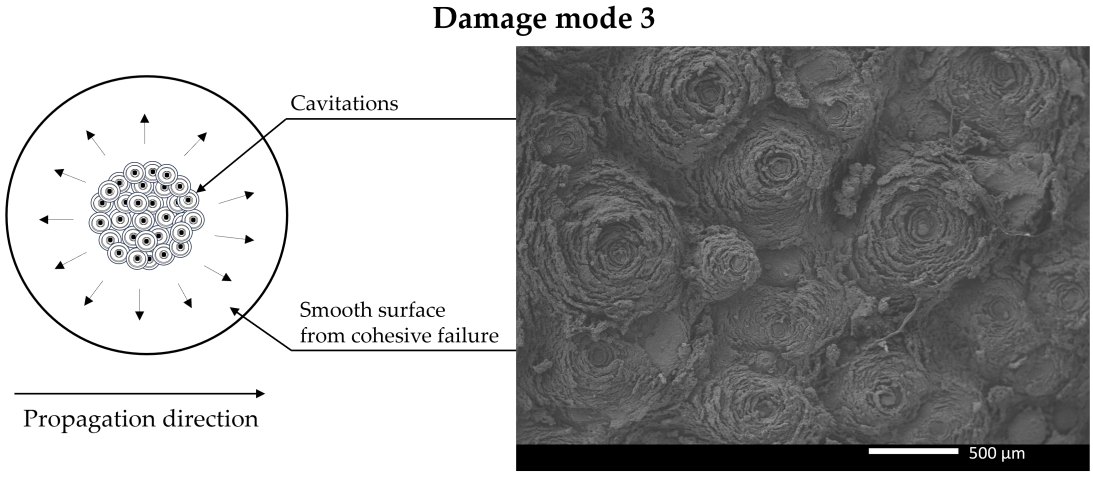

Figure 4.7: Schematic representation of a fracture surface of a filled NR Diabolo specimen tested under highly non-relaxing fatigue loading conditions at $R_U = 0.25$.

4.3 Results and discussion

4.3.1 Relaxing tension loadings

First of all, it should be recalled that results are plotted in terms of endurance curves representing the fatigue predictor, *i.e.*, the Cauchy stress σ, and the lifetime N_i.

4.3.1.1 Effect of the vulcanization system on the fatigue resistance

As discussed in the Introduction section, the accelerator [A] and sulphur [S] contents drive the macromolecular network structure, *i.e.*, ν_{ac} and cross-link length. The effect of these two parameters on the fatigue response are here independently addressed.

Active chain density effect

Figure 4.8 presents the endurance curves for NR with [A]/[S] of (a) 0.2 and (b) 0.6 for CV systems, and (c) 1.5 and (d) 2.5 for SEV ones. For each endurance curve, the effect of the ν_{ac} is shown through three materials. First, Fig. 4.8 (a) shows the endurance curves for materials with long cross-links (CV), with [A]/[S]=0.2. Increasing ν_{ac} increases the stress. This is also observed for the other [A]/[S] ratios, and is due to the increase in stiffness caused by the higher ν_{ac} [47]. Even though, for a given displacement, the fatigue lives decrease as ν_{ac} increases, it seems they follow the same behavior as they can be fitted with a unique power law. This suggests that ν_{ac} does not have a significant effect on the fatigue life for [A]/[S]=0.2. Then, again for CV, but with [A]/[S]=0.6 (Fig. 4.8 (b)), a similar fatigue response was obtained for $NR^2_{0.6}$ and $NR^4_{0.6}$, traducing only minor effect of ν_{ac} on the fatigue life. However, for $NR^6_{0.6}$ presenting the highest ν_{ac}, the fatigue life is drastically reduced in comparison to the $NR^2_{0.6}$ and $NR^4_{0.6}$. This could be interpreted by the network mobility restrictions caused by too much active chains. To continue, the endurance curves for [A]/[S]=1.5 are presented in Fig. 4.8 (c). Increasing ν_{ac} increases the stress as well as the fatigue life. In particular, above $0.95 \times 10^4\,\mathrm{mol/cm^3}$, the fatigue resistance is significantly enhanced. This suggests that for these materials, a higher ν_{ac} and consequently a higher stiffness is truly efficient to enhance fatigue resistance. However, it is worth noting that the range of ν_{ac} for [A]/[S]=1.5 are significantly lower than the ones [A]/[S]=0.2 and 0.6. Finally, for the SEV with [A]/[S]=2.5 (Fig. 4.8 (d)), a similar fatigue response is obtained for $NR^{1.2}_{2.5}$ and $NR^{1.6}_{2.5}$, which is significantly better than the $NR^{0.8}_{2.5}$ having a lower ν_{ac}. This suggests that for this type of SEV, a certain stiffness is required to maximize the fatigue resistance: above $1.11 \times 10^4\,\mathrm{mol/cm^3}$, the fatigue resistance is drastically improved. Nevertheless, there is no gain in fatigue resistance with the higher ν_{ac} of $1.71 \times 10^4\,\mathrm{mol/cm^3}$, which suggests a threshold effect.

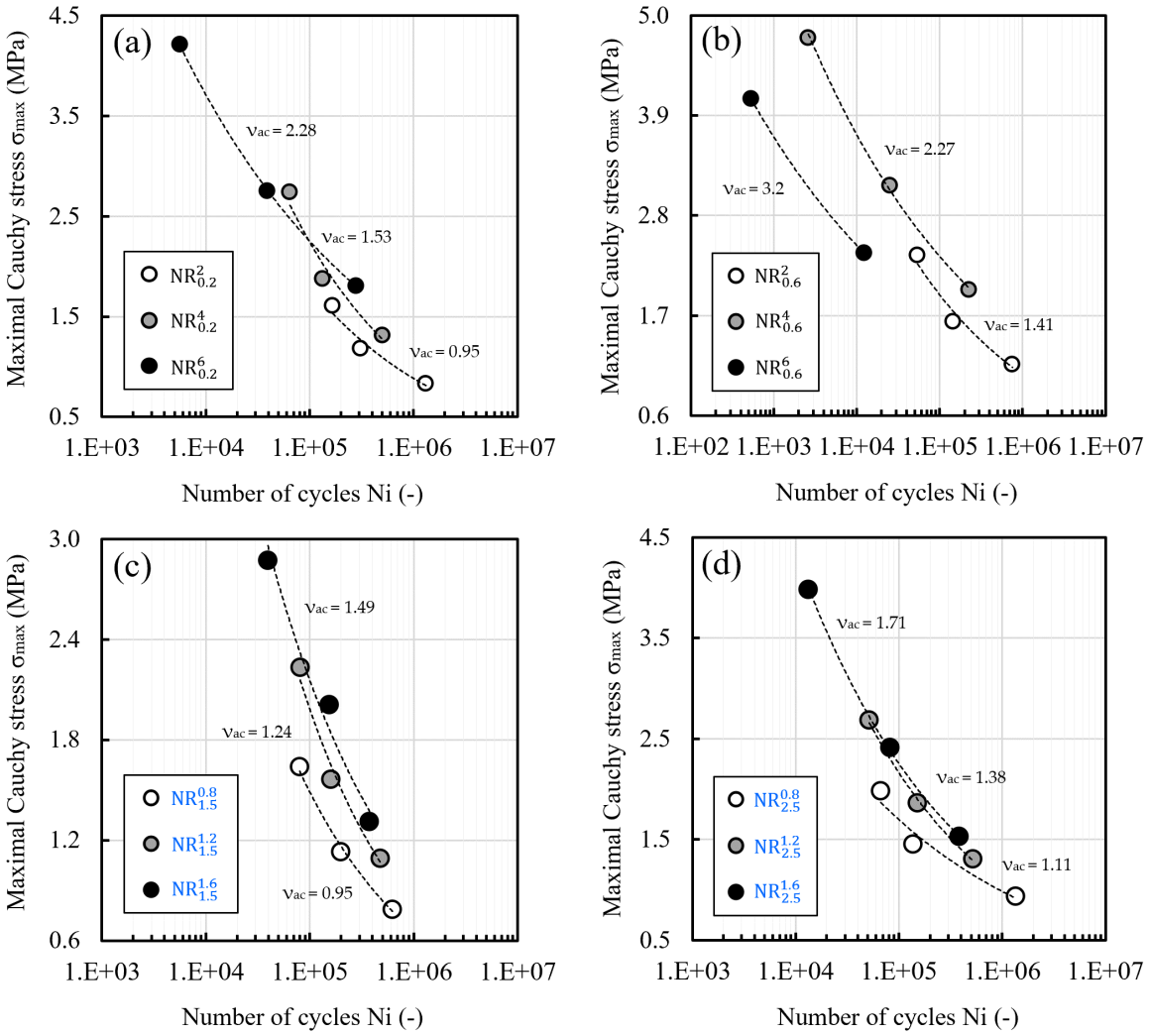

Figure 4.8: Endurance curves for [A]/[S] ratio of (a) 0.2, (b) 0.6, (c) 1.5 and (d) 2.5, for different ν_{ac}.

To sum-up, ν_{ac} is found to strongly affect the fatigue properties of filled NR, by impacting the mechanical response. However, the effect of ν_{ac} on the fatigue life differs depending on the [A]/[S] ratio, *i.e.*, the cross-link length. For example, increasing the ν_{ac} and consequently the stiffness is of benefit for the filled NR with an [A]/[S] ratio of 1.5, while it was not the case for the filled NR with an [A]/[S] ratio of 0.6. It is noteworthy that the ν_{ac} ranges varied between the different [A]/[S] studied, making the comparison difficult. Finally, this suggests a twofold possibility, either that there is an optimum value of ν_{ac} as mentioned in Refs [1, 3, 45], or that the cross-link length affects the fatigue response. To go further and provide an answer to this question, we now focus on the effect of the cross-link length on the fatigue properties.

Cross-link length effect

The effect of the cross-link length on the fatigue properties is evaluated based on a comparison of filled NR having similar ν_{ac} and different [A]/[S] ratios. Four groups of filled NR were defined in order to cover a wide range of ν_{ac}. It is to be noted that results from these comparisons need to be analyzed with caution, since the ν_{ac} of each group *(i)* is not constant (except for Group n°1), and *(ii)* they are based on a measurement that implies an experimental error. These couples are presented in Table 4.7.

Group n°	**Materials**	**Range of ν_{ac}**
1	$NR^{2}_{0.2} \Leftrightarrow NR^{0.8}_{1.5}$	0.95
2	$NR^{1.2}_{1.5} \Leftrightarrow NR^{0.8}_{4}$	1.24-1.29
3	$NR^{2}_{0.6} \Leftrightarrow NR^{1.2}_{2.5} \Leftrightarrow NR^{1.6}_{1.5}$	1.38-1.49
4	$NR^{4}_{0.2} \Leftrightarrow NR^{1.6}_{1.5}$	1.49-1.53

Table 4.7: Summary of the groups used to evaluate the effect of the cross-link length. Values of ν_{ac} are given in $\times 10^4$ mol/cm^3.

Figure 4.9 presents the endurance curves of the four material groups listed in Tab. 4.7. The individual fatigue lives are also reported for the sake of clarity.
First, Fig. 4.9 (a) compares the endurance curves of $NR^{2}_{0.2}$ and $NR^{0.8}_{1.5}$ having low ν_{ac}. The longer cross-link length of $NR^{2}_{0.2}$ significantly increases the fatigue lives, and confirms that polysulphide cross-links improves the fatigue life [173, 176, 177] in comparison to shorter mono- and- disulphide cross-links. Hence, CV systems are better than SEV ones for a low ν_{ac}. Then, Fig. 4.9 (b) presents the endurance curves of $NR^{1.2}_{1.5}$ and $NR^{0.8}_{4}$. The SEV system shows better fatigue resistance than the EV one, which indicates, once more, that longer cross-links could enhance the fatigue resistance. This effect is less pronounced than with CV system in Fig. 4.9 (a). To continue, Fig. 4.9 (c) shows that $NR^{2}_{0.6}$, having mainly polysulphide cross-links, is less resistant to fatigue than the $NR^{1.6}_{1.5}$ and $NR^{1.2}_{2.5}$. This suggests for this range of ν_{ac} that longer cross-links do not improve the fatigue resistance, contrarily to what was observed for lower ν_{ac}. This raises the question of whether ν_{ac} has a stronger effect than cross-links length on the fatigue life improvement, for this range of ν_{ac}. Finally, Fig. 4.9 (d) shows that comparable fatigue lives were obtained between CV and SEV with ν_{ac} around 1.50×10^4 mol/cm^3. Thus, it can be concluded CV system is no longer better than the SEV, for this ν_{ac} value. This could indicate that the beneficial effect of long cross-links on the network mobility [175], is reduced at high ν_{ac}.

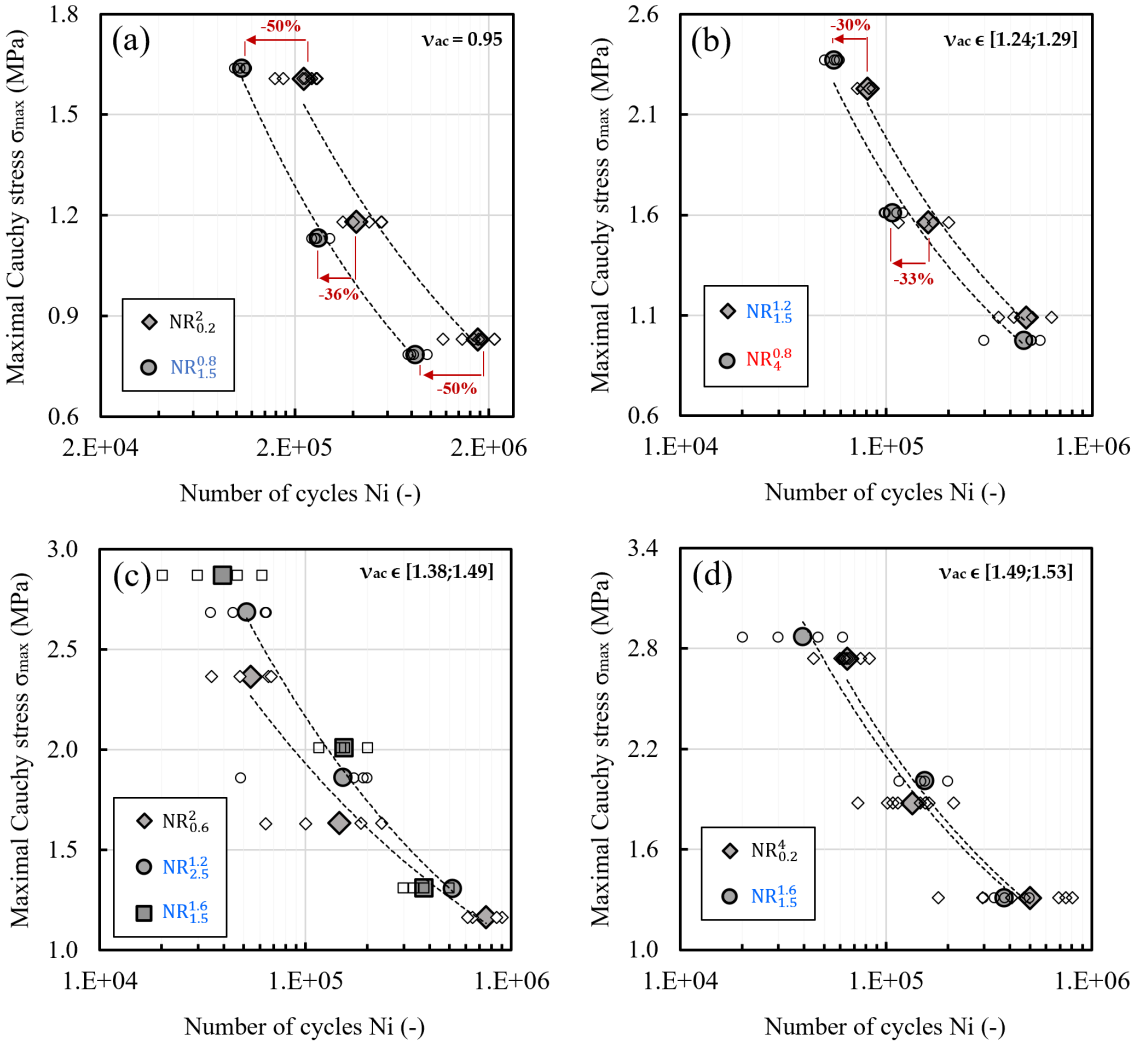

Figure 4.9: The effect of the cross-link length on the fatigue response, in which four groups of NR are compared: Groups (a) n°1 (b) n°2 (c) n°3 and (d) n°4 in Table 4.7, respectively.

To sum-up, the effect of the cross-link length depends on ν_{ac}. Low ν_{ac} combined to polysulphide cross-links lead to significantly higher fatigue lives. This confirms the results obtained previously in the literature [173, 176, 177] and could be explained by structural rearrangements, without being able to establish the exact phenomenon in question. Increasing ν_{ac} will decrease this effect until it completely disappears. This could be explained by possible mobility restrictions overcoming the benefits of polysulphide cross-links.

4.3.1.2 Effect of the vulcanization conditions on the fatigue resistance

Vulcanization time and temperature have an effect on the macromolecular network structure, driven by ν_{ac} and cross-link length. As reviewed by Akiba and Hashim [12], CV systems are more prone to reversion than SEV and EV ones, which have shorter cross-links and are much more thermally stable. Thus, a vulcanization carried out for a

too long time is known to reduce the mechanical properties [12]. This can be explained by *(i)* the formation of elastically inactive structures, such as "cyclic sulphides" [35] that decreases ν_{ac} and *(ii)* NR chains modifications causing the macromolecules to lose their stereoregularity due to the change from *cis* to *trans* configurations [45]. These effects are presented in Figures 4.10 and 4.11, which sum-up the effect of vulcanization time and temperature on the fatigue response, respectively.

Vulcanization time

Fig. 4.10 presents the endurance curves for (a) the $NR^4_{0.2}$, (b) the $NR^{1.2}_{1.5}$ and (c) the $NR^{0.8}_4$, corresponding to CV, SEV and EV, respectively. Fig. 4.10 (a) shows that for $NR^4_{0.2}$, the stress response as well as the fatigue life significantly decrease after over-curing. This illustrates the effect of the reversion, which is known to decrease ν_{ac} [44] as well as the cross-link length [42, 43]. This suggests that even with a decrease in ν_{ac} and thus less energy available for crack growth, over-curing involves other phenomena that significantly reduce the fatigue life. To continue, SEV systems (see Fig. 4.10 (b)) show no significant dependence to the over-vulcanization, as endurance curves are similar between optimally and over-vulcanized materials. However, the fatigue lives are significantly enhanced in the case of under-vulcanization. Since ν_{ac} is relatively similar for them all, the better fatigue resistance of SEV system when under-vulcanized could be related to the higher cross-link length, or to the formation of inactive structures above t_{80} such as pendant cross-links or cyclic cross-links. This result correlates well with the fact that SEV systems are more resistant than CV ones to long time vulcanization, with only a few changes in ν_{ac} [12]. No effect on the fatigue resistance above t_{98} was observed. For EV systems (see Fig. 4.10 (c)), the endurance curves for the three vulcanization conditions are superimposed. This is expected as EV systems are much more thermally stable than CV [44]. This indicates that ν_{ac} does not evolve when additional thermal energy is provided. Furthermore, the fact that the under-vulcanized EV is similar to the others correlates well with the fact that polysulphide cross-links decomposed early in the vulcanization process of EV systems [12]. As a result, lifetime cannot be improved by under-vulcanization, but this material will not suffer from over-vulcanization.

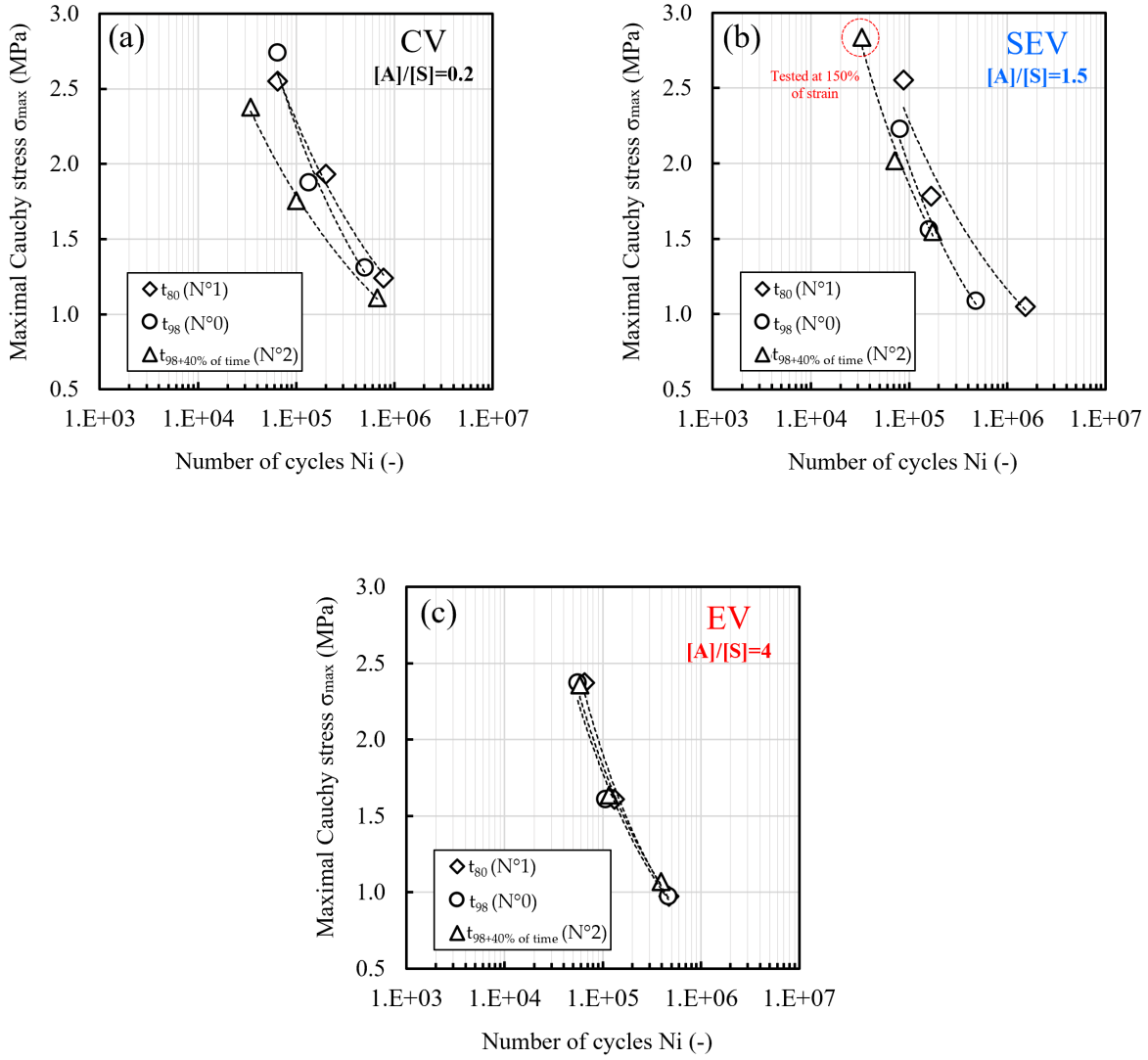

Figure 4.10: Effect of the vulcanization time on the fatigue response for the (a) $NR^{4}_{0.2}$ (CV) (b) $NR^{1.2}_{1.5}$ (SEV) and (c) $NR^{0.8}_{4}$ (EV), respectively.

Vulcanization temperature

Fig. 4.11 presents the endurance curves for (a) the $NR^{4}_{0.2}$, (b) the $NR^{1.2}_{1.5}$ and (c) the $NR^{0.8}_{4}$, corresponding to CV, SEV and EV, respectively. The vulcanization temperature significantly changed ν_{ac} for the CV system $NR^{4}_{0.2}$, the lowest ν_{ac} was unexpectedly obtained at 160°C (Fig. 4.11 (a)). Consequently, ν_{ac} and stresses for CV vulcanized at 150 and 170°C are higher than at 160°C, especially at high strain. The corresponding fatigue lives are slightly higher, but this is not significant. This indicates that the effect of the vulcanization temperature on the fatigue properties is minor as long as the vulcanization time is adjusted accordingly. To continue on the endurance curves for SEV and EV systems (Figs. 4.11 (b) and (c)), the same conclusions can be addressed as the endurance

curves are superimposed. To sum-up, the vulcanization temperature has no effect on the fatigue resistance. This result differs from that of Gehling *et al.* who found a higher crack growth resistance for CB filled NBR vulcanized at 170°C, with a EV system [182]. This suggests that the effect of vulcanization temperature is different for this type of rubber.

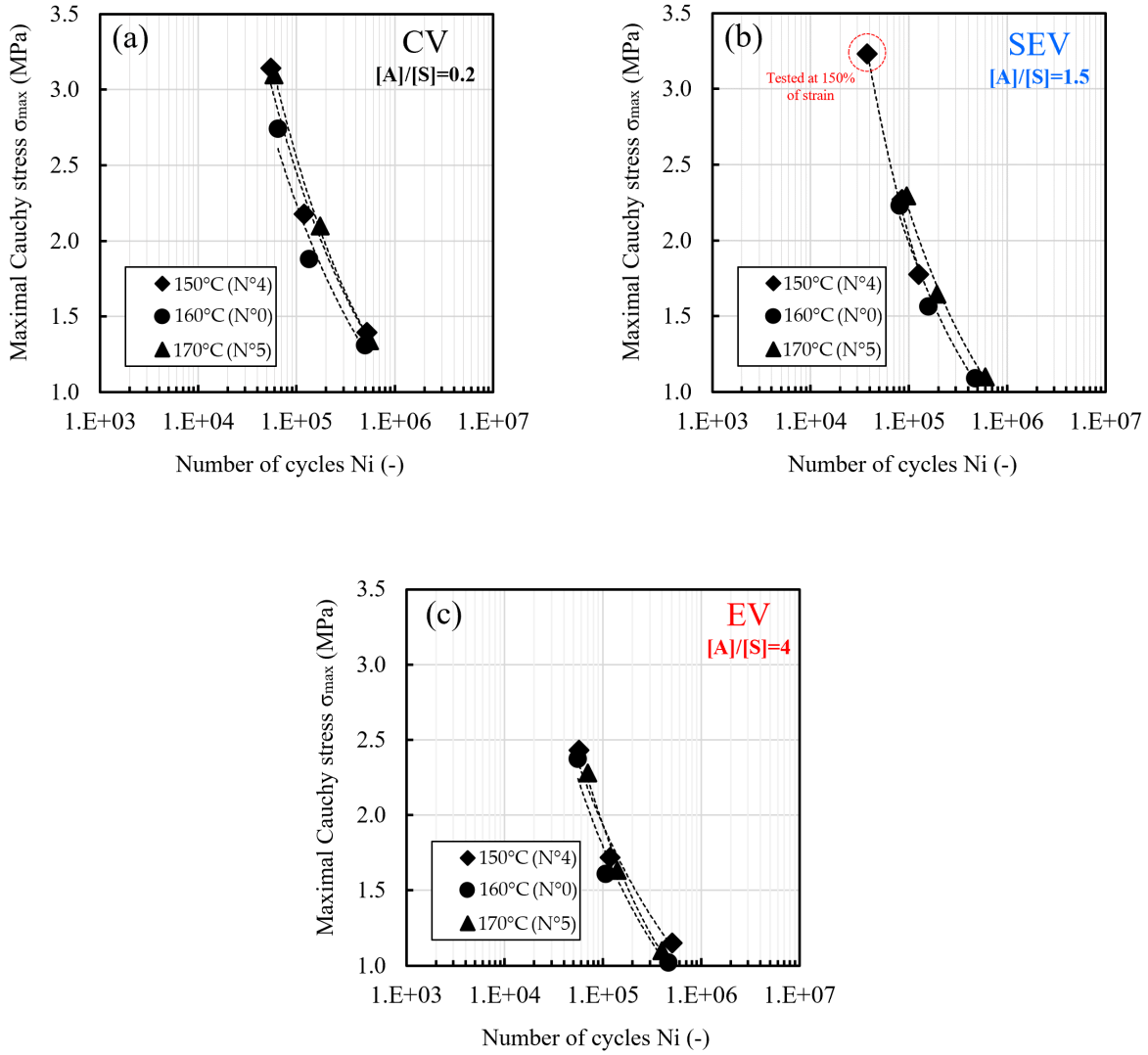

Figure 4.11: Effect of the vulcanization temperature on the fatigue response for the (a) $NR^{4}_{0.2}$ (CV) (b) $NR^{1.2}_{1.5}$ (SEV) and (c) $NR^{0.8}_{4}$ (EV), respectively.

4.3.1.3 Damage modes analysis

The Diabolo tested under relaxing tension, *i.e.*, for $R_U = 0$ only, failed under Damage mode 1. Some of the materials have been chosen to illustrate the changes induced by the vulcanization system, namely ν_{ac} and the cross-link length. For the sake of clarity, since the results regarding the effect of vulcanization conditions do not provide any truly

significant insights into fracture surfaces, they are not presented here[8].

Effect of the active chain density on the damage mechanisms

Figure 4.12 presents representative failure surfaces of $NR^{0.8}_{2.5}$, $NR^{1.2}_{2.5}$ and $NR^{1.6}_{2.5}$, tested at 60, 90 and 120%. The Figure is constructed as follows: *(i)* ν_{ac} increases per column from the left to the right, and *(ii)* the strain level increases per row, from the top to the bottom.

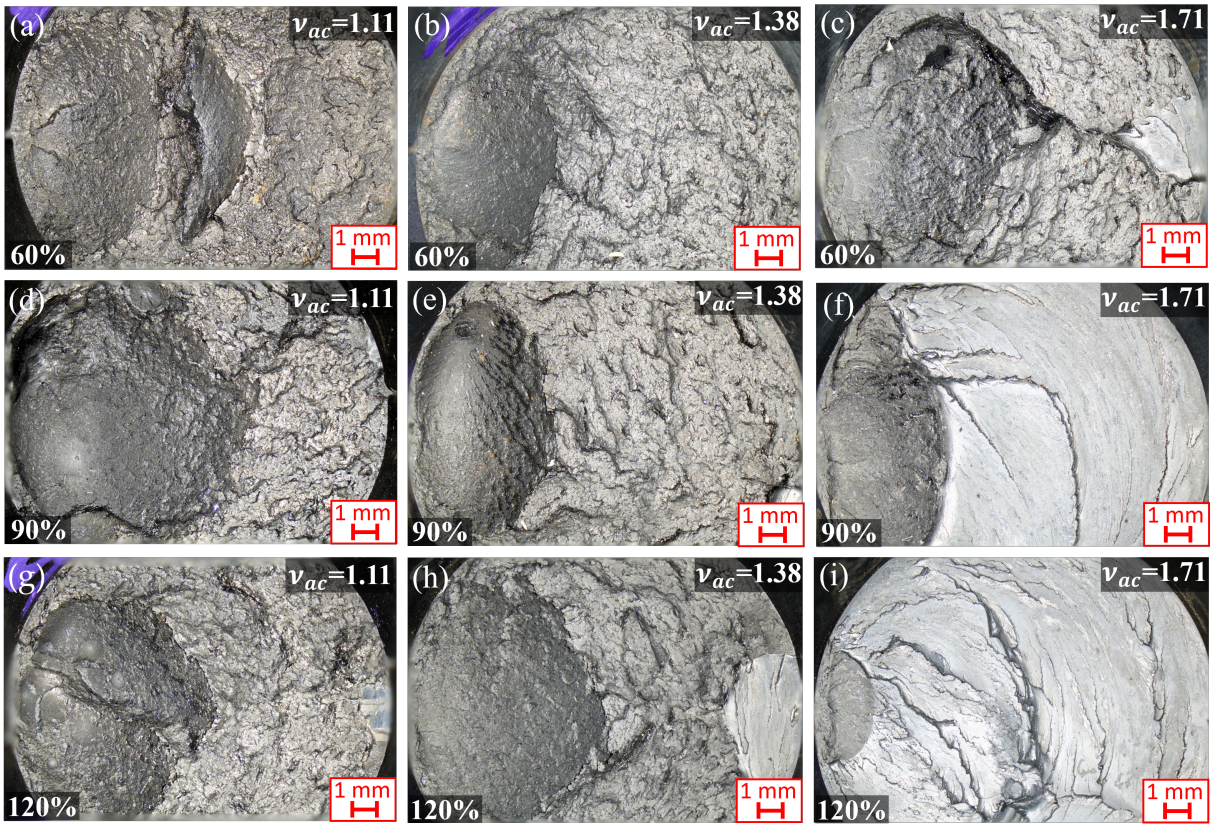

Figure 4.12: Fractographies of $NR^{0.8}_{2.5}$, $NR^{1.2}_{2.5}$ and $NR^{1.6}_{2.5}$, tested in fatigue under relaxing tension loadings. The effect of the maximal strain for $NR^{0.8}_{2.5}$ at (a) 60, (d) 90 and (g) 120%, $NR^{1.2}_{2.5}$ at (b) 60, (e) 90 and (h) 120% and $NR^{1.6}_{2.5}$ at (c) 60, (f) 90 and (i) 120% is given.

For each failure surface, the crack propagates from the left to the right, showing a wide stable propagation surface, wrenchings and a smooth final ligament surface. Increasing the strain level increases the final ligament surface area, indicating an earlier catastrophic failure as a higher strain level induces more energy used for crack growth. Also, wrenchings are significantly more inclined. For $NR^{0.8}_{2.5}$ and $NR^{1.2}_{2.5}$, having the same ν_{ac}, fatigue striations were observed at 120% of strain. This indicates that SIC markers are promoted

[8]The results obtained by varying the vulcanization time and temperature has no significant effect; however, they do confirm the observations made under optimal conditions. For instance, for non-relaxing loading conditions, $NR^{0.8}_{4}$ exhibited a competition between Damage modes 2 and 3 regardless of the vulcanization temperature.

by a specific range of ν_{ac}, and suggests that SIC depends on ν_{ac} [90]. By increasing ν_{ac}, the final ligament surface increases. This effect is much more pronounced at high strain levels traducing a catastrophic failure. This could be explained by the fact that a high ν_{ac} *(i)* implies a high stiffness and provide a high strain energy quantity for crack growth, *(ii)* but drastically reduces the macromolecular network mobility and consequently its ability to dissipate this energy. To go further, increasing ν_{ac} leads to an increase and then a decrease of fatigue striations number, suggesting that there may be an ν_{ac} maximizing SIC. This is in a strong analogy with what was found by Chenal *et al.* [116] under quasi-static loadings.
As a summary, it has been shown that both ν_{ac} and strain level have an effect on the fracture surface, which is consistent with the previous results obtained in Section 4.3.1.2.

Effect of the cross-link length on the damage mechanisms

The effect of the cross-link length on the fracture surface is addressed by comparing materials with similar ν_{ac} and different [A]/[S]. Table 4.8 summarizes the materials to be compared. Figure 4.13 presents a comparison of materials having close ν_{ac} value: (a) $NR^{6}_{0.2}$ is compared with (b) $NR^{4}_{0.6}$, (c) $NR^{4}_{0.2}$ is compared with (d) $NR^{1.6}_{1.5}$ and (e) $NR^{1.2}_{1.5}$ is compared with (f) $NR^{0.8}_{4}$. Since the fractographic images showed comparable changes at 60, 90 and 120% of maximum strain, only the fracture surfaces obtained at 120 % are shown.

Pair n°	**Materials**	**Range of ν_{ac}**
1	$NR^{6}_{0.2} \Leftrightarrow NR^{4}_{0.6}$	2.27-2.28
2	$NR^{4}_{0.2} \Leftrightarrow NR^{1.6}_{1.5}$	1.49-1.53
3	$NR^{1.2}_{1.5} \Leftrightarrow NR^{0.8}_{4}$	1.24-1.29

Table 4.8: Summary of the three pairs used to evaluate the effect of the cross-link length on the damage mechanisms. Values of ν_{ac} are given in $\times 10^4$ mol/cm^3.

Figs. 4.13 (a) and (b) are both CV materials of [A]/[S] ratio of 0.2 and 0.6, respectively. Clearly, fracture surfaces are very similar with a tiny stable propagation zone and a very large smooth surface, characteristic of a catastrophic failure. This suggests that their high ν_{ac} drives the damage mechanisms. Since they are both CV systems, this does not exclude a potential effect of the cross-link length. To continue with the second pair (Figs. 4.13 (c) for CV and (d) for SEV), no major difference was observed. Indeed, both fracture surfaces consist of a stable propagation surface, wrenchings, and a smooth area characteristic of a catastrophic failure. Finally, results shown no significant effect of the cross-link length on the fracture surface for last Pair n°3 (Figs. 4.13 (e) and (f)). Indeed, both exhibit similar stable propagation surface and wrenchings, presence of fatigue striations, and a

comparable final ligament surface. To sum-up, it can be concluded that the cross-link length has no significant effect on the fracture surface.

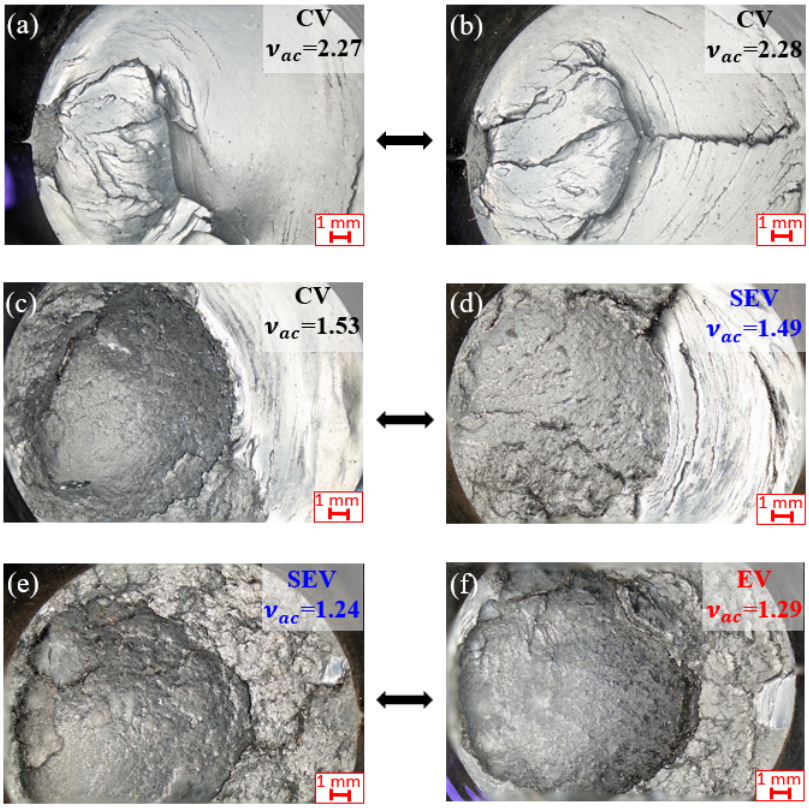

Figure 4.13: Fractographies of the NR pairs used to evaluate the effect of the cross-link length on the damage mechanisms: (a) $NR^{6}_{0.2}$, (b) $NR^{4}_{0.6}$, (c) $NR^{4}_{0.2}$,(d) $NR^{1.6}_{1.5}$, (e) $NR^{1.2}_{1.5}$ and (f) $NR^{0.8}_{4}$. These correspond to fracture surfaces tested at 120% strain.

4.3.1.4 Summary

In this section dedicated to the fatigue results under relaxing tension loadings, the effect of the vulcanization system and conditions was studied. ν_{ac} was found to drive the fatigue properties and damage mechanisms. Clearly, a sufficient stiffness must be achieved to maximize the fatigue resistance, although it should not be too high, as this would leads to reduced lifetime and catastrophic failure. Moreover, the effect of the cross-link length on damage mechanisms was found to be negligible, suggesting that stiffness drives the damage modes. However, the cross-link length showed a slight effect on the fatigue resistance which depends on ν_{ac}. Notably, no effect of cross-link length on fatigue resistance was found for high ν_{ac}, but low ν_{ac} has proved to be significantly improved by longer cross-link length. In terms of the vulcanization conditions, it was shown that vulcanization temperature had no effect on fatigue resistance when vulcanized at the appropriate optimum time. However, increasing the vulcanization time tends to decrease the fatigue resistance for CV systems. It is to be noted that for both CV and SEV, under-vulcanized Diabolo specimens showed better fatigue resistance, while EV showed

no difference in lifetime. In summary, vulcanization systems and conditions provide a wide range of parameters to drive the macromolecular network structure and, thereby, the fatigue resistance of filled NR.

4.3.2 Non-relaxing tension loadings

As above-mentioned, non-relaxing loading conditions lead to a lifetime reinforcement. This reinforcement is generally represented by the Haigh diagram, as a typical "V shape" of iso-lifetime is observed. In this section, iso-lifetimes of 10^4 ($\cdots$), 10^5 (- -) and 10^6 (–) cycles are plotted with respect to the amplitude σ_{amp} and mean σ_{mean} Cauchy stresses. They are both calculated by using σ_{min} and σ_{max}: $\sigma_{amp} = 0.5 \times (\sigma_{max} - \sigma_{min})$ and $\sigma_{mean} = 0.5 \times (\sigma_{max} + \sigma_{min})$, respectively. Depending on the material and the experimental life obtained, only the interpolated iso-lifetimes are shown. Furthermore, it should be noted that the "V-shape" does not appear in the following Haigh diagrams as only R ratios superior or equal to zero have been tested.

4.3.2.1 Effect of the vulcanization system on the lifetime reinforcement

Active chain density effect

Figure 4.14 presents the Haigh diagram for NR with [A]/[S] of (a) 0.2, (b) 0.6, (c) 1.5 and (d) 2.5. For each Haigh diagram, the effect of the ν_{ac} is shown through three materials.
The lifetime reinforcement can be discussed with Fig. 4.14 (a) for CV, *i.e.*, $NR^2_{0.2}$, $NR^4_{0.2}$ and $NR^6_{0.2}$. The slope of each iso-lifetimes displayed are different, which means that ν_{ac} has a strong effect on the lifetime reinforcement magnitude. Clearly, increasing ν_{ac} decreases the slope, suggesting that a too much ν_{ac} is detrimental for CV of [A]/[S]=0.2. To continue with CV, $NR^2_{0.6}$, $NR^4_{0.6}$ and $NR^6_{0.6}$ showed very different slopes (Fig. 4.14 (b)). Thus, results are consistent with the previous ones (Fig. 4.14 (a)): ν_{ac} drives the slope of the iso-lifetimes, with low ν_{ac} values leading to the highest lifetime reinforcement. A different trend is obtained for SEV with [A]/[S]=1.5 (Fig. 4.14 (c)). These materials are highly reinforced, with the higher the ν_{ac} the higher the lifetime reinforcement. This suggests that the cross-link length may have an effect, or as the ν_{ac} range is different, it may have a different effect to the one previously observed. Finally, Fig. 4.14 (d) shows a higher slope for $NR^{1.2}_{2.5}$, corresponding to a higher lifetime reinforcement. For higher and lower ν_{ac}, the lifetime reinforcement is significantly decreased. This shows that ν_{ac} drives the lifetime reinforcement for [A]/[S]=2.5.
To sum-up, ν_{ac} was found to have a strong effect on the fatigue life reinforcement. Since *(i)* the effects were different depending on [A]/[S], and *(ii)* considering that they have different range of ν_{ac}, this does not exclude the existence of an optimum ν_{ac} range maximizing the

reinforcement. However, it is difficult to analyze and generalize the effect of ν_{ac} on the lifetime reinforcement. This is further addressed in Section 4.3.

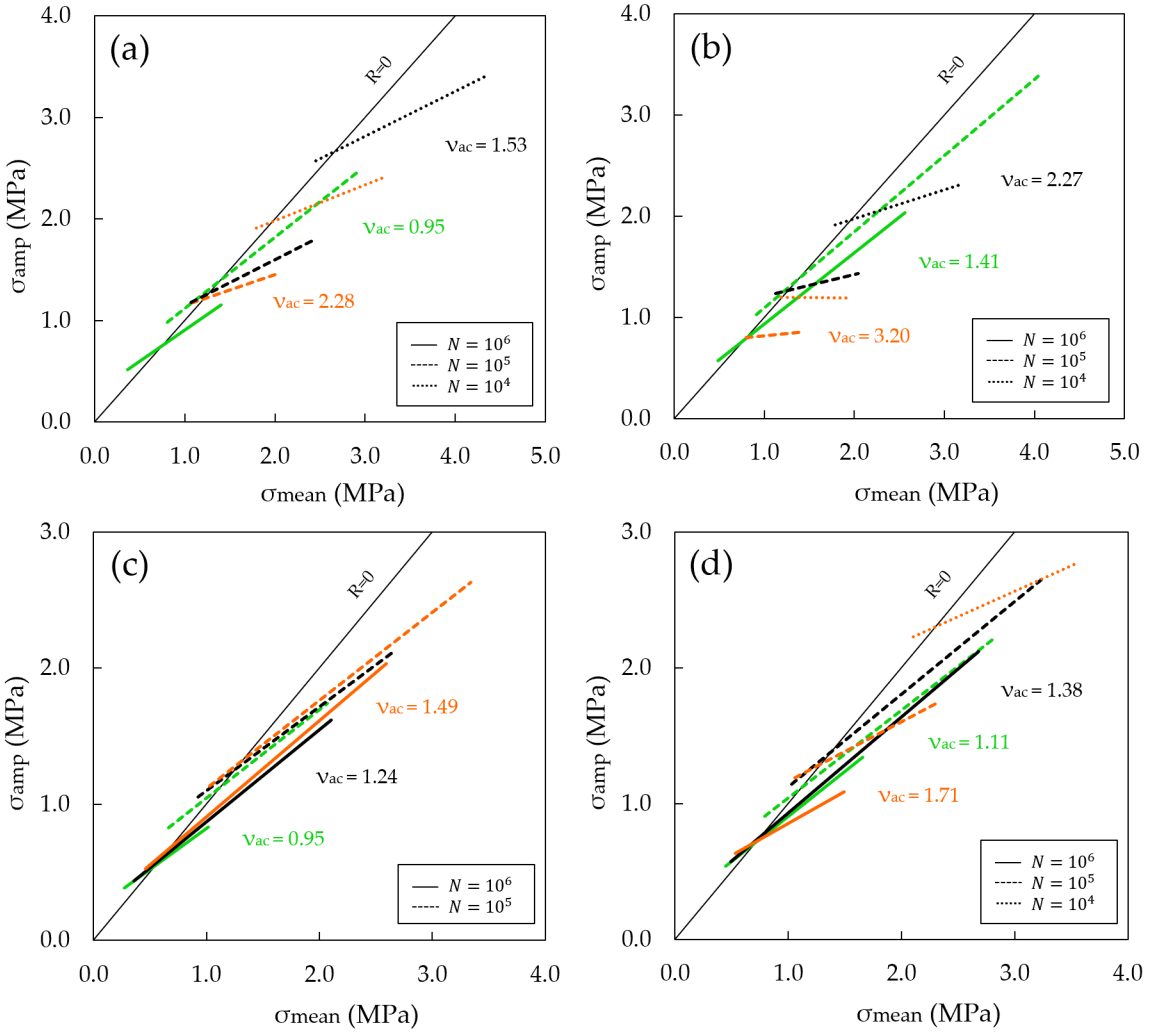

Figure 4.14: Effect of ν_{ac} on the lifetime reinforcement for [A]/[S] of (a) 0.2 (b) 0.6 (c) 1.5 and (d) 2.5.

Cross-link length effect

Figure 4.14 presents the effect of the cross-link length on the lifetime reinforcement. Fig. 4.14 (a) shows the lifetime reinforcement for Group n°1. The slope of each iso-lifetime displayed are very similar indicating a comparable lifetime reinforcement. Similarly, Group n°2 and 3 (Fig. 4.14 (b) and (c)) showed no difference in lifetime trends, suggesting that the cross-link length does not affect the lifetime reinforcement for these ranges of ν_{ac}. However, Group n°4 showed higher slope for SEV than CV systems $NR_{1.5}^{1.6}$ (Fig. 4.14 (d)). This is surprising, and could be due to excessive ν_{ac} inhibiting the SIC for CV. Without going into further explanation of these results, it should be noted that the CV system is less reinforced.

To sum-up, the cross-link length has a negligible effect on the lifetime reinforcement, further demonstrating the strong effect of ν_{ac} on fatigue response. Nevertheless, we note that $NR^4_{0.2}$ showed a difference with $NR^{1.6}_{1.5}$.

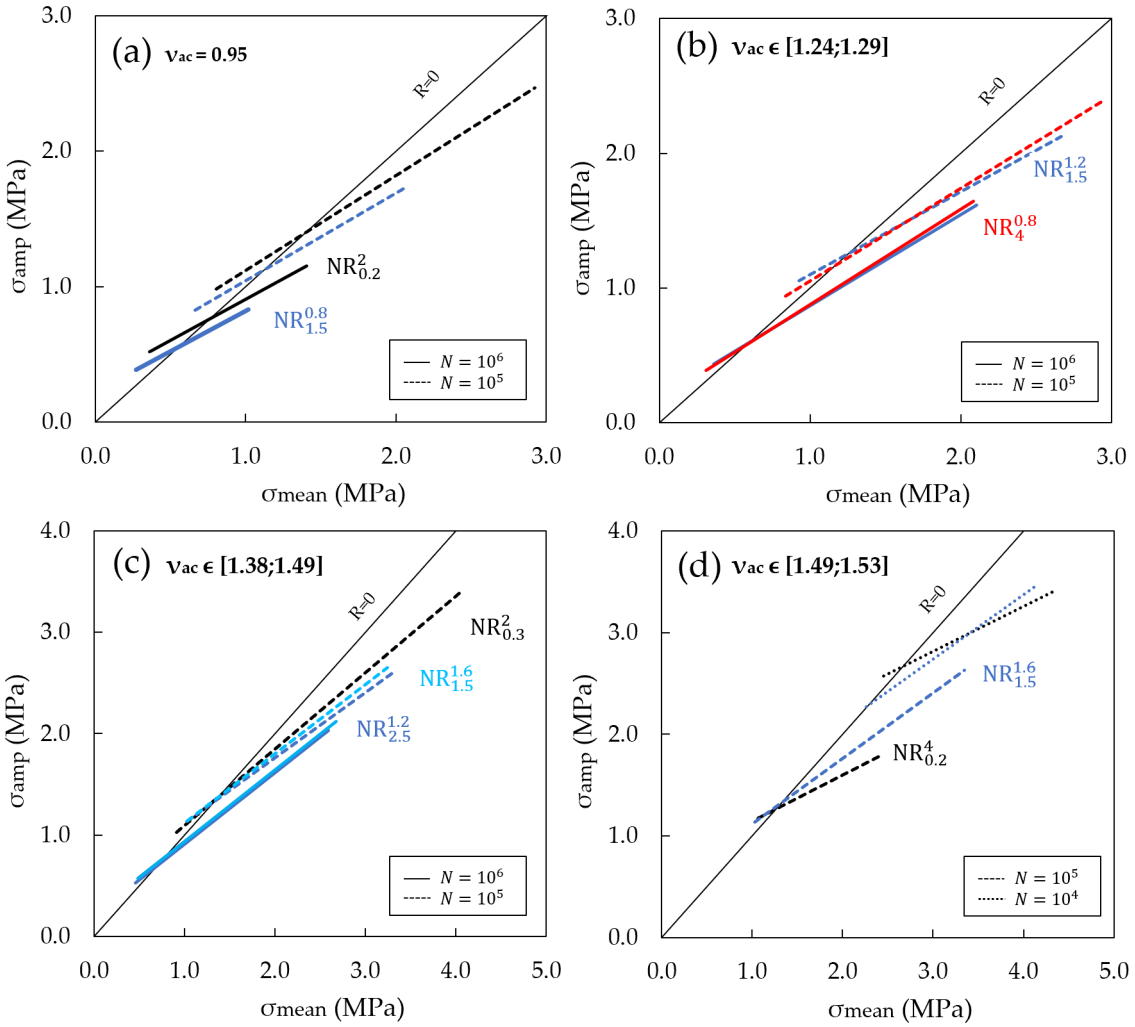

Figure 4.15: Effect of the cross-link length on the lifetime reinforcement for Groups (a) n°1 (b) n°2 (c) n°3 and (d) n°4 defined in Table 4.7.

4.3.2.2 Effect of the vulcanization conditions on the lifetime reinforcement

The effect of the vulcanization conditions on the lifetime reinforcement are independently addressed. It is recalled that vulcanization conditions are changed accordingly to Table 4.5.

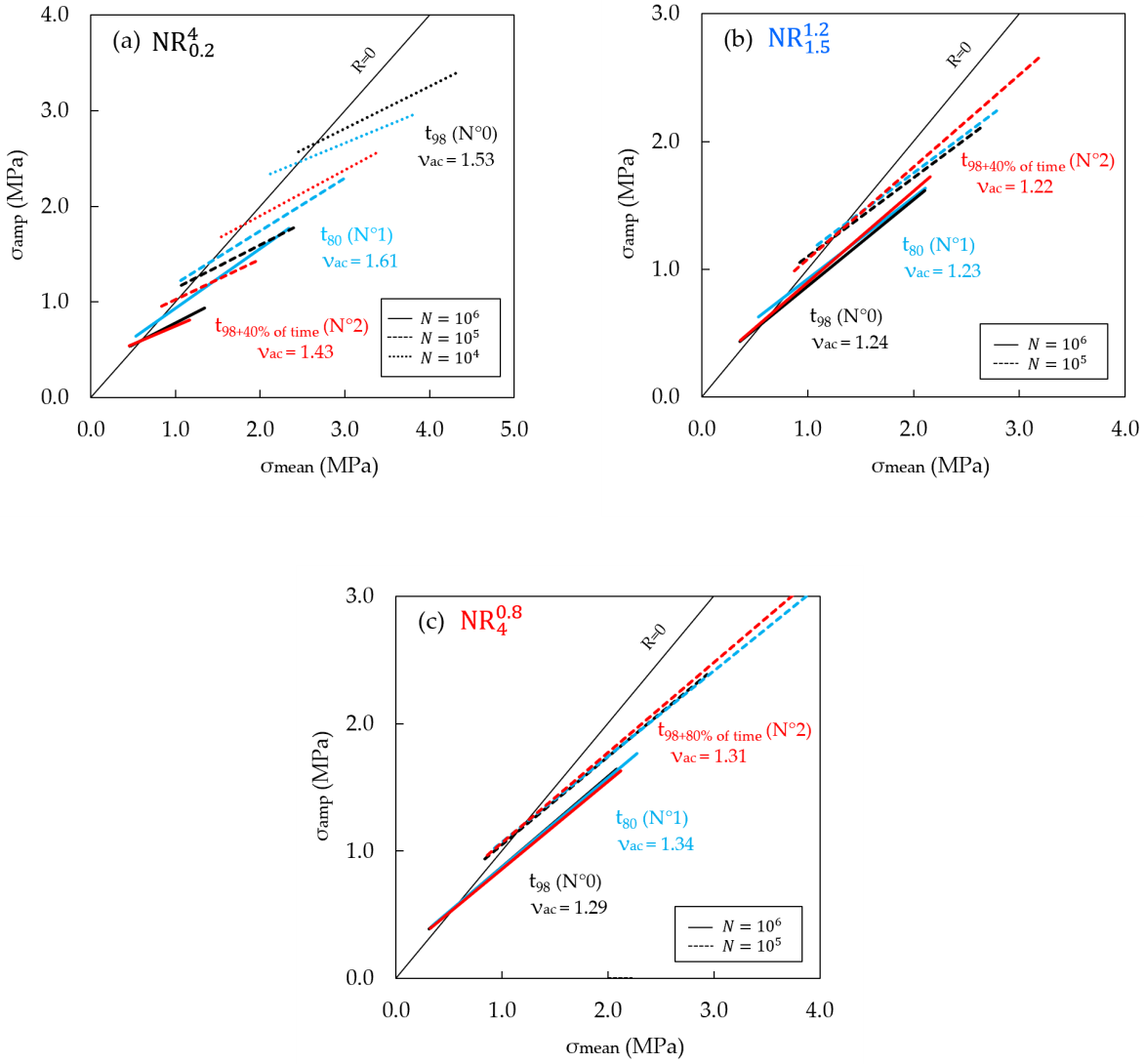

Figure 4.16: Effect of the vulcanization time on the lifetime reinforcement for (a) $NR^4_{0.2}$ (CV) (b) $NR^{1.2}_{1.5}$ (SEV) and (c) $NR^{0.8}_4$ (EV).

Vulcanization time

Figure 4.16 presents the effect of the vulcanization time on fatigue response for (a) $NR^4_{0.2}$ (b) $NR^{1.2}_{1.5}$ and (c) $NR^{0.8}_4$. Fig. 4.16 (a) presents the effect of the vulcanization time on fatigue response for $NR^4_{0.2}$. For too much time (N°2), a decrease in the slope is obtained, indicating a lower lifetime reinforcement. On the other hand, under-vulcanized $NR^4_{0.2}$ (N°1), shows higher slope and consequently a higher lifetime reinforcement. This suggests that under-vulcanization significantly enhance the lifetime reinforcement for CV system. However, for 10^4 cycles it is noticeable that the optimal $NR^4_{0.2}$ (N°0) was slightly more reinforced. Figs. 4.16 (b) and (c) shows the results obtained for $NR^{1.2}_{1.5}$ and $NR^{0.8}_4$, respectively. There was no significant effect of the vulcanization time on the lifetime

reinforcement. This could be due to the fact that SEV and EV systems are less thermally sensitive, resulting in few structural changes.

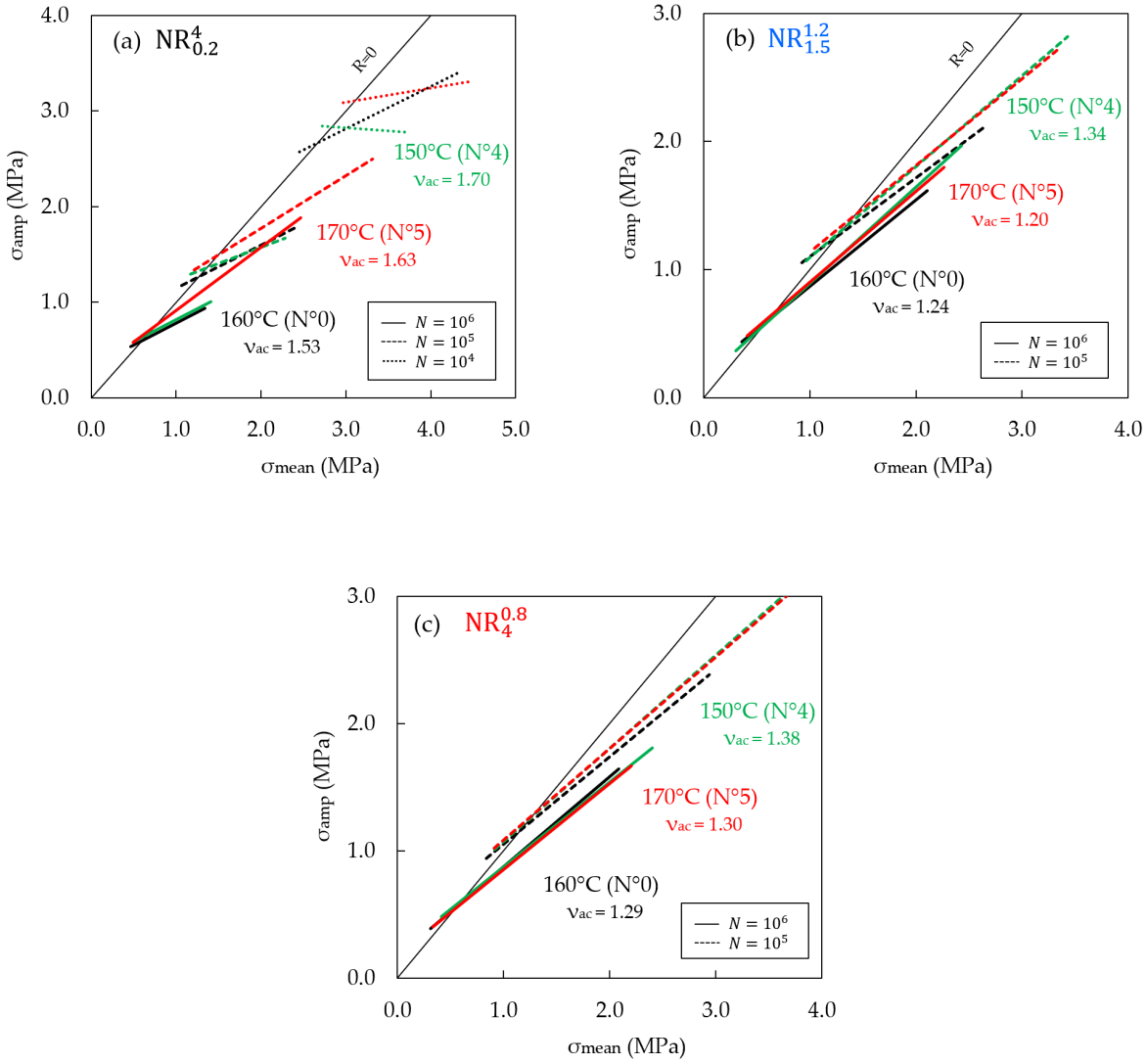

Figure 4.17: Effect of the vulcanization temperature on the lifetime reinforcement for (a) $NR^4_{0.2}$ (CV) (b) $NR^{1.2}_{1.5}$ (SEV) and (c) $NR^{0.8}_4$ (EV).

Vulcanization temperature

Figure 4.17 presents the effect of the vulcanization temperature on fatigue response for (a) $NR^4_{0.2}$ (b) $NR^{1.2}_{1.5}$ and (c) $NR^{0.8}_4$. Fig. 4.17 (a) shows the effect of the vulcanization temperature for $NR^4_{0.2}$. A vulcanization temperature of 170°C exhibits a slightly higher slope than the two other temperatures. Nevertheless, it appears that slopes of 10^4 cycles iso-lifetimes decrease drastically for 150°C and 170°C. It is noteworthy that they have much higher ν_{ac} than 160°C. This could induce a ν_{ac} threshold, and above this threshold

a decrease in fatigue response at high stress is obtained. Fig. 4.17 (b) presents the fatigue response for $NR^{1.2}_{1.5}$ vulcanized at 150°C, 160°C and 170°C. Comparable results are obtained, suggesting no effect of the vulcanization temperature for SEV system. The same results were obtained for EV system (Fig. 4.17 (c)). This is again correlated with the better thermal resistance of short cross-links, *i.e.*, SEV and EV systems.

4.3.2.3 Damage modes analysis

For non-relaxing loading, three damage modes are observed, namely Damage modes 1, 2 and 3 as defined in Sub-section 4.2.4.2. These damage modes are used in order to investigate the effect of ν_{ac} on the damage mechanisms. For the sake of clarity, the same three NR presented in Section 4.3.1 in Tab. 4.8 are used again. Moreover, since most of the Diabolo specimens did not fail during the fatigue tests at 90% of maximum strain, no result at this strain level will be presented.

Effect of the active chain density on the damage mechanisms

Figure 4.18 shows the effect of maximum strain on the fracture surfaces of $NR^{0.8}_{2.5}$, $NR^{1.2}_{2.5}$, and $NR^{1.6}_{2.5}$.

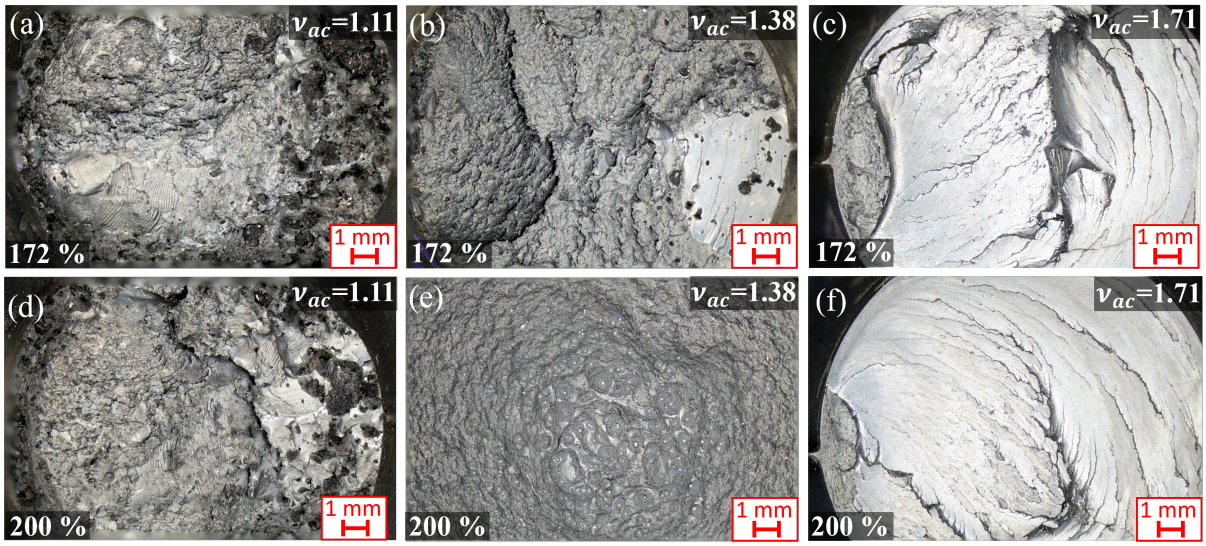

Figure 4.18: Fractographies of $NR^{0.8}_{2.5}$, $NR^{1.2}_{2.5}$ and $NR^{1.6}_{2.5}$, tested in fatigue under non-relaxing loading conditions. The effect of the maximal strain for $NR^{0.8}_{2.5}$ at (a) 172% and (d) 200%, $NR^{1.2}_{2.5}$ at (b) 172% and (e) 200% and $NR^{1.6}_{2.5}$ at (c) 172% and (f) 200% is given.

Figs. 4.18 (a), (b) and (c) present the fracture surfaces obtained at 172% of maximum strain. For the lower ν_{ac}, Damage mode 2 was obtained, with wrenchings, cones along the edge and well-defined fatigue striations and a slight final ligament. For ν_{ac} of 1.38×10^4 mol/cm^3, the same damage mode was obtained, but with a more prominent final ligament. Then, for the highest ν_{ac}, *i.e.*, $NR^{1.6}_{2.5}$ an almost unique smooth surface

characteristic of a catastrophic failure in Damage mode 1 is observed. Furthermore, no SIC marker was observed, which questions the effect of SIC and the ability to crystallize for this material with a high ν_{ac}. Subsequently, the second row, corresponding to maximum of 200% strain (Fig. 4.18 (d), (e) and (f)), exhibited some differences. For $NR^{0.8}_{2.5}$ the only difference is a larger final ligament. However, $NR^{1.2}_{2.5}$ was altered by Damage mode 3 with cavitations under the metallic inserts, due to a higher reinforcement than the others. This suggests that ν_{ac} is strongly correlated with the fatigue resistance. It is perhaps worth emphasizing that $NR^{1.6}_{2.5}$ (Fig. 4.18) is almost solely composed of a wide and smooth surface, characteristic of a catastrophic failure. This could be due to an excessively high ν_{ac}. More importantly, analogous outcomes were observed for [A]/[S] ratios of 0.2, 0.6, and 1.5.

To sum-up, as for relaxing tension loadings, both ν_{ac} and strain level influence the fracture surface. Smooth fracture surfaces are found in the case of high ν_{ac} while low ν_{ac} enables SIC markers, *i.e.*, fatigue striations and cones as well as cavitation to form. This questions once more the relationship between SIC and ν_{ac}. This topic is fully addressed in Section 4.3.3.

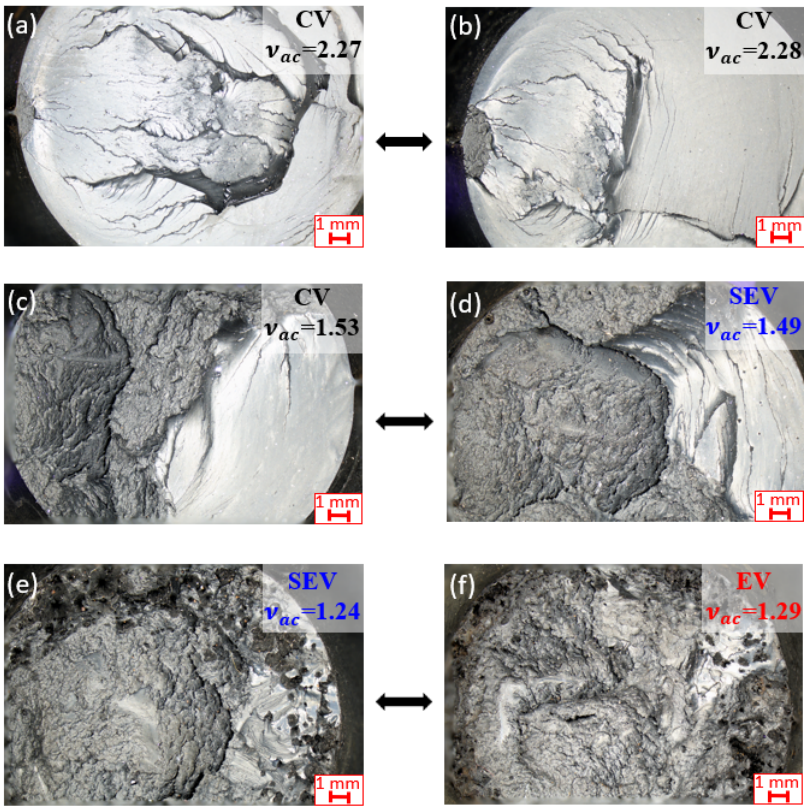

Figure 4.19: Fractographies of (a) $NR^{6}_{0.2}$, (b) $NR^{4}_{0.6}$, (c) $NR^{4}_{0.2}$,(d) $NR^{1.6}_{1.5}$, (e) $NR^{1.2}_{1.5}$ and (f) $NR^{0.8}_{4}$. Diabolos were tested under non-relaxing loading conditions at 172% of maximum strain.

Effect of the cross-link length on the damage mechanisms

The effect of the cross-link length on the fracture surface is evaluated by comparing the same materials as those presented in Table 4.8, with similar ν_{ac} but different [A]/[S]. Since fractographic images showed similar changes at 172%, and 200% of maximum strain, the 172% strain condition will be used as a reference example hereafter. Figure 4.19 presents a comparison of materials with close values of ν_{ac}. Similarly to relaxing tension loadings, Pair n°1 showed a comparable fracture surface with a tiny stable propagation area and a very large smooth surface, characteristic of a catastrophic failure. For this high ν_{ac}, it suggests that the cross-link length is not a first order parameter driving the damage mechanisms. Continuing with Pair n°2, there is no significant difference between the two surfaces. Indeed, both fracture surfaces consist of wrenchings, and a consequent smooth area characteristic of a catastrophic failure. Finally, no differences were obtained with Pair n°3. Both exhibited wrenchings, fatigue striations and cones along the edge. From these observations it is concluded that the cross-link length has no significant effect on the fracture surface.

4.3.2.4 Summary

In this section dedicated to the fatigue results under non-relaxing loading conditions, the effect of the vulcanization system and conditions have been studied. ν_{ac} was found to govern the fatigue properties and damage modes. Smooth fracture surfaces, especially for high ν_{ac}, are possibly explained by the stiffness and mobility restriction induced by an excessive ν_{ac}. Some materials exhibited fatigue striations, cones and fracture under metallic inserts, which indicates a strong reinforcement. These results obtained with the fractrographic analysis is in a strong agreement with the results obtained in terms of end-of-life and lifetime reinforcement. Indeed, ν_{ac} was also found to drive the lifetime reinforcement evaluated on Haigh diagram, with specific ranges showing a very sharp reinforcement. It is perhaps worth emphasizing that the effect of the cross-link length on damage mechanisms was found to be negligible, while the latter showed slight effect for the fatigue resistance analysis. Concerning the vulcanization conditions effect on lifetime reinforcement, vulcanization time showed a strong effect for CV while no effect for vulcanization temperature was observed. In view of these results, the question of the relationship between the network structure, SIC markers and lifetime reinforcement is of primary importance in order to better understand and model the fatigue behavior of NR.

4.3.3 Discussion

The relationship between ν_{ac}, the fatigue response and the damage modes is discussed in this section. A new representation based on the clustering of the different materials

regarding their ν_{ac} is here proposed. Fatigue response and damage modes are independently addressed in Sub-sections 4.3.3.1 and 4.3.3.2, respectively. Finally, a comparison between them is performed in Sub-section 4.3.3.3.

4.3.3.1 Effect of the active chain density on the fatigue life

Relaxing tension loading conditions

The different materials were clustered into groups with respect to their fatigue resistance. Five categories were defined as they minimize the regression coefficient of the fitted endurance curves. The materials categories are summarized in Table 4.9.

Category	Range of ν_{ac}	Materials	Power law	R^2
1	0.95 - 1.20	$NR^{2}_{0.2}$, $NR^{0.8}_{2.5}$	$\sigma_{max} = 34.836 \times N_i^{-0.262}$	0.95
2	1.20 - 1.30	$NR^{1.2}_{1.5}$, $NR^{0.8}_{4}$	$\sigma_{max} = 167.76 \times N_i^{-0.391}$	0.94
3	1.30 - 1.70	$NR^{1.6}_{1.5}$, $NR^{1.2}_{2.5}$, $NR^{2}_{0.6}$, $NR^{4}_{0.2}$, $NR^{1.6}_{2.5}$	$\sigma_{max} = 75.518 \times N_i^{-0.309}$	0.97
4	2.20 - 2.30	$NR^{6}_{0.2}$, $NR^{4}_{0.6}$	$\sigma_{max} = 24.534 \times N_i^{-0.206}$	0.99
5	0.95 and $>$ 3.20	$NR^{0.8}_{1.5}$, $NR^{6}_{0.6}$	$\sigma_{max} = 18.701 \times N_i^{-0.228}$	0.98

Table 4.9: Materials categorization according to the fatigue life for relaxing tension loading.

Figure 4.20 presents the (a) endurance curves of each category (b) summarized in the [A]/[S] diagram. Categories 4 and 5 correspond to the highest and the lowest fatigue resistance, respectively. Surprisingly, the best fatigue resistance is reach for 2.27×10^4 mol/cm^3, while it drastically drops above 3.20×10^4 mol/cm^3 for category 5. This demonstrates that a high ν_{ac} increases the number of active chains contributing to the network strength, and therefore increases the strain energy required to break the active chains [135]. However, a too high ν_{ac} leads to too high energy input for crack growth [130], and causes a premature rupture. Thus, this suggests the existence of an optimum value of ν_{ac} maximizing the fatigue resistance. The fatigue resistance and the stress response decrease progressively, from category 4 to 1 corresponding to 2.30 to 0.95×10^4 mol/cm^3, respectively. This is consistent with what reported Mars and Fatemi: "There is an optimum crosslink density, which results in the longest fatigue life." [1]. It is perhaps worth emphasizing that $NR^{0.8}_{1.5}$, which has a ν_{ac} corresponding to 0.95×10^4 mol/cm^3, does not follow this trend. As demonstrated in Section 4.3.1, a low ν_{ac} combined with short cross-links is responsible for a lower fatigue life. To continue, the two endurance curves for Categories 4 and 5 are almost parallel. On the other hand, the endurance curves for Categories 1, 2 and 3 has a much higher slope. This could be due to a stiffening effect that depends on the level of strain. Since SIC is driven by the strain level, it could be related to this stiffening effect [223]. It is noteworthy that Tosaka *et al.* found an optimum ν_{ac} maximizing SIC around

1.50×10^4 mol/cm^3 [126, 128], which is very close to the values of Categories 2 and 3. Furthermore, Chenal *et al.* reported an optimum ν_{ac} of 1.20×10^4 mol/cm^3 [116], which corresponds to Category 1.

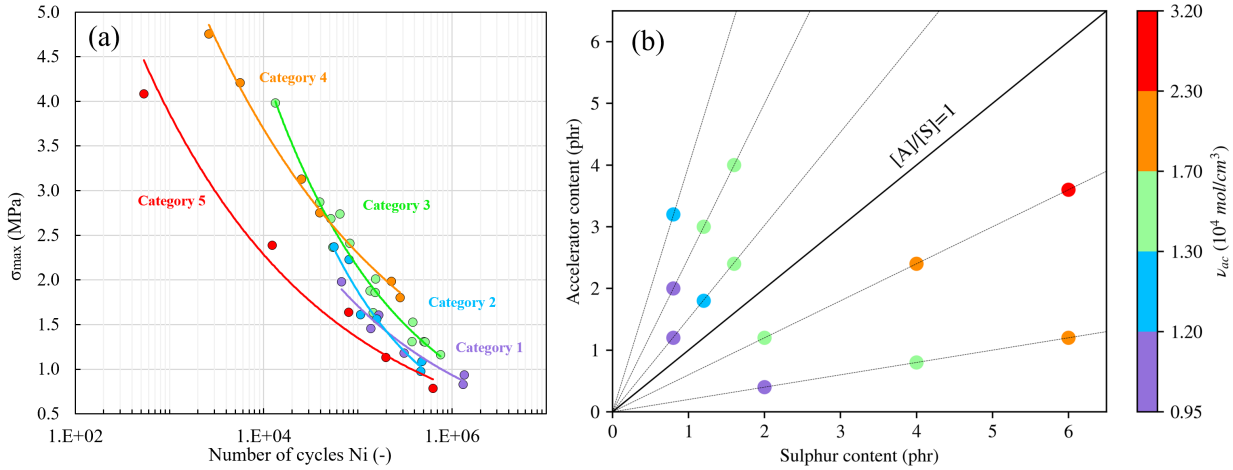

Figure 4.20: Clustering of the vulcanization system depending on their fatigue resistance: (a) endurance curves and (b) cartography of ν_{ac} categories in the [A]/[S] diagram.

Non-relaxing tension loading conditions

Materials were clustered into groups regarding their lifetime reinforcement. Figure 4.21 (a) presents the 10^4 cycles iso-lifetime associated with these groups. These iso-lifetimes correspond to a given reference material providing an example of the reinforcement corresponding to its ν_{ac} range. The categories are given in Table 4.10.

Category	Range of ν_{ac}	Materials	Equation
1	0.95 - 1.20	$NR^2_{0.2}$, $NR^{0.8}_{1.5}$, $NR^{0.8}_{2.5}$	$\sigma_{amp} = 0.6472 \times {\sigma_{mean}}^{0.3913}$
2	1.20 - 1.30	$NR^{1.2}_{1.5}$, $NR^{0.8}_{4}$	$\sigma_{amp} = 0.6886 \times {\sigma_{mean}}^{0.363}$
3	1.30 - 1.50	$NR^{1.6}_{1.5}$, $NR^{1.2}_{2.5}$, $NR^2_{0.6}$	$\sigma_{amp} = 0.682 \times {\sigma_{mean}}^{0.4397}$
4	1.50 - 1.70	$NR^4_{0.2}$, $NR^{1.6}_{2.5}$	$\sigma_{amp} = 0.4518 \times {\sigma_{mean}}^{0.4965}$
5	1.70 - 2.30	$NR^6_{0.2}$, $NR^4_{0.6}$	$\sigma_{amp} = 0.2195 \times {\sigma_{mean}}^{0.9849}$
6	3.20	$NR^6_{0.6}$	$\sigma_{amp} = 0.0913 \times {\sigma_{mean}}^{0.7262}$

Table 4.10: Material categorization according to the fatigue life reinforcement for non-relaxing tension loading.

Categories 1, 2 and 3 show a very similar reinforcement as they have the same slopes. In particular, ranges of 1.20 - 1.50 $\times 10^4$ mol/cm^3 demonstrates a slightly higher lifetime

reinforcement. This indicates that ν_{ac} drives the lifetime reinforcement, suggesting therefore better ability to crystallize for these categories. This is in good agreement with ν_{ac} ranges that maximized SIC, according to the results of Tosaka *et al.* [126, 128]. By increasing ν_{ac} above 1.50×10^4 mol/cm^3, which corresponds to Category 4, this lifetime reinforcement is much less pronounced. It weakens further above 1.70 $\times 10^4$ mol/cm^3 for Category 5 and almost disappears for Category 6. Hence, ν_{ac} showed a strong correlation with the lifetime reinforcement, suggesting that a too high ν_{ac} decreases the ability to crystallize and the lifetime reinforcement. It is to be noted that the most interesting materials differ from the results found at $R_U = 0$, *i.e.*, 0.95 - 1.50 $\times 10^4$ mol/cm^3 *vs* 1.20 - 1.70 $\times 10^4$ mol/cm^3 at $R_U = 0.25$ and $R_U = 0$, respectively.

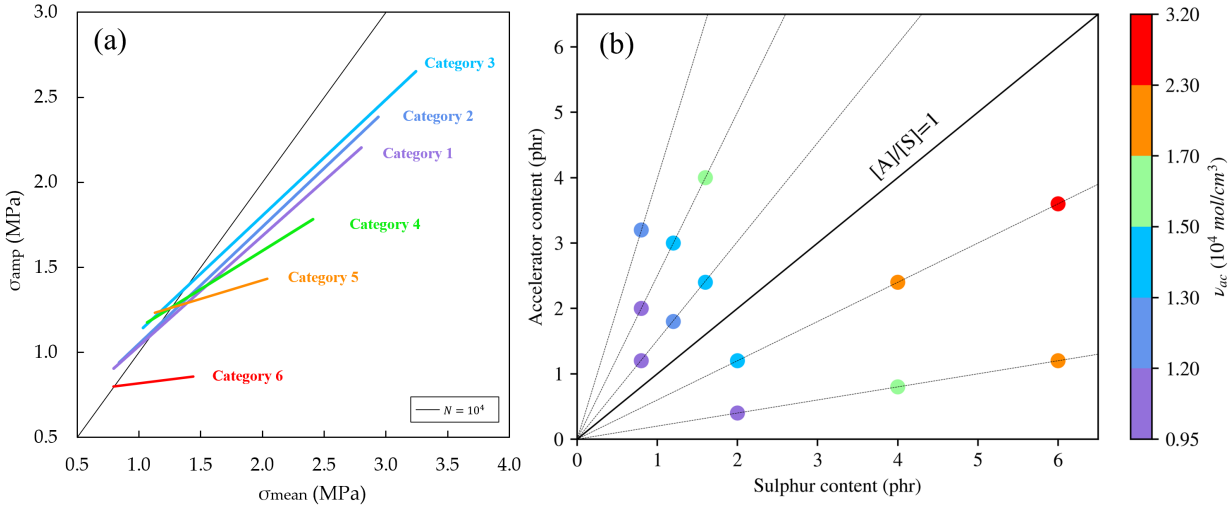

Figure 4.21: Effect of ν_{ac} on the fatigue resistance. In (a) the fatigue response was classified with respect to ν_{ac}, leading to five categories of responses. In (b) these categories are recalled in terms of the vulcanization system.

4.3.3.2 Effect of the active chain density on the damage modes

Relaxing tension loading conditions

In Section 4.3.1, ν_{ac} was found to be the main parameter driving the damage mechanisms. The fracture surfaces were clustered into 4 categories regarding the size of the stable and unstable crack propagation zones, the presence and size of striations and the size of the final ligament. The material categories are given in Table 4.11, as well as the corresponding ν_{ac} and damage mode. Figures 4.22 (a), (b), (c) and (d) presents characteristic failure surfaces of materials in Categories 1, 2, 3 and 4, respectively, for a test carried out at $\epsilon_{max} = 120\%$ and for $R_U = 0$. It has to be noted that similar conclusions were drawn at other strain levels.

Category	**Range of ν_{ac}**	**Materials**	**Damage mode**
1	0.95 - 1.20	$NR^{2}_{0.2}$, $NR^{0.8}_{1.5}$	1
2	1.20 - 1.50	$NR^{0.8}_{2.5}$, $NR^{1.2}_{1.5}$, $NR^{0.8}_{4}$, $NR^{1.2}_{2.5}$, $NR^{2}_{0.6}$, $NR^{1.6}_{1.5}$	1
3	1.50 - 1.70	$NR^{1.6}_{2.5}$, $NR^{4}_{0.2}$	1
4	1.70 - 3.20	$NR^{4}_{0.6}$, $NR^{6}_{0.2}$, $NR^{6}_{0.6}$	1

Table 4.11: Material categorization according to the damage mechanisms, for relaxing tension loadings at ϵ_{max}=120%.

First, the size of the stable crack propagation zone increases with ν_{ac}. However, this trend is not followed for ν_{ac} above $1.70 \times 10^4\,\mathrm{mol/cm^3}$. Since the transition between the stable and unstable crack propagation zoneis correlated with the resistance to crack growth, this goes in the sense that increasing ν_{ac} increases the fatigue resistance. Then, the size of the final ligament increases with ν_{ac}. It almost constitutes the whole fracture surface for filled NR in Category 4. This could be explained by the too high ν_{ac} and stiffening, which leads to catastrophic failure. The fatigue striations were only observed for ν_{ac} from 0.95 and to $1.50 \times 10^4\,\mathrm{mol/cm^3}$. This suggests that this range of ν_{ac} presents good ability to crystallize. Above $1.50 \times 10^4\,\mathrm{mol/cm^3}$, fatigue striations completely disappeared. It has to be noted that the damage mechanism is fully driven and evolves continuously with ν_{ac}, which is in opposition with the fatigue life categorization, see Table 4.9, for which materials having ν_{ac} below 0.95 and above $2.30 \times 10^4\,\mathrm{mol/cm^3}$ had comparable fatigue resistance. This shows that the post-mortem analysis, and fatigue lifetime have to be put into perspectives and compared systematically.

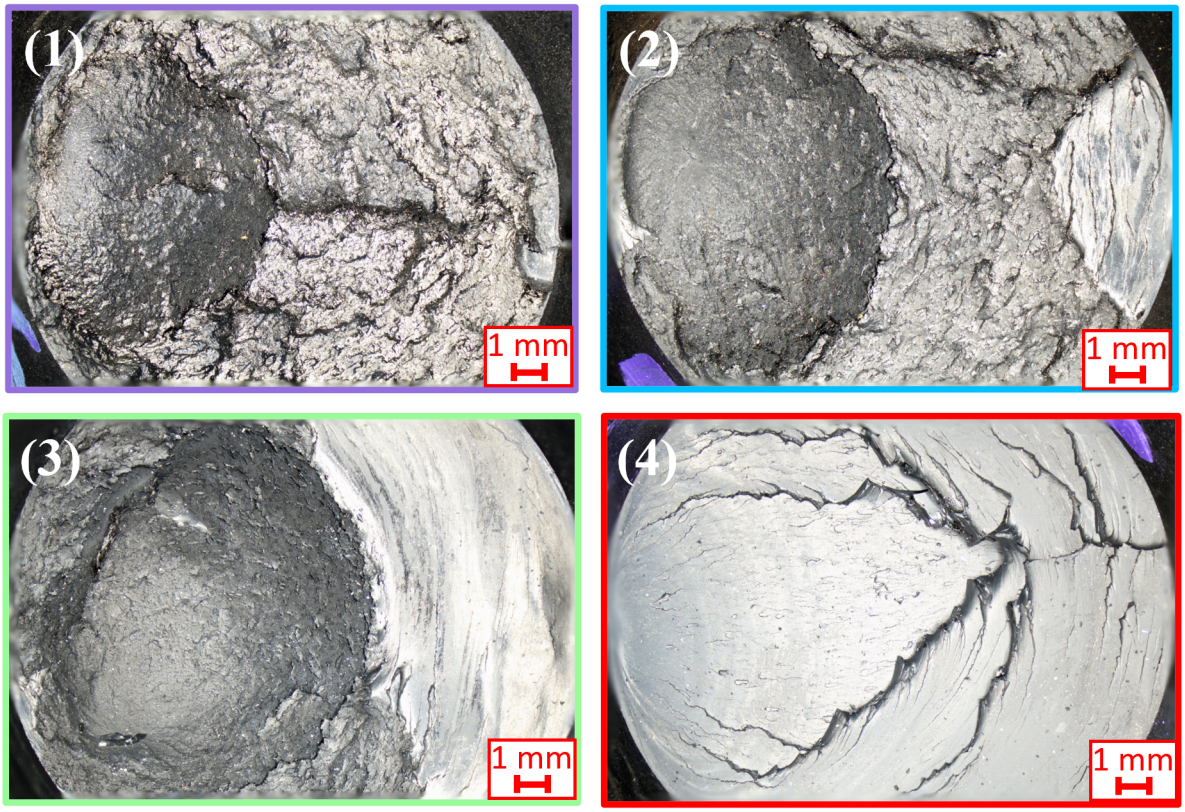

(a)

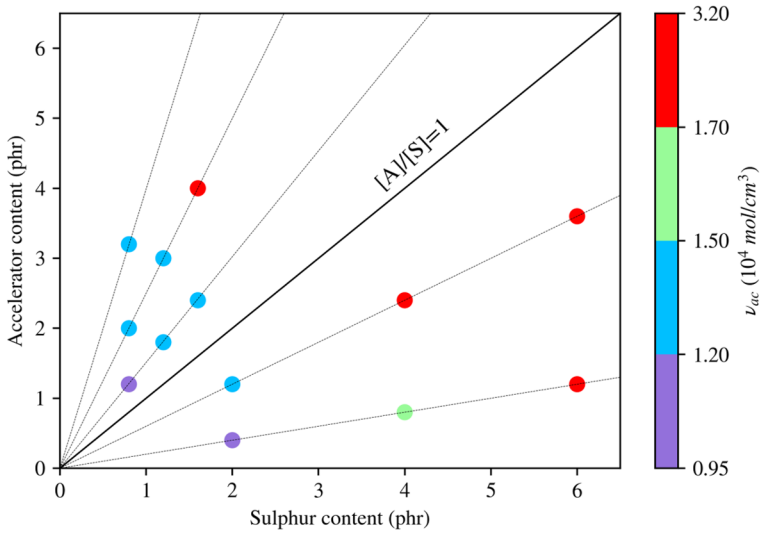

(b)

Figure 4.22: Effect of ν_{ac} on the damage mechanisms, for relaxing tension loading condition at ϵ_{max}=120%. Fracture surfaces are given in (a) and corresponds to the groups numbered 1 to 4, represented in (b).

Non-relaxing tension loading conditions

As above-mentioned, the damage modes under non-relaxing loading conditions evolve with the strain level. At 90% of maximum strain, there are solely two groups: *(i)* those that do not break and *(ii)* those that experience early catastrophic failure above 1.70×10^4 mol/cm^3. There is no in-between, supporting the possibility that a threshold exists, above which fatigue properties are reduced. Figure 4.23 (a) (1, 2, 3 and 4) illustrates the four failure surfaces identified for each category at 172% of strain, which are given in Table 4.12. In addition, Figure 4.24 (a) (1, 2, 3 and 4) shows the four characteristic failure surfaces at 200% of strain. Categories are given in Table 4.13.

Category	**Range of ν_{ac}**	**Materials**	**Damage mode**
1	0.95 - 1.25	$NR^{2}_{0.2}$, $NR^{0.8}_{1.5}$, $NR^{0.8}_{2.5}$, $NR^{1.2}_{1.5}$	2
2	1.25 - 1.50	$NR^{0.8}_{4}$, $NR^{1.2}_{2.5}$, $NR^{1.6}_{1.5}$	2
3	1.50 - 1.55	$NR^{4}_{0.2}$	2
4	1.55 - 3.20	$NR^{1.6}_{2.5}$, $NR^{4}_{0.6}$, $NR^{6}_{0.2}$	1
No failure	1.41	$NR^{2}_{0.6}$	-
Not tested	3.20	$NR^{6}_{0.6}$	-

Table 4.12: Material categorization according to the damage mechanisms, for non-relaxing loadings at ϵ_{max}=172%.

At 172% of strain, fracture surfaces of Categories 1 and 2 were similar and composed of cones at the edges of the Diabolo specimen, well defined fatigue striations, rough wrenchings, and a small final ligament. Therefore, from 0.95 and to 1.50×10^4 mol/cm^3, fatigue resistance is very high. By further increasing ν_{ac}, fatigue striations disappeared for Category 3. Indeed, failure surfaces are composed solely of rough wrenchings and a larger smooth area similar to a final ligament. This suggests a lower lifetime reinforcement. Finally, Category 4 consists of materials of ν_{ac} ranging from 1.55 to 3.20×10^4 mol/cm^3, whose fracture surfaces are composed solely of a completely smooth surface, indicative of a catastrophic failure. For these materials, the fracture surface is comparable to those obtained for relaxing tension loading conditions, which suggests no significant differences in fatigue life, *i.e.*, no lifetime reinforcement. Finally, for highly non-relaxing loading conditions (*i.e.*, R_U = 0,25 and 200% strain), the behavior of the materials continue to evolve, leading to a new classification, given in Table 4.13.

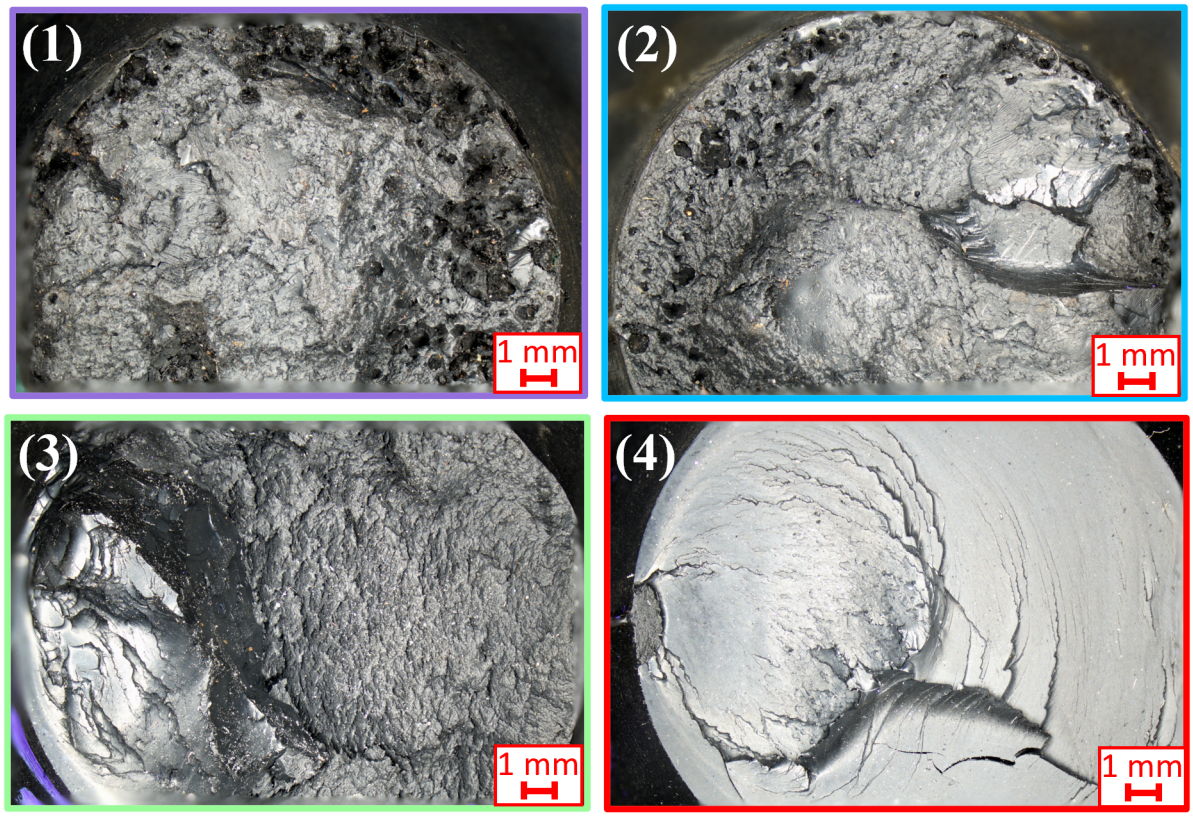

(a)

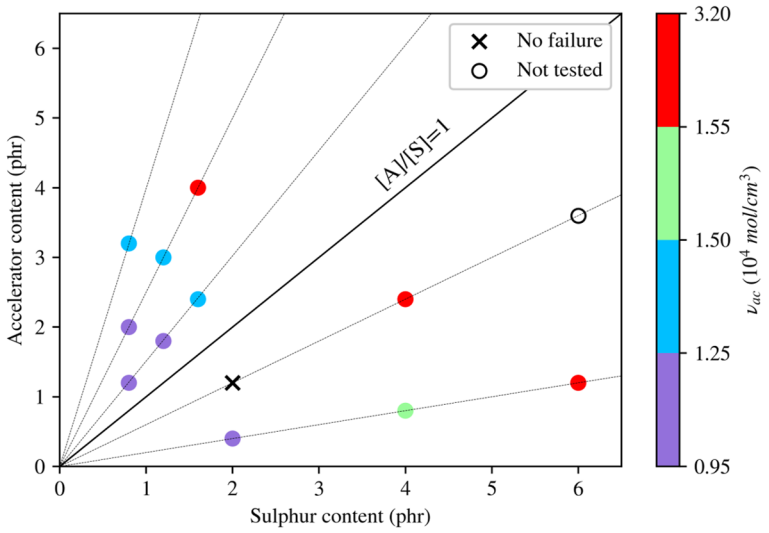

(b)

Figure 4.23: Effect of ν_{ac} on damage mechanisms, for non-relaxing loadings at ϵ_{max}=172%. Fracture surfaces are given in (a) and corresponds to the groups numbered 1 to 4, represented in (b).

Category	**Range of ν_{ac}**	**Materials**	**Damage mode**
1	0.95 - 1.20	$NR^{2}_{0.2}$, $NR^{0.8}_{1.5}$, $NR^{0.8}_{2.5}$	2
2	1.29	$NR^{0.8}_{4}$	2 & 3
3	1.20 - 1.50	$NR^{1.2}_{1.5}$, $NR^{1.2}_{2.5}$, $NR^{2}_{0.6}$, $NR^{1.6}_{1.5}$	3
4	1.50 - 1.70	$NR^{1.6}_{2.5}$, $NR^{4}_{0.2}$	1
Not tested	1.70 - 3.20	$NR^{4}_{0.6}$, $NR^{6}_{0.2}$, $NR^{6}_{0.6}$	-

Table 4.13: Material categorization according to the damage mechanisms, for non-relaxing loadings at ϵ_{max}=200%.

At 200% of strain, for Category 1, *i.e.*, ν_{ac} ranging between 0.95 and 1.20×10^4 mol/cm^3, cones at the edges of the Diabolo specimen, well-defined fatigue striations, rough wrenchings, and a small final ligament were obtained. This corresponds to a significant lifetime reinforcement. On the other hand, Category 2 solely includes the $NR^{0.8}_{4}$ with ν_{ac} equal to 1.29×10^4 mol/cm^3. For this material, both Damage modes 2 and 3 were reported. Category 3, with ν_{ac} between 1.20 and 1.50×10^4 mol/cm^3, shows a fracture shifted under the metallic inserts as indicated by the presence of cavitations, traducing a high reinforcement in the center of the Diabolo specimens. Then, Category 4 with ν_{ac} ranging from 1.50 to 1.70×10^4 mol/cm^3 presents fracture surfaces composed of some wrenchings and a very large smooth surface, characteristic of a catastrophic failure. Thus, a too high ν_{ac} shows the absence of SIC markers. Finally, there is also three materials not tested, with ν_{ac} ranging from 1.70 to 3.20×10^4 mol/cm^3 ($NR^{4}_{0.6}$, $NR^{6}_{0.2}$ and $NR^{6}_{0.6}$). The white color is used for those materials that cannot be classified.

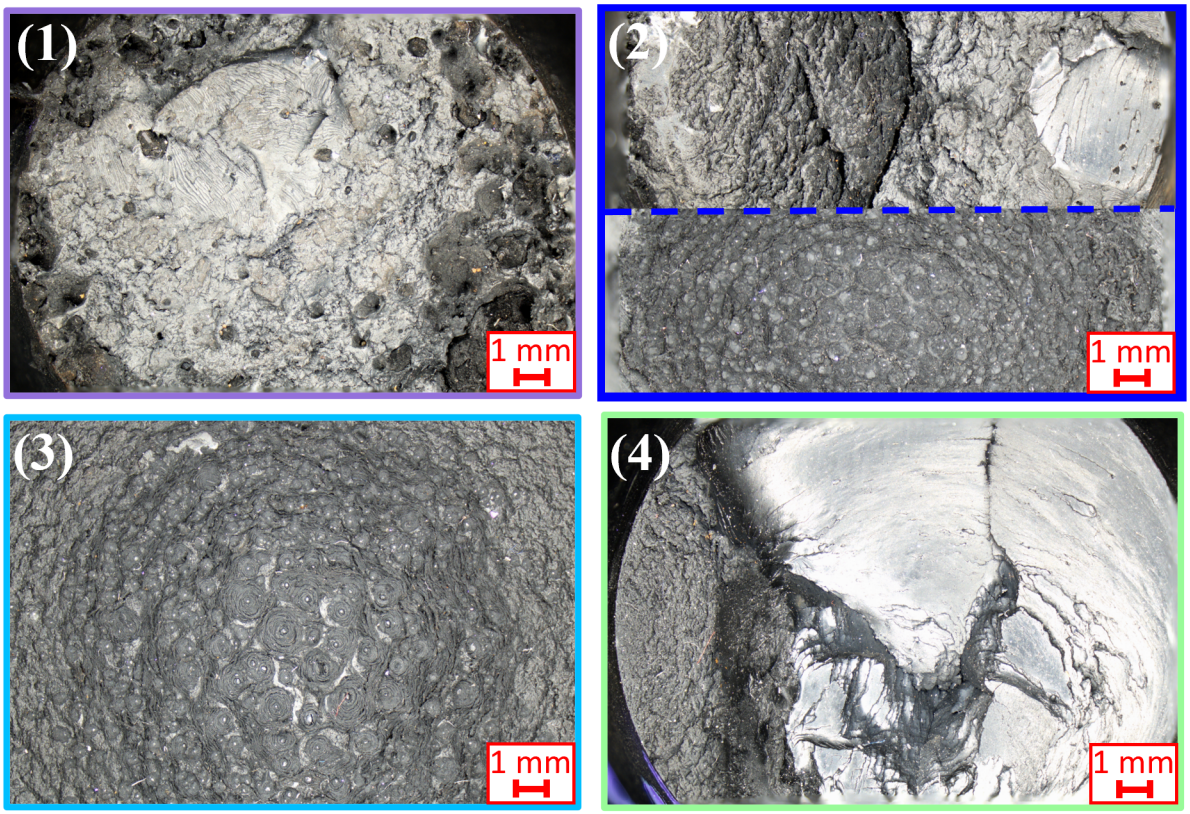

(a)

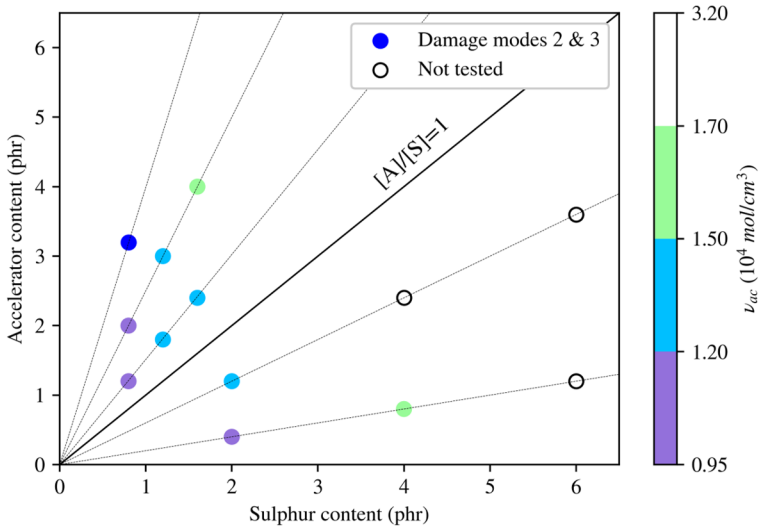

(b)

Figure 4.24: Effect of ν_{ac} on the damage mechanisms, for non-relaxing loadings at ϵ_{max}=200%. Fracture surfaces are given in (a) and corresponds to the groups numbered 1 to 4, represented in (b).

4.3.3.3 Relationship between the active chain density, fatigue response and damage mechanisms

Mappings realized for fatigue resistance and damage mechanisms showed similarities and differences. This is discussed in the present sub-section.

Relaxing tension loading conditions

At high ν_{ac}, active chains are restricted, which results in the network losing its ability to dissipate the strain energy [224]. Furthermore, network rearrangements are limited which may lead to local stress concentrations. This corresponds to the smooth fracture surface previously observed. However, even though they have a high ν_{ac} and a smooth fracture surface, $NR^6_{0.2}$ and $NR^4_{0.6}$ showed good fatigue response. This suggests that fracture surface mechanisms are governed by stress, and should be carefully analyzed with respect to endurance curves. Furthermore, SIC seems activated only for ν_{ac} between 0.95 and $1.50 \times 10^4\,\mathrm{mol/cm^3}$, as evidenced by SIC markers such as fatigue striations. This is correlated with the ν_{ac} range showing endurance curves with a higher slope. More importantly, the range of ν_{ac} for these materials is closed to optimal ν_{ac} values maximizing SIC and ranging from 1.20 to $1.50 \times 10^4\,\mathrm{mol/cm^3}$ [65, 116, 126, 128].

Non-relaxing tension loading conditions

As explained by Le Cam and Toussaint, high stress at the crack tip locally increases the crystallinity, preventing the crack from propagating in a direction perpendicular to the applied load and therefore causing the crack to bifurcate. As a result, the fracture surfaces experience simultaneous tearing, sliding and relaxation along the highly crystallized tip, leading to the formation of fatigue striations [186]. This is typically encountered below $1.20 \times 10^4\,\mathrm{mol/cm^3}$. Nevertheless, for ν_{ac} ranges between 1.20 and $1.50 \times 10^4\,\mathrm{mol/cm^3}$, cavitations were indicative of a reinforcement so significant that failure no longer occurs in the middle of the Diabolo specimen but under the metallic inserts. For this range of ν_{ac}, a strong lifetime reinforcement was also evidenced in the Haigh diagram. This proves that the SIC markers are correlated with the lifetime reinforcement, and ν_{ac}. However, since each filled NR demonstrated a lifetime reinforcement, this questions the origin of the lifetime reinforcement. Hence, we note that SIC seems to drive the level of reinforcement, but it may not be the only reason for the activation of the lifetime reinforcement.

4.4 Conclusions and perspectives

This study explores the effect of the macromolecular network structure on the fatigue response of CB filled NR. Different active chain densities and cross-link lengths were

studied, by varying vulcanization conditions and system. The active chain density of each material was evaluated by using swelling tests and the Flory-Rehner relationship. Fatigue tests at two different loading ratios and post-mortem analyses were performed in order to study the effect of the macromolecular network on the fatigue resistance and the lifetime reinforcement. For relaxing tension loading conditions, fatigue resistance was found to depend on the active chain density. A sufficient active chain density is necessary to ensure good fatigue properties. In addition, a certain range of materials showed a fatigue curve which was strongly dependent on the strain level. However, it was found that increasing the active chain density leads to an increase in the final ligament on the fracture surface which suggests catastrophic failure. For non-relaxing tension loading conditions, it was found that both lifetime reinforcement and SIC markers are related to the active chain density. There is an optimum range of active chain density maximizing both the SIC markers, and the lifetime reinforcement. For highly cross-linked materials, SIC markers disappeared, and the lifetime reinforcement was weakened. This study provides the first relationship between the macromolecular network structure, the fatigue properties and the damage mechanisms.

Conclusion générale

Ces travaux de thèse portent sur l'effet de la structuration du réseau macromoléculaire sur les propriétés mécaniques quasi-statiques et en fatigue du caoutchouc naturel. La boucle de conception de pièces en caoutchouc s'avère à la fois longue et coûteuse, impliquant plusieurs itérations. Comprendre comment la formulation et les conditions de vulcanisation modifient le réseau macromoléculaire, et de facto les propriétés mécaniques, est nécessaire afin d'optimiser la conception de ces pièces. La caractérisation d'une large gamme de matériaux aux structures de réseau macromoléculaire différentes, obtenues en faisant varier les conditions et systèmes de vulcanisation, a été menée.

Avant d'aborder les résultats obtenus sur les propriétés mécaniques, il convient de rappeler que la méthode de gonflement, et plus précisément les hypothèses de calculs employées lors du traitement de données, a fait l'objet d'un verrou scientifique. En effet, la littérature n'étant pas unanime sur la prise en compte des particules insolubles, nous avons alors mis en lumière leur effet notable sur le calcul de la densité de chaînes actives. L'effet de la fraction volumique du CB et du ZnO, ainsi que les interactions CB-matrice, ont donc été prises en compte afin d'assurer une évaluation représentative de la densité de chaînes actives et donc de la structuration du réseau macromoléculaire.
La caractérisation mécanique en quasi-statique a confirmé que la densité de chaînes actives et les charges pilotent la raideur. Pour les matériaux non-chargés, l'effet Mullins dépend de la densité de chaînes actives. Ce résultat questionne de fait la contribution de la SIC, puisque cette dernière dépend elle-même de la densité de chaînes actives. Cependant, pour les matériaux chargés, l'effet Mullins est principalement dû à la présence de charges si bien que l'effet de la densité de chaînes actives devient négligeable, voire non-détectable.
En ce qui concerne la caractérisation en fatigue, plusieurs contributions originales ont été obtenues. Pour un matériau chargé d'une même quantité et d'un même type de CB, la structuration du réseau macromoléculaire :

1. pilote la résistance à la fatigue. La densité de chaînes actives, la raideur et la longueur des ponts soufrés ont un effet pour les chargements relaxants, alors que

la densité de chaînes actives semble à elle seule piloter le niveau de renforcement atteint dans le cas de chargements non-relaxants,

2. et plus précisément la densité de chaînes actives, affecte la morphologie des faciès de rupture, *e.g.*, la zone de propagation stable, la taille du ligament final et les marqueurs de la SIC.

Ces résultats peuvent être plus pertinemment mis en perspective avec le phénomène de cristallisation, puisque le renforcement de la durée de vie lui est généralement imputé. Si la cristallisation dépend de la densité de chaînes actives, alors il devrait exister des liens entre le renforcement et les marqueurs de la SIC sur les faciès de rupture. Dans cette étude, nous avons montré que :

- les marqueurs de la SIC (stries et cônes) sont corrélés à la densité de chaînes actives, et une plage de densité de chaînes actives maximise l'apparition de ces marqueurs. Pour des densités de chaînes actives inférieure, les marqueurs de la SIC sont toujours observés dans une moindre mesure. En revanche, pour des densités de chaînes actives supérieures, ils ne sont plus observés.

- la plage de densité de chaînes actives maximisant la SIC identifiée dans l'état de l'art est proche de celle maximisant les marqueurs de la SIC,

- la plage de densité de chaînes actives présentant le meilleur renforcement présente également le plus grand nombre de marqueurs de la SIC. Cela suggère un lien entre la cristallisation et le renforcement observé.

D'un point de vue industriel, établir les effets de la structuration du réseau macromoléculaire sur les propriétés mécaniques du NR a permis d'orienter et de consolider les choix de formulation et de conditions de mise en œuvre des pièces en fonction des propriétés recherchées. Pour terminer, plusieurs questions et perspectives découlent de cette étude :

- est-ce que plus le matériau cristallise, plus il présente de marqueurs de la SIC et plus il se renforce ? La question de la représentativité des mesures de cristallisation, qui se font généralement sur des échantillons fins et pour un champ de déformation homogène, se pose alors pour faire le lien avec les résultats de fatigue obtenus sur Diabolo.

- compte-tenu du fait que même les matériaux très pontés, sans marqueurs de la SIC et qui a priori ne devraient pas présenter de bonnes propriétés cristallines, se renforcent ; quel est l'origine du renforcement ? Est-elle tout d'abord induite de l'orientation de la phase amorphe, puis promue par la cristallisation ?

Par ailleurs d'autres travaux non reportés dans le manuscrit pour des raisons de confidentialité, ont permis de déterminer si une analyse calorimétrique associée aux essais quasi-statiques permettent de classer les matériaux vis-à-vis de leur performance en fatigue.

Appendix A

A comprehensive review on active chain density evaluation from swelling and insights for better accounting for insoluble particles

Preamble

The present appendix provides a state of the art on methods for evaluating active chain density of rubbers from swelling experiments. This review focuses more particularly on the effects of components that are known to limit the swelling, and which typically results in an overestimation of the active chain density. These components are commonly considered as insoluble. Different corrections dealing with the two principal insoluble components, namely zinc oxide (ZnO) and carbon black (CB) filler, are thoroughly investigated. A comparative study on the same natural rubber (NR), either filled and unfilled, vulcanized with three different vulcanization systems, is performed to evaluate the relevance of each predictive approach. The results obtained highlight their respective limitations. In particular, it is shown that the swelling ratio of unfilled and filled natural rubbers are linearly related, suggesting that fillers have no significant effect on the overall number of cross-links formed during vulcanization. As a result, we propose a unified approach for correcting the ZnO content for unfilled NR and both the ZnO and CB contents for filled NR. By comparing with results issued from uniaxial tensile tests, it is shown that the use of a mechanical response is a relevant alternative for determining the active chain density.

Keywords: swelling, active chain density, filler effects, rubber, vulcanization system effects.

A.1 Introduction

The elastic properties of rubber are mainly driven by the vulcanization process that consists in cross-linking macromolecules into a network. The length, the atomic composition, and the number of formed cross-links can differ from one vulcanization process to another. For example, in the case of sulphur vulcanization, the number and length of cross-links depends on *(i)* the sulphur and accelerator contents and *(ii)* the processing conditions, typically time, temperature, and pressure of molding. Sulphur vulcanization is classically divided into three types of vulcanization system; the conventional vulcanization system (CV), which leads mainly to the formation of polysulphide cross-links, while much shorter cross-links, *i.e.*, mono- and- disulphide are obtained with efficient vulcanization system (EV). The semi-efficient vulcanization system (SEV) is midway between the two of them since it has an equal proportion of long and short cross-links. There are several ways of differentiating them, the most widely used being the distinction proposed by Quirck: the type of vulcanization system depends on the accelerator (A) and sulphur (S) weight content, and also their content ratio denoted [A]/[S] [23]. The final mechanical properties are triggered by both the length and the number of the cross-links, the number of cross-links being directly related to the number of elastically active chains. It was found that polysulphide cross-links enhance the crack growth resistance while mono- and- disulphide cross-links increase the thermal degradation resistance [37, 173]. Therefore, for a given vulcanization system, mechanical properties are mainly driven by the number of active chains [13].

Various methods have been proposed in the literature to determine the number of active chains. The reader can refer for instance to Refs [53, 193, 203]. One of the most commonly used approach is the swelling by solvent, which enables linking the macromolecular network expansion to the swelling ratio through the Flory-Rehner relationship [52]. The main advantage of this method lies in its easy applicability on an experimental point of view. For example, it was used to address the effect of the type of vulcanization accelerator on the mechanical properties, of the vulcanization system on the viscoelastic properties and to characterize the macromolecular network, *i.e.*, chain scission or cross-linking for temperature-accelerated ageing [16, 58, 152]. Of note, this method is applicable to all rubbers, regardless of their nature: nitrile butadiene rubber (NBR), butadiene rubber (BR), natural rubber (NR), etc.), as long as the type of solvent is appropriate [188, 225, 226]. This insight is fully addressed in Section A.2.1.

The experimental conditions, the calculation assumptions, and the data-processing reported in the literature vary from a study to another, which may induce a bias in the interpretation of the results. As mentioned by Gros, the definition of the framework is of major importance [227]. Among the hypotheses used to process the experimental data, one of the principal issues lies in the fact that some components are considered as insoluble in any solvent, *i.e.*, they are not extracted during the swelling. It is typically the case with ZnO and CB, which are used in rubber formulations to *(i)* activate the cross-linking and *(ii)* to optimize mechanical properties, respectively [12, 228]. Thus, some methodologies include a correction of the swelling ratio to account for these insoluble components. Nevertheless, there is no scientific consensus on the type of correction. This is even truer when both are used in the formulation. Therefore, this

raises the question of the most appropriate methodology for comparing materials in terms of the active chain density. The question is even more justified in the case of crystallizable rubbers in which active chain density significantly affects the strain-induced crystallization (SIC) [65, 116, 120].

In this work, a comparative study of the different approaches based on the same NR, both filled and unfilled. The objective is to identify the relevance and limitations of each method, and to develop a unified approach. The study is divided in five sections. Section A.2 is dedicated to the state of the art of the swelling methodologies reported in the literature. Then, a concise review of Flory-Rehner's relationship fundamental notions is recalled. This section also introduces the corrections for accounting contribution of CB and ZnO on the active chain density. In Section A.3, the experimental set-up is presented. Materials of the study and sample geometry are given as well as the test protocol. The results are next reported and discussed in Section A.4. The relevance of each correction factor is investigated with our materials. Finally, Section A.5 describes a new methodology that unifies approaches for correcting the ZnO content for unfilled NR and both ZnO and CB contents for filled NR. Concluding remarks and perspectives close the paper.

A.2 State of the art

A swelling test typically consists in immersing a sample in a solvent. The solvent molecules incorporate and spread the polymer chains while filling the free spacing in the network. The solvent penetrates the available empty spaces until an equilibrium state is reached. However, the insoluble components, when present, limit the swelling process. At the equilibrium, the network is fully constrained by topological constraints such as cross-link junction points and entanglements. Then, the samples are dried, and the solvent trapped evaporates. By following the sample's mass during these two successive stages, the swelling ratio, which is used to calculate the active chain density, can be evaluated.
This state of the art on swelling methodologies is divided in three sub-sections. The classical experimental conditions used in literature are first recalled. Then, the Flory-Rehner theory on the swelling of polymers is presented. The section ends with the correction of insoluble components in solvent through a non-exhaustive review from 1940.

A.2.1 Experimental conditions

The main experimental conditions reported in the literature are given in Table A.1. This table gives a non-exhaustive list of the most commonly used weights and dimensions of the sample, as well as the type of solvent employed, the time at swelling equilibrium, and the time and temperature of drying. Non-filled rows are due to lack of information. As a brief summary, it is to be noted that the toluene is the most widely used solvent, especially since the 1990s. The time of swelling decreases through the years and it is nowadays most often set to 72 h. When authors used a vacuum oven to dry, only 24 h are sufficient to reach constant weight,

regardless of the temperature between 60 and 80 °C. One can also note that the samples are most commonly rectangular, and the cutting method is not always mentioned.

A.2.2 Active chain density determination

A.2.2.1 The Flory-Rehner relationship

Swelling by solvent is considered as the property of a polymer to absorb a large amount of an organic liquid. Without chemical bonds between macromolecules, a rubber could theoretically swell to an unlimited extent. Vulcanized rubber can only absorb a limited amount of solvent due to cross-links resulting in a lower ability to swell [52]. Thus, the maximum absorption corresponds to the point where to the osmotic pressure of solvent molecules, and the deformation of the network (*i.e.*, the relative displacement of the mechanically active chains) are counterbalanced. As a result, a so-called equilibrium state is reached. In terms of thermodynamics, it is associated with the evolution of the free energy of mixing. The free energy is given by $\frac{\partial G}{\partial n_s}$, which is calculated by the partial derivatives of the free energy by the number of solvent molecules absorbed [47]. Two entropic contributions of the free energy of mixing exist: the energy of mixing $\frac{\partial G_m}{\partial n_s}$ (denoted $\Delta F_{m,1}$ by Flory) and the energy of deformation $\frac{\partial G_e}{\partial n_s}$ (denoted $\Delta F_{e,1}$ by Flory) [22]. G_m is related to the free energy of mixing, *i.e.*, the osmotic contribution, while Ge is related to the network expansion, *i.e.*, the elastic contribution of the free energy. The enthalpic contribution due to the deformation of the network is generally neglected [230]. The expression of $\frac{\partial G}{\partial n_s}$ is given by:

$$\frac{\partial G}{\partial n_s} = \frac{\partial G_m}{\partial n_s} + \frac{\partial G_e}{\partial n_s} \tag{A.1}$$

As solvent absorption takes place, the active chains are spread: their chain ends are displaced from their original position, and their entropy changes. However, retraction forces tend to bring back the ends of the active chains to their original position. The total free energy of mixing is therefore governed by the competition between these two phenomena. An equilibrium state is obtained when the Gibbs free energy is stable, which results in writing:

$$\frac{\partial G}{\partial n_s} = 0 \tag{A.2}$$

Flory and Huggins calculated independently the first term $\frac{\partial G_m}{\partial n_s}$ and obtained similar results, as written below [189, 206, 248]:

$$\frac{\partial G_m}{\partial n_s} = RT[\ln(1-\upsilon_r) + \upsilon_r + \chi\upsilon_r^2] \tag{A.3}$$

with R the gaz constant, T the absolute temperature and υ_r the volume fraction of rubber at equilibrium state corresponding to the inverse of the swelling ratio Q. The swelling ratio is defined as the ratio of the swollen state over the non-swollen[1] state volumes. The semi-empiric

[1]It is not referred to the initial state volume. Indeed, the dry state weight may be different from the initial state one. The choice of the weight depends on the assumptions used and the material studied.

References	Weight (g)	Dimension (mm^3)	Solvent	Swelling time (h)	Drying time (h)	Drying temperature (°C)
[229]	-	24.4*24.4*2.032	decalin	72	48	70
[230]	0.1	25*4*1	-	-	-	-
[231, 232]	-	-	cyclohexane	24	-	-
[233]	-	5*25*2	toluene	-	-	-
[234]	1.5	-	benzene/ n-heptane	144	16	70
[235]	-	-	benzene	336	-	-
[207]	1	-	benzene	48	4*	80
[187]	0.2	-	-	-	-	-
[236]	2	-	benzene	-	-	-
[237]	1.5	31.75*12.7*2.032	Isooctane/n-heptane cyclohexane/chloroform	48	-	70
[209]	1	-	n-decane	168	until cst	70
[238]	-	25.4*25.4*1.905	isooctane	-	12 (a night)	70
[239]	-	-	heptane/toluene	168	-	80
[240]	0.2-0.3	-	toluene	-	-	-
[40]	-	0.8*10*10	toluene	168	until cst	80
[65]	-	-	toluene	-	-	-
[241]	-	-	naphthenic/ paraffinic oil	48	-	-
[242]	-	20*10*0.2	toluene	72	-	-
[116]	-	-	toluene	-	-	-
[188]	-	-	toluene	72	24	60
[243]	-	π*3^2*2	toluene	24	-	-
[203]	-	π*3^2*2	toluene	72	24	60
[244]	-	10*10*1	n-decane	48	-	50
[245]	-	-	toluene	72	until cst	23
[246]	-	-	toluene	72	24	60
[247]	0.5-0.9	-	toluene	72	24	23
[120]	-	-	toluene	-	-	-
[41]	1	-	toluene	72	24	-
[53]	-	-	toluene	120	24	80

Table A.1: Summary of the experimental conditions used in the literature.

term $\chi \upsilon_r^2$ depends on the solvent-polymer couple studied. The calculation of the Flory-Huggins parameter χ is detailed in Sub-section A.2.2.
The second term $\frac{\partial G_e}{\partial n_s}$, associated to the entropic deformation of the network, can be calculated through the pioneering works of Guth and Mark, Kuhn, and Treloar as [47]:

$$\frac{\partial G_e}{\partial n_s} = RT[\ln(1-\upsilon_r) + \upsilon_r + \chi \upsilon_r^2] + \frac{\rho RT}{M_c} \upsilon_s \upsilon_r^{\frac{1}{3}} \tag{A.4}$$

with M_c the molecular weight between cross-link, ρ the density of the polymer, and υ_s the molar volume of the solvent. For further details about the modeling of single chain and an entire network deformation, the reader can refer to Treloar [47]. By applying the equilibrium condition $\frac{\partial G_m}{\partial n_s} = -\frac{\partial G_e}{\partial n_s}$, M_c can be expressed as follows:

$$M_c = -\frac{\rho \upsilon_s \upsilon_r^{\frac{1}{3}}}{\log(1-\upsilon_r) + \upsilon_r + \chi \upsilon_r^2} \tag{A.5}$$

As explained by Treloar, this relation is modified when the network expansion is taken into account by using another relation proposed by Flory [50]:

$$M_c = -\frac{\rho \upsilon_s (\upsilon_r^{\frac{1}{3}} - \frac{\upsilon_r}{2})}{\log(1-\upsilon_r) + \upsilon_r + \chi \upsilon_r^2} \tag{A.6}$$

It is to be noted that M_c is intrinsic to the macromolecular network. However, other quantities, expressed in g/mol or mol/cm^3, are generally preferred such as *(i)* the cross-link density ν_{cl}, which refers to as the number of cross-links, and *(ii)* the active chain density ν_{ac}, which is related to the number of chains between cross-linking knots. The cross-link density is related to M_c through the two following relations depending on the unit used: $\nu_{cl} = \frac{1}{2M_c}$ in g/mol, and $\nu_{cl} = \frac{\rho}{2M_c}$ in mol/cm^3. In this work, results are expressed in terms of active chain density ν_{ac} in mol/cm^3, which writes as:

$$\nu_{ac} = \frac{\rho}{M_c} \tag{A.7}$$

Note that for tetra-functional cross-links, both quantities are related by a factor two, *i.e.*, $\nu_{ac} = 2 * \nu_{cl}$ [47].

A.2.2.2 The modeling of the macrolecular network

The Flory-Rehner relation (Equation A.6) is based on the classical molecular theory of an "affine network". Even though this relationship is the most frequently used in the literature, other authors developed other theories from which different expressions of M_c can be derived. These theories are briefly recalled hereafter.

Affine network model

The "affine network" considers that the rubber chains are independent from one another. In other words, no interactions or entanglement effects occur. In this case, the cross-link junction points are constrained; they are fixed relatively to the rubber chains. In this way, the deformation of the network is considered the same at the macroscopic and the microscopic scales. Such an assumption leads every active chain to be displaced and rotated similarly. The functionality of the network ϕ is taken as four, *i.e.*, a cross-link junction point joins on average four rubber chains [10]. These assumptions depend on the free strain energy density W, described by the Kuhn model [47]. Thus, for a given ϕ , the Flory-Rehner relation in affine deformation assumption can be written as:

$$M_c = -\frac{\rho \upsilon_s (\upsilon_r^{\frac{1}{3}} - \frac{2\upsilon_r}{\phi})}{\log(1-\upsilon_r) + \upsilon_r + \chi \upsilon_r^2} \tag{A.8}$$

Phantom network model

James and Guth proposed an alternative to the "affine network", namely the "phantom network" model [190]. In this model, rubber chains are also considered as independent. Nevertheless, in contrast to the affine network model, cross-link junction points have a certain mobility, *i.e.*, fluctuations are possible and only few cross-link junction points are really fixed. In this sense, the active chains are not displaced and rotated similarly. It leads to the following calculation of M_c:

$$M_c = -\frac{\rho \upsilon_s \upsilon_r^{\frac{1}{3}} (1 - \frac{2}{\phi})}{\log(1-\upsilon_r) + \upsilon_r + \chi \upsilon_r^2} \tag{A.9}$$

According to Valentín and coworkers, these two models are both representative of the most extreme cases [188]. It is to note that they are yet the most widely used ones. Since the type of modeling affect the calculation of M_c, it is necessary to choose appropriately the physical network model. Vilgis pointed out that these two classical models do not account *(i)* for the chain dependency and *(ii)* for the network heterogeneity [249]. This provides a partial description of the real behavior. Further information on the comparison between the affine and phantom network as well as on others model is given by Han, Horka and McKenna [192].

Tube network model

More recently, Basterra-Beroiz *et al.* worked on the tube model network, which significantly differs from the previous ones. This model is more faithful to the actual behavior of rubber materials. They applied the approach by Helmis-Heinrich-Straube (HHS) to process their swelling results [193, 250]. In the HHS model, the rubber chains are considered as dependent from one to another, and the topological constraints and the entanglements are taken into account. This means introducing in the calculation of M_c, a factor $F(x_m)$ that accounts for the cross-links, the topological constraints, and the entanglements as follows:

$$M_c = -\frac{\upsilon_s \upsilon_r^{\frac{1}{3}} A_c \rho F(x_m)}{\log(1-\upsilon_r) + \upsilon_r + \chi \upsilon_r^2} \tag{A.10}$$

It also includes a microstructure factor A_c considering the fluctuations of the cross-link junction points [246]. One can note that the phantom model somehow gives results close to the ones obtained from HHS one, while the affine model is less predictive.

A.2.2.3 The Flory-Huggins interaction

The Flory-Huggins interaction χ is generally referred to the affinity of a solvent-polymer pair. There are numerous methods to calculate χ. One of them is described in Equation A.11. It is made under the assumption that the term χ is dependent to the polymer concentration υ_r [22]. This relation is used in recent articles, for example by Horkay *et al.*, Vieyres *et al.*, and Valentín *et al.* also [188, 192, 203].

$$\chi = \chi_0 + \chi_1 \upsilon_r + \chi_2 \upsilon_r^2 \tag{A.11}$$

A second method lies in the assumption that χ is equal to the addition of an entropic χ_S and an enthalpic χ_H contributions [251]. It is also known as the Hildebrand relation, and it is given by Equation A.12.

$$\chi = \chi_S + \chi_H \tag{A.12}$$

For the entropic contribution χ_S, it is a constant equal to 0.34, one can found more information in the literature [251, 252]. For the enthalpic contribution χ_H, it can be calculated with Equation A.13. For a polar polymer, the cohesive energy density A_{sp} for a solvent-polymer pair depends on their solubility parameters. It is equal to $A_{sp} = (\delta_s - \delta)^2$, with δ_s and δ_p the solubility parameters of the solvent and the polymer, respectively. In practice, the smaller A_{sp}, the more compatible the polymer and the solvent are. Contrarily, for a significant difference between δ_s and δ_p, the solvent is likely to dissolve the polymer, which will make the solvent test inefficient. By knowing the solubility parameters δ_s and δ_p, we can determine χ_H by using the Equation A.13 [253].

$$\chi_H = \frac{\upsilon_s}{RT} A_{sp} \tag{A.13}$$

For a χ higher than 0.5, one can consider the solvent-polymer incompatible with solvent swelling. The value must be less than 0.5, the solvents were better as this value decrease [254]. In general, for the toluene-NR pair, χ is taken as constant and is equal to 0.39 or 0.393 [53, 247].

A.2.3 Accounting for the insoluble components

Since the 20^{th} century and the pioneering work of Mote, the rubber industry commonly employed CB in rubber formulation to enhance some mechanical properties [172, 238]. Indeed, it increases the material's stiffness, stress at break, and also its wear resistance [255]. As the Flory-Rehner theory is generally assumed to provide a realistic description of the macromolecular network of rubbers, the swelling method has been used to characterize both filled and unfilled rubbers [24, 52]. However, filled rubbers showed a swelling ratio significantly lower than their unfilled namesakes. In other words, adding CB leads to an increase in the active chain density. This result raises at least two questions: *(i)* what is the origin of this difference? and *(ii)* how can the same rubbers filled and unfilled be compared? Moreover, ZnO is often added to formulations, the main reason being for the vulcanization activation. The ZnO amount can be significant (10 phr for example). Such a quantity has non-negligible effects on the macromolecular network swelling and raises the same questions as for CB fillers. The present section reviews the answers found in the literature for these two types of insoluble particles. In the following, Q_0 refers to the swelling ratio of the corrected rubber and Q to the swelling ratio of the composites ones, *i.e.*, filled or unfilled but containing ZnO.

A.2.3.1 Accounting for fillers

Only the CB effects are reviewed in this part. However, it is to be noted that the conclusions drawn are not directly applicable to other types of filler, *i.e.*, filler having different chemical structure. It is particularly true when considering filler which have strong interaction with the rubber matrix such as the silica.

Dannenberg studied the filler-matrix interaction of a SBR vulcanized with sulphur and accelerated with N-cyclohexyl-2-benzothiazole sulphenamide (CBS) [229]. The author showed through swelling tests that the restriction of swelling induced by fillers only happened for vulcanized rubber. Lately, Zapp and Guth showed that CB induces a much more pronounced swelling restriction than other fillers; this result suggests that CB leads to stronger filler-matrix interaction [231, 232]. They highlighted that the restriction is solely a function of the surface area. Bueche also worked on different filler types, and on a silicone rubber [233]. The author showed the dependency of the polymer volume fraction υ_r on the volume fraction of filler φ, *i.e.*, the filler content. It is to note that this can also be transposed to other fillers. During the same year, Kraus investigated the effect of the curing state of rubbers, and also focused on the swelling behaviors of filled and unfilled like SBR, BR and NR [234]. For SBR, sulphur and peroxide

vulcanization agents were used. In the case of sulphur, its content was varied as well as the CBS one. The author also highlighted the restriction of swelling when fillers are added and showed that restriction is affected by the vulcanization degree, the vulcanization system and the filler type and content. Then, the author proposed to distinguish the apparent and effective swelling ratios of the materials. The author suggests that a correction should be done to the swelling ratio to account for the filler effect on swelling. Bevilacqua also came to the same conclusion and suggested to establish a correction of the swelling ratio based on Guth and Gold model [256].

In the early 1960s, Westlinning and Buthenuth studied the effect of the accelerator and the CB contents on the swelling ratio [235]. They fixed the sulphur content to 2.5 phr. With the accelerator content being variable, the [A]/[S] content ratio varied from 0.24 to 1.92. A value of 0.24 corresponds to a CV system and 1.92 to a SEV one. Increasing the accelerator content led to an increase in the active chain density, and consequently to a decrease in the swelling ratio. The authors showed that the swelling ratio decreased by increasing the volume fraction of CB, for every accelerator content. This result highlights that the cross-links mean length does not affect swelling behavior. During the same year, Lorenz and Parks presented new results on many different compositions of NR, vulcanized by CV peroxide and sulphur systems, and also accelerated with several different accelerators [207]. Results on sulphur vulcanized materials NR showed the dependency of the swelling ratio of filled material to the unfilled one through the following relation $Q = aQ_0$. The authors hypothesized on a limited swelling in the vicinity of the fillers, mainly due to topological constraints, which has been defined on the basis of the results of the CV system, for [A]/[S]=0.5. The weight fraction of filler z is defined as the weight of filler over the weight of rubber, as follow: $z = w_{CB}/w_{NR}$ (Equation A.14). The coefficients a and b were the same for all the materials studied, which suggests that high-abrasion furnace (HAF) CB does not have any significant effect on the active chain density.

$$\frac{Q}{Q_0} = ae^{-z} + b \tag{A.14}$$

Few years later, Lorenz and Parks relation was analyzed by Kraus [208]. The latter took into account conclusions of Lorenz and Park and considered that two phases coexist: the bulk having no restriction and the surroundings of filler particles being restricted. Kraus studied several rubbers, solvents, fillers type and contents of filler. The author developed two relations, taking into account the filler volume fraction φ. The first one is defined by Equation A.15. It is the consequence of a weak filler-matrix interaction, leading to the absence of adhesion of the rubber chains on the filler particles. It represents the ideal insertion of the solvent within the network, without any constraints for the solvent to propagate in the macromolecular network.

$$Q_0 = \frac{Q - \varphi}{1 - \varphi} \tag{A.15}$$

The second one, defined by Equation A.16, is the consequence of an existing strong filler-matrix interaction. In this case, the swelling is limited in the filler surrounding due to the filler-matrix interactions. The coefficient m corresponds to the curve slope, depending on Q_0.

One can note that this relation was used for example by Boonstra and Taylor in order to better understand the filler-matrix interaction [237].

$$\frac{Q}{Q_0} = 1 - \frac{m\varphi}{1-\varphi} \tag{A.16}$$

Lorenz and Parks and Kraus relations lead to very different results, which have been highlighted by Porter in the first part of its article dedicated to the characterization of filled rubbers [207–209]. The author proposed different assumptions on the nature of the swelling restriction due to fillers: *(i)* fillers promote the formation of cross-links, *(ii)* fillers limit the quantity of absorbed solvent, *(iii)* the filler-matrix interaction nodes act as actual cross-links and can be considered as such and *(iv)* the fillers affect the interaction between the solvent and the rubber. Furthermore, the author suggested studying an EV system with an extremely small amount of sulphur, in which no sulphur would be available to create additional cross-links. This could provide information on the nature of the restriction, namely, the fillers itself, the physical bonding or the chemical bonding. Porter studied several compositions, including a CV compound accelerated with CBS with [A]/[S]=0.24, and a SEV compound with MBT within [A]/[S]=1. The author also investigated sulphur vulcanization with 4 phr of Tetramethylthiuram disulphide (TMTD) accelerator and peroxide vulcanization with variables contents. Results indicated that the apparent active chain density increases linearly with the filler amount. A relation was proposed to link the cross-link density of the filled and unfilled materials. It is given in Equation A.17, with k a constant.

$$\frac{\nu_Q}{\nu_{Q_0}} = 1 + k\varphi \tag{A.17}$$

As highlighted by Saville and Watson, the work of Porter, Lorenz and Parks, and Kraus provides major contributions to the understanding of CB effect on rubber swelling [257].
Stickney et Mueller studied the swelling kinetics of filled and unfilled SBRs accelerated with Dibenzothiazyl disulphide (MBTS) and [A]/[S]=1.5 [238]. HAF CB contents varied from 5 to 50 phr. Their results showed that at least two different types of swelling restriction exist: a permanent restriction and a swelling kinetics restriction. The authors attributed this result to the geometry of the fillers, or to an effect of the filler-matrix interaction. During the following years, no further significant correction of CB content was proposed, but several articles used the existing ones. Indeed, Diamant and Foldman used Kraus relation, while other studies have instead focused on a description of the swelling heterogeneity, which is a function of the expression of the mixing energy and the strain energy density [239, 258, 259].

In the early 2000s, Gent, Hartwell and Lee introduced a method to accurately estimate the apparent active chain density [241]. The authors were interested in several NR, accelerated with CBS and TMTD, and with a fixed [A]/[S]=0.5, which corresponds to CV systems. In both cases, they varied the sulphur content to increase the active chain density by keeping the mean cross-links length constant. They found the relation given by Equation A.18, with a and b being equal to 0.875 and 0.125, respectively. This relation shows that the swelling ratio of filled rubber

evolves linearly with the one of unfilled material. This indicates that CB does not affect the degree of cross-linking in the rubbers studied, which meets Lorenz and Parks conclusions [207]. The authors imputed the restriction of swelling to the filler-matrix interaction, and pointed out that these interactions are strong enough to withstand swelling stresses. The authors also suggested to estimate the active chain density through tension tests and the classical theory of rubber elasticity [47].

$$\frac{1}{Q} = \frac{a}{Q_0} + b \tag{A.18}$$

Since the work of Gent, Hartwell and Lee, no other correction was proposed [241]. The relation of Kraus was later used in numerous studies [242, 259–261]. Candau observed a deviation of the corrected Q from the reference Q_0 values of the unfilled NR [123]. The author attributed this result to a possible additional cross-linking phenomenon in the vicinity of the fillers, without providing any further detail. Lorenz and Parks relation was more recently used by Grasland, which is justified by the unchanged length distribution of active chains after incorporating the fillers [120]. Even more recently, the work of Basterra-Beroiz *et al.* on unfilled materials could lead in new suggested corrections through a finer modelling of the macromolecular network [246].

A.2.3.2 Accounting for zinc oxide

In the early 1960s, Scott, Lorenz and Parks worked on a NR containing 5 phr of ZnO [236]. They proposed an experimental protocol to perform a preliminary extraction of rubber sample by using acetone followed by a swelling in benzene. One can note that this protocol was used in their previous work [262]. They corrected the swelling ratio, according to Equation A.19, by using an empirical relation obtained by Pierson *et al.*, in which ν_0 refers to the ratio between the rubber gel network and the total weight within all soluble components [263]. The insoluble components were not considered, ZnO being the only one mentioned by the authors.

$$Q_0 = \nu_0(Q + 1) - 1 \tag{A.19}$$

The swelling ratio was calculated accordingly to Equation A.20, where w_{ini} is the initial weight of the samples (2 g). It becomes wext after a first acetone extraction. The weights w_{swo} and w_{dry} characterizes the weight at the swollen state and the dry state, respectively. The total weight of the rubber composition is given by w_{tot}. It is interesting to note that soluble components are defined as the extracted components by the different solvents.

$$Q = \frac{w_{swo} - w_{dry}}{w_{tot} * \frac{100}{w_{ini}} - (w_{ext} - w_{dry})} \tag{A.20}$$

Ellis and Welding also used a similar weighing procedure. Nevertheless, they considered a weight fraction of insoluble components ($f_{ins} = (g.\ of\ ins)/(g.\ of\ total)$) in their calculation. They defined the accelerator, sulphur, and ZnO as part of this fraction, corresponding to 10 phr in total. According to the authors, neglecting these insoluble components leads to errors

of up to 10% in the calculation of Q. In practice, they corrected the initial weight with the weight fraction given in Equation A.21. It was a first and major contribution dedicated to the correction of the ZnO contribution [187]. It has then been used for example by Kurian [240].

$$Q = \frac{\frac{w_s}{\rho_s} + \frac{w_{dry} - f_{ZnO} w_{ini}}{\rho_r}}{\frac{w_{dry} - f_{ZnO} w_{ini}}{\rho_r}} \tag{A.21}$$

Lately, Bristow and Porter proposed a quite similar correction since they also subtracted the insoluble components. The only difference between the two approaches being the weight fraction f applied on the weight on the swollen state [264]. No other correction was dedicated to ZnO since the early 2000, Valentín *et al.* worked on incertitude about swelling tests upon addressing the correction of insoluble components on the basis of the work of Ellis and Welding [187, 188]. However, their approach focuses only on ZnO since the accelerator and the sulphur are considered as part of the network. According to the authors, it would be preferable to take into account a correction of the excess solvent contained at the ZnO-matrix interface, in order to better estimate the swelling ratio of NR. This interface forms a so-called vacuole.

$$Q = \frac{\frac{\frac{w_{dry} - f_{ZnO} w_{ini}}{\rho_r} + \frac{w_s}{\rho_s}}{\frac{w_{dry} - f_{ZnO} w_{ini}}{\rho_r}} + \frac{\frac{f_{ZnO} w_{ini}}{\rho_{ZnO}}}{\frac{w_{swo} - f_{ZnO} w_{ini}}{\rho_r}}}{1 + \frac{\frac{f_{ZnO} w_{ini}}{\rho_{ZnO}}}{\frac{w_{swo} - f_{ZnO} w_{ini}}{\rho_r}}} \tag{A.22}$$

A few years later, Valentín *et al.* adapted their correction given in Equation A.22, in the case of filled NR as it is described in Equation A.23 [265]. Nevertheless, the authors did not compare their method with those reported in the literature. The following equation does not consider the swelling ratio of filled and unfilled rubber being the same.

$$Q = \frac{\frac{\frac{w_{dry} - f_{ins} w_{ini}}{\rho_r} + \frac{w_s}{\rho_s}}{\frac{w_{dry} - f_{ins} w_{ini}}{\rho_r}} + \frac{\frac{f_{ins} w_{ini}}{\rho_{ins}}}{\frac{w_{swo} - f_{ins} w_{ini}}{\rho_r}}}{1 + \frac{\frac{f_{ins} w_{ini}}{\rho_{ins}}}{\frac{w_{swo} - f_{ins} w_{ini}}{\rho_r}}} \tag{A.23}$$

During the 2010s, no further correction was applied to ZnO. Equation A.20 was recently used by several authors [203, 243]. In 2018, one can cite the works of Howse *et al.* and Bornstein *et al.*, which employed Kraus method but for ZnO and not for CB [41, 208, 247]. Finally, it has to be mentioned that most studies do not use any ZnO correction.

A.2.4 Summary and conclusions of the state of the art

The state of the art highlights that swelling restrictions are due to insoluble components, mostly CB and ZnO. The restriction induced by ZnO and CB depends on several parameters. For CB, the type, the structure and the quantity has an effect on swelling, while for ZnO, only the quantity has an impact. Thus, for both, the quantity seems to be the most important significant parameter on swelling. Furthermore, it is to be noted that CB induces strong interactions with

the rubber matrix, which complicates the interpretation of the swelling process. For NR, the swelling restriction was observed for CV and SEV sulphur vulcanization system.
Taking both the ZnO and CB effect into account in the active chain density calculation therefore appears of major importance. To the best of our knowledge, there is no admitted procedure to correct the effect of the insoluble components in the swelling of NR. For filled NR, with a significant content of ZnO, it is essential to consider at least both CB and ZnO. Regarding the literature, a remaining question still needs to be addressed: what is the limit of what is considered as insoluble components? The authors herein report the questions initially raised by Valentín and coworkers [188]. Indeed, this is highly questionable since other components such as vulcanization "wastes", elastically ineffective, like residual accelerators, pendant chains, or ZnS clusters and non-rubber components interfere with the macromolecular network [177]. To our opinion and in accordance with the answers provided by the literature, it is worth considering only ZnO and CB, which why our following study focuses only on these two components.
In summary, at least two paths can be followed to correct the effect of CB and ZnO on the swelling results:

1. the first one is to consider the macromolecular network un-modified by adding insoluble components: it is in this case necessary to identify a relation like the one of Lorenz and Parks or Gent and coworkers [207, 241]. It raises the question of how to correct the unfilled rubber with high proportion of ZnO since it is no more a representative reference. Using a reference without any ZnO would however be impossible.

2. the second one is to correct the swelling ratio relatively to the fraction of insoluble components, as done by Kraus and lately by Valentín and coworkers [208, 265]. If there is still a difference between the corrected filled and unfilled NR, one need to hypothesize on the nature of this difference and to determine if it is rather due to filler-matrix interaction such as additional chemically bonds, or other contributions.

The next following part of the present article aims at defining a holistic criterion. For that purpose, the existing corrections of the literature are applied to a large number of formulations of NR. So, unfilled and filled NR formulations, containing a high content of ZnO, have been used in our study to evaluate the relevancy of each method. The materials and method are presented in Section A.3. In Section A.4, as a function of the results obtained, a methodology inspired by the existing corrections of the literature has been proposed to process our data. The proposed methodology has been evaluated by comparing the results of active chain density with the one obtained by exploiting quasi-static stress-strain curves in low strain area. This comparison is carried out using very different vulcanization systems.

	[A]	[S]	[A]/[S]
CV	0.4 - 3.5	2 - 3.5	0.1 - 0.6
SEV	1.2 - 2.4	1 - 1.7	0.7 - 2.5
EV	2 - 5	0.4 - 0.8	2.5 - 12

Table A.2: Summary of the vulcanization system distinction proposed by Quirk [23]. Values for [A] and [S] are given in parts per hundred rubber in weight (phr).

A.3 Experimental section

A.3.1 Experimental section

The materials considered here are composed of the same *cis*-1,4-polyisoprene polymer matrix, from NR of Standard Malaysian Rubber (SMR) grade. This type of rubber presents a highly stereoregular configuration with 99.9% of cis-1,4 monomer units. All materials were vulcanized with sulphur and accelerated with sulfenamide type CBS. They were filled with 20 phr of CB N330 of HAF grade and 10 phr of ZnO in order to be representative of the of the formulations used for automotive applications [5]. Standard contents of stearic acid and antioxidants were added; 2 and 3 phr, respectively. It should be noted that several vulcanization systems were considered, in accordance with the classification proposed by Quirck given in Table A.2 [23]. In this table, conventional (CV), semi-efficient (SEV) and efficient (EV) systems are defined with respect to the accelerator and sulphur contents, as well as the [A]/[S] ratio.

The difference between these lies in the length of the cross-links formed. For CV system, the CBS and sulphur contents can vary while their ratio is kept constant at 0.2. As a result, the active chain density can be varied while ensuring a fairly identical mean length of the sulphur cross-links [120]. Thus, five accelerator-to-sulphur content ratios ([A]/[S]) are defined. For each ratio, a unfilled reference material is also prepared. All the formulations are detailed in the Table A.3. The materials are denoted NR_I^J, I the sulphur content and J the accelerator-to-sulphur content ratio, respectively. One can note that our formulations are similar in composition to those studied in the literature, allowing them to be compared and discussed.

The samples were obtained by standard mixing and molding process. All the components are incorporated into the internal mixer except for the vulcanization system, which is added during external mixing, in an open-roll mill, at a lower temperature to prevent early reactions. Samples were molded at a temperature of 160 °C, at a time corresponding to t_{98}, determined with a rheometer (Rubber Process Analyzer 1000, Alpha Technologies).

A.3.2 Equilibrium swelling tests

A.3.2.1 Preliminary tests

Numerous parameters can affect the swelling behavior, and therefore the active chain density calculation. These parameters are the nature of the solvent, the time of immersion to

	$NR^{2}_{0.2}$	$NR^{4}_{0.2}$	$NR^{6}_{0.2}$	$NR^{4}_{0.6}$	$NR^{1.5}_{1.2}$	$NR^{2.5}_{1.2}$	$NR^{0.8}_{4}$
Components	Content (in phr)						
NR TSR	100	100	100	100	100	100	100
CB N330	20	0 - 20	20	0 - 20	0 - 20	0 - 20	0 - 20
ZnO	10	10	10	10	10	10	10
Stearic acid	2	2	2	2	2	2	2
Antioxidants	3	3	3	3	3	3	3
Plasticizer	2	2	2	2	2	2	2
Sulphur	2	4	6	4	1.2	1.2	0.8
CBS	0.4	0.8	1.2	2.4	1.8	3	3.2
[A]/[S]	0.2	0.2	0.2	0.6	1.5	2.5	4

Table A.3: Formulations used in the present study. The formulations with "0 – 20" in CB content indicated that a 20 phr filled and an unfilled version exists.

equilibrium, the drying procedure, the sample geometry and the sample initial weight.

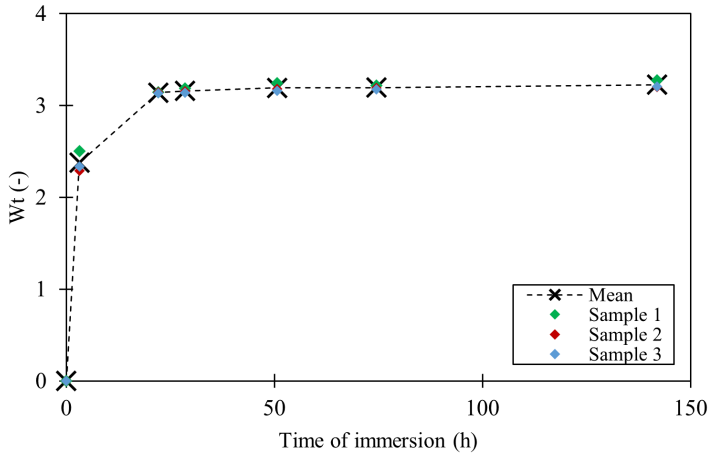

Figure A.1: Weight evolution of filled $NR^{2}_{0.2}$, during a swelling experiment in toluene.

In order to ease the comparison with results from the literature, toluene has been chosen as the solvent since it is the most widely used one. According to the literature, an immersion time of 72 h is chosen. To justify this time, the swelling kinetics of filled $NR^{2}_{0.2}$ has been characterized by measuring the evolution of the weight of the samples during several days, while immersed in a toluene vial to determine the equilibrium swelling time. The results are presented in Figure A.1 that plots the crude weight ratio wt as a function of the time of immersion. The crude weight ratio is calculated thanks to the relation given by Ellis and Welding, which is the weight at swollen state, at a given time, divided by the initial weight [187]. While three samples were evaluated, results show a 3% dispersion on the weight measurements, which evidences a correct test repeatability. The weight stabilizes after 50 h, indicating that the equilibrium state is then reached. Furthermore, the 72 h to equilibrium time were verified by performing two consecutive swelling tests to ensure that all the solvent-soluble components were extracted during the first

test.
The drying procedure, is defined accordingly to the literature to 24 h at 60 °C. The drying temperature is below that required to cause accelerated ageing of the material. A vacuum oven was used to extract the toluene trapped in samples, during the drying phase. By weighing the samples at 24 h and 48 h, the same results were obtained, indicating that 24 h at 60 °C is sufficient to completely dry the samples.

Filled $NR^2_{0.2}$, $NR^4_{0.2}$ and $NR^6_{0.2}$ were used to investigate the effect of the sample weight and geometry. Figure A.2 (a) shows the effect of the initial weight on the active chain density calculation, for a fixed rectangular section, by using 3 samples for each material. The calculated active chain densities are very similar for an initial weight of 0.2 ad 0.4 g, except for filled $NR^6_{0.2}$, for which the weight is overestimated. This could be attributed to the fact that a smaller initial weight is more sensitive to the drying of the toluene in excess at the surface, when samples are taken out from the toluene vial. So, an initial weight of 0.4 g is more appropriate and is used in the protocol. For the effect of the geometry, circular and rectangular section samples were used to conduct a comparative study since the surface exposed to solvent is thereby changed. Once again, each test was carried out using three samples, and for an initial weight fixed at 0.4 g. The results presented in Figure A.2 (b) shows no effect of the geometry on the calculated active chain density for all the tested materials. To conclude, both geometries can thus be used.

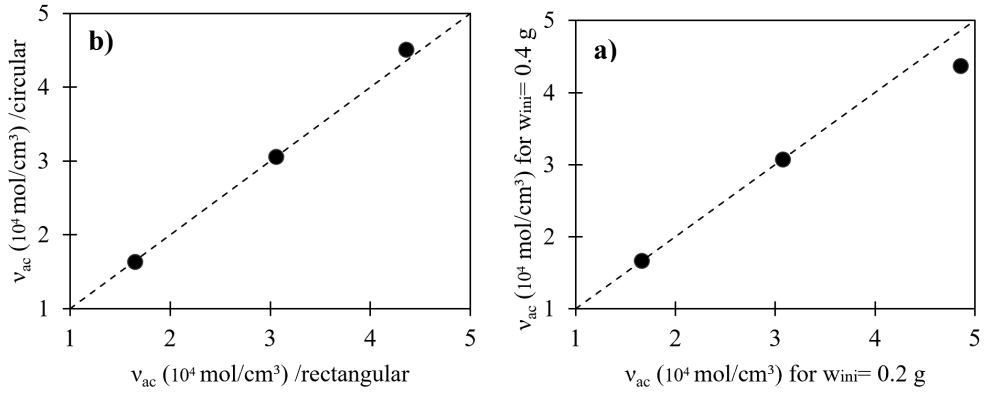

Figure A.2: The effect of (a) the initial weight and (b) the geometry on the non-corrected active chain density. The assumptions used to calculate the active chain density are given in A.3.2.2.

A.3.2.2 Experimental protocol and data-processing

The protocol to perform swelling tests as well as assumptions used for the calculation of active chain density are described hereafter.
The equilibrium swelling experiments are performed by using 3 circular section samples with a weight of 0.4 g, cut with a punch. The samples are weighed (w_{ini}) and immersed for 72 h in toluene ($\upsilon_s = 106.2\, cm^3/mol$, $\rho_s = 0.87\, kg/m^3$), in a closed vial. Then, samples are recovered, and a paper cloth is used to rapidly dry the excess of solvent from their surface, and after which the weight at swollen state (w_{swo}) is measured. In order to evaporate the toluene trapped in the samples, they are dried in a vacuum-oven until constant weight is obtained, typically for

24 h at 60 °C. The samples are finally weighed at the considered dry state (w_{dry}). The weight is measured with an accuracy of 10^{-4} g (model XT-220A, Precisa scale). One can note that tests were performed at ambient temperature, without isolating the vial from the light. UV light is known to cause a chemical degradation of unfilled NR leading to a decreasing of the weight in the equilibrium state [188]. However, by looking at the swelling kinetics of Candau, no degradation occurred up to 300 h, which is considerably longer than the chosen immersion time [123].

For the results presented in sub-sections A.4.1 and A.4.2, the assumptions as well as the relationship used for the calculations are described hereafter. The analysis is carried out by using the Flory-Rehner relationship with the affine network model, given in Equation (8). For this purpose, M_c is calculated by considering a constant Flory-Huggins interaction χ of 0.39, corresponding to the NR-toluene pair (see A.2.2.3). As a first approach, these relatively simple assumptions were chosen to focus the analysis on the correction of insoluble components. Note that in most of studies from literature, these assumptions are used. In Equation A.8, the term υ_r needs to be calculated from the weight measurements, as the inverse of the swelling ratio Q. As a reminder, Q is equivalent to V/V_0 , with $V = w_{swo}/\rho_r$ and $V_0 = w_{dry}/\rho_r$. It is recalled that the weight at dried state is considered since it does not account for soluble components in toluene such as un-reacted rubber chains or components with a low molecular weight (antioxidants, accelerator residual...), which are extracted during the swelling process. Finally, the active chain density is calculated, from M_c, by using Equation A.7.

A.3.3 Quasi-static mechanical characterization

Uniaxial tests were carried out in the laboratory with a home-made biaxial testing machine. The samples used were cut by waterjet cutting within a pure shear molded sheet. Further information is given in reference [5]. Tests are prescribed under displacement. The samples are uniaxially stretched to $\lambda = 7$, with λ representing the ratio between current and initial lengths. The loading rate is set to 250 mm/min, per grip.

A.4 Results

The objective of this part is to establish a methodology to account for ZnO and CB in the calculation of active chain density. An evaluation of the relevancy of the corrections, presented in the literature review, is first carried out on filled and unfilled formulations. Then, the effect of combined corrections on CB and ZnO is addressed, leading to the proposal of a new methodology. This part ends with the comparison of results issued from the methodology proposed and from the mechanical tests.

A.4.1 Application of the corrections from the literature

In order to estimate the effect of the insoluble components on the calculation of the active chain density, unfilled NR are taken as references. They correspond to formulations denoted unfilled $NR^4_{0.2}$, $NR^4_{0.6}$, $NR^{1.2}_{1.5}$, $NR^{1.2}_{2.5}$ and $NR^{0.8}_{4}$ referred to as "UNR", in opposition to their parent filled pairs "FNR". As a first experiment, Figure A.3 (a) presents the active chain densities of UNR as a function of FNR ones, calculated as defined in the protocol in Sub-section A.3.2.2. without using any correction. In such a graph, data on the bisector are equal. The active chain densities of the five UNR tested are lower than FNR ones, which is shown on the Figure A.3 (b) by the deviation from the plotted line. This result is in good agreement with the literature review and shows that CB leads to a strong overestimation of the active chain density. However, the ZnO effect cannot be interpretated here since it is contained in both UNR and FNR.

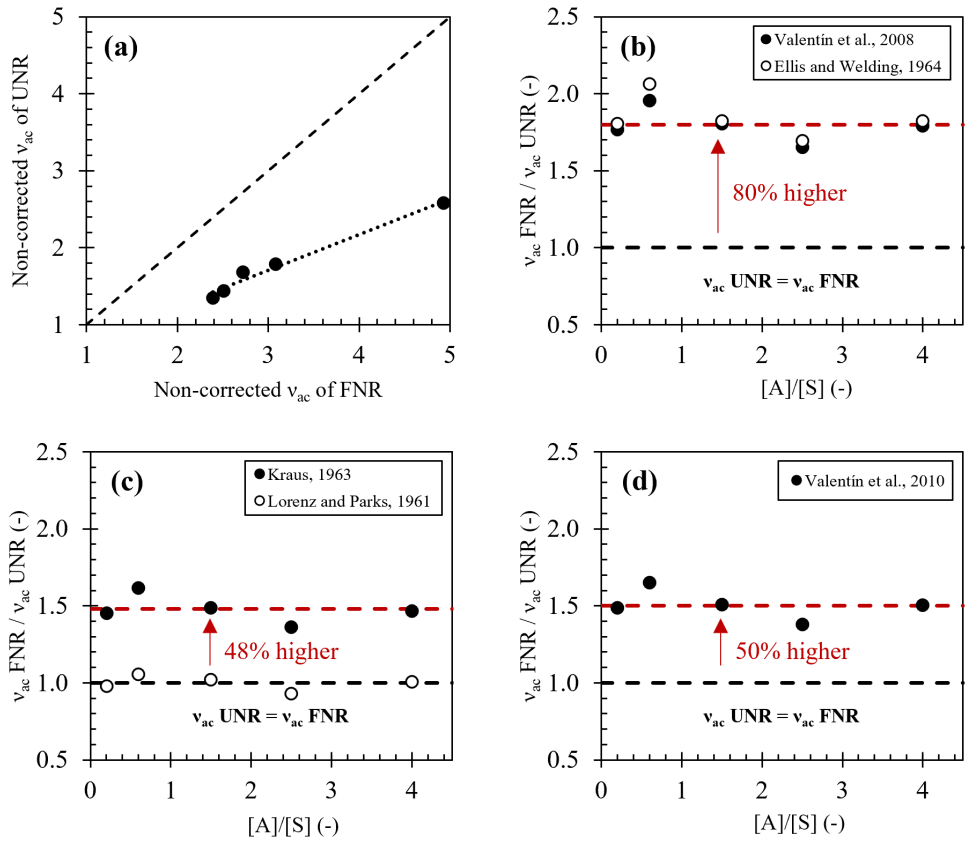

Figure A.3: Representation of (a) the active chain densities, expressed in 10^4 mol/cm^3, for UNR and FNR for a calculation without any correction. The ratio of active chain densities of FNR and UNR are expressed as a function of the [A]/[S] ratio for different corrections: (b) by correcting the ZnO effect, (c) by correcting the CB effect and (d) by correcting the CB and ZnO effect. The assumptions used for the calculation are given in A.3.2.2.

In the following, corrections from the literature are applied with the objective to unify the active chain densities between FNR and UNR. In other words, we are trying to correct the data to be as close as possible to the $y = x$ plotted line in Figure A.3 (a). To facilitate the reading,

results are presented in terms of the ratio of active chain densities, *i.e.*, FNR over UNR ones, as a function of the [A]/[S] ratio ranging from 0.2 to 4. First, it is necessary to investigate the corrections of the ZnO content. Then, CB corrections are addressed. Finally, a correction on both ZnO and CB is used.

A.4.1.1 Correction of the ZnO effect

Figure A.3 (b) presents the active chain densities of UNR and FNR. By applying the correction proposed by Ellis and Welding, the active chain densities of FNR are 80% higher than those of UNR. Similar results are obtained from the correction proposed by Valentín and coworkers[188]. The two corrections give results in the same order of magnitude. However, since both UNR and FNR were corrected, it is not surprising to obtain such a difference. This can be explained because CB effects are not taken into account in the correction, while CB leads to a strong restriction of swelling and consequently a miscalculation of active chain densities of FNR. These results evidence that correcting only the ZnO effect does not return satisfactory results.

A.4.1.2 Correction of the CB effect

Figure A.3 (c) presents the effect of the correction proposed by Kraus and Lorenz and Parks [207, 208]. Firstly, by using the Kraus correction, the difference in active chain densities is significantly lowered, results for FNR being about 50% higher than those for UNR. This can be explained because CB content is higher than the ZnO one. Therefore, taking it into account drastically improves the accuracy of the calculation, as expected. One can note that the results of Candau on NR accelerated with CBS were very similar: $NRS1.2$, a NR vulcanized with 1.2 phr of sulphur and accelerated with CBS, presents a comparable difference in comparison to NRS1.2 filled with 20 phr of CB [123]. Secondly, the correction proposed by Lorenz and Parks does not lead to any significant difference [207]. This is anticipated, since it is the aim of Equation A.14. One should note that the z value is the same for all materials, the filler content as well, taken as 0.2. This result is interesting because it is the first one that gives the same calculated values of active chain density for all the formulations. The question of the most representative approach between the one of Kraus and Lorenz and Parks is addressed in Section A.4.2. However, since the ZnO content is not considered for both Kraus, and Lorenz and Parks corrections, the active chain densities of UNR and FNR are de facto overestimated. In this case, the ratio (ν_{ac} FNR)/(ν_{ac} UNR) is non informative, since UNR and FNR materials are biased. As a result, correcting both ZnO and CB is required.

A.4.1.3 Correction of both the CB and ZnO effect

The last correction investigated is the one proposed by Valentín *et al.* which takes into account both CB and ZnO [265]. The results are presented in Figure A.3 (d). The active chain densities of FNR are 50% higher compared to UNR ones. This result shows a significant difference between them even though the CB and ZnO contents are taken into account. Since ZnO contents are the same between UNR and FNR, the difference cannot be reduced any further

than 50%. However, the ratio between active chain densities is surely properly calculated and has a physical significance. This highlights the necessity to take both contributions of CB and ZnO. It would then be possible to compare materials with different levels of CB and ZnO. Nevertheless, the correction proposed by Valentín *et al.* still leads to differences between UNR and FNR, which raises several questions: *(i)* Is the difference between UNR and FNR properly estimated? *(ii)* Could it be lowered by considering new corrections? *(iii)* If this difference is properly estimated, what is its physical origin? *(iv)* Is the difference to be considered as part of the results? These questions are addressed in the next section with the proposal for new corrections.

A.4.2 Correcting both CB and ZnO effects

Previous results have evidenced the necessity of correcting both ZnO and CB effects. This is first addressed by combining existing corrections from the literature.

A.4.2.1 Correction of CB and ZnO effects by combining corrections from literature

The previous results gained by using the correction of Valentín *et al.* showed higher active chain densities for FNR than UNR, even though a correction on CB and ZnO was employed [265]. One can wonder if such a difference would be the same by using another method. Indeed, it is necessary to verify whether or not it can be lowered. To the best of our knowledge, except for their model, no one used a correction simultaneously on both CB and ZnO. In our opinion, it seems appropriate to combine the existing corrections. Table A.4 presents a proposition of three combinations. Combination 1 couples Kraus and Ellis and Welding corrections, Combination 2 couples Kraus and Valentín corrections and Combination 3 is the re-defined Kraus correction. For the latter Kraus correction, the total volume fraction of insoluble components is included, leading to: $\varphi_{ins} = \varphi_{CB} + \varphi_{ZnO}$ [208]. The results are given in terms of the mean difference of active chain density between UNR and FNR. From Table A.4, combinations 1 and 2 led to very similar results. Furthermore, these results are the same as the one established from the Valentín *et al.* relation [265]. For Combination 3, FNR is less overestimated with values 46% higher in average, which is slightly lower than the others. These results show a noticeable difference between UNR and FNR, whichever the correction used, and the type of combination made. In this sense, it is possible to consider that the active chain densities of FNR are at least 46% higher than those of UNR, and properly estimated. Consequently, the last two questions *(iii)* and *(iv)*, previously raised, still need to be investigated. They are addresses in the following Sub-section A.4.2.2.

A.4.2.2 Proposal of a new methodology based on existing corrections

In order to have a clear understanding of the remaining difference of active chain densities between UNR and FNR, it is essential to understand correctly the nature of the filler-rubber interactions. In other words, we wondered what type of interactions between the CB particles

	Combination 1	Combination 2	Combination 3
ZnO correction	Kraus [208]	Kraus [208]	Kraus [208] redefined
CB correction	Ellis and Welding [187]	Valentín *et al.* [188]	
% of increasing of ν_{ac} for FNR compared to UNR	51%	51%	46%

Table A.4: The mean difference in active chain density between UNR and FNR, by applying three different combinations.

and the rubber bulk occurred, and if they are truly to be considered as part of the active chain density.

The pioneering work of Studebaker questioned about the possibility of somehow filler-rubber bonds resulting in an increase in the overall number of cross-linking [219]. However, Dannenberg argued that no strong interaction between the filler and the matrix should occur [229]; it is in fact correlate with the theory of rubber chain slipping, which is only possible under the assumption of no interaction or for weak ones only, *i.e.*, the interface is composed of physical bonding [200]. In the work of Leblanc, a non-negligible amount of the rubber is considered bounded to filler particles, in which rubber chains are attached to filler surface [25]. One can note that there also exists occluded or immobilized rubber between fillers aggregates and un-bounded rubber to filler particles also exist, resulting in the absence of interaction in the bulk [25, 131, 266]. According to the result of Porter, CB coupled within CV system (mainly composed of long sulphur cross-links) could enhance the cross-linking, by creating additional cross-links [41]. However, for a wide range of materials comprising CV system, Gent showed no effect of the CB on the degree of cross-linking: the swelling ratios Q and Q_0 of filled and unfilled NR were linearly related [241]. As shown by Valentín *et al.* through swelling and NMR tests, strong filler-rubber interactions – comparable to giant cross-links – do exist in the vicinity of the filler particles while the bulk seems un-affected [265]. By comparing these few works, it is very difficult to interpret the nature of filler-rubber interactions. As mentioned by Robertson *et al.*, the more realistic rubber-filler interactions could probably be a combination of rubber chains adsorption by filler along with covalent bonding of rubber chains to filler particles and with a cross-linking clustering effect in the vicinity of the fillers [27]. But, to our knowledge, filler-rubber interactions are not yet fully clear.

In the present study, we are more interested in whether or not the filler-rubber interaction is to be considered as part of the macromolecular network. Furthermore, it is also essential to wonder if it contributes to the mechanical properties. To our opinion, it is necessary to verify if additional cross-links are responsible for swelling restriction. If it is the case, they must be considered by employing the relation of Valentín and coworkers [265]. If not, they must be totally corrected thanks to a relation like the one of Lorenz and Parks [207]. So, in response to these issues, the question raised whether the vulcanization system could influence the swelling since it drives the amount of sulphur available to operate the cross-linking of rubber chains.

Thus, depending on the sulphur and accelerator contents initially introduced, vulcanization obviously operates differently. It may be suggested that a high sulphur content promotes such bonding resulting in highly cross-linked CV system. In order to understand the effect of the vulcanization system on the swelling and to verify if possible additional cross-links formation, the swelling ratio of UNR and FNR are compared. The results, presented in Figure A.4 (a), clearly highlight that swelling ratio of FNR evolved linearly with the one of UNR. This suggests that fillers do not modify the network for the range of vulcanization studied that is [A]/[S] $\in$ [0.2;4]. In other words, the average number of active chains is not affected by the presence of CB. This result is in good agreement with a few literature works on similar NR, but for different [A]/[S] [120, 207, 241]. Thus, the vulcanization system has no significant effect on the results. The difference between UNR and FNR may be explained by physical interactions between the filler and the rubber matrix, or by a restriction of the mobility of the active chain in the vicinity of the CB particles. This result proves that the swelling ratio of FNR must be corrected with respect to the one of UNR.

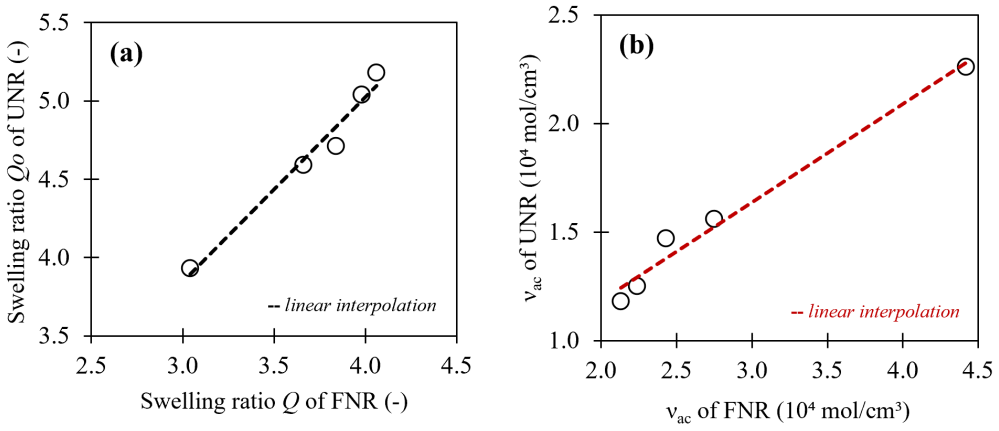

Figure A.4: Representation of the (a) linearly related swelling ratio of UNR and FNR and (b) the active chain density relationship between UNR and FNR. The assumptions used for the calculation are given in A.3.2.2.

Consequently, we propose to use a new methodology to correct our values. It consists of two steps: *(i)* firstly the UNR values are corrected by using the ZnO correction of Valentín *et al.* and (ii) secondly the FNR are corrected by using the correction of Lorenz and Parks [188, 207]. Without using the preliminary correction of ZnO on UNR, the active chain densities are, on the average overestimated by 13%. This further demonstrates the importance to take ZnO into account, which enables comparing materials having different contents of CB and ZnO. Finally, since our formulations have fixed ZnO and CB contents, the active chain density can be corrected from the affine relation presented in the Figure A.4 (b) instead of the Lorenz and Parks one. This affine relation is considered effective over the range of vulcanization systems defined.

A.4.3 Discussion on the relevance of the predicted active chain density

This section is dedicated to the interpretation of the predicted active chain density, in order to discuss about the relevancy of the methodology. The objective is to evaluate if our methodology is still valid under more realistic assumptions, and if the results thus gained to calculate the active chain density are the same as when using another technique.

A.4.3.1 Verification of the methodology under other assumptions

Since the calculation is performed by using the classical Flory-Rehner relation, given in Equation A.8, we wondered if our results would have been the same when using other assumptions. So, the same calculation is made with a phantom network model, given in Equation A.9. Results are presented in Figure A.5 (a). The values of active chain densities have changed, as a consequence of the changes in assumption, but they are still linearly related. As a result, the conclusions drawn previously are not affected by the type of network model. Then, the calculation is carried out by using a phantom network model and also by using the Equation A.11 to calculate the Flory-Huggins interaction. These two assumptions were shown to be more representative of the true behavior of our materials [188]. Results are presented in Figure A.5 (b) in which active chain densities of UNR and FNR are following the same trend, again. To conclude, the proposed methodology is considered to suitably apply to every assumption.

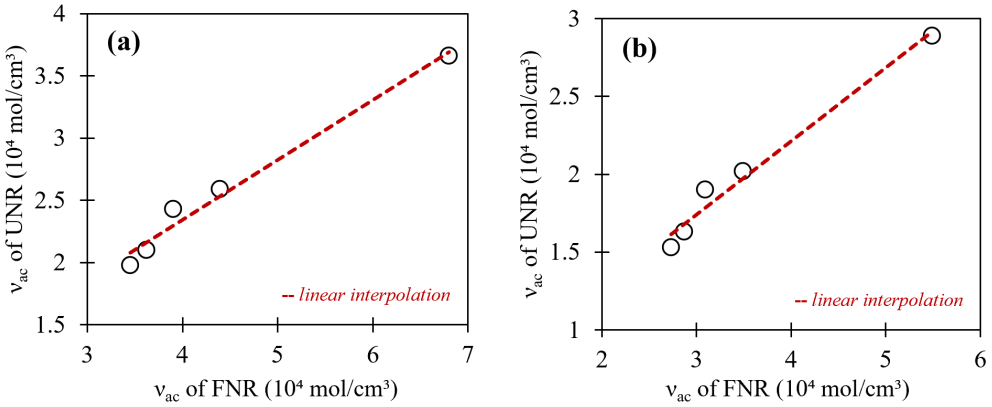

Figure A.5: The effect of using (a) a phantom model and a constant Flory-Huggins interaction, and (b) a phantom model and a variable Flory-Huggins interaction. The changes in assumptions used for the calculation are given in A.4.3.1.

A.4.3.2 Comparison with stress-strain analysis technique

Among the other techniques to estimate the active chain density, the stress-strain analysis is the simplest one. From the work due to Treloar [47, 50], the stress-strain relationship for uniaxial simple extension is given by:

$$\sigma = NkT(\lambda^2 - \lambda^{-1}) \tag{A.24}$$

with σ the true or Cauchy stress, N the active chain density (in g/mol), k the Boltzmann constant and T the absolute temperature. The shear modulus is expressed as $G = NkT = \rho RT/M_c$. By considering that $M_c = 1/N$ and by including ψ to take into account the network model, the Equation A.24 can be modified as follows:

$$\sigma = N\rho RT\psi(\lambda^2 - \lambda^{-1}) \tag{A.25}$$

Note that the term ψ refers to either affine for $\psi = 1$ or phantom for $\psi = 0.5$. The stress-strain response determined from uniaxial tensile test, in the range of small strains, is used to calculate the active chain density. Figure A.6 presents the stress-strain curves for unfilled materials, UNR, previously presented in Table A.2. The results are plotted in terms of Cauchy stress σ vs $\lambda^2 - \lambda^{-1}$ in the low stretch area. These stress-strain responses can be fitted by using the Mooney-Rivlin model [195], which is defined as:

$$\sigma = 2 * (C_1 + \frac{C_2}{\lambda})(\lambda^2 - \lambda^{-1}) \tag{A.26}$$

with C_1 and C_2 the independent constants, to be identified. The shear modulus is given by $G = 2(C_1 + C_2)$ [267].

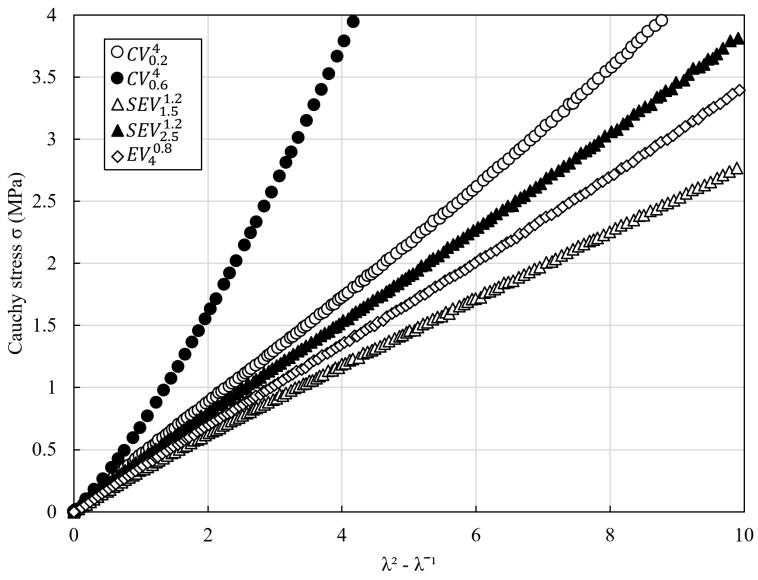

Figure A.6: The stress-strain response plotted as Cauchy stress σ vs stretch λ, for all the [A]/[S] content ratio investigated.

Finally, the Equation A.27, gives a relation between the active chain density N and the coefficients identified from the Mooney-Rivlin model. For the sake of clarity, the term ν_{ac} will be used instead of N, as the result is given in mol/cm^3. It is generally considered that the active chain density corresponds to the parameter C_1 only. By also using the parameter C_2, it is believed to include a contribution from entanglements, as explained by Vieyres and coworkers [203]. In this sense, the value of ν_{ac} calculated by using the Equation A.27 is considered to include every contribution to the elasticity.

$$\nu_{ac} = \frac{2(C_1 + C_2)}{RT\rho\psi} \tag{A.27}$$

Figure A.7 presents the comparison between the active chain densities of UNR obtained from swelling method and stress-strain analysis, for an assumption of an affine model. Also, the Flory-Huggins interaction χ is taken as 0.39.

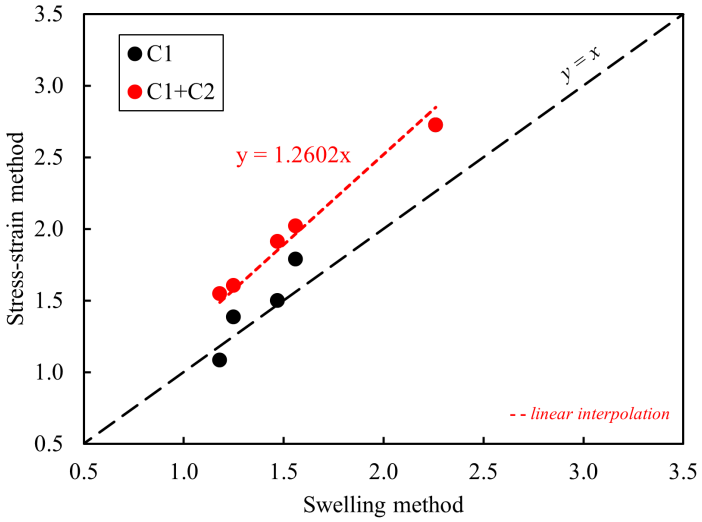

Figure A.7: The active chain density obtained by the stress-strain method as a function of the active chain density obtained by the swelling methodology, for the UNR materials.

The results obtained by considering C_1 only are fairly the same for both techniques, indicating a good correlation between them. The active chain densities of UNR are properly calculated. This confirmed that the results of filled materials can be corrected on the basis of the unfilled ones, for the swelling technique. Furthermore, by considering both C_1 and C_2, results are linearly related, with an intercept value of zero. This suggests that the stress-strain method is sensitive to entanglements.

A.4.4 Summary

As a summary, Figure A.8 provides a synthetic view on the motivation of the present paper. When determined by using the Flory-Rehner relationship of both filled and unfilled NR, vulcanized with different vulcanization systems, the active chain density is strongly overestimated. Insoluble components in toluene are responsible for this overestimation, due to a restriction of swelling. It is highlighted by the green circles surrounding ZnO and CB particles. Contrarily to CB particles, ZnO particles do not have strong interaction with the rubber matrix. To better estimate the active chain density, a correction of both ZnO and CB was proposed and validated.

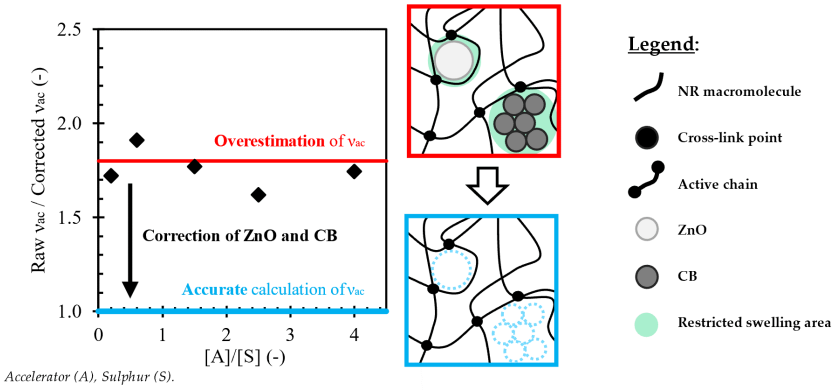

Figure A.8: Representation of the overestimation of the active chain density induced by ZnO and CB particles (this figure corresponds to the graphical abstract).

Finally, a new representation of the results is proposed to map the effect of the formulation on the active chain density. This representation is given by the Figure A.9. It is proposed to represent the data with a 3D graphical in which the vulcanization system is represented in the X and Y axess, corresponding to the sulphur and accelerator contents, respectively. In addition, different areas (blue, green and red) are plotted in order to provide an information on the type of vulcanization system, *i.e.*, a qualitative information on the length of the sulphur cross-links. The corrected active chain density is plotted as an iso-value, for every formulation used in this study. Note that the values are calculated under the assumptions of a phantom network and a variable Flory-Huggins interaction.

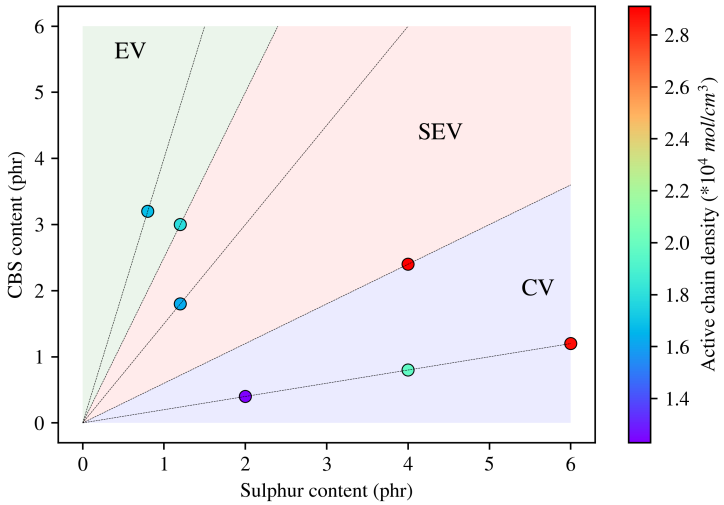

Figure A.9: Mapping of the effect of the formulation on the active chain density of the macromolecular network. The accelerator and sulphur contents are given in parts per hundred of rubber, and the active chain density in mol/cm^3. The green, red and blue areas correspond to EV, SEV and CV vulcanization systems, respectively.

A.5 Conclusions and perspectives

This paper investigates the effect of the insoluble components on the swelling properties of unfilled and CB-filled NR. Swelling tests were performed accordingly to the classical Flory-Rehner relation in order to estimate the active chain densities of the filled and unfilled NR. Several corrections from the literature were applied to take into account the effect of the ZnO and CB. The results showed that without any corrections, or by correcting only ZnO or only CB, an overestimation of the active chain density was observed. By employing a correction on both of them, a difference between active chain densities of filled and unfilled NR remained. However, the swelling ratios of unfilled Q_0 and filled Q NR were linearly related, independently of the vulcanization system type. Consequently, it was proposed to correct the active chain densities of FNR with respect to the UNR ones. Thus, a methodology based on the correction of the ZnO for unfilled NR and ZnO and CB for filled NR was proposed. In order to verify the relevance of the methodology proposed, different calculation assumptions were employed. Furthermore, a comparison with active chain densities obtained by stress-strain analysis was carried out. As a perspective, using materials with different contents of ZnO and CB would be ideal. It also raises several outcomes, such as *(i)* the effect for very different vulcanization system such as peroxide and *(ii)* the effect for very different content and type of fillers, such as recovered CB.

Appendix B

Monotonic stress-strain curves

Preamble

The stress-strain responses not shown in Chapter 2, are presented in this second appendix. It corresponds to the stress-strain responses under monotonic tension loading conditions.

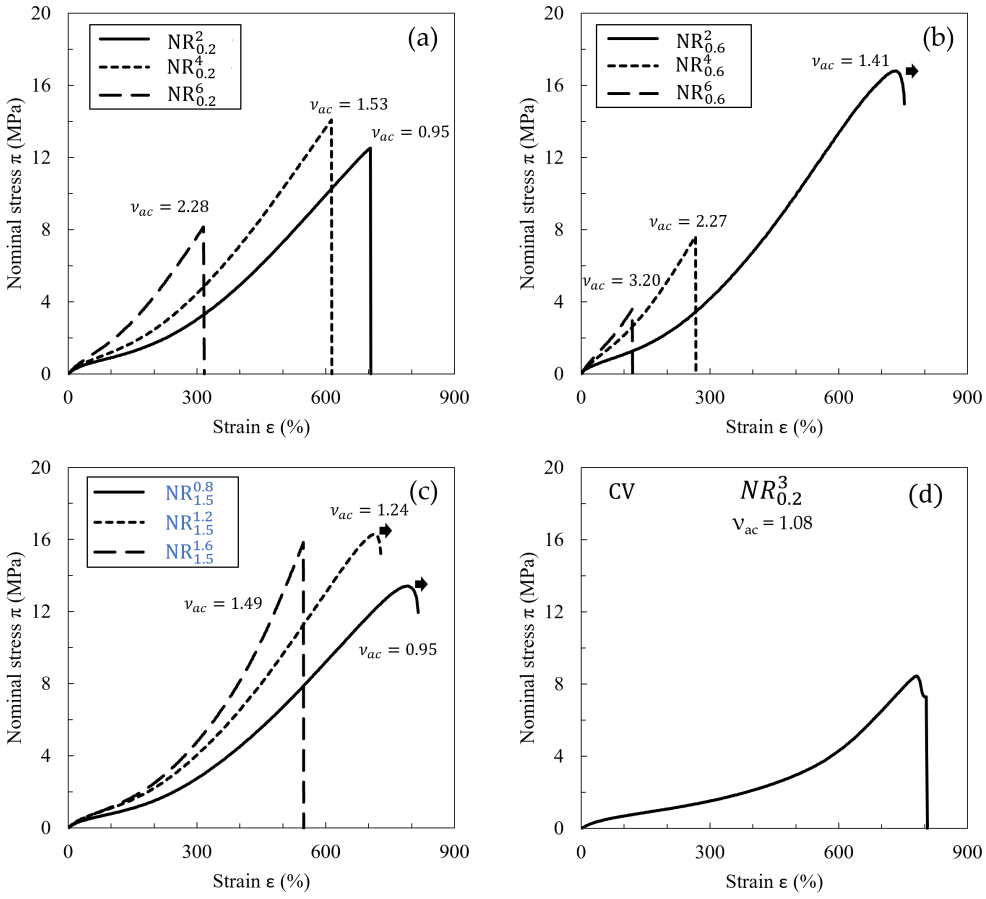

Figure B.1: Mechanical responses of (a) filled $NR^2_{0.2}$, $NR^4_{0.2}$ and $NR^6_{0.2}$, (b) filled $NR^2_{0.6}$, $NR^4_{0.6}$ and $NR^6_{0.6}$, (c filled) $NR^{0.8}_{1.5}$, $NR^{1.2}_{1.5}$ and $NR^{1.6}_{1.5}$, and (d) unfilled $NR^3_{0.2}$. The vertical lines highlight the stretch at break. ν_{ac} is given in 10^4 mol/cm^3, and calculated by using the Flory-Rehner relationship with the assumption of an affine network, and for χ=0.39.

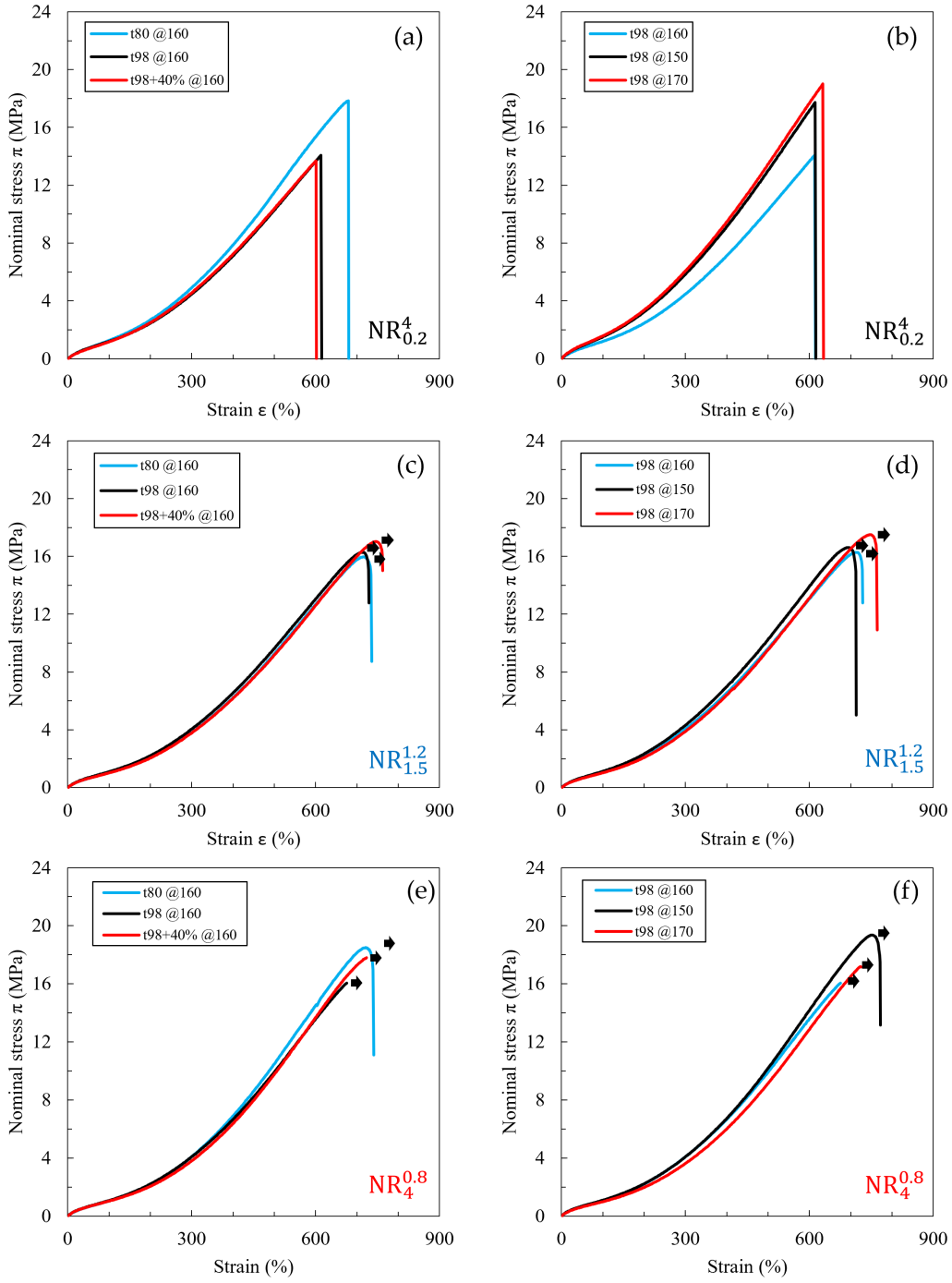

Figure B.2: Mechanical responses of filled $NR^4_{0.2}$ ((a) and (b)), $NR^{1.2}_{1.5}$ ((c) and (d)) and $NR^{0.8}_{4}$ ((e) and (f)) vulcanized for different conditions. The vertical lines highlight the stretch at break. ν_{ac} is given in 10^4 mol/cm^3, and calculated by using the Flory-Rehner relationship with the assumption of an affine network, and for χ=0.39.

Appendix C

Cyclic stress-strain curves

Preamble

The stress-strain responses not shown in Chapter 3, are presented in this third appendix. It corresponds to the stress-strain responses under cyclic tension loading conditions.

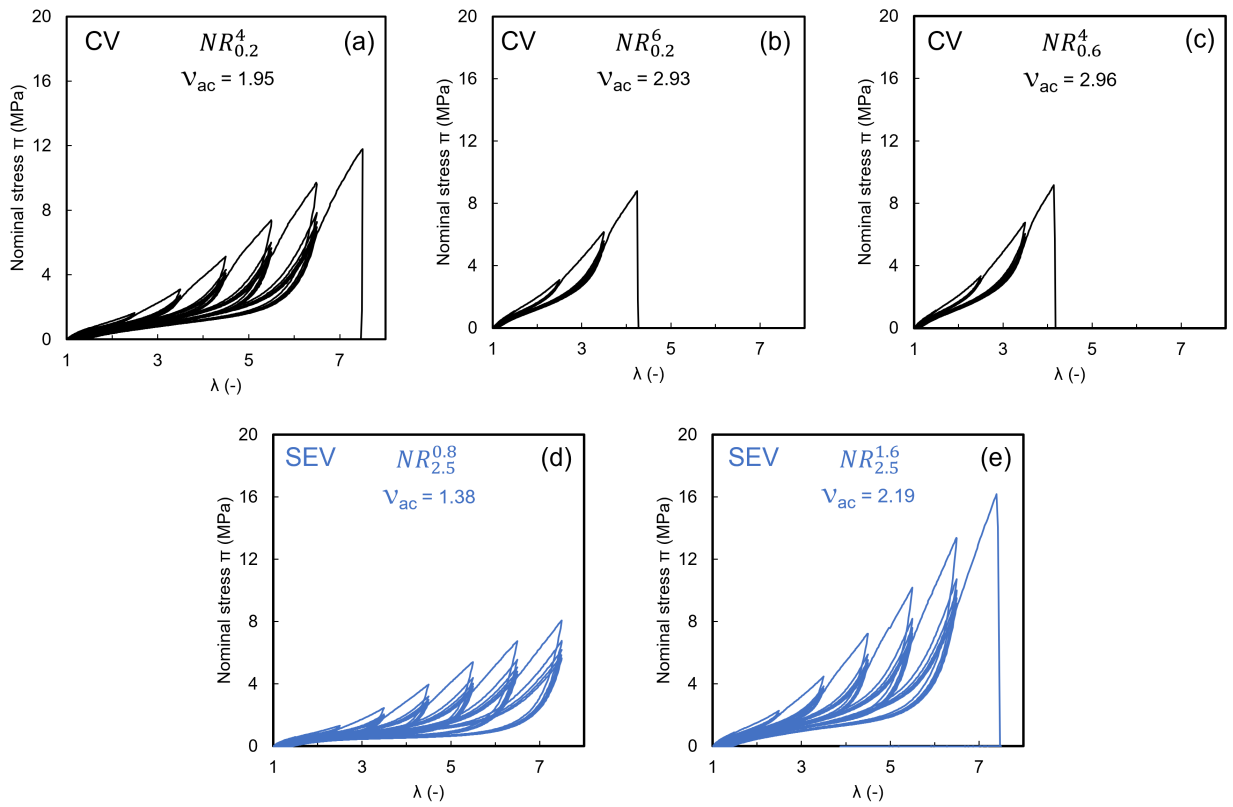

Figure C.1: Mechanical responses of filled (a) $NR^4_{0.2}$ (b) $NR^6_{0.2}$ (c) $NR^4_{0.6}$ (d) $NR^{0.8}_{2.5}$ and (e) $NR^{1.6}_{2.5}$. The vertical lines highlight the stretch at break. ν_{ac} is given in 10^4 mol/cm^3, and calculated by using the Flory-Rehner relationship with the assumption of a phantom network, and for $\chi = f(\upsilon_r)$.

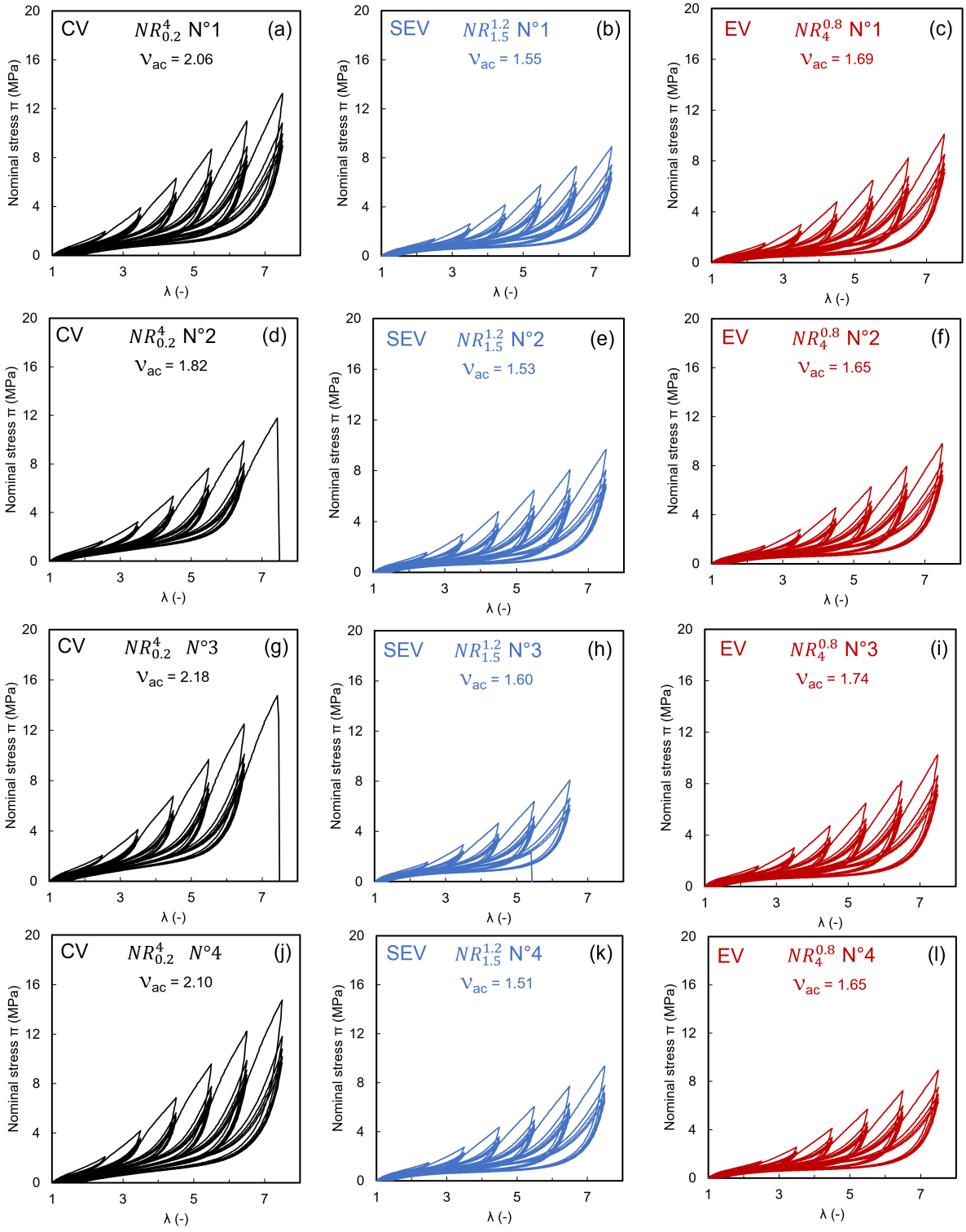

Figure C.2: Mechanical responses of filled $NR^4_{0.2}$ ((a), (d), (g) (j)), $NR^{1.2}_{1.5}$ ((b), (e), (h), (k)) and $NR^{0.8}_4$ ((c), (f), (i), (l)) vulcanized for different conditions. The "N°X" refers to the vulcanization condition given in the Table 2.3. The vertical lines highlight the stretch at break. ν_{ac} is given in 10^4 mol/cm^3, and calculated by using the Flory-Rehner relationship with the assumption of a phantom network, and for $\chi = f(\upsilon_r)$.

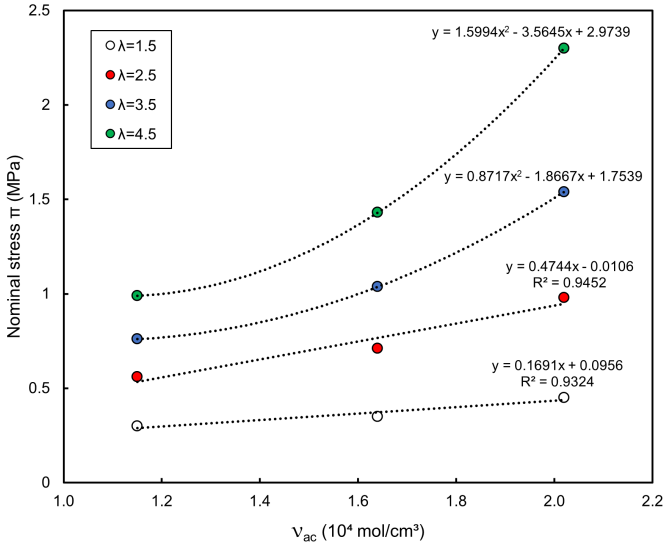

Figure C.3: Effect of ν_{ac} on stiffness for unfilled $NR^2_{0.2}$, $NR^4_{0.2}$ and $NR^6_{0.2}$ for stretch levels of 1.5, 2.5, 3.5 and 4.5. ν_{ac} is given in 10^4 mol/cm^3, and calculated by using the Flory-Rehner relationship with the assumption of a phantom network, and for $\chi = f(\upsilon_r)$.

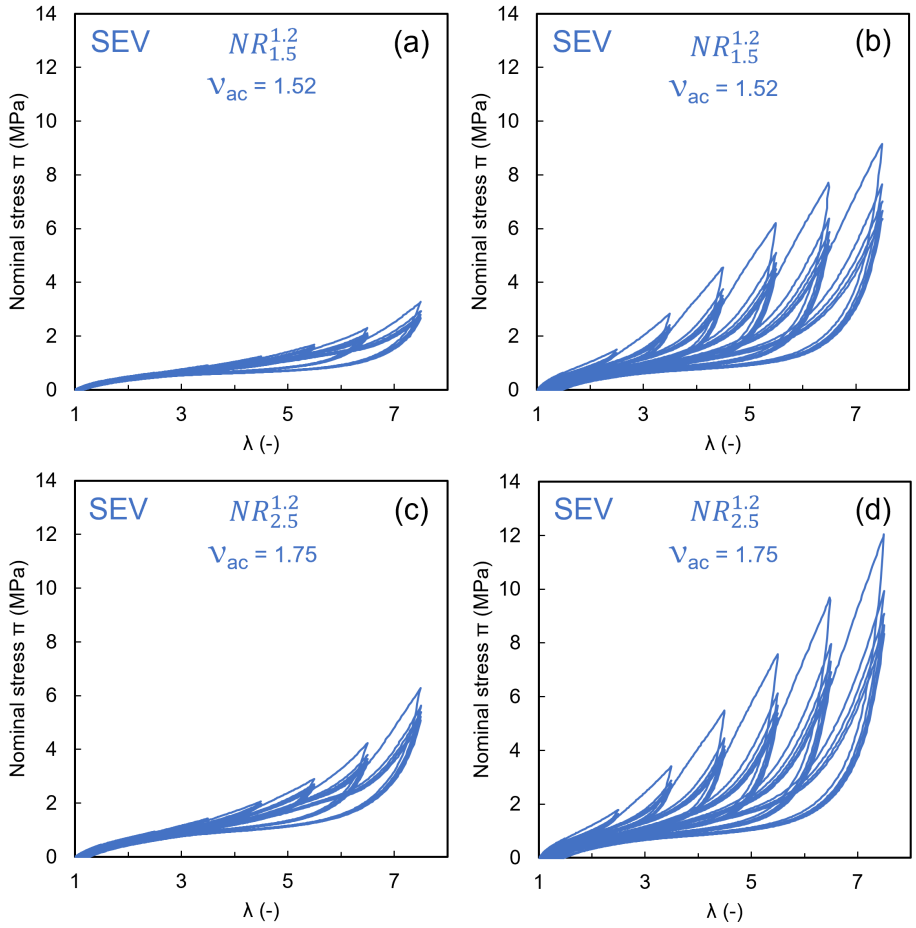

Figure C.4: Mechanical responses for both filled and unfilled $NR^{1.2}_{1.5}$ ((a) and (b)) and $NR^{1.2}_{2.5}$ ((c) and (d)), plotted in terms of the nominal stress as a function of the prescribed stretch. ν_{ac} is given in 10^4 mol/cm^3, and calculated by using the Flory-Rehner relationship with the assumption of a phantom network, and for $\chi = f(\upsilon_r)$.

Bibliography

[1] W. V. Mars and A. Fatemi. "Factors that affect the fatigue life of rubber: a literature survey". In: *Rubber Chemistry and Technology* 77.3 (2004), pp. 391–412. DOI: https://doi.org/10.5254/1.3547831.

[2] L. Chazeau, J. -M. Chenal, C. Gauthier, J. Kallungal, and J. Caillard. "About the Influence of Materials Parameters on the Ultimate and Fatigue Properties of Elastomers". In: *Fatigue Crack Growth in Rubber Materials*. Springer International Publishing, 2020, pp. 297–329. DOI: https://doi.org/10.1007/12_2020_80.

[3] T. Gehling, J. Schieppati, W. Balasooriya, R. C. Kerschbaumer, and G. Pinter. "Fatigue Behavior of Elastomeric Components: A Review of the Key Factors of Rubber Formulation, Manufacturing, and Service Conditions". In: *Polymer Reviews* 63.3 (2023), pp. 763–804. DOI: https://doi.org/10.1080/15583724.2023.2166955.

[4] S. M. Cadwell, R. A. Merrill, C. M. Sloman, and F. L. Yost. "Dynamic fatigue life of rubber". In: *Rubber Chemistry and Technology* 13.2 (1940), pp. 304–315. DOI: https://doi.org/10.5254/1.3539515.

[5] B. Ruellan. "Fatigue of natural rubber at different temperatures: reinforcement due to strain-induced crystallization and modelling the non-linear damage evolution". PhD thesis. University of Rennes 1, 2019.

[6] A. K. Bhowmick and H. Stephens. *Handbook of elastomers*. CRC Press, 2000. DOI: https://doi.org/10.1201/9781482270365.

[7] S. Kohjiya and Y. Ikeda. *Chemistry, manufacture and applications of natural rubber*. Woodhead Publishing, 2021. DOI: https://doi.org/10.1016/C2018-0-04686-1.

[8] Y. Tanaka. "Structural characterization of natural polyisoprenes: solve the mystery of natural rubber based on structural study". In: *Rubber chemistry and technology* 74.3 (2001), pp. 355–375. DOI: https://doi.org/10.5254/1.3547643.

[9] S.-H. Chough and D.-H. Chang. "Kinetics of sulfur vulcanization of NR, BR, SBR, and their blends using a rheometer and DSC". In: *Journal of Applied Polymer Science* 61.3 (1996), pp. 449–454. DOI: https://doi.org/10.1002/(SICI)1097-4628(19960718)61:3<449::AID-APP7>3.0.CO;2-I.

[10] P. J. Flory. "Network Structure and the Elastic Properties of Vulcanized Rubber." In: *Chemical reviews* 35.1 (1944), pp. 51–75. DOI: https://doi.org/10.1021/cr60110a002.

[11] P. Nun-anan, S. Wisunthorn, S. Pichaiyut, C. D. Nathaworn, and C. Nakason. "Influence of nonrubber components on properties of unvulcanized natural rubber". In: *Polymers for Advanced Technologies* 31.1 (2020), pp. 44–59. DOI: https://doi.org/10.1002/pat.4746.

[12] M. Akiba and A. S. Hashim. "Vulcanization and crosslinking in elastomers". In: *Progress in polymer science* 22.3 (1997), pp. 475–521. DOI: https://doi.org/10.1016/S0079-6700(96)00015-9.

[13] A. Y. Coran. "Vulcanization". In: *Science and Technology of Rubber*. Elsevier, 1994. Chap. 7, pp. 339–385. DOI: https://doi.org/10.1016/b978-0-08-051667-7.50012-3.

[14] N. P. Cheremisinoff. *Elastomer technology handbook*. CRC press, 1993. DOI: https://doi.org/10.1201/9780138758851.

[15] G. Heideman, R. N. Datta, J. W. M. Noordermeer, and B. Van Baarle. "Activators in accelerated sulfur vulcanization". In: *Rubber chemistry and technology* 77.3 (2004), pp. 512–541. DOI: https://doi.org/10.5254/1.3547834.

[16] A. S. Aprem, K. Joseph, T. Mathew, V. Altstaedt, and S. Thomas. "Studies on accelerated sulphur vulcanization of natural rubber using 1-phenyl-2, 4-dithiobiuret/tertiary butyl benzothiazole sulphenamide". In: *European Polymer Journal* 39.7 (2003), pp. 1451–1460. DOI: https://doi.org/10.1016/S0014-3057(02)00382-8.

[17] A. S. Aprem, K. Joseph, R. Laxminarayanan, and S. Thomas. "Physical, mechanical, and viscoelastic properties of natural rubber vulcanizates cured with new binary accelerator system". In: *Journal of Applied Polymer Science* 87.14 (2003), pp. 2193–2203. ISSN: 1097-4628. DOI: https://doi.org/10.1002/app.11473.

[18] A. S. Aprem, S. Thomas, K. Joseph, N. M. Barkoula, and J. K. Kocsis. "Sulphur Vulcanisation of Styrene Butadiene Rubber Using New Binary Accelerator Systems". In: *Journal of Elastomers & Plastics* 35.1 (2003), pp. 29–55. ISSN: 1530-8006. DOI: https://doi.org/10.1177/009524403031095.

[19] A. S. Aprem, K. Joseph, S. Thomas, N. M. Barkoula, and J. Karger-Kocsis. "Effect of 1-phenyl-2,4-dithiobiuret as secondary accelerator on cure characteristics and vulcanisate properties of natural rubber-styrene/butadiene rubber blends". In: *Plastics, Rubber and Composites* 32.1 (2003), pp. 3–10. ISSN: 1743-2898. DOI: https://doi.org/10.1179/146580103225009130.

[20] C. M. Kok. "The effects of compounding variables on the reversion process in the sulphur vulcanization of natural rubber". In: *European Polymer Journal* 23.8 (1987), pp. 611–615. DOI: https://doi.org/10.1016/0014-3057(87)90006-1.

[21] S.-S. Choi, C. Nah, and B.-W. Jo. "Properties of natural rubber composites reinforced with silica or carbon black: influence of cure accelerator content and filler dispersion". In: *Polymer international* 52.8 (2003), pp. 1382–1389. DOI: https://doi.org/10.1002/pi.1232.

[22] P. J. Flory. *Principles of polymer chemistry*. Cornell university press, 1953. DOI: https://doi.org/10.1007/978-1-4614-2212-9.

[23] R. P. Quirk. "Overview of curing and crosslinking of elastomers". In: *Progress in rubber and plastics technology* 4.1 (1988), pp. 31–45. URL: https://api.semanticscholar.org/CorpusID:137770036.

[24] D. Parkinson. "The reinforcement of rubber by carbon black". In: *British Journal of Applied Physics* 2.10 (1951), pp. 273–280. ISSN: 0508-3443. DOI: https://doi.org/10.1088/0508-3443/2/10/301.

[25] J. L. Leblanc. "Rubber–filler interactions and rheological properties in filled compounds". In: *Progress in polymer science* 27.4 (2002), pp. 627–687. DOI: https://doi.org/10.1016/S0079-6700(01)00040-5.

[26] E. Farida, N. Bukit, E. M. Ginting, and B. F. Bukit. "The effect of carbon black composition in natural rubber compound". In: *Case Studies in Thermal Engineering* 16 (2019), p. 100566. DOI: https://doi.org/10.1016/j.csite.2019.100566.

[27] C. G. Robertson and N. J. Hardman. "Nature of Carbon Black Reinforcement of Rubber: Perspective on the Original Polymer Nanocomposite". In: *Polymers* 13.4 (2021), p. 538. ISSN: 2073-4360. DOI: https://doi.org/10.3390/polym13040538.

[28] R. S. Stearns and B. L. Johnson. "Interaction between Carbon Black and Polymer in Cured Elastomers". In: *Industrial & Engineering Chemistry* 43.1 (1951), pp. 146–154. ISSN: 1541-5724. DOI: https://doi.org/10.1021/ie50493a042.

[29] P. B. Stickney and R. D. Falb. "Carbon Black-Rubber Interactions and Bound Rubber". In: *Rubber Chemistry and Technology* 37.5 (1964), pp. 1299–1340. ISSN: 0035-9475. DOI: https://doi.org/10.5254/1.3540401.

[30] I. Surya, H. Ismail, and A. R. Azura. "Alkanolamide as an accelerator, filler-dispersant and a plasticizer in silica-filled natural rubber compounds". In: *Polymer testing* 32.8 (2013), pp. 1313–1321. DOI: https://doi.org/10.1016/j.polymertesting.2013.07.015.

[31] Y. Fan, G. D. Fowler, and M. Zhao. "The past, present and future of carbon black as a rubber reinforcing filler – A review". In: *Journal of Cleaner Production* 247 (2020), p. 119115. ISSN: 0959-6526. DOI: https://doi.org/10.1016/j.jclepro.2019.119115.

[32] H. P. Boehm. "Some aspects of the surface chemistry of carbon blacks and other carbons". In: *Carbon* 32.5 (1994), pp. 759–769. ISSN: 0008-6223. DOI: 10.1016/0008-6223(94)90031-0.

[33] F. Othman and N. A. Ismail. "Coconut Oil Plasticizer as a Replacement of Petroleum Oil in Natural Rubber Compound: Physical and Mechanical Properties". In: *Charting the Sustainable Future of ASEAN in Science and Technology*. Springer, 2020, pp. 203–213. DOI: https://doi.org/10.1007/978-981-15-3434-8_18.

[34] F. W. H. Kruger and W. J. McGill. "A DSC study of curative interactions. I. The interaction of ZnO, sulfur, and stearic acid". In: *Journal of applied polymer science* 42.10 (1991), pp. 2643–2649. DOI: https://doi.org/10.1002/app.1991.070421002.

[35] J. Kruželák, R. Sỳkora, and I. Hudec. "Sulphur and peroxide vulcanisation of rubber compounds–overview". In: *Chemical Papers* 70.12 (2016), pp. 1533–1555. DOI: https://doi.org/10.1515/chempap-2016-0093.

[36] D. Craig. "The Vulcanization of Rubber with Sulfur". In: *Rubber Chemistry and Technology* 30.5 (1957), pp. 1291–1346. ISSN: 0035-9475. DOI: https://doi.org/10.5254/1.3542761.

[37] N. M. Mathew and S. K. De. "Thermo-oxidative ageing and its effect on the network structure and fracture mode of natural rubber vulcanizates". In: *Polymer* 24.8 (1983), pp. 1042–1054. DOI: https://doi.org/10.1016/0032-3861(83)90158-1.

[38] F. Grasland, L. Chazeau, J.-M. Chenal, J. Caillard, and R. Schach. "About thermo-oxidative ageing at moderate temperature of conventionally vulcanized natural rubber". In: *Polymer Degradation and Stability* 161 (2019), pp. 74–84. DOI: https://doi.org/10.1016/j.polymdegradstab.2018.12.029.

[39] J. Y. Buzaré, G. Silly, J. Emery, G. Boccaccio, and E. Rouault. "Aging effects on vulcanized natural rubber studied by high resolution solid state 13C-NMR". In: *European Polymer Journal* 37.1 (2001), pp. 85–91. DOI: https://doi.org/10.1016/S0014-3057(00)00081-1.

[40] R. L. Fan, F. Zhang Y.and Li, Y. X. Zhang, K. Sun, and Y. Z. Fan. "Effect of high-temperature curing on the crosslink structures and dynamic mechanical properties of gum and N330-filled natural rubber vulcanizates". In: *Polymer testing* 20.8 (2001), pp. 925–936. DOI: https://doi.org/10.1016/S0142-9418(01)00035-6.

[41] D. Bornstein and R. J. Pazur. "The sulfur reversion process in natural rubber in terms of crosslink density and crosslink density distribution". In: *Polymer Testing* 88 (2020), p. 106524. DOI: https://doi.org/10.1016/j.polymertesting.2020.106524.

[42] C. T. Loo. "High temperature vulcanization of elastomers: 2. Network structures in conventional sulphenamide-sulphur natural rubber vulcanizates". In: *Polymer* 15.6 (1974), pp. 357–365. DOI: https://doi.org/10.1016/0032-3861(74)90177-3.

[43] C. T. Loo. "High temperature vulcanization of elastomers: 3. Network structure of efficiently vulcanized natural rubber mixes". In: *Polymer* 15.11 (1974), pp. 729–737. DOI: https://doi.org/10.1016/0032-3861(74)90025-1.

[44] R. Mukhopadhyay, S. K. De, and S. N. Chakraborty. "Effect of vulcanization temperature and vulcanization systems on the structure and properties of natural rubber vulcanizates". In: *Polymer* 18.12 (1977), pp. 1243–1249. DOI: https://doi.org/10.1016/0032-3861(77)90287-7.

[45] A. Y. Coran. "Chemistry of the vulcanization and protection of elastomers: a review of the achievements". In: *Journal of Applied Polymer Science* 87.1 (2003), pp. 24–30. DOI: https://doi.org/10.1002/app.11659.

[46] F. Lin, W. Jia, L. Zhong, F. Liu, H. Zhang, B. Wang, and Y. Song. "Effect of main chain modification during reversion on strain-induced crystallization of polyisoprene rubbers". In: *Polymer Engineering & Science* 62.5 (2022), pp. 1710–1719. DOI: https://doi.org/10.1002/pen.25958.

[47] L. R. G. Treloar. "The elasticity and related properties of rubbers". In: *Reports on progress in physics* 36.7 (1973), p. 755. DOI: https://doi.org/10.1088/0034-4885/36/7/001.

[48] K. H. Meyer and C. Ferri. "The Elasticity of Rubber". In: *Rubber Chemistry and Technology* 8.3 (1935), pp. 319–334. ISSN: 0035-9475. DOI: https://doi.org/10.5254/1.3539443.

[49] P. J. Flory, A. Ciferri, and C. A. J. Hoeve. "The thermodynamic analysis of thermoelastic measurements on high elastic materials". In: *Journal of Polymer Science* 45.145 (1960), pp. 235–236. ISSN: 1542-6238. DOI: https://doi.org/10.1002/pol.1960.1204514527.

[50] L. R. G. Treloar. "The physics of rubber elasticity". In: (1975). DOI: https://doi.org/10.1093/oso/9780198570271.001.0001.

[51] I. Masquelier. “Influence de la formulation sur les propriétés en fatigue d’élastomères industriels”. PhD thesis. Brest, 2014.

[52] P. J. Flory and J. Rehner Jr. “Statistical mechanics of cross-linked polymer networks I. Rubberlike elasticity”. In: *The journal of chemical physics* 11.11 (1943), pp. 512–520. DOI: https://doi.org/10.1063/1.1723791.

[53] C. T. Hiranobe, G. D. Ribeiro, G. B. Torres, E. A. P. D. Reis, F. C. Cabrera, A. E. Job, L. L. Paim, and R. J. D. Santos. “Cross-Linked Density Determination of Natural Rubber Compounds by Different Analytical Techniques”. In: *Materials Research* 24 (2021). DOI: https://doi.org/10.1590/1980-5373-mr-2021-0041.

[54] L. Mullins and N. R. Tobin. “Stress softening in rubber vulcanizates. Part I. Use of a strain amplification factor to describe the elastic behavior of filler-reinforced vulcanized rubber”. In: *Journal of Applied Polymer Science* 9.9 (1965), pp. 2993–3009. ISSN: 1097-4628. DOI: https://doi.org/10.1002/app.1965.070090906.

[55] G. R. Hamed and N. Rattanasom. “Effect of Crosslink Density on Cut Growth in Black-Filled Natural Rubber Vulcanizates”. In: *Rubber Chemistry and Technology* 75.5 (2002), pp. 935–942. DOI: https://doi.org/10.5254/1.3547693.

[56] G. Chagnon. “Modélisation de l’effet Mullins dans les élastomères”. PhD thesis. Ecole Centrale de Nantes, 2003.

[57] K. Yamaguchi, A. G. Thomas, and J. J. C. Busfield. “Stress relaxation, creep and set recovery of elastomers”. In: *International Journal of Non-Linear Mechanics* 68 (2015), pp. 66–70. ISSN: 0020-7462. DOI: https://doi.org/10.1016/j.ijnonlinmec.2014.07.004.

[58] R. Hagen, L. Salmén, and B. Stenberg. “Effects of the type of crosslink on viscoelastic properties of natural rubber”. In: *Journal of Polymer Science Part B: Polymer Physics* 34.12 (1996), pp. 1997–2006. DOI: https://doi.org/10.1002/(SICI)1099-0488(19960915)34:12<1997::AID-POLB5>3.0.CO;2-N.

[59] R. L. Fan, Y. Zhang, C. Huang, Y. Zhang, Y. Fan, and K. Sun. “Effect of crosslink structures on dynamic mechanical properties of natural rubber vulcanizates under different aging conditions”. In: *Journal of Applied Polymer Science* 81.3 (2001), pp. 710–718. DOI: https://doi.org/10.1002/app.1488.

[60] A. F. Baruel, S. A. C. de Mello, F. Menezes, and S. N. Cassu. “Effect of Vulcanization System on Damping Properties of Natural Rubber”. In: *Macromolecular Symposia* 406.1 (2022). ISSN: 1521-3900. DOI: https://doi.org/10.1002/masy.202200040.

[61] J.-M. Chenal, C. Gauthier, L. Chazeau, L. Guy, and Y. Bomal. "Parameters governing strain induced crystallization in filled natural rubber". In: *Polymer* 48.23 (2007), pp. 6893–6901. DOI: https://doi.org/10.1016/j.polymer.2007.09.023.

[62] J. R. Samaca Martinez, J.-B. Le Cam, X. Balandraud, E. Toussaint, and J. Caillard. "Mechanisms of deformation in crystallizable natural rubber. Part 1: thermal characterization". In: *Polymer* 54.11 (2013), pp. 2717–2726. DOI: https://doi.org/10.1016/j.polymer.2013.03.011.

[63] J. R. Samaca Martinez, J.-B. Le Cam, X. Balandraud, E. Toussaint, and J. Caillard. "Mechanisms of deformation in crystallizable natural rubber. Part 2: Quantitative calorimetric analysis". In: *Polymer* 54.11 (2013), pp. 2727–2736. DOI: https://doi.org/10.1016/j.polymer.2013.03.012.

[64] J.-B. Le Cam. "Energy storage due to strain-induced crystallization in natural rubber: The physical origin of the mechanical hysteresis". In: *Polymer* 127 (2017), pp. 166–173. ISSN: 0032-3861. DOI: https://doi.org/10.1016/j.polymer.2017.08.059.

[65] S. Trabelsi, P.-A. Albouy, and J. Rault. "Crystallization and melting processes in vulcanized stretched natural rubber". In: *Macromolecules* 36.20 (2003), pp. 7624–7639. DOI: https://doi.org/10.1021/ma030224c.

[66] M.T. Loukil, G. Corvec, E. Robin, M. Miroir, J.-B. Le Cam, and P. Garnier. "Stored energy accompanying cyclic deformation of filled rubber". In: *European Polymer Journal* 98 (2018), pp. 448–455. ISSN: 0014-3057. DOI: https://doi.org/10.1016/j.eurpolymj.2017.11.035.

[67] V. N. Khiêm, J.-B. Le Cam, S. Charlès, and M. Itskov. "Thermodynamics of strain-induced crystallization in filled natural rubber under uni- and biaxial loadings, Part I: Complete energetic characterization and crystallinity evaluation". In: *Journal of the Mechanics and Physics of Solids* 159 (2022), p. 104701. ISSN: 0022-5096. DOI: https://doi.org/10.1016/j.jmps.2021.104701.

[68] J.-B. Le Cam. "Fast Evaluation and Comparison of the Energy Performances of Elastomers from Relative Energy Stored Identification under Mechanical Loadings". In: *Polymers* 14.3 (2022), p. 412. ISSN: 2073-4360. DOI: https://doi.org/10.3390/polym14030412.

[69] H. Bouasse and Z. Carrière. "Sur les courbes de traction du caoutchouc vulcanisé". In: *Annales de la Faculté des sciences de Toulouse: Mathématiques*. Vol. 5. 3. 1903, pp. 257–283.

[70] L. Mullins. "Effect of Stretching on the Properties of Rubber". In: *Rubber Chemistry and Technology* 21.2 (1948), pp. 281–300. ISSN: 0035-9475. DOI: https://doi.org/10.5254/1.3546914.

[71] Y. Mouslih. "Fatigue multiaxiale du caoutchouc naturel : renforcement de la durée de vie sous chargement en torsion à différentes températures". PhD thesis. Université de Rennes, 2023.

[72] J. A. C. Harwood, L. Mullins, and A. R. Payne. "Stress softening in natural rubber vulcanizates. Part II. Stress softening effects in pure gum and filler loaded rubbers". In: *Journal of Applied Polymer Science* 9.9 (1965), pp. 3011–3021. ISSN: 1097-4628. DOI: https://doi.org/10.1002/app.1965.070090907.

[73] J. A. C. Harwood and A. R. Payne. "Stress softening in natural rubber vulcanizates. Part V. The anomalous tensile behavior of natural rubber". In: *Journal of Applied Polymer Science* 11.10 (1967), pp. 1825–1834. ISSN: 1097-4628. DOI: https://doi.org/10.1002/app.1967.070111001.

[74] R. Diaz, J. Diani, and P. Gilormini. "Physical interpretation of the Mullins softening in a carbon-black filled SBR". In: *Polymer* 55.19 (2014), pp. 4942–4947. ISSN: 0032-3861. DOI: https://doi.org/10.1016/j.polymer.2014.08.020.

[75] N. Candau, O. Oguz, E. Peuvrel-Disdier, J.-L. Bouvard, M. L. Maspoch, G. Corvec, C. Pradille, and N. Billon. "Heat source and voiding signatures of Mullins damage in filled EPDM". In: *Polymer Testing* 91 (2020), p. 106838. ISSN: 0142-9418. DOI: https://doi.org/10.1016/j.polymertesting.2020.106838.

[76] M. S. Loo, J.-B. Le Cam, A. Andriyana, and E. Robin. "Inelastic responses of swollen nitrile rubber under cyclic loading". In: *Rubber Chemistry and Technology* 91.1 (2018), pp. 136–150. ISSN: 1943-4804. DOI: https://doi.org/10.5254/rct.18.83713.

[77] G. Machado, G. Chagnon, and D. Favier. "Analysis of the isotropic models of the Mullins effect based on filled silicone rubber experimental results". In: *Mechanics of Materials* 42.9 (2010), pp. 841–851. ISSN: 0167-6636. DOI: https://doi.org/10.1016/j.mechmat.2010.07.001.

[78] G. Machado, G. Chagnon, and D. Favier. "Induced anisotropy by the Mullins effect in filled silicone rubber". In: *Mechanics of Materials* 50 (2012), pp. 70–80. ISSN: 0167-6636. DOI: https://doi.org/10.1016/j.mechmat.2012.03.006.

[79] J. A. C. Harwood and A. R. Payne. "Stress softening in natural rubber vulcanizates. Part IV. Unfilled vulcanizates". In: *Journal of Applied Polymer Science* 10.8 (1966), pp. 1203–1211. ISSN: 1097-4628. DOI: https://doi.org/10.1002/app.1966.070100811.

[80] P. A. Kakavas. "Mechanical properties of bonded elastomer discs subjected to triaxial stress". In: *Journal of Applied Polymer Science* 59.2 (1996), pp. 251–261. ISSN: 1097-4628. DOI: https://doi.org/10.1002/(sici)1097-4628(19960110)59:2<251::aid-app9>3.0.co;2-w.

[81] J. Diani, B. Fayolle, and P. Gilormini. "A review on the Mullins effect". In: *European Polymer Journal* 45.3 (2009), pp. 601–612. ISSN: 0014-3057. DOI: https://doi.org/10.1016/j.eurpolymj.2008.11.017.

[82] G. Kraus, C. W. Childers, and K. W. Rollmann. "Stress softening in carbon black-reinforced vulcanizates. Strain rate and temperature effects". In: *Journal of Applied Polymer Science* 10.2 (1966), pp. 229–244. ISSN: 1097-4628. DOI: https://doi.org/10.1002/app.1966.070100205.

[83] E. M. Dannenberg and J. J. Brennan. "Strain Energy as a Criterion for Stress Softening in Carbon-Black-Filled Vulcanizates". In: *Rubber Chemistry and Technology* 39.3 (1966), pp. 597–608. ISSN: 0035-9475. DOI: https://doi.org/10.5254/1.3544867.

[84] C. M. Roland. "The Mullins Effect in Crosslinked Rubber". In: *Journal of Rheology* 33.4 (1989), pp. 659–670. ISSN: 1520-8516. DOI: https://doi.org/10.1122/1.550032.

[85] H. Wan, K. Gao, S. Li, L. Zhang, X. Wu, X. Wang, and J. Liu. "Chemical Bond Scission and Physical Slippage in the Mullins Effect and Fatigue Behavior of Elastomers". In: *Macromolecules* 52.11 (2019), pp. 4209–4221. ISSN: 1520-5835. DOI: https://doi.org/10.1021/acs.macromol.9b00128.

[86] J.-B. Le Cam. "Thermomechanical and Energetic Behavior of Elastomers Investigated with IR Thermography-Based Surface Calorimetry: Revisiting Rubber Elasticity, Viscosity, Stress Softening, Strain-Induced Crystallization, and Energy Stored". In: *Advances in Polymer Science*. Springer Berlin Heidelberg, 2024. DOI: https://doi.org/10.1007/12_2024_174.

[87] X. Balandraud and J.-B. Le Cam. "Some specific features and consequences of the thermal response of rubber under cyclic mechanical loading". In: *Archive of Applied Mechanics* 84.6 (2014), pp. 773–788. DOI: https://doi.org/10.1007/s00419-014-0832-3.

[88] J.-B. Le Cam. "Strain-induced crystallization in rubber: A new measurement technique". In: *Strain* 54.1 (2018), e12256. DOI: https://doi.org/10.1111/str.12256.

[89] P.-A. Albouy and P. Sotta. "Strain-Induced Crystallization in Natural Rubber". In: *Advances in Polymer Science*. Springer International Publishing, 2015, pp. 167–205. ISBN: 9783319506845. DOI: https://doi.org/10.1007/12_2015_328.

[90] B. Huneau. "Strain-induced crystallization of natural rubber: a review of X-ray diffraction investigations". In: *Rubber chemistry and technology* 84.3 (2011), pp. 425–452. DOI: https://doi.org/10.5254/1.3601131.

[91] S. Toki. "The effect of strain-induced crystallization (SIC) on the physical properties of natural rubber (NR)". In: *Chemistry, Manufacture and Applications of Natural Rubber*. Elsevier, 2014, pp. 135–167. ISBN: 9780857096838. DOI: https://doi.org/10.1533/9780857096913.1.135.

[92] M. Tosaka, S. Murakami, S. Poompradub, S. Kohjiya, Y. Ikeda, I. Toki S.and Sics, and B. S. Hsiao. "Orientation and crystallization of natural rubber network as revealed by WAXD using synchrotron radiation". In: *Macromolecules* 37.9 (2004), pp. 3299–3309. DOI: https://doi.org/10.1021/ma0355608.

[93] J. R. Katz. "Röntgenspektrographische Untersuchungen am gedehnten Kautschuk und ihre mögliche Bedeutung für das Problem der Dehnungseigenschaften dieser Substanz". In: *Die Naturwissenschaften* 13.19 (1925), pp. 410–416. ISSN: 1432-1904. DOI: https://doi.org/10.1007/bf01560952.

[94] M. Tosaka, S. Kohjiya, S. Murakami, S. Poompradub, Y. Ikeda, S. Toki, I. Sics, and B. S. Hsiao. "Effect of Network-Chain Length on Strain-Induced Crystallization of NR and IR Vulcanizates". In: *Rubber Chemistry and Technology* 77.4 (2004), pp. 711–723. DOI: https://doi.org/10.5254/1.3547846.

[95] S. Trabelsi, P.-A. Albouy, and J. Rault. "Effective Local Deformation in Stretched Filled Rubber". In: *Macromolecules* 36.24 (2003), pp. 9093–9099. ISSN: 1520-5835. DOI: https://doi.org/10.1021/ma0303566.

[96] J.-B. Le Cam, P.-A. Albouy, and S. Charlès. "Comparison between x-ray diffraction and quantitative surface calorimetry based on infrared thermography to evaluate strain-induced crystallinity in natural rubber". In: *Review of Scientific Instruments* 91.4 (2020), p. 044902. DOI: https://doi.org/10.1063/1.5141851.

[97] J.-B. Le Cam, W. A. Kyei-Manu, A. Tayeb, P.-A. Albouy, and J. J. C. Busfield. "Strain-induced crystallisation of reinforced elastomers using surface calorimetry". In: *Polymer Testing* 131 (2024), p. 108341. ISSN: 0142-9418. DOI: https://doi.org/10.1016/j.polymertesting.2024.108341.

[98] P. J. Flory. "Thermodynamics of crystallization in high polymers. I. Crystallization induced by stretching". In: *The Journal of Chemical Physics* 15.6 (1947), pp. 397–408. DOI: https://doi.org/10.1063/1.1746537.

[99] A. N. Gent, S. Kawahara, and J. Zhao. "Crystallization and Strength of Natural Rubber and Synthetic cis-1,4-Polyisoprene". In: *Rubber Chemistry and Technology* 71.4 (1998), pp. 668–678. DOI: https://doi.org/10.5254/1.3538496.

[100] S. Toki and B. S. Hsiao. "Nature of strain-induced structures in natural and synthetic rubbers under stretching". In: *Macromolecules* 36.16 (2003), pp. 5915–5917. DOI: https://doi.org/10.1021/ma034729e.

[101] S. Amnuaypornsri, J. Sakdapipanich, S. Toki, B. S. Hsiao, N. Ichikawa, and Y. Tanaka. "Strain-Induced Crystallization of Natural Rubber: Effect of Proteins and Phospholipids". In: *Rubber Chemistry and Technology* 81.5 (2008), pp. 753–766. ISSN: 0035-9475. DOI: https://doi.org/10.5254/1.3548230.

[102] S. Toki, B. S. Hsiao, S. Amnuaypornsri, and J. Sakdapipanich. "New insights into the relationship between network structure and strain-induced crystallization in un-vulcanized and vulcanized natural rubber by synchrotron X-ray diffraction". In: *Polymer* 50.9 (2009), pp. 2142–2148. DOI: https://doi.org/10.1016/j.polymer.2009.03.001.

[103] G. L. Clark, M. Kabler, E. Blaker, and J. M. Ball. "Hysteresis in Crystallization of Stretched Vulcanized Rubber from X-Ray Data. Correlation with Stress-Strain Behavior and Resilience". In: *Rubber Chemistry and Technology* 14.1 (1941), pp. 27–34. ISSN: 0035-9475. DOI: https://doi.org/10.5254/1.3540018.

[104] M. Zaghdoudi, Z. Tourki, and P.-A. Albouy. "Characterisation of vulcanised natural rubber behaviour by monotonic andin situcyclic X-ray scattering tests". In: *Plastics, Rubber and Composites* 44.6 (2015), pp. 211–217. ISSN: 1743-2898. DOI: https://doi.org/10.1179/1743289815y.0000000011.

[105] S. Beurrot-Borgarino, B. Huneau, E. Verron, and P. Rublon. "Strain-induced crystallization of carbon black-filled natural rubber during fatigue measured by in situ synchrotron X-ray diffraction". In: *International Journal of fatigue* 47 (2013), pp. 1–7. DOI: https://doi.org/10.1016/j.ijfatigue.2012.07.001.

[106] K. Brüning, K. Schneider, S. V. Roth, and G. Heinrich. "Strain-induced crystallization around a crack tip in natural rubber under dynamic load". In: *Polymer* 54.22 (2013), pp. 6200–6205. ISSN: 0032-3861. DOI: https://doi.org/10.1016/j.polymer.2013.08.045.

[107] S. Trabelsi, P.-A. Albouy, and J. Rault. "Stress-Induced Crystallization around a Crack Tip in Natural Rubber". In: *Macromolecules* 35.27 (2002), pp. 10054–10061. ISSN: 1520-5835. DOI: https://doi.org/10.1021/ma021106c.

[108] P. Rublon, B. Huneau, E. Verron, N. Saintier, S. Beurrot, A. Leygue, C. Mocuta, D. Thiaudière, and D. Berghezan. "Multiaxial deformation and strain-induced crystallization around a fatigue crack in natural rubber". In: *Engineering Fracture Mechanics* 123 (2014), pp. 59–69. ISSN: 0013-7944. DOI: https://doi.org/10.1016/j.engfracmech.2014.04.003.

[109] Q. Demassieux, D. Berghezan, and C. Creton. "Microfocused Beam SAXS and WAXS Mapping at the Crack Tip and Fatigue Crack Propagation in Natural Rubber". In: *Advances in Polymer Science*. Springer International Publishing, 2020, pp. 467–491. ISBN: 9783030689209. DOI: https://doi.org/10.1007/12_2020_79.

[110] S. Beurrot. "Cristallisation sous contrainte du caoutchouc naturel en fatigue et sous sollicitation multiaxiale". PhD thesis. Ecole Centrale de Nantes, 2012.

[111] N. Candau, R. Laghmach, L. Chazeau, J.-M. Chenal, C. Gauthier, T. Biben, and E. Munch. "Influence of strain rate and temperature on the onset of strain induced crystallization in natural rubber". In: *European Polymer Journal* 64 (2015), pp. 244–252. ISSN: 0014-3057. DOI: https://doi.org/10.1016/j.eurpolymj.2015.01.008.

[112] N. Candau, L. Chazeau, J.-M. Chenal, C. Gauthier, and E. Munch. "Complex dependence on the elastically active chains density of the strain induced crystallization of vulcanized natural rubbers, from low to high strain rate". In: *Polymer* 97 (2016), pp. 158–166. ISSN: 0032-3861. DOI: https://doi.org/10.1016/j.polymer.2016.05.020.

[113] K. Brüning, K. Schneider, S. V. Roth, and G. Heinrich. "Kinetics of strain-induced crystallization in natural rubber: A diffusion-controlled rate law". In: *Polymer* 72 (2015), pp. 52–58. ISSN: 0032-3861. DOI: https://doi.org/10.1016/j.polymer.2015.07.011.

[114] N. Candau, L. Chazeau, J.-M. Chenal, C. Gauthier, and E. Munch. "Compared abilities of filled and unfilled natural rubbers to crystallize in a large strain rate domain". In: *Composites Science and Technology* 108 (2015), pp. 9–15. DOI: https://doi.org/10.1016/j.compscitech.2014.12.014.

[115] J. Rault, J. Marchal, P. Judeinstein, and P. A. Albouy. "Stress-induced crystallization and reinforcement in filled natural rubbers: 2H NMR study". In: *Macromolecules* 39.24 (2006), pp. 8356–8368. DOI: https://doi.org/10.1021/ma0608424.

[116] J.-M. Chenal, L. Chazeau, L. Guy, Y. Bomal, and C. Gauthier. "Molecular weight between physical entanglements in natural rubber: A critical parameter during strain-induced crystallization". In: *Polymer* 48.4 (2007), pp. 1042–1046. DOI: https://doi.org/10.1016/j.polymer.2006.12.031.

[117] P.-A. Albouy, J. Marchal, and J. Rault. "Chain orientation in natural rubber, Part I: The inverse yielding effect". In: *The European Physical Journal E* 17.3 (2005), pp. 247–259. ISSN: 1292-895X. DOI: https://doi.org/10.1140/epje/i2004-10145-6.

[118] S. Beurrot-Borgarino, B. Huneau, E. Verron, P. Rublon, D. Thiaudière, C. Mocuta, and A. Zozulya. "In situ synchrotron X-ray diffraction study of strain induced crystallisation of natural rubber during fatigue tests". In: *Plastics, rubber and composites* 41.7 (2012), pp. 290–295. DOI: https://doi.org/10.1179/1743289812Y.0000000028.

[119] W. Sainumsai, K. Suchiva, and S. Toki. "Influence of sulphur crosslink type on the strain-induced crystallization of natural rubber vulcanizates during uniaxial stretching by in situ WAXD using a synchrotron radiation". In: *Materials today: Proceedings* 17 (2019), pp. 1539–1548. DOI: https://doi.org/10.1016/j.matpr.2019.06.179.

[120] F. Grasland. "Vieillissement du caoutchouc naturel par thermo-oxydation: Etudes de ses conséquences sur la cristallisation sous déformation, la fissuration et la rupture". PhD thesis. Université de Lyon, 2018.

[121] W. Sainumsai, S. Toki, S. Amnuaypornsri, A. Nimpaiboon, J. Sakdapipanich, L. Rong, B. S. Hsiao, and K. Suchiva. "dependence of the onset of strain-induced crystallization of natural rubber and its synthetic analogue on crosslink and entanglement by using synchrotron x-ray". In: *Rubber Chemistry and Technology* 90.4 (2017), pp. 728–742. ISSN: 1943-4804. DOI: https://doi.org/10.5254/rct.18.82693.

[122] Y. Ikeda, Y. Yasuda, K. Hijikata, M. Tosaka, and S. Kohjiya. "Comparative study on strain-induced crystallization behavior of peroxide cross-linked and sulfur cross-linked natural rubber". In: *Macromolecules* 41.15 (2008), pp. 5876–5884. DOI: https://doi.org/10.1021/ma800144u.

[123] N. Candau. "Compréhension des mécanismes de cristallisation sous tension des élastomères en conditions quasi-statiques et dynamiques". PhD thesis. INSA de Lyon, 2014.

[124] Y. Ikeda, Y. Yasuda, S. Makino, S. Yamamoto, M. Tosaka, K. Senoo, and S. Kohjiya. "Strain-induced crystallization of peroxide-crosslinked natural rubber". In: *Polymer* 48.5 (2007), pp. 1171–1175. DOI: https://doi.org/10.1016/j.polymer.2007.01.006.

[125] J. M. Goppel. "On the degree of crystallinity in natural rubber I". In: *Flow, Turbulence and Combustion* 1.1 (1949). DOI: https://doi.org/10.1007/bf02120311.

[126] M. Tosaka, S. Kohjiya, Y. Ikeda, S. Toki, and B. S. Hsiao. "Molecular orientation and stress relaxation during strain-induced crystallization of vulcanized natural rubber". In: *Polymer journal* 42.6 (2010), pp. 474–481. DOI: https://doi.org/10.1038/pj.2010.22.

[127] Y. Wang, L. Liao, R. Wang, H. Yu, T. Zheng, Y. Lian, M. Luo, S. Liao, H. Liu, and Z. Peng. "Research of strain induced crystallization and tensile properties of vulcanized natural rubber based on crosslink densities". In: *Industrial Crops and Products* 202 (2023), p. 117070. ISSN: 0926-6690. DOI: https://doi.org/10.1016/j.indcrop.2023.117070.

[128] M. Tosaka, D. Kawakami, K. Senoo, S. Kohjiya, Y. Ikeda, S. Toki, and B. S. Hsiao. "Crystallization and stress relaxation in highly stretched samples of natural rubber and its synthetic analogue". In: *Macromolecules* 39.15 (2006), pp. 5100–5105. DOI: https://doi.org/10.1021/ma061798v.

[129] Q. Demassieux, D. Berghezan, D. Cantournet, H. Proudhon, and C. Creton. "Temperature and aging dependence of strain-induced crystallization and cavitation in highly crosslinked and filled natural rubber". In: *Journal of Polymer Science Part B: Polymer Physics* 57.12 (2019), pp. 780–793. DOI: https://doi.org/10.1002/polb.24832.

[130] J. R. Beatty. "Fatigue of rubber". In: *Rubber Chemistry and Technology* 37.5 (1964), pp. 1341–1364. DOI: https://doi.org/10.5254/1.3540402.

[131] C. G. Robertson, R. Stoček, C. Kipscholl, and W. V. Mars. "Characterizing the intrinsic strength (fatigue threshold) of natural rubber/butadiene rubber blends". In: *Tire Science and Technology* 47.4 (2019), pp. 292–307. DOI: https://doi.org/10.1007/12_2020_71.

[132] R. S. Rivlin and A. G. Thomas. "Rupture of rubber. I. Characteristic energy for tearing". In: *Journal of Polymer Science* 10.3 (1953), pp. 291–318. ISSN: 1542-6238. DOI: https://doi.org/10.1002/pol.1953.120100303.

[133] A. G. Thomas. "Rupture of rubber. V. Cut growth in natural rubber vulcanizates". In: *Journal of Polymer Science* 31.123 (1958), pp. 467–480. ISSN: 1542-6238. DOI: https://doi.org/10.1002/pol.1958.1203112324.

[134] A. N. Gent, P. B. Lindley, and A. G. Thomas. "Cut growth and fatigue of rubbers. I. The relationship between cut growth and fatigue". In: *Journal of Applied Polymer Science* 8.1 (1964), pp. 455–466. ISSN: 1097-4628. DOI: https://doi.org/10.1002/app.1964.070080129.

[135] G. J. Lake and A. G. Thomas. "The strength of highly elastic materials". In: *Proceedings of the Royal Society of London. Series A. Mathematical and Physical Sciences* 300.1460 (1967), pp. 108–119. ISSN: 2053-9169. DOI: https://doi.org/10.1098/rspa.1967.0160.

[136] N. André. "Haigh diagram for fatigue crack initiation prediction of natural rubber components". In: *Kautschuk Gummi Kunststoffe* (1999). URL: https://api.semanticscholar.org/CorpusID:136601611.

[137] N. Saintier. "Fatigue multiaxiale dans un élastomère de type NR chargé : mécanismes d'endommagement et critère local d'amorçage de fissure". PhD thesis. Ecole Nationale Supérieure des Mines de Paris, 2001.

[138] G. Ayoub, M. Naït-Abdelaziz, F. Zaïri, J. M. Gloaguen, and P. Charrier. "Fatigue life prediction of rubber-like materials under multiaxial loading using a continuum damage mechanics approach: Effects of two-blocks loading and R ratio". In: *Mechanics of Materials* 52 (2012), pp. 87–102. ISSN: 0167-6636. DOI: https://doi.org/10.1016/j.mechmat.2012.03.012.

[139] I. Warneboldt, Y. Marco, P. Charrier, W. Hervouet, C. Champy, I. Raoult, V. Le Saux, and F. Szmytka. "Experimental investigations about complex non-relaxing fatigue loads for carbon-black filled natural rubber". In: *International Journal of Fatigue* 156 (2022), p. 106696. ISSN: 0142-1123. DOI: https://doi.org/10.1016/j.ijfatigue.2021.106696.

[140] C. Neuhaus, A. Lion, M. el Johlitz, P. Heuler, M. Barkhoff, and F. Duisen. "Fatigue behaviour of an elastomer under consideration of ageing effects". In: *International Journal of Fatigue* 104 (2017), pp. 72–80. DOI: https://doi.org/10.1016/j.ijfatigue.2017.07.010.

[141] A. Dinari, M. Chaabane, T. Benameur, Q. Guo, J.-M. Gloaguen, and F. Zaïri. "Multiscale Observation of the Fatigue-Induced Damage Mechanisms in Carbon-Black Filled Styrene-Butadiene Rubber". In: *Macromolecular Materials and Engineering* 305.8 (2020). ISSN: 1439-2054. DOI: https://doi.org/10.1002/mame.202000227.

[142] Y. L. Tee, M. S. Loo, and A. Andriyana. "Recent advances on fatigue of rubber after the literature survey by Mars and Fatemi in 2002 and 2004". In: *International Journal of Fatigue* 110 (2018), pp. 115–129. DOI: https://doi.org/10.1016/j.ijfatigue.2018.01.007.

[143] E. Ostoja Kuczynski, P. Charrier, E. Verron, G. Marckmann, L. Gornet, and G. Chagnon. "Crack initiation in filled natural rubber: experimental database and macroscopic observations". In: *Constitutive Models for Rubber III: Proceedings of the Third European Conference on Constitutive Models for Rubber, London, UK, 15-17 September 2003*. CRC Press. 2003, p. 41. URL: https://www.tib.eu/de/suchen/id/BLCP:CN049725620.

[144] I. Raoult. "Structures élastomères sous chargement cyclique: comportement, fatigue, durée de vie". PhD thesis. Ecole Polytechnique X, 2005.

[145] F. Abraham, T. Alshuth, and S. Jerrams. "The effect of minimum stress and stress amplitude on the fatigue life of non strain crystallising elastomers". In: *Materials & Design* 26.3 (2005), pp. 239–245. ISSN: 0261-3069. DOI: https://doi.org/10.1016/j.matdes.2004.02.020.

[146] A. Bennani. "Elaboration, comportement et durée de vie en fatigue du caoutchouc naturel renforcé de silice". PhD thesis. École Nationale Supérieure des Mines de Paris, 2006.

[147] C. Champy, V. Le Saux, Y. Marco, T. Glanowski, P. Charrier, and W. Hervouet. "Fatigue of crystallizable rubber: Generation of a Haigh diagram over a wide range of positive load ratios". In: *International Journal of Fatigue* 150 (2021), p. 106313. ISSN: 0142-1123. DOI: 10.1016/j.ijfatigue.2021.106313.

[148] S. Svensson. "Testing methods for fatigue properties of rubber materials and vibration isolators". In: *Polymer Testing* 2.3 (1981), pp. 161–174. ISSN: 0142-9418. DOI: https://doi.org/10.1016/0142-9418(81)90002-7.

[149] C. Lu. "Étude du comportement mécanique et des mécanismesd'endommagement des élastomères en fatigue et en fissuration par fatigue". PhD thesis. Conservatoire National des Arts et Métiers, 1991.

[150] Y. Le Chenadec. "Autoéchauffement, fatigue thermomécanique des élastomères." PhD thesis. Ecole Polytechnique X, 2008.

[151] V. Le Saux, Y. Marco, S. Calloch, C. Doudard, and P. Charrier. "Fast evaluation of the fatigue lifetime of rubber-like materials based on a heat build-up protocol and micro-tomography measurements". In: *International Journal of Fatigue* 32.10 (2010), pp. 1582–1590. ISSN: 0142-1123. DOI: https://doi.org/10.1016/j.ijfatigue.2010.02.014.

[152] M. Broudin. "Vieillissement thermo-oxydatif d'un élastomère industriel pour applications automobiles antivibratoires: caractérisations, compréhension, outils de dimensionnement". PhD thesis. Brest, 2017.

[153] N. Saintier, G. Cailletaud, and R. Piques. "Multiaxial fatigue life prediction for a natural rubber". In: *International Journal of Fatigue* 28.5-6 (2006), pp. 530–539. DOI: https://doi.org/10.1016/j.ijfatigue.2005.05.011.

[154] B. Ruellan, J.-B. Le Cam, E. Robin, I. Jeanneau, F. Canévet, G. Mauvoisin, and D. Loison. "Fatigue crack growth in natural rubber: The role of SIC investigated through post-mortem analysis of fatigue striations". In: *Engineering Fracture Mechanics* 201 (2018), pp. 353–365. DOI: https://doi.org/10.1016/j.engfracmech.2018.07.001.

[155] Y. Mouslih, J.-B. Le Cam, B. Ruellan, I. Jeanneau, and F. Canevet. "Temperature effects on the lifetime reinforcement due to strain-induced crystallization in carbon black filled natural rubber under non-relaxing torsion: comparison with non-relaxing tensile loadings". In: *Mechanics of Materials* 196 (2024), p. 105045. ISSN: 0167-6636. DOI: https://doi.org/10.1016/j.mechmat.2024.105045.

[156] Y. Mouslih, J.-B. Le Cam, B. Ruellan, I. Jeanneau, and F. Canévet. "Fatigue life reinforcement of carbon black filled natural rubber under non-relaxing torsion loadings and comparison with non-relaxing tension loadings". In: *Fatigue & Fracture of Engineering Materials & Structures* 47.5 (2024), pp. 1620–1637. ISSN: 1460-2695. DOI: https://doi.org/10.1111/ffe.14250.

[157] J.-B. Le Cam. "Endommagement en fatigue des élastomères". PhD thesis. Nantes, 2005.

[158] J. H. Fielding. "Flex Life and Crystallization of Synthetic Rubber". In: *Rubber Chemistry and Technology* 17.2 (1944), pp. 398–403. ISSN: 0035-9475. DOI: https://doi.org/10.5254/1.3546660.

[159] D. G. Young. "Dynamic Property and Fatigue Crack Propagation Researchon Tire Sidewall and Model Compounds.pdf. Rubber Chemistryand Technology". In: *Rubber Chemistryand Technology* (1986). DOI: https://doi.org/10.5254/1.3536093.

[160] A. I. Medalia. "Heat Generation in Elastomer Compounds: Causes and Effects". In: *Rubber Chemistry and Technology* 64.3 (1991), pp. 481–492. ISSN: 0035-9475. DOI: https://doi.org/10.5254/1.3538565.

[161] O. Kratina, M. Pöschl, and R. Stoček. "The effect of apparent density of sulfidic crosslink and their chemical nature on self-heat build-up in carbon black filled Natural Rubber under cyclic mechanical loading". In: *Polymer Degradation and Stability* 227 (2024), p. 110871. ISSN: 0141-3910. DOI: https://doi.org/10.1016/j.polymdegradstab.2024.110871.

[162] F. Stadlbauer, T. Koch, V.-M. Archodoulaki, F. Planitzer, W. Fidi, and A. Holzner. "Influence of Experimental Parameters on Fatigue Crack Growth and Heat Build-Up in Rubber". In: *Materials* 6.12 (2013), pp. 5502–5516. ISSN: 1996-1944. DOI: https://doi.org/10.3390/ma6125502.

[163] G. J. Lake. "Fracture Mechanics and its Application to Failure in Rubber Articles". In: *Rubber Chemistry and Technology* 76.3 (2003), pp. 567–591. ISSN: 0035-9475. DOI: https://doi.org/10.5254/1.3547761.

[164] J. Schieppati, B. Schrittesser, A. Wondracek, S. Robin, A. Holzner, and G. Pinter. "Impact of temperature on the fatigue and crack growth behavior of rubbers". In: *Procedia Structural Integrity* 13 (2018), pp. 642–647. ISSN: 2452-3216. DOI: https://doi.org/10.1016/j.prostr.2018.12.106.

[165] S. Seichter, V.-M. Archodoulaki, T. Koch, A. Holzner, and A. Wondracek. "Investigation of different influences on the fatigue behaviour of industrial rubbers". In: *Polymer Testing* 59 (2017), pp. 99–106. ISSN: 0142-9418. DOI: https://doi.org/10.1016/j.polymertesting.2017.01.018.

[166] W. A. Kyei-Manu, L. B. Tunnicliffe, C. R. Herd, K. Akutagawa, O. Kratina, R. Stoček, and J. J. C. Busfield. "Effect of Carbon Black on Heat Build-up and Energy Dissipation in Rubber Materials". In: *Advances in Polymer Science*. Springer Berlin Heidelberg, 2024. DOI: https://doi.org/10.1007/12_2024_171.

[167] K. K. Kar and A. K. Bhowmick. "Hysteresis loss in filled rubber vulcanizates and its relationship with heat generation". In: *Journal of Applied Polymer Science* (1997). DOI: https://doi.org/10.1002/(SICI)1097-4628(19970523)64:8<1541::AID-APP12>3.0.CO;2-0.

[168] B. Ruellan, J.-B. Le Cam, I. Jeanneau, F. Canévet, F. Mortier, and E. Robin. "Fatigue of natural rubber under different temperatures". In: *International Journal of Fatigue* 124 (2019), pp. 544–557. DOI: https://doi.org/10.1016/j.ijfatigue.2018.10.009.

[169] M. Broudin, Y. Marco, V. Le Saux, P. Charrier, W. Hervouet, and P.-Y. Le Gac. "Investigation of thermo-oxidative ageing effects on the fatigue design of automotive anti-vibration parts". In: *MATEC Web of Conferences*. Vol. 165. 08004. EDP Sciences. 2018. DOI: https://doi.org/10.1051/matecconf/201816508004.

[170] M. Broudin, V. Le Saux, Y. Marco, P. Charrier, and W. Hervouet. "Investigation of thermal aging effects on the fatigue design of automotive anti-vibration parts". In: *Constitutive Models for Rubber IX* (2015), pp. 53–59. DOI: https://doi.org/10.1201/b18701-11.

[171] P.-Y Le Gac, M. Broudin, G. Roux, J. Verdu, P. Davies, and B. Fayolle. "Role of strain induced crystallization and oxidative crosslinking in fracture properties of rubbers". In: *Polymer* 55.10 (2014), pp. 2535–2542. DOI: https://doi.org/10.1016/j.polymer.2014.03.023.

[172] B. A. Dogadkin and Z. N. Tarasova. "Vulcanization Structures and Their Influence on the Heat Resistance and Fatigue of Rubber". In: *Rubber Chemistry and Technology* 27.4 (1954), pp. 883–898. DOI: https://doi.org/10.5254/1.3543540.

[173] L. C. Yanyo. "Effect of crosslink type on the fracture of natural rubber vulcanizates". In: *Structural Integrity*. Springer, 1989, pp. 103–110. DOI: https://doi.org/10.1007/BF00047443.

[174] A. K. Bhowmick, A. N. Gent, and C. T. R. Pulford. "Tear Strength of Elastomers under Threshold Conditions". In: *Rubber Chemistry and Technology* 56.1 (1983), pp. 226–232. DOI: https://doi.org/10.5254/1.3538115.

[175] G. J. Lake and P. B. Lindley. "The mechanical fatigue limit for rubber". In: *Journal of Applied Polymer Science* 9.4 (1965), pp. 1233–1251. DOI: https://doi.org/10.1002/app.1965.070090405.

[176] W. L. Cox and C. R. Parks. "Effect of Curing Systems on Fatigue of Natural Rubber Vulcanizates". In: *Rubber Chemistry and Technology* 39.3 (1966), pp. 785–797. DOI: https://doi.org/10.5254/1.3544883.

[177] B. L. Chan, D. J. Elliott, M. Holley, and J. F. Smith. "The influence of curing systems on the properties of natural rubber". In: *Journal of Polymer Science: Polymer Symposia* 48.1 (1974), pp. 61–86. DOI: https://doi.org/10.1002/polc.5070480108.

[178] A. N. Gent and R. H. Tobias. "Threshold tear strength of elastomers". In: *Journal of Polymer Science: Polymer Physics Edition* 20.11 (1982), pp. 2051–2058. ISSN: 1542-9385. DOI: https://doi.org/10.1002/pol.1982.180201107.

[179] S. G. Kim and S.-H. Lee. "Effect of crosslink structures on the fatigue crack growth behavior of NR vulcanizates with various aging conditions". In: *Rubber chemistry and technology* 67.4 (1994), pp. 649–661. DOI: https://doi.org/10.5254/1.3538700.

[180] Y. Nie, B. Wang, G. Huang, L. Qu, P. Zhang, G. Weng, and J. Wu. "Relationship between the material properties and fatigue crack-growth characteristics of natural rubber filled with different carbon blacks". In: *Journal of applied polymer science* 117.6 (2010), pp. 3441–3447. DOI: https://doi.org/10.1002/app.32098.

[181] A. K. Bhowmick. "Threshold fracture of elastomers". In: *Polymer Reviews* 28.3-4 (1988), pp. 339–370. DOI: https://doi.org/10.1080/15583728808085379.

[182] T. Gehling, R. C. Kerschbaumer, G. Pinter, M. A. Fasching, T. Schwarz, and J. Schieppati. "Investigating the impact of manufacturing conditions on crack growth rate in nitrile butadiene rubber for enhanced service life - part 01". In: *Results in Engineering* 20 (2023), p. 101484. ISSN: 2590-1230. DOI: https://doi.org/10.1016/j.rineng.2023.101484.

[183] J.-B. Le Cam, B. Huneau, and E. Verron. "Fatigue damage in carbon black filled natural rubber under uni- and multiaxial loading conditions". In: *International Journal of Fatigue* 52 (2013), pp. 82–94. ISSN: 0142-1123. DOI: https://doi.org/10.1016/j.ijfatigue.2013.02.022.

[184] J.-B. Le Cam, B. Huneau, and E. Verron. "Description of fatigue damage in carbon black filled natural rubber". In: *Fatigue & Fracture of Engineering Materials & Structures* 31.12 (2008), pp. 1031–1038. ISSN: 1460-2695. DOI: https://doi.org/10.1111/j.1460-2695.2008.01293.x.

[185] J.-B. Le Cam, B. Huneau, E. Verron, and L. Gornet. "Mechanism of Fatigue Crack Growth in Carbon Black Filled Natural Rubber". In: *Macromolecules* 37.13 (2004), pp. 5011–5017. ISSN: 1520-5835. DOI: https://doi.org/10.1021/ma0495386.

[186] J.-B. Le Cam and E. Toussaint. "The mechanism of fatigue crack growth in rubbers under severe loading: the effect of stress-induced crystallization". In: *Macromolecules* 43.10 (2010), pp. 4708–4714. DOI: https://doi.org/10.1021/ma100042n.

[187] B. Ellis and G. N. Welding. "Estimation, from swelling, of the structural contribution of chemical reactions to the vulcanization of natural rubber. Part II. Estimation of equilibrium degree of swelling". In: *Rubber Chemistry and Technology* 37.2 (1964), pp. 571–575. DOI: https://doi.org/10.5254/1.3540348.

[188] J. L. Valentin, J. Carretero-Gonzalez, I. Mora-Barrantes, W. Chasse, and K. Saalwachter. "Uncertainties in the determination of cross-link density by equilibrium swelling experiments in natural rubber". In: *Macromolecules* 41.13 (2008), pp. 4717–4729. DOI: https://doi.org/10.1021/ma8005087.

[189] P. J. Flory. "Thermodynamics of high polymer solutions". In: *The Journal of chemical physics* 10.1 (1942), pp. 51–61. DOI: https://doi.org/10.1063/1.1723621.

[190] H. M. James and E. Guth. "Theory of the elastic properties of rubber". In: *The Journal of Chemical Physics* 11.10 (1943), pp. 455–481. DOI: https://doi.org/10.1063/1.1723785.

[191] G. Delahaye, A. Redon, B. Ruellan, I. Jeanneau, J. Rosselgong, S. M. Guillaume, and J.-B. Le Cam. "A comprehensive review on active chain density evaluation from swelling and insights for better accounting for insoluble particles". In: *Journal of Applied Polymer Science* 141.35 (2024). ISSN: 1097-4628. DOI: https://doi.org/10.1002/app.55899.

[192] F. Horkay, G. B. McKenna, P. Deschamps, and E. Geissler. "Neutron scattering properties of randomly cross-linked polyisoprene gels". In: *Macromolecules* 33.14 (2000), pp. 5215–5220. DOI: https://doi.org/10.1021/ma0003001.

[193] B. Basterra-Beroiz, R. Rommel, F. Kayser, S. Westermann, J. L. Valentín, and G. Heinrich. "New insights into rubber network structure by a combination of experimental techniques". In: *Rubber Chemistry and Technology* 90.2 (2017), pp. 347–366. DOI: https://doi.org/10.5254/rct.16.83732.

[194] G. Marckmann and E. Verron. "Comparison of Hyperelastic Models for Rubber-Like Materials". In: *Rubber Chemistry and Technology* 79.5 (2006), pp. 835–858. ISSN: 0035-9475. DOI: https://doi.org/10.5254/1.3547969.

[195] M. Mooney. "A Theory of Large Elastic Deformation". In: *Journal of Applied Physics* 11.9 (1940), pp. 582–592. ISSN: 1089-7550. DOI: https://doi.org/10.1063/1.1712836.

[196] R. S. Rivlin. "Large elastic deformations of isotropic materials IV. further developments of the general theory". In: *Philosophical Transactions of the Royal Society of London. Series A, Mathematical and Physical Sciences* 241.835 (1948), pp. 379–397. ISSN: 2054-0272. DOI: https://doi.org/10.1098/rsta.1948.0024.

[197] A. F. Blanchard and D. Parkinson. "Breakage of Carbon-Rubber Networks by Applied Stress". In: *Rubber Chemistry and Technology* 25.4 (1952), pp. 808–842. ISSN: 0035-9475. DOI: https://doi.org/10.5254/1.3543444.

[198] J. M. Clough, C. Creton, S. L. Craig, and R. P. Sijbesma. "Covalent Bond Scission in the Mullins Effect of a Filled Elastomer: Real-Time Visualization with Mechanoluminescence". In: *Advanced Functional Materials* 26.48 (2016), pp. 9063–9074. ISSN: 1616-3028. DOI: https://doi.org/10.1002/adfm.201602490.

[199] R. Houwink. "Slipping of Molecules during the Deformation of Reinforced Rubber". In: *Rubber Chemistry and Technology* 29.3 (1956), pp. 888–893. ISSN: 0035-9475. DOI: https://doi.org/10.5254/1.3542602.

[200] E. M. Dannenberg. "The Effects of Surface Chemical Interactions on the Properties of Filler-Reinforced Rubbers". In: *Rubber Chemistry and Technology* 48.3 (1975), pp. 410–444. ISSN: 0035-9475. DOI: https://doi.org/10.5254/1.3547460.

[201] S. Cantournet, R. Desmorat, and J. Besson. "Mullins effect and cyclic stress softening of filled elastomers by internal sliding and friction thermodynamics model". In: *International Journal of Solids and Structures* 46.11–12 (2009), pp. 2255–2264. ISSN: 0020-7683. DOI: https://doi.org/10.1016/j.ijsolstr.2008.12.025.

[202] M. Hernandez, J. L. Valentin, M. A. Lopez-Manchado, and T. A. Ezquerra. "Influence of the vulcanization system on the dynamics and structure of natural rubber: Comparative study by means of broadband dielectric spectroscopy and solid-state NMR spectroscopy". In: *European Polymer Journal* 68 (2015), pp. 90–103. DOI: https://doi.org/10.1016/j.eurpolymj.2015.04.021.

[203] A. Vieyres, R. Perez-Aparicio, P.-A. Albouy, O. Sanseau, K. Saalwachter, D. R. Long, and P. Sotta. "Sulfur-cured natural rubber elastomer networks: correlating cross-link density, chain orientation, and mechanical response by combined techniques". In: *Macromolecules* 46.3 (2013), pp. 889–899. DOI: https://doi.org/10.1021/ma302563z.

[204] W. A. Kyei-Manu, C. R. Herd, M. Chowdhury, J. J. C. Busfield, and L. B. Tunnicliffe. "The Influence of Colloidal Properties of Carbon Black on Static and Dynamic Mechanical Properties of Natural Rubber". In: *Polymers* 14.6 (2022), p. 1194. ISSN: 2073-4360. DOI: https://doi.org/10.3390/polym14061194.

[205] H. M. James and E. Guth. "Theory of the increase in rigidity of rubber during cure". In: *The Journal of Chemical Physics* 15.9 (1947), pp. 669–683. DOI: https://doi.org/10.1063/1.1746626.

[206] M. L. Huggins. "Theory of solutions of high polymers1". In: *Journal of the American Chemical Society* 64.7 (1942), pp. 1712–1719. DOI: https://doi.org/10.1021/ja01259a068.

[207] O. Lorenz and C. R. Parks. "The crosslinking efficiency of some vulcanizing agents in natural rubber". In: *Journal of Polymer Science* 50.154 (1961), pp. 299–312. DOI: https://doi.org/10.1002/pol.1961.1205015404.

[208] G. Kraus. "Swelling of filler-reinforced vulcanizates". In: *Journal of Applied Polymer Science* 7.3 (1963), pp. 861–871. DOI: https://doi.org/10.5254/1.3540317.

[209] M. Porter. "Structural Characterization of Filled Vulcanizates Part 1. Determination of the Concentration of Chemical Crosslinks in Natural Rubber Vulcanizates Containing High Abrasion Furnace Black". In: *Rubber Chemistry and Technology* 40.3 (1967), pp. 866–882. DOI: https://doi.org/10.5254/1.3539101.

[210] Z. Li, H. Xu, X. Xia, Y. Song, and Q. Zheng. "Energy dissipation accompanying Mullins effect of nitrile butadiene rubber/carbon black nanocomposites". In: *Polymer* 171 (2019), pp. 106–114. ISSN: 0032-3861. DOI: https://doi.org/10.1016/j.polymer.2019.03.043.

[211] T.-T. Mai, Y. Morishita, and K. Urayama. "Novel features of the Mullins effect in filled elastomers revealed by stretching measurements in various geometries". In: *Soft Matter* 13.10 (2017), pp. 1966–1977. ISSN: 1744-6848. DOI: https://doi.org/10.1039/c6sm02833k.

[212] A. Lachhab, E. Robin, J.-B. Le Cam, F. Mortier, Y. Tirel, and F. Canevet. "Thermomechanical analysis of polymeric foams subjected to cyclic loading: Anelasticity, self-heating and strain-induced crystallization". In: *Polymer* 126 (2017), pp. 19–28. ISSN: 0032-3861. DOI: https://doi.org/10.1016/j.polymer.2017.08.010.

[213] P. Junkong, K. Cornish, and Y. Ikeda. "Characteristics of mechanical properties of sulphur cross-linked guayule and dandelion natural rubbers". In: *RSC Advances* 7.80 (2017), pp. 50739–50752. ISSN: 2046-2069. DOI: https://doi.org/10.1039/c7ra08554k.

[214] P. Junkong, Y. Matsushima, T. Phakkeeree, K. Cornish, and Y. Ikeda. "Influence of strain-induced crystallization on stress softening of sulfur cross-linked unfilled guayule and dandelion natural rubbers". In: *Rubber Chemistry and Technology* 92.2 (2019), pp. 388–398. ISSN: 1943-4804. DOI: https://doi.org/10.5254/rct.19.81481.

[215] X. Liang and K. Nakajima. "Study of the Mullins Effect in Carbon Black-Filled Styrene–Butadiene Rubber by Atomic Force Microscopy Nanomechanics". In: *Macromolecules* 55.14 (2022), pp. 6023–6030. ISSN: 1520-5835. DOI: https://doi.org/10.1021/acs.macromol.2c00776.

[216] R. N. Datta. *Rubber curing systems*. Vol. 12. iSmithers Rapra Publishing, 2002. DOI: https://doi.org/10.1201/9781420007183.sec3.

[217] Y. S. Rohana Yahya, A. R. Azura, and Z. Ahmad. "Effect of curing systems on thermal degradation behaviour of natural rubber (SMR CV 60)". In: *Journal of Physical Science* 22.2 (2011), pp. 1–14. DOI: https://doi.org/10.13140/RG.2.1.1419.5683.

[218] S.-S. Choi. "Influence of rubber composition on change of crosslink density of rubber vulcanizates with EV cure system by thermal aging". In: *Journal of Applied Polymer Science* 75.11 (2000), pp. 1378–1384. DOI: https://doi.org/10.1002/(SICI)1097-4628(20000314)75:11<1378::AID-APP9>3.0.CO;2-I.

[219] M. L. Studebaker and J. R. Beatty. "Effects of Compounding on Dynamic Mechanical Properties of Rubber". In: *Rubber Chemistry and Technology* 47.4 (1974), pp. 803–824. ISSN: 0035-9475. DOI: https://doi.org/10.5254/1.3540466.

[220] K. Le Gorju-Jago. "Fatigue life of rubber components: 3D damage evolution from X-ray computed microtomography". In: *Constitutive Models for Rubber V*. 2007.

[221] J.-B. Le Cam, E. Verron, B. Huneau, L. Gornet, and F. Pérocheau. "Micromechanism of fatigue crack growth: comparison between carbon black filled NR and SBR". In: *Constitutive Models for Rubber IV*. 2005.

[222] K. Le Gorju-Jago and C. Bathias. "Fatigue initiation and propagation in natural and synthetic rubbers". In: *International Journal of Fatigue* 24.2–4 (2002), pp. 85–92. ISSN: 0142-1123. DOI: https://doi.org/10.1016/s0142-1123(01)00062-7.

[223] S. Toki, T. Fujimaki, and M. Okuyama. "Strain-induced crystallization of natural rubber as detected real-time by wide-angle X-ray diffraction technique". In: *Polymer* 41.14 (2000), pp. 5423–5429. DOI: https://doi.org/10.1016/S0032-3861(99)00724-7.

[224] J. Zhao and G. N. Ghebremeskel. "A Review of Some of the Factors Affecting Fracture and Fatigue in SBR and BR Vulcanizates". In: *Rubber Chemistry and Technology* 74.3 (2001), pp. 409–427. ISSN: 0035-9475. DOI: https://doi.org/10.5254/1.3547645.

[225] A. Redon, J.-B. Le Cam, E. Robin, M. Miroir, and J.-C. Fralin. "Aging characterization of different nitrile butadiene rubbers for sealing in a pneumatic system: Linking the change of the physicochemical state to the mechanical properties". In: *Journal of Applied Polymer Science* 140.29 (2023). ISSN: 1097-4628. DOI: https://doi.org/10.1002/app.54068.

[226] A. J. Marzocca. "Evaluation of the polymer–solvent interaction parameter χ for the system cured styrene butadiene rubber and toluene". In: *European polymer journal* 43.6 (2007), pp. 2682–2689. DOI: https://doi.org/10.1016/j.eurpolymj.2007.02.034.

[227] A. Gros. "Modélisation de la cristallisation sous tension du caoutchouc naturel". PhD thesis. École centrale de Nantes, 2016.

[228] E. A. Meinecke and M. I. Taftaf. "Effect of Carbon Black on the Mechanical Properties of Elastomers". In: *Rubber Chemistry and Technology* 61.3 (1988), pp. 534–547. ISSN: 0035-9475. DOI: https://doi.org/10.5254/1.3536199.

[229] E. M. Dannenberg. "Carbon Black-Loaded GR-S Stocks. Relationship between Reinforcement and Swelling Properties". In: *Rubber Chemistry and Technology* 22.3 (1949), pp. 805–811. ISSN: 0035-9475. DOI: https://doi.org/10.5254/1.3542999.

[230] R. L. Scott and M. Magat. "Thermodynamics of high-polymer solutions. III. Swelling of cross-linked rubber". In: *Journal of Polymer Science* 4.5 (1949), pp. 555–571. ISSN: 1542-6238. DOI: 10.1002/pol.1949.120040502.

[231] R. L. Zapp and E. Guth. "Elastic Modulus and Swelling of Butyl Vulcanizates. Influence of Fillers". In: *Rubber Chemistry and Technology* 24.4 (1951), pp. 894–913. ISSN: 0035-9475. DOI: https://doi.org/10.5254/1.3543118.

[232] R. L. Zapp and E. Guth. "Elastic Modulus and Swelling of Butyl Vulcanizates". In: *Industrial & Engineering Chemistry* 43.2 (1951), pp. 430–438. ISSN: 1541-5724. DOI: https://doi.org/10.1021/ie50494a040.

[233] A. M. Bueche. "Filler reinforcement of silicone rubber". In: *Journal of Polymer Science* 25.109 (1957), pp. 139–149. ISSN: 1542-6238. DOI: https://doi.org/10.1002/pol.1957.1202510902.

[234] G. Kraus. "Degree of Cure in Filler-Reinforced Vulcanizates by the Swelling Method". In: *Rubber Chemistry and Technology* 30.3 (1957), pp. 928–951. ISSN: 0035-9475. DOI: https://doi.org/10.5254/1.3542738.

[235] H. Westlinning and G. Butenuth. "Swelling and Network (Crosslink) Density of Carbon Black-Filled Natural Rubber Vulcanizates". In: *Rubber Chemistry and Technology* 35.2 (1962), pp. 274–283. ISSN: 0035-9475. DOI: https://doi.org/10.5254/1.3539900.

[236] K. W. Scott, O. Lorenz, and C. R. Parks. "Network degradation accompanying the vulcanization of natural rubber with a sulfur–diphenylguanidine system". In: *Journal of Applied Polymer Science* 8.6 (1964), pp. 2909–2922. ISSN: 1097-4628. DOI: https://doi.org/10.1002/app.1964.070080634.

[237] B. B. Boonstra and G. L. Taylor. "Swelling of Filled Rubber Vulcanizates". In: *Rubber Chemistry and Technology* 38.4 (1965), pp. 943–960. ISSN: 0035-9475. DOI: https://doi.org/10.5254/1.3535712.

[238] P. B. Stickney and W. J. Mueller. "Influence of Carbon Black on Swelling Rate of Polymer in Filled Vulcanizates". In: *Rubber Chemistry and Technology* 42.2 (1969), pp. 604–612. ISSN: 0035-9475. DOI: https://doi.org/10.5254/1.3539240.

[239] Y. Diamant and M. Folman. "Influence of dewetting on the damping properties of a filled polymer system: 1. Static characterization". In: *Polymer* 20.8 (1979), pp. 1025–1033. ISSN: 0032-3861. DOI: https://doi.org/10.1016/0032-3861(79)90203-9.

[240] T. Kurian, K. E. George, and D. J. Francis. "Effect of vulcanization temperature on the cure characteristics and vulcanizate properties of natural rubber and styrene-butadiene rubber". In: *Die Angewandte Makromolekulare Chemie* 162.1 (1988), pp. 123–134. ISSN: 1522-9505. DOI: https://doi.org/10.1002/apmc.1988.051620108.

[241] A. N. Gent, J. A. Hartwell, and G. Lee. "Effect of Carbon Black on Crosslinking". In: *Rubber Chemistry and Technology* 76.2 (2003), pp. 517–532. ISSN: 0035-9475. DOI: https://doi.org/10.5254/1.3547758.

[242] L. Bokobza and M. Kolodziej. "On the use of carbon nanotubes as reinforcing fillers for elastomeric materials". In: *Polymer International* 55.9 (2006), pp. 1090–1098. ISSN: 1097-0126. DOI: https://doi.org/10.1002/pi.2064.

[243] S. P. Thomas, E. J. Mathew, and C. V. Marykutty. "Synthesis and effect of surface modified nano ZnO in natural rubber vulcanization". In: *Journal of Applied Polymer Science* 124.4 (2011), pp. 3099–3107. ISSN: 1097-4628. DOI: https://doi.org/10.1002/app.35349.

[244] K. Boonkerd, C. Deeprasertkul, and K. Boonsomwong. "Effect of sulfur to accelerator ratio on crosslink structure, reversion, and strength in natural rubber". In: *Rubber chemistry and technology* 89.3 (2016), pp. 450–464. DOI: https://doi.org/10.5254/rct.16.85963.

[245] L. M. Palacios-Pineda, I. A. Perales-Martinez, L. M. Lozano-Sanchez, O. Martínez-Romero, J. Puente-Córdova, E. Segura-Cárdenas, and A. Elías-Zúniga. "Experimental investigation of the magnetorheological behavior of PDMS elastomer reinforced with iron micro/nanoparticles". In: *Polymers* 9.12 (2017), p. 696. DOI: https://doi.org/10.3390/polym9120696.

[246] B. Basterra-Beroiz, R. Rommel, F. Kayser, S. Westermann, J. L. Valentín, and G. Heinrich. "Swelling of polymer networks with topological constraints: Application of the Helmis-Heinrich-Straube model". In: (2018). DOI: https://doi.org/10.3144/expresspolymlett.2018.62.

[247] S. Howse, C. Porter, T. Mengistu, and R. J. Pazur. "Experimental determination of the quantity and distribution of chemical crosslinks in unaged and aged natural rubber, part 1: Peroxide vulcanization". In: *Polymer Testing* 70 (2018), pp. 263–274. DOI: https://doi.org/10.1016/j.polymertesting.2018.07.002.

[248] M. L. Huggins. "Some Properties of Solutions of Long-chain Compounds." In: *The Journal of Physical Chemistry* 46.1 (1942), pp. 151–158. ISSN: 1541-5740. DOI: https://doi.org/10.1021/j150415a018.

[249] T. A. Vilgis. "Rubber elasticity and inhomogeneities in crosslink density". In: *Macromolecules* 25.1 (1992), pp. 399–403. DOI: https://doi.org/10.1021/ma00027a061.

[250] G. Heinrich, E. Straube, and G. Helmis. "Rubber elasticity of polymer networks: Theories". In: *Advances in Polymer Science*. Springer Berlin Heidelberg, 1988, pp. 33–87. ISBN: 9783662151167. DOI: https://doi.org/10.1007/bfb0024050.

[251] R. F. Blanks and J. M. Prausnitz. "Thermodynamics of polymer solubility in polar and non-polar systems". In: *Industrial & Engineering Chemistry Fundamentals* 3.1 (1964), pp. 1–8. DOI: https://doi.org/10.1021/ie50650a011.

[252] C. J. Sheehan and A. L. Bisio. "Polymer/solvent interaction parameters". In: *Rubber Chemistry and Technology* 39.1 (1966), pp. 149–192. DOI: https://doi.org/10.5254/1.3544827.

[253] C. M. Hansen. *Hansen solubility parameters: a user's handbook*. CRC press, 2007. DOI: https://doi.org/10.1201/9781420006834.

[254] M. Fontanille, Y. Gnanou, and J.-L. Six. *Chimie et physico-chimie des polymères - 4e édition*. Dunod, 2021. URL: https://www.dunod.com/sciences-techniques/chimie-et-physico-chimie-polymeres-0.

[255] S. Wolff. "Chemical Aspects of Rubber Reinforcement by Fillers". In: *Rubber Chemistry and Technology* 69.3 (1996), pp. 325–346. ISSN: 0035-9475. DOI: https://doi.org/10.5254/1.3538376.

[256] E. M. Bevilacqua. "Oxidation of Hevea Vulcanizates Containing Carbon Black". In: *Rubber Chemistry and Technology* 33.1 (1960), pp. 60–71. ISSN: 0035-9475. DOI: https://doi.org/10.5254/1.3542134.

[257] B. a Saville and A. A. Watson. "Structural characterization of sulfur-vulcanized rubber networks". In: *Rubber chemistry and technology* 40.1 (1967), pp. 100–148. DOI: https://doi.org/10.5254/1.3539039.

[258] T. Kotani and S. S. Sternstein. "Birefringence Analysis of Inhomogeneous Swelling in Filled Elastomers". In: *Polymer Networks*. Springer US, 1971, pp. 273–291. ISBN: 9781475762105. DOI: https://doi.org/10.1007/978-1-4757-6210-5_13.

[259] S. S. Sternstein. "Inhomogeneous swelling in filled elastomers". In: *Journal of Macromolecular Science, Part B* 6.1 (1972), pp. 243–262. ISSN: 1525-609X. DOI: https://doi.org/10.1080/00222347208224800.

[260] L. Bokobza. "The Reinforcement of Elastomeric Networks by Fillers". In: *Macromolecular Materials and Engineering* 289.7 (2004), pp. 607–621. ISSN: 1439-2054. DOI: https://doi.org/10.1002/mame.200400034.

[261] D. Y. Kim, J. W. Park, D. Y. Lee, and K. H. Seo. "Correlation between the crosslink characteristics and mechanical properties of natural rubber compound via accelerators and reinforcement". In: *Polymers* 12.9 (2020). DOI: https://doi.org/10.3390/polym12092020.

[262] C. R. Parks and O. Lorenz. "Effect of Network Structure on Aging of Natural Rubber Vulcanizates". In: *Industrial & Engineering Chemistry Product Research and Development* 2.4 (1963), pp. 279–284. ISSN: 1943-2976. DOI: https://doi.org/10.1021/i360008a007.

[263] R. M. Pierson, A. J. Costanza, and F. J. Naples. "American Chemical Society Meeting - 126th edition." In: 1954.

[264] G. M. Bristow and M. Porter. “Structural characterization of vulcanizates. Part V. Determination of degree of chemical crosslinking of natural rubber gum vulcanizate networks”. In: *Journal of Applied Polymer Science* 11.11 (1967), pp. 2215–2226. ISSN: 1097-4628. DOI: https://doi.org/10.1002/app.1967.070111111.

[265] J. L. Valentín, I. Mora-Barrantes, J. Carretero-González, M. A. López-Manchado, P. Sotta, D. R. Long, and K. Saalwächter. “Novel Experimental Approach To Evaluate Filler-Elastomer Interactions”. In: *Macromolecules* 43.1 (2009), pp. 334–346. ISSN: 1520-5835. DOI: https://doi.org/10.1021/ma901999j.

[266] A. I. Medalia. “Effective Degree of Immobilization of Rubber Occluded within Carbon Black Aggregates”. In: *Rubber Chemistry and Technology* 45.5 (1972), pp. 1171–1194. ISSN: 0035-9475. DOI: https://doi.org/10.5254/1.3544731.

[267] L. R. G. Treloar. “The mechanics of rubber elasticity.” In: *Proceedings of the Royal Society of London. A. Mathematical and Physical Sciences* 351.1666 (1976), pp. 301–330. ISSN: 0080-4630. DOI: https://doi.org/10.1098/rspa.1976.0144.

COLLEGE DOCTORAL BRETAGNE
SCIENCES DE LA MATIERE DES MOLECULES ET MATERIAUX

Université de Rennes

Titre : Effets de la structuration du réseau macromoléculaire sur les propriétés mécaniques quasi-statiques et en fatigue du caoutchouc naturel.

Mots clés : densité de chaînes actives ; effet Mullins ; propriétés en fatigue ; conditions et système de vulcanisation ; noir de carbone ; caoutchouc naturel.

Résumé : Les propriétés mécaniques du caoutchouc naturel (CN) dépendent fortement de la structure du réseau macromoléculaire (densité de chaînes actives et longueur des ponts) formée lors de la vulcanisation. Cependant, la relation entre structure et propriétés mécaniques demeure incomprise, en particulier en matière de comportement en fatigue. Dans cette étude, une large gamme de réseaux macromoléculaires, chargés et non-chargés de noir de carbone, a été définie. Chaque matériau est caractérisé en évaluant la densité de chaînes actives par la méthode de gonflement. Le comportement mécanique quasi-statique dépend de la densité de chaînes actives, des charges et de la longueur des ponts. Pour les CN chargés, l'effet Mullins est peu sensible aux variations de structure. Ce n'est pas le cas de leur réponse en fatigue. Pour les chargements relaxants, la réponse dépend de la densité de chaînes actives, de la longueur des ponts et du temps de vulcanisation. Pour les chargements non-relaxants, la densité de chaînes actives pilote à elle seule le renforcement de la durée de vie. L'analyse *post mortem* des faciès de rupture montre une corrélation entre les marqueurs de la cristallisation et le niveau de renforcement. Le lien entre formulation, densité de chaînes actives et propriétés en fatigue a ainsi pu être établi. Le rôle de la structure du réseau sur la cristallisation sous étirement, et par voie de conséquence sur la fatigue, a été clarifié.

Title: Macromolecular network structuring effects on quasi-static and fatigue properties of natural rubber.

Keywords: active chain density; Mullins effect; fatigue properties; vulcanization system and conditions; carbon black filler; natural rubber.

Abstract: The mechanical properties of natural rubber (NR) are mainly driven by the macromolecular network structure (active chain density and cross-link length), formed during the vulcanization process. Nevertheless, the relationship between network structure and mechanical properties remains unclear, particularly with regard to fatigue properties. In the present study, a wide range of macromolecular network structures, both filled and unfilled, were defined on the same NR. Swelling test is used to characterize each material by evaluating of the active chain density. The quasi-static mechanical behavior depends on both the active chain density and cross-link length. The Mullins effect is similar for each filled NR. For relaxing loading conditions, the fatigue behavior shows that the lifetime for filled NR is mainly driven by the active chain density, cross-link length, and vulcanization time. However, for non-relaxing loading conditions, the lifetime reinforcement is predominantly driven by the active chain density. The *post-mortem* analysis showed a strong correlation between the level of reinforcement and relative number of SIC markers on the failure surfaces. Finally, a relationship between formulation, active chain density and fatigue properties was established. In addition, the role of the macromolecular network structure on the strain-induced crystallization, and consequently on fatigue resistance, has been clarified.